

Negative Stiffness Device for Seismic Protection of Structures

by
Apostolos A. Sarlis, Dharma Theja R. Pasala,
Michael C. Constantinou, Andrei M. Reinhorn,
Satish Nagarajaiah and Douglas P. Taylor

Technical Report MCEER-13-0005

June 12, 2013

NOTICE

This report was prepared by the University at Buffalo, State University of New York and Rice University as a result of research supported primarily by the George E. Brown, Jr. Network for Earthquake Engineering Simulation (NEES) Program of the National Science Foundation. Neither MCEER, associates of MCEER, its sponsors, the University at Buffalo, State University of New York, Rice University, nor any person acting on their behalf:

- a. makes any warranty, express or implied, with respect to the use of any information, apparatus, method, or process disclosed in this report or that such use may not infringe upon privately owned rights; or
- b. assumes any liabilities of whatsoever kind with respect to the use of, or the damage resulting from the use of, any information, apparatus, method, or process disclosed in this report.

Any opinions, findings, and conclusions or recommendations expressed in this publication are those of the author(s) and do not necessarily reflect the views of MCEER, the National Science Foundation, or other sponsors.

Negative Stiffness Device for Seismic Protection of Structures

by

Apostolos A. Sarlis¹, Dharma Theja R. Pasala,² Michael C. Constantinou,³
Andrei M. Reinhorn,⁴ Satish Nagarajaiah⁵ and Douglas P. Taylor⁶

Publication Date: June 12, 2013

Submittal Date: December 19, 2012

Technical Report MCEER-13-0005

NSF Grant Number CMMI-NEESR-0830391

- 1 Ph.D. Candidate, Department of Civil, Structural and Environmental Engineering, University of Buffalo, State University of New York
- 2 Senior Riser Engineer, Intecsea; Former Graduate Student, Department of Civil and Environmental Engineering, Rice University
- 3 Professor, Department of Civil, Structural and Environmental Engineering, University at Buffalo, State University of New York
- 4 Clifford C. Furnas Professor, Department of Civil, Structural and Environmental Engineering, University at Buffalo, State University of New York
- 5 Professor, Department of Civil and Environmental Engineering & Mechanical Engineering and Material Science, Rice University
- 6 President, Taylor Devices Inc.

MCEER

University at Buffalo, State University of New York

133A Ketter Hall, Buffalo, NY 14260

Phone: (716) 645-3391; Fax (716) 645-3399

E-mail: mceer@buffalo.edu; Website: <http://mceer.buffalo.edu>

Project Overview

Development of Next Generation Adaptive Seismic Protection Systems

Design of conventional structures specified by the codes is based on the philosophy that the structure should withstand seismic loads while sustaining an acceptable level of damage. Structures are designed to prevent collapse but their serviceability and functionality in the aftermath of strong earthquake ground motion are not taken into consideration. This is achieved by designing structures to be ductile and letting them yield when subjected to strong earthquake ground motions. Yielding leads to stiffness and strength degradation, increased interstory drifts, and damage with permanent drifts, which render the structure non-functional.

Alternatively, the yielding can be emulated in a structural system by adding an adaptive “negative stiffness device” (NSD) and shifting the yielding away from the main structural system, leading to the new idea of “apparent weakening” that occurs to ensure structural stability at all displacement amplitudes. This is achieved through an adaptive negative stiffness system, a combination of NSD and a fluid damper. By engaging the NSD at an appropriate displacement (apparent yield displacement that is well below the actual yield displacement of the primary structural system), the composite structure-device assembly behaves like a yielding structure (while the primary structure remains mostly elastic). The concept and the NSD have been developed by the project team. The feasibility of this new concept has been experimentally verified at the University at Buffalo-NEES facility on different structures.

Structural weakening and the addition of damping is an approach previously proposed to reduce seismic forces and drifts in the retrofit of structures. It is also used in the design of new buildings with damping systems. While this approach is efficient, it does not significantly reduce and may even amplify inelastic excursions and permanent deformations of the structural system during a seismic event. A novel negative stiffness device (NSD) is developed in this project that can emulate weakening of the structural system without inelastic excursions and permanent deformations. The NSD produces yielding by engaging at a prescribed displacement and generating negative stiffness, thus reducing the stiffness of the combined primary structure and NSD system, and leading to a bilinear inelastic system.

The new transformative ideas of “Negative Stiffness Device” and “apparent weakening” have been demonstrated in this project by means of experimental and analytical study. The new concept results in significant damage and response reduction. The system can be used in new buildings as well as for retrofit situations. NSD is the first practical negative stiffness device implementable in large structures; such a device did not exist prior to this project. The NSD is adaptive but passive, and exhibits true negative stiffness behavior by possessing predesigned variations of stiffness as a function of structural displacement amplitude. The NSD properties can be easily adapted by changing the lever arm to ac-

commodate any change in the properties of the structure observed over time. It is likely to impact the state of practice of supplemental devices in earthquake protection. Extensive analytical modeling has also been developed and validated using the shake table test results. The nonlinear analytical models have been incorporated into 3D-BASIS, IDARC and Opensees computer programs, thus enabling technology transfer.

The concept of negative stiffness and apparent yielding/weakening has been experimentally verified in a three-story base-isolated structure and base isolated bridge with the NSD at the isolation level and also in a three-story fixed-base steel structure (moment frame) with the NSD in the first story. To accentuate the advantages of incorporating the NSD in structures, the responses of different systems including (1) base structure; (2) base structure with damper; (3) base structure with NSD; and (4) base structure with NSD and damper; are compared for a suite of ground motions. The behavior of all four systems are predicted analytically and the predicted results are in excellent agreement with the experiments. Shake table tests confirmed that by adding the NSD and damper, acceleration, base shear and deformations of the structure can be significantly reduced. In bilinear inelastic structures, the addition of the NSD and damper will prevent collapse as well as reduce its response during severe earthquakes.

This report contains the following: (a) a description of the development and operation of the NSD, (b) analytical and computational tools that describe the behavior of the device, (c) experimental results that represent proof-of-concept for weakening with the use of the Negative Stiffness Device, (d) validation of the developed analytical models by comparison of analytical and experimental results, and (e) reports of design imperfections and proposed improvements in the design of the device.

Project Management Committee

Satish Nagarajaiah, Principal Investigator, Rice University, Department of Civil and Environmental Engineering and Mechanical Engineering and Material Science, Houston, TX-77005; *Satish.Nagarajaiah@rice.edu*.

Andrei M. Reinhorn, Co-Principal Investigator, Department of Civil and Environmental Engineering, University at Buffalo, State University of New York, Buffalo, NY-14260; *reinhorn@buffalo.edu*.

Michael C. Constantinou, Co-Principal Investigator, Department of Civil and Environmental Engineering, University at Buffalo, State University of New York, Buffalo, NY-14260; *constan1@buffalo.edu*.

Michael Symans, Co-Principal Investigator, Department of Civil and Environmental Engineering, Rensselaer Polytechnic Institute, Troy, NY-12180; *symans@rpi.edu*.

Jian Zhang, Co-Principal Investigator, Department of Civil and Environmental Engineering, University of California, Los Angeles, CA- 90095; *zhangj@ucla.edu*.

Douglas P. Taylor, Co-Principal Investigator, Taylor Devices Inc., North Tonawanda, NY-14120; *taylordevi@aol.com*.

ABSTRACT

Seismic forces and displacements in existing structures can be effectively reduced in an approach where the structure is intentionally weakened (stiffness and strength are reduced) and damping is added. However, the approach also results in inelastic excursions and permanent deformation of the structural system during a seismic event. A new concept previously proposed by the authors simulates weakening by incorporating a mechanical system that produces true negative stiffness in the structural system. In doing so, inelastic excursions and permanent deformations may be substantially reduced or eliminated.

The Negative Stiffness Device (NSD) is a device that produces a force which is in the same direction as the imposed displacement thus the name “negative stiffness.” The NSD consists of (a) a highly compressed spring that produces the negative stiffness, (b) a magnification mechanism to magnify the negative stiffness, (c) a self-containment system so that the large forces needed for developing the negative stiffness are not resisted by the structure, and (d) a "gap spring assembly" (GSA) mechanism which delays the development of negative stiffness until the structural system undergoes a prescribed displacement. The prototype of the negative stiffness device was designed by researchers at the University at Buffalo (UB), Rice University and Taylor Devices Inc., built at Taylor Devices Inc., and was first tested on a shake table by researchers at UB and Rice University in a three story structural model isolated with elastomeric bearings.

This report contains the following: (a) a description of the development and operation of the NSD, (b) analytical and computational tools that describe the behavior of the device, (c) experimental results that represent proof-of-concept for weakening with the use of the Negative Stiffness Device, (d) validation of the developed analytical models by comparison of analytical and experimental results, and (e) reports of design imperfections and proposed improvements in the design of the device.

ACKNOWLEDGEMENTS

The work described in this report has been funded by the National Science Foundation through grant NSF-CMMI--NEESR-0830391 and by Taylor Devices, Inc. of North Tonawanda, NY. This support is greatly acknowledged.

The authors would like to thank David Lee, PhD, from Taylor Devices Western Technical Center, who provided the project with candidate linkage arrangements for the NSD, the Structural Engineering and Earthquake Simulation Laboratory (SEESL) staff at the University at Buffalo for their assistance in the assembly and testing of the structure, Mr. John Metzger of Taylor Devices, Inc. for detailing the NSD, Mr. Jonathan Rivera, an undergraduate student at UB, for helping with data management, Mr. Tathagatha Ray, a graduate student at the University at Buffalo, for his help in the experimental preparations and Professor Dhiman Basu of IIT-Gandhinagar, India, and former graduate student at the University at Buffalo, for conducting preliminary analysis of the NSD.

TABLE OF CONTENTS

Section	Title	Page
1	INTRODUCTION.....	1
2	DESCRIPTION AND OPERATION OF NEGATIVE STIFFNESS DEVICE	7
2.1	NSD Description and Operation	7
2.2	Gap Spring Assembly Description and Operation.....	11
3	BASIC FORCE-DISPLACEMENT RELATIONS OF NEGATIVE DEVICE.....	15
3.1	Introduction.....	15
3.2	Analysis of Negative Stiffness Device	15
3.3	Basic Force-Displacement Relations for Gap Spring Assembly	26
3.4	Modeling of Negative Stiffness Device in General Purpose Analysis Programs.....	29
3.5	Considerations in the Implementation of NSD in Structures.....	31
4	ADVANCED FORCE-DISPLACEMENT RELATIONS OF NEGATIVE STIFFNESS DEVICE.....	33
4.1	Introduction.....	33
4.2	NSD Relations Considering Large Deformation Effects.....	33
4.3	NSD Relations Considering Inertia Effects	39
4.4	NSD Relations Considering Friction	45
4.4.1	Hysteresis due to pin friction	45
4.4.2	Hysteresis in SAP2000 model of NSD	50
4.5	NSD Relations Considering Member Flexibility.....	55
4.6	Advanced Force-Displacement Relation of Gap Spring Assembly.....	60
4.7	Detailed Model of NSD in Program SAP2000	64
5	EXPERIMENTAL SETUP	67
5.1	Introduction.....	67
5.2	Specimen Description	67
5.3	Instrumentation	74
6	EXPERIMENTAL RESULTS.....	85
6.1	Introduction.....	85
6.2	Experiment Outline.....	85
6.3	Testing of Elastomeric Bearings.....	87
6.4	Testing of GSA	89

TABLE OF CONTENTS (CONT'D)

Section	Title	Page
6.5	Testing of Linear Viscous Dampers	92
6.6	Testing of NSD	94
6.7	Identification of Properties of Fixed Superstructure.....	106
6.8	Shake Table Testing Results.....	109
7	ANALYTICAL PREDICTION OF RESPONSE	141
7.1	Introduction.....	141
7.2	Modeling of Superstructure in Program SAP2000	141
7.3	Modeling of Elastomeric Bearings	144
7.4	Modeling of Viscous Dampers	147
7.5	Modeling of GSA.....	148
7.6	Modeling of NSD.....	150
7.7	Implementation of NSD Model in Program SAP2000	155
7.8	Comparison of Experimental and Analytical Results.....	159
8	REPORT SUMMARY.....	177
9	CONCLUSIONS	181
10	REFERENCES.....	185
 Appendices		
A	EXPERIMENTAL RESULTS.....	217
B	INSTRUMENTATION VERIFICATION	393
C	COMPARISON OF ANALYTICAL AND EXPERIMENTAL RESULTS.....	403

LIST OF FIGURES

Figure	Title	Page
1-1	True negative stiffness concept (Pasala et al., 2012)	2
1-2	View of 3-story structure with NSD	4
2-1	View of Negative Stiffness Device as installed on the 3-story isolated structure	7
2-2	Gap Spring Assembly Mechanism.....	8
2-3	Terminology used for the elements of the Negative Stiffness Device.....	8
2-4	NSD at its deformed configuration	9
2-5	Qualitative force-displacement relations of NSD	10
2-6	Detailed view of Gap Spring Assembly.....	11
2-7	Photograph of un-deformed GSA installed at the NSD.....	12
2-8	Views of NSD and idealized force-displacement relations with and without the gap spring assembly	13
3-1	Forces acting on pivot plate	16
3-2	Free body diagram of bottom chevron.....	16
3-3	Force-displacement relations of GSA and of NSD with and without the GSA for the properties of Table 3-1	20
3-4	Effective stiffness as function of displacement for GSA and NSD with and without the GSA for the properties of Table 3-1	21
3-5	Instantaneous stiffness as function of displacement for GSA and for NSD with and without the GSA for the properties of Table 3-1	22
3-6	Effect of the double hinged column axial load on the NSD force-displacement relation without the GSA and for the properties of Table 3-1	22
3-7	Simple negative stiffness device without magnification	23
3-8	Comparison of normalized force-displacement relations of NSD and negative stiffness magnification factor.....	24
3-9	Adjustable lever arm connection used for negative stiffness magnification	25
3-10	Force-displacement relations of NSD without GSA for various values of length l_2	25
3-11	Free body diagrams of housing plates of gap spring assembly at three deformed stages.....	26
3-12	Force-displacement loops that can be produced using the nonlinear elastic element in program SAP2000	29
3-13	SAP2000 NSD element with and without GSA	30
3-14	Comparison of results of program SAP2000 to analytical results for NSD with properties of Table 3-1	31
3-15	Plan view of a structure with positive and negative stiffness elements	32

LIST OF FIGURES (Cont'd)

Figure	Title	Page
4-1	Deformed NSD when considering large deformation effects.....	34
4-2	Free body diagram of pivot plate.....	34
4-3	Free body diagram of bottom chevron.....	34
4-4	Comparisons of NSD force without the GSA predicted without due (small rotations) and with due (large rotations) consideration of large deformation effects for the device with properties of Table 3-1.....	37
4-5	Force-displacement relations of NSD without GSA for varied lever length and for very large column height.....	38
4-6	Force-displacement relations of NSD without GSA for varied column height and for very large lever length.....	38
4-7	Modeling of NSD for dynamic effects.....	39
4-8	Force-displacement relations of NSD without GSA with due and without due consideration of inertia effects.....	42
4-9	Comparison of force histories of NSD without GSA with due and without due consideration of inertia effects.....	43
4-10	Comparison of force-displacement relations and force histories of NSD without GSA with due and without due consideration of inertia effects for random motion measured in shake table test.....	43
4-11	Comparison of contributions of acceleration ($M_a \ddot{u}$) and velocity ($M_v \dot{u}^2$) terms in NSD force.....	44
4-12	Comparison of exact and approximate expressions for NSD force-displacement relation for case of motion with 4Hz frequency.....	44
4-13	Pin friction model.....	45
4-14	Free body diagrams (bodies in bold) used for deriving NSD force-displacement relations with effects of joint friction.....	46
4-15	Force-displacement loops of NSD without GSA with properties of Table 3-1 and various values of pin friction coefficient.....	50
4-16	Comparison of force-displacement loops of NSD without GSA produced by analytical model and by SAP2000 constant friction model.....	51
4-17	SAP2000 model of NSD capable of generating complex hysteresis.....	53
4-18	Experimental force-displacement relation of NSD without GSA and quantities for model calibration.....	54
4-19	Comparison of force displacement loops of NSD without GSA produced by the analytical model with hysteresis and the SAP2000 force-proportional hysteresis model.....	55
4-20	Model of NSD with top and bottom chevron flexibility.....	56

LIST OF FIGURES (Cont'd)

Figure	Title	Page
4-21	Force-displacement relations of NSD without GSA for rigid top and for flexible bottom chevron	59
4-22	Force-displacement relations of NSD with GSA for flexible top and for rigid bottom chevron	59
4-23	Free body diagrams of housing plates 1 and 2 and rod of GSA	61
4-24	Force-displacement relation of modified GSA	64
4-25	Detailed model of NSD in program SAP2000	65
4-26	Comparison of force-displacement relations of the NSD without GSA produced by the analytical model with due consideration of large rotation effects and by the detailed model in SAP2000	66
5-1	East view of model structure with NSD on shake table.....	68
5-2	North-West view of model structure with NSD on shake table.....	68
5-3	Schematics of 3-story base-isolated structure used in testing.....	69
5-4	Views of viscous dampers and elastomeric bearings in isolation system.....	70
5-5	Viscous damper assembly.....	70
5-6	Angle used to connect the bottom of the NSD to the shake table.....	70
5-7	Schematic of connection of bottom of NSD to shake table	71
5-8	Schematic of connection of NSD to superstructure	72
5-9	Photographs of NSD connection to superstructure	72
5-10	View of transverse cables used for torsional stability in tests of NSD without the GSA.....	73
5-11	Connectors of model base-mat to reaction frame	73
5-12	Reaction frame and connector view.....	74
5-13	List of potentiometers for superstructure and shake table	75
5-14	List of accelerometers for superstructure and shake table	75
5-15	Five-component load cell channels.....	76
5-16	View of load cells below elastomeric bearings.....	76
5-17	LED installed at four points of the East NSD.....	76
5-18	Complete LED instrumentation of NSD on East side	77
5-19	String pot, accelerometer and load cell instrumentation of NSD East	78
5-20	String pot, accelerometer and load cell instrumentation of NSD West	78
5-21	Views of accelerometer and string pot installed on NSD.....	78
5-22	Damper instrumentation.....	79
5-23	Comparison of base shear-base displacement loops obtained from processing of acceleration records (force F_{acc}) and directly measured by load cells (force F_{ld}) in structure on elastomeric bearings.....	80

LIST OF FIGURES (Cont'd)

Figure	Title	Page
5-24	Load cell calibration fixture.....	81
5-25	Comparison of viscous damper horizontal force obtained from processing of acceleration records and isolator load cells ($F_{acc}-F_{ld}$) and from damper load cells (F_{vd}).....	81
5-26	Comparison of NSD force-displacement loops (two devices) obtained from NSD load cells (F_{nsd}) and from records of base shear (acceleration-based) and isolator load cells ($F_{acc}-F_{ld}$).....	83
5-27	Comparison of measured NSD East to NSD West force-displacement loops.....	83
5-28	Comparison of NSD East (left) and West (right) force-displacement relations based on measurement by the NSD load cells and predicted by analysis for the nominal NSD properties of Table 3-1.....	84
5-29	Comparison of experimental and analytical total NSD force-displacement relations.....	84
6-1	Section of elastomeric bearing (Wolff and Constantinou, 2004)	87
6-2	Schematic of single bearing testing machine (Kasalanati et al, 1999)	87
6-3	Recorded force-displacement loops of elastomeric bearings at shear strain of 145%, compressive load of 50kN and frequency of 0.01Hz	88
6-4	Recorded force-displacement loops of elastomeric bearings at shear strain of 145%, compressive load of 50kN and frequency of 1Hz	88
6-5	Testing arrangement for GSA.....	89
6-6	Experimental force-displacement relations of GSA	90
6-7	Schematic of revised GSA	91
6-8	Deformed GSA of West NSD in displacement-controlled test at 2.5in amplitude and 0.02Hz frequency (observe uneven coil movement).....	92
6-9	Wear on housing plate due to friction between housing plate and spring	92
6-10	Experimental results for dampers obtained in displacement-controlled tests at frequency of 0.5Hz.....	94
6-11	Deformed NSD West (left) and NSD East (right) during displacement-controlled test at 6.4cm amplitude and 0.02Hz frequency.....	95
6-12	Displacement histories of points on NSD for configuration ENB (without GSA) in test at 0.02 Hz frequency.....	96
6-13	Displacement histories of points on NSD for configuration ENA (with GSA) in test at 0.02 Hz frequency.....	97
6-14	Displacement histories of points on NSD for configuration ENB-LA (with GSA) in test at 0.02 Hz frequency.....	98

LIST OF FIGURES (Cont'd)

Figure	Title	Page
6-15	Displacement histories of points on NSD for configuration ENB (with GSA) in test at 1 Hz frequency.....	99
6-16	Displacement histories of points on NSD for configuration ENA (with GSA) in test at 1 Hz frequency.....	100
6-17	Displacement histories of points on NSD for configuration ENB-LA (with GSA) in test at 1 Hz frequency.....	101
6-18	Displacement histories of additional points on NSD for configuration ENA (with GSA) in test at 1 Hz frequency.....	102
6-19	Force-displacement relations of NSD obtained in displacement-controlled test at 0.02Hz frequency for configurations ENB and ENB-LA (without GSA) and ENA (with GSA).....	104
6-20	Force-displacement relations of isolation system (bearings-LD and NSD) obtained in displacement-controlled test at 0.02Hz frequency for configurations ENB and ENB-LA (without GSA) and ENA (with GSA).....	105
6-21	Effect of frequency on NSD East force-displacement relation.....	106
6-22	Amplitude of transfer functions (T.F.) of superstructure obtained in low amplitude white noise testing.....	107
6-23	Amplitude of transfer functions of superstructure obtained in low amplitude seismic testing with motion ATL 270.....	108
6-24	Target and table motion 5%-damped acceleration response spectra.....	112
6-25	Base shear divided by weight and NSD force versus base displacement loops recorded for motion PS10317 and configurations without dampers.....	116
6-26	Base shear divided by weight, NSD force and viscous damper force versus base displacement loops recorded for motion PS10317 and configurations with dampers.....	117
6-27	Base displacement histories recorded for motion PS10317 and configurations without dampers.....	118
6-28	Base displacement histories recorded for motion PS10317 and configurations with dampers.....	119
6-29	2 nd story drift ratio recorded for motion PS10317 and configurations without dampers.....	120
6-30	2 nd story drift ratio recorded for motion PS10317 and configurations with dampers.....	121
6-31	3 rd floor acceleration histories recorded for motion PS10317 and configurations without dampers.....	122
6-32	3 rd floor acceleration histories recorded for motion PS10317 and configurations with dampers.....	123

LIST OF FIGURES (Cont'd)

Figure	Title	Page
6-33	Axial load histories (for pair of load cells) for ground motion PS10317 for systems without dampers	124
6-34	Axial load histories (for pair of load cells) for ground motion PS10317 for systems with dampers	125
6-35	Base 5%-damped acceleration response spectra	126
6-36	First floor 5%-damped acceleration response spectra	128
6-37	Second floor 5%-damped acceleration response spectra	130
6-38	Third floor 5%-damped acceleration response spectra	132
6-39	Comparison of recorded peak inter-story drift ratio for all configurations and tests (left column is for systems without dampers; right column is for systems with dampers).....	137
6-40	Comparison of recorded peak floor acceleration for all configurations and tests (left column is for systems without dampers; right column is for systems with dampers).....	138
6-41	Comparison of recorded peak base displacement and base shear force for all configurations and tests (left column is for systems without dampers; right column is for systems with dampers).....	139
7-1	Comparison of analytical and experimental results for inner-story drift of fixed structure obtained for ground motion ATL-270	142
7-2	Comparison of analytical and experimental results for floor acceleration of fixed structure obtained for ground motion ATL-270	143
7-3	Comparison of analytical and experimental results for 5%-damped floor acceleration spectra of fixed structure obtained for ground motion ATL-270	144
7-4	Force-displacement relations of five parallel elements representing an elastomeric bearing.....	145
7-5	Analytical force-displacement loop of and elastomeric bearings obtained by the combination of the five parallel elements of Figure 7-4.....	145
7-6	Comparison of analytical and experimental force-displacement loops of elastomeric isolation system	146
7-7	Comparison of analytical and experimental damper force-displacement loops	147
7-8	Comparison of experimental and analytically predicted (program SAP2000) damper longitudinal component of damper force versus base displacement in test of configuration ED and ground motion PS10317	148
7-9	Comparison of analytical and experimental force-displacement relations of individual GSA	149

LIST OF FIGURES (Cont'd)

Figure	Title	Page
7-10	Comparison of GSA analytical results using the basic equation of Section 3.2 (Equation (3-13) and the detailed equations of Section 4.6 for modeling GSA abnormal behavior	150
7-11	Comparison of experimental and basic analytical force-displacement relations of NSD in test with configuration ENB (without GSA)	151
7-12	Comparison of experimental and analytical force-displacement relations with inertia effects of NSD in test with configuration ENB (without GSA)	152
7-13	Comparison of experimental and analytical force-displacement relations with flexibility effects of NSD in test with configuration ENB (without GSA).....	152
7-14	Comparison of experimental and analytical force-displacement loops with pin friction effects of NSD in test with configuration ENB (without GSA).....	153
7-15	Comparison of experimental and analytical force-displacement loops of NSD with GSA in configuration ENA in test with motion PS10317	153
7-16	Comparison of experimental and analytical force-displacement loops of NSD with GSA in configuration ENA in test with motion 0637-270	154
7-17	Shimming of GSA resulting in modified gap opening	155
7-18	Comparison of experimental and response history analysis (program SAP2000) results for NSD force-displacement loops for configuration ENA in test with motion 0637-270.....	156
7-19	NSD with initial curvature of the pre-compressed spring	157
7-20	NSD force-displacement relation with initial spring curvature	158
7-21	Comparison of experimental and analytical (program SAP2000 with initial curvature of spring) force-displacement loops of NSD without GSA for configurations ENB and ENB-LA and motion PS10317	158
7-22	Comparison of experimental and analytical results for configuration E and ground motion PS-10317	160
7-23	Comparison of experimental and analytical results for configuration ENA and ground motion PS-10317	162
7-24	Comparison of experimental and analytical results for configuration ENB and ground motion PS-10317	164
7-25	Comparison of experimental and analytical results for configuration ENB-LA and ground motion PS-10317	166
7-26	Comparison of experimental and analytical results for configuration ED and ground motion PS-10317	168
7-27	Comparison of experimental and analytical results for configuration EDNA and ground motion PS-10317	170

LIST OF FIGURES (Cont'd)

Figure	Title	Page
7-28	Comparison of experimental and analytical results for configuration EDNB and ground motion PS-10317	172
7-29	Comparison of experimental and analytical results for configuration EDNB-LA and ground motion PS-10317	174

LIST OF TABLES

Table	Title	Page
3-1	Nominal NSD properties used in the experimental study.....	20
3-2	SAP2000 NSD element parameters	30
4-1	Masses and mass moment of inertia of elements of NSD with properties of Table 3-1	42
4-2	Description of elements of SAP2000 model of NSD with complex hysteresis.....	54
6-1	Notation and tested configurations	85
6-2	Earthquake motions used for shake table testing.....	86
6-3	Earthquake motions and tested configurations	86
6-4	Mode shape, period and damping ratio for three modes of vibration of superstructure obtained in low amplitude white noise testing.....	107
6-5	Mode shape, period and damping ratio for three modes of vibration of superstructure obtained in low amplitude seismic testing with motion ATL 270	108
6-6	Stiffness and damping matrices of superstructure constructed from modal data in identification tests	108
6-7	Peak recorded inter-story drift ratio	134
6-8	Peak recorded floor acceleration.....	135
6-9	Peak recorded base displacement and base shear force	136
7-1	Modal characteristics of analytical model in SAP2000	142
7-2	Properties of five elements representing each elastomeric bearing	146
7-3	Properties of individual GSA.....	148
7-4	Properties used in modeling GSA per theory of Section 4.6	155

ABBREVIATIONS

NSD: Negative Stiffness Device

GSA: Gap spring assembly mechanism

VD: Linear viscous dampers

LD: Low damping elastomeric bearings

SECTION 1

INTRODUCTION

Current practice for designing structures against seismic actions relies on reduced design strength with ductile behavior and allows the development of significant inelastic deformations in strong earthquakes so that reduction of inertia forces is achieved. At best, this approach ensures life safety in the design earthquake event and collapse prevention in the maximum earthquake event. Large drifts, permanent deformations and loss of functionality of the structure are common observations of performance after strong seismic events. Reinhorn et al. (2005) and Viti et al. (2006) introduced the concept of weakening (reducing further the strength and implicitly stiffness) and introduction of supplemental viscous damping to simultaneously reduce structural accelerations and inter-story drifts in the retrofit of structures.

Moreover, the approach described in ASCE 7, Chapter 18 (American, 2010) for the design of structures with damping systems is based on the concept of reduced strength and stiffness and addition of damping to achieve the same objective for new construction (Ramirez et al., 2001). Specifically, new buildings designed with viscous damping systems per minimum criteria of the ASCE 7 Standard, Chapter 18 have strength and stiffness approximately half of that of a comparable building without the damping system that also meets the drift criteria (Ramirez et al., 2001). However, the approach does not reduce inelastic action or improves the performance of the structural system unless enhanced viscous damping is used to achieve a higher performance level (Ramirez et al., 2001; Pavlou et al., 2006).

An alternative approach is to “simulate yielding” by introducing true negative stiffness at prescribed displacements leading to the concept of “apparent weakening” (Nagarajaiah et al., 2010 and Pasala et al., 2012). A true negative stiffness system develops forces that assist motion, not oppose it as it is in the case of a positive stiffness system.

The development, construction, modeling and testing of a large scale, practical and passive device that generates true negative stiffness (termed Negative Stiffness Device or NSD) is presented in this report. Earlier attempts to achieve “weakening” included active or semiactive hydraulic devices that effectively simulated the behavior of negative stiffness devices (Iemura et al., 2009). The NSD described in this report is capable of generating true negative stiffness and it does not need external power, sensors and controllers to generate the desired forces.

In order to visualize the effect of adding true negative stiffness to a structure where viscous dampers and negative stiffness devices have been added, consider the force-displacement relations shown in Figure 1-1(a) (the dashed line is the force-displacement relation for the structure, the dotted line is the force-displacement relation for the viscous damper and the solid line is the force-displacement relation for the negative stiffness device). By adding the NSD to the structure, as schematically shown in Figure 1-1(b), the assembly stiffness reduces from the

value K_e to $K_a = K_e - K_n$ for displacements beyond the limit u'_y . If, F_2 and u_2 are the maximum restoring force and maximum displacement of a perfectly-linear system (dashed line in Figure 1-1(b)) then for the same excitation, the maximum restoring force and the maximum displacement of the assembly of the structure and NSD are F_3 and u_3 , respectively. Stiffness K_n is selected to achieve the desired reduction in base shear. Although a reduction in base shear is achieved, the maximum deformation of the system may increase when compared to the system without the NSD. Reduction of displacements to acceptable levels is achieved by adding passive damping devices in parallel to the NSD, as schematically shown in Figure 1-1(c). To demonstrate the concept, a linear viscous damper is used. The maximum displacement is reduced, resulting in $u'_3 < u_2$.

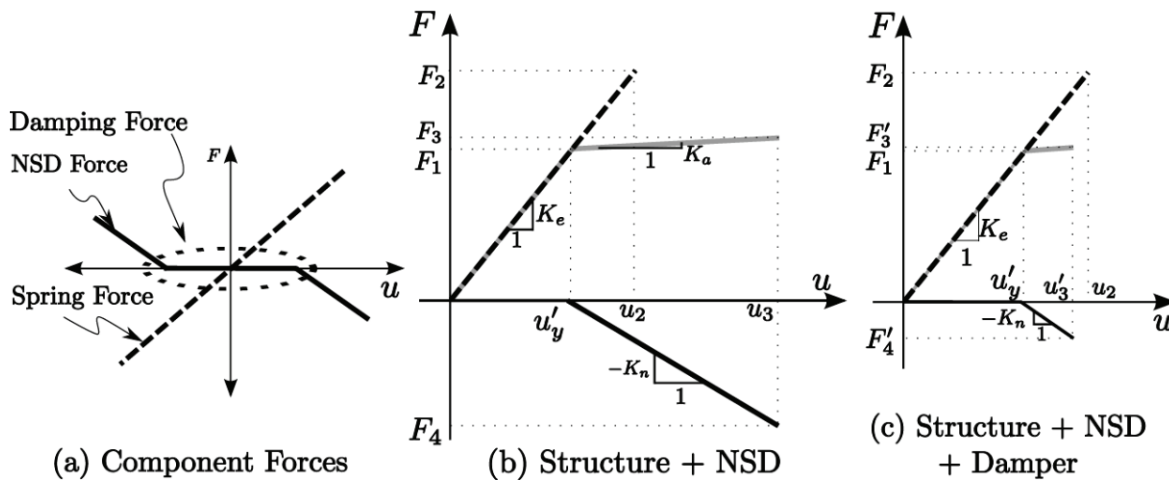


Figure 1-1: True negative stiffness concept (Pasala et al., 2012)

The concept of negative stiffness was first introduced in the pioneering publication of Molyneux (1957) in several proposals for vibration isolation systems. This original idea recently became reality in the development of highly effective vibration isolation systems (e.g., see US patent 6676101BB2; Platus, 2004). Thus far the application of negative stiffness devices has been limited to vibration isolation of small, highly sensitive equipment and of seats in automobiles (Lee et al., 2007). The reason that this technology has been restricted to small mass applications is due to the requirement for large forces in preloaded springs in order to develop the necessary negative stiffness. These preload forces are typically of the order of the weight of the isolated structure. The application of negative-stiffness concept to massive structures, like buildings and bridges, requires modification of the existing mechanisms to reduce the demand for preload force and to “package” the negative stiffness device in a system that does not impose any additional loads on the structure, other than those needed for achieving the goal of seismic protection. These requirements led to the development of a true negative system device with the following components and characteristics:

- 1) A highly compressed machined spring (CS) that develops a force in the direction of motion (thus, negative stiffness). The magnitude of the force reduces with increasing displacement so that stability of the system is ensured at large displacements.
- 2) A double chevron self-containing system to resist the preload in the compressed spring and also to prevent the transfer of the vertical component of the preload to the structure.
- 3) A double negative stiffness magnification mechanism that substantially reduces the requirement for preload so that a practical system is achieved.
- 4) A system (called *Gap Spring Assembly* or GSA) that provides positive stiffness up to a predefined displacement such that the combined effective stiffness of NSD and GSA is almost zero until a predefined displacement is reached. The GSA is essential to simulate a bi-linear elastic behavior with an apparent-yield displacement which is smaller than the actual yield displacement of the structure.
- 5) Viscous damping devices in parallel to the negative stiffness device in order to reduce displacement demands to within acceptable limits.

Note that other negative stiffness concepts have also been developed and tested for structures, but they lack the important characteristics that can be achieved using the NSD described above. One example is the pseudo-negative stiffness system mentioned earlier (Iemura et al., 2009) which makes use of active or semiactive hydraulic devices to develop the negative stiffness. Another example is the one described by Iemura et al. (2008) in which a structure is placed on top of convex pendulum bearings. Negative stiffness is generated by the structural weight loads applied on the convex surface (as opposed to the behavior of Friction Pendulum bearings that utilize concave surfaces-see Fenz et al., 2008a,b-and in similarity to the behavior of the uplift-restraining Friction Pendulum bearing-see Roussis et al., 2006) while elastomeric bearings are placed in parallel to provide positive stiffness. The combined system has low effective stiffness that emulates the behavior of single Friction Pendulum bearings. Additionally the convex bearings represent an unstable system which constantly generates negative stiffness for all displacement amplitudes-an undesirable feature.

This report describes the Negative Stiffness Device and its components, presents analytical and computational models of its behavior and presents component and shake table experimental results that validate the analytical and computational models.

The experimental study presented in this report is the first of a series of experiments that demonstrate the utility of negative stiffness in various structural applications. This study focuses on the application to a seismically isolated building. Future studies will include applications to non-isolated yielding structures and to bridges. The isolated structure of the current study is the three-story structure supported by low damping elastomeric bearings shown in Figure 1-2. It is a modification of the six-story structure which was extensively used in the past at the University at Buffalo (Reinhorn et al., 1989; Mokha et al., 1990; Wolff and Constantinou, 2004; Fenz and

Constantinou, 2008b). Two negative stiffness devices and two linear viscous dampers were installed between the shake table and the base of the isolated model.

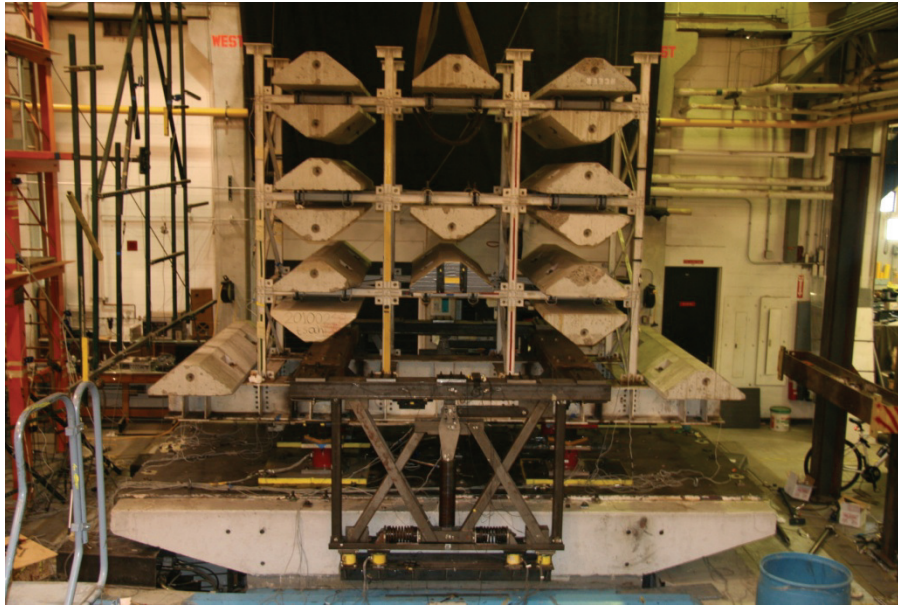


Figure 1-2: View of 3-story structure with NSD

The structure was tested in shake table tests in a total of 8 different configurations. Two benchmark systems were considered: a) the structure isolated with elastomeric bearings, without NSD and without dampers (undamped benchmark system) and b) the structure similar to a) but for the addition of dampers (damped benchmark system). When the shake table testing results from the two benchmark systems are compared (damped and undamped), the damped case showed reductions by an average (for all ground motions tested) of 15% for base shear, 10% for inter-story drifts and 36% for base displacements however peak floor accelerations were increased by 6%. The NSD was added in each of the two benchmark systems using three different configurations. When the results from the NSD configuration that showed the largest response reduction (without dampers) is compared to the undamped benchmark system, reductions by an average (for all ground motions tested) of 52% for base shear, 41% for inter-story drifts, 35% for peak floor accelerations and 2% increase for base displacements were observed. When the NSD configuration that showed the largest response reduction was added to the damped benchmark system and results are compared to the results of the damped benchmark system, the NSD reduced the response by an average of 43% for the base shear, 26% for drifts, 3% for base displacement and 31% for peak floor accelerations. When the results of the same configuration are compared to the results of the undamped benchmark system, reductions by an average of (for all ground motions tested) 54% for the base shear, 36% for the inter-story drifts, 27% for base displacements and 39% for peak floor accelerations were observed.

This report contains:

- In Section 2, a qualitative description of operation of the NSD is presented.
- In Section 3, analytical and computational models of the behavior of the NSD are presented. Also this section includes an analytical study that demonstrates the advantages of the NSD over other simpler systems.
- In Section 4, a study is presented that identifies sources of potential sensitivities and deviations from ideal behavior of the NSD. It is shown that these deviations typically have negligible effects. In the unlikely case that these sensitivities become important, modeling techniques are presented to include them in the NSD analysis.
- In Section 5, a description of an experimental program is presented. The experimental program includes displacement-controlled tests of individual NSD and shake table tests of a model structure equipped with NSD.
- In Section 6, the results of experiments on individual NSD are presented. Also in Section 6, the results of shake table experiments of the model structure with or without NSD, with or without viscous dampers and for different NSD configurations are presented.
- In Section 7, results of selected shake table experiments are compared to analytical predictions in order to establish the validity and accuracy of the analytical prediction.

SECTION 2

DESCRIPTION AND OPERATION OF NEGATIVE STIFFNESS DEVICE

2.1 NSD Description and Operation

The Negative Stiffness Device (NSD) is shown in the photograph of Figure 2-1 and schematically in Figure 2-3 (in un-deformed shape) and Figure 2-4 (in deformed shape). The negative stiffness device is a device that produces a force which is in the same direction as the imposed displacement thus the name “negative stiffness”. The device itself is inherently unstable. It can be installed in an isolated structure between the ground and the isolation level or in between the floors of any fixed and/ or isolated structure. Its effect is to reduce the total force at its installation level. In effect this is equivalent to reduction of stiffness and strength, which results in reduction of acceleration and inertia forces.

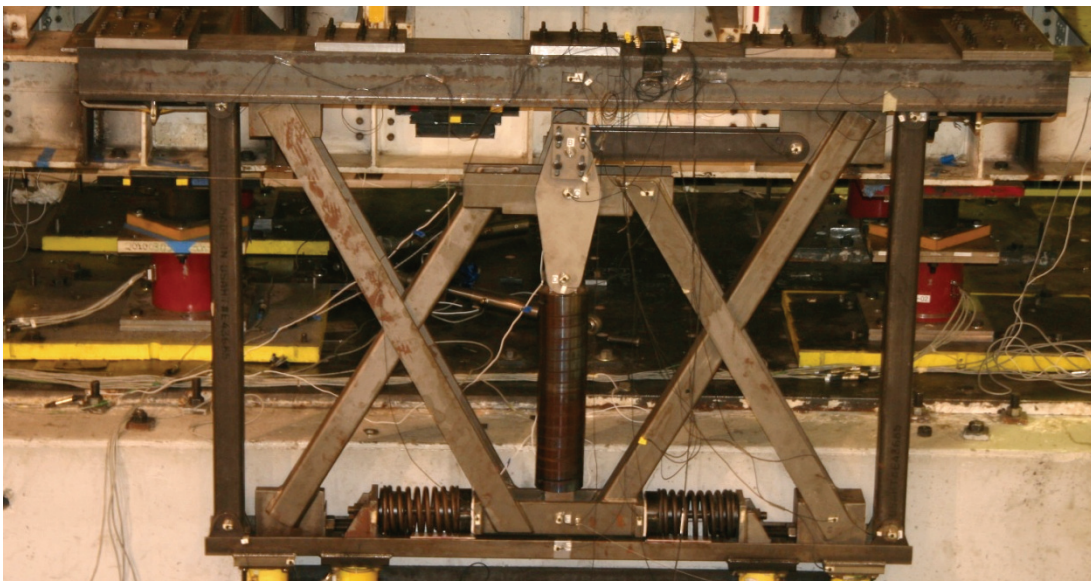


Figure 2-1: View of Negative Stiffness Device as installed on the 3-story isolated structure

In order to ensure a considerable amount of positive stiffness for small displacements and satisfy serviceability requirements (e.g., wind loading), a, so called, Gap Spring Assembly mechanism (GSA) is included in the NSD. The GSA is an assembly of springs (shown at the bottom of the NSD in Figure 2-1 and in a close view in Figure 2-2) that add stiffness to the negative stiffness device for displacements between zero and a predetermined limit. The GSA exhibits a bilinear elastic behavior. In doing so, the combined system has zero or small negative or positive stiffness for displacements less than the predetermined limit. For larger displacements, the system has the negative stiffness of the NSD. The NSD (see Figure 2-3) is composed of a pre-compressed spring shown in the center of the device, the GSA at the bottom, the pivot plate, the

lever, the top and bottom chevron braces and the two double hinged columns. When the device deforms as shown in Figure 2-4, the pre-compressed spring rotates and exerts a force in the direction of the displacement (introducing negative stiffness or “apparent weakened strength”). For small values of displacement, the GSA counteracts the NSD function so that the device provides zero or some small negative or positive stiffness until a predetermined value of displacement. The force in the pre-compressed spring reduces as displacement increases so that the negative stiffness value reduces with increasing displacement. At some large value of displacement, the NSD provides positive stiffness (stiffening) which is a desirable feature for limiting displacement demands in large earthquakes.

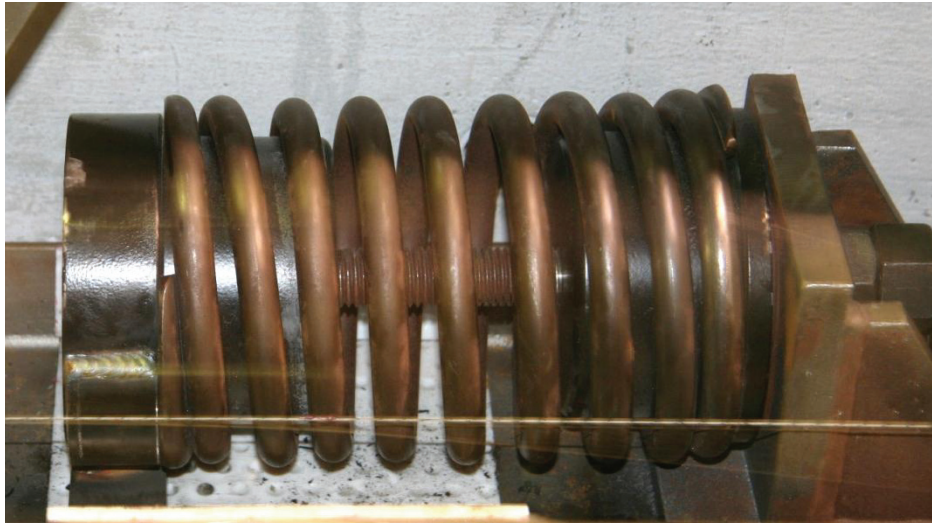


Figure 2-2: Gap Spring Assembly Mechanism

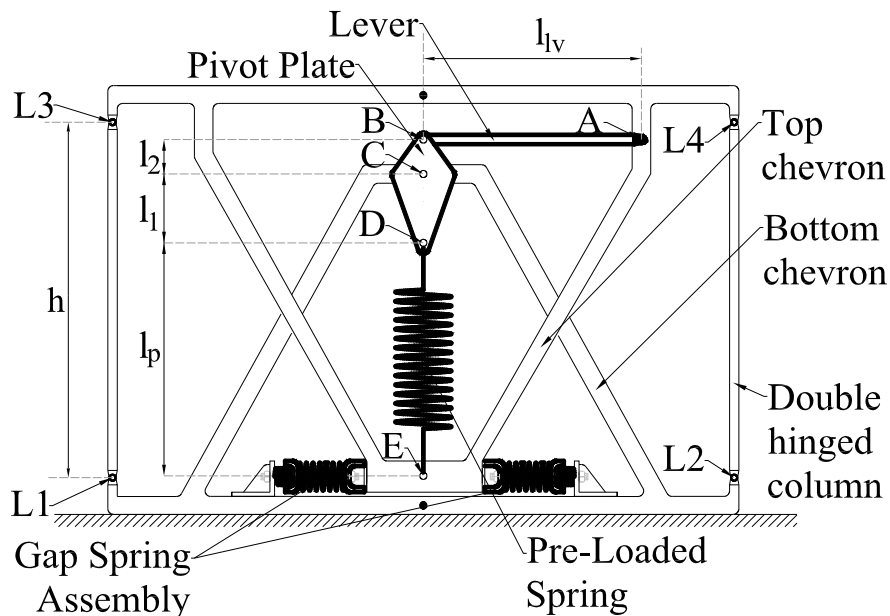


Figure 2-3: Terminology used for the elements of the Negative Stiffness Device

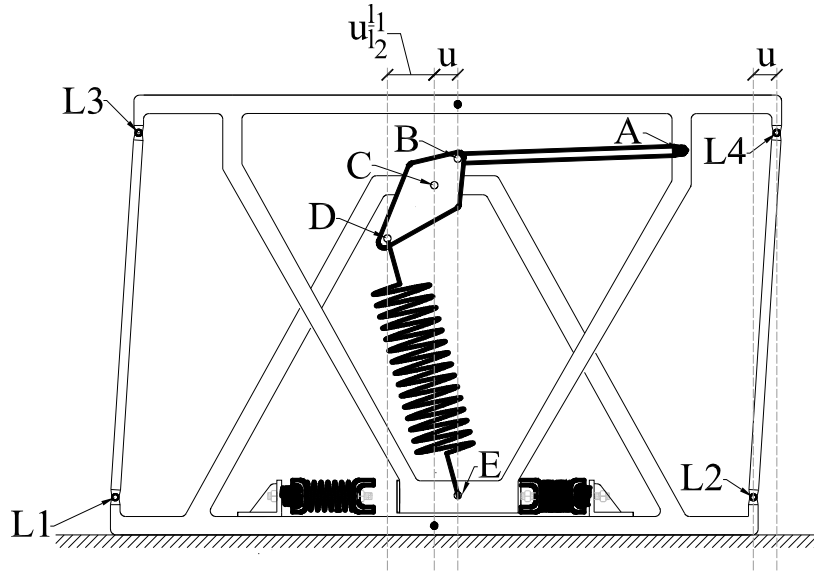
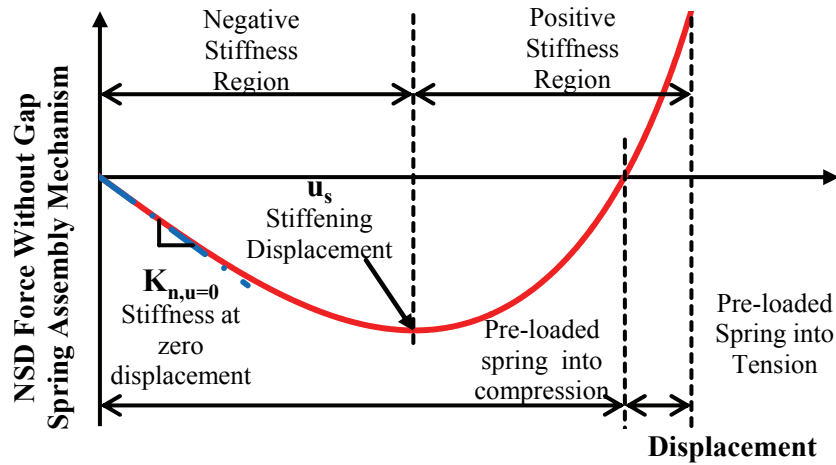


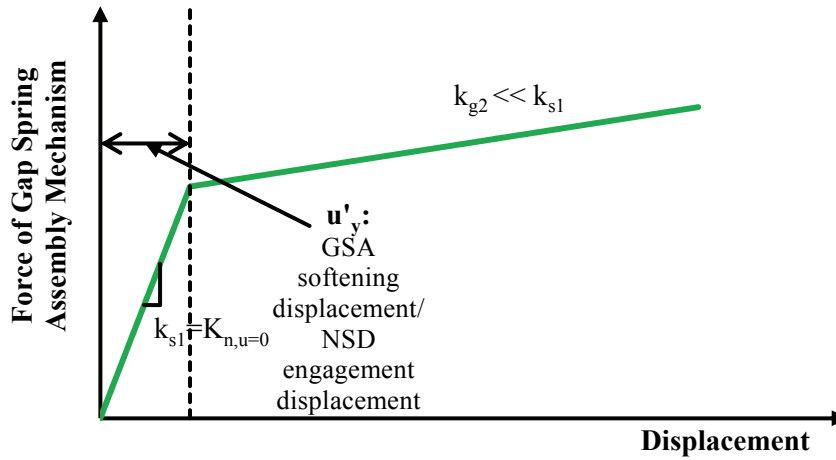
Figure 2-4: NSD at its deformed configuration

The NSD behavior is determined by the motion of the pivot plate and pre-loaded spring (thus, the motion of points A, B, C, D, E) and by the spring properties of initial length DE , pre-load P_{in} and stiffness K_s . Consider the motion of the top of the NSD by displacement u towards the right as shown in Figure 2-4. The lever imposes a displacement on the top of the pivot plate (point B) making the pivot plate to rotate about point C. Due to the axial rigidity of the lever and its negligible rigid body rotation, the imposed displacement and the displacement of Point B are essentially equal. Since the pivot plate rotates about C, point D moves in the opposite direction from the imposed displacement. It should be noted that the bottom pin of the pre-compressed spring (point E) is rigidly connected to the top of the device via the top chevron brace and therefore has a displacement equal to the one imposed on the top. The kinematics of the spring's top and bottom pins cause the pre-compressed spring to rotate. Since the spring is pre-compressed and rotated in the direction opposite to the imposed displacement, it facilitates the motion rather than opposing it. This gives rise to negative stiffness.

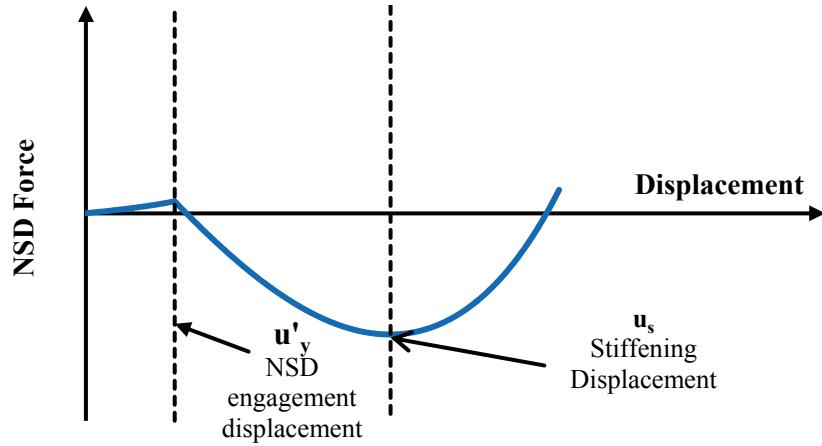
It can be seen from Figure 2-4 that the spring exhibits its minimum length when the device is undeformed. As the device deforms, the spring extends so that its force reduces. Moreover, as the device deforms, due to the increase of the spring inclination angle, the horizontal component of the force generated by the device reduces. The combination of these two events leads to a gradual reduction of the negative stiffness generated by the device which eventually leads to positive stiffness. This occurs at larger displacements and it is termed stiffening throughout this report. The behavior of the device without and with the GSA is qualitatively depicted in the graphs of Figure 2-5.



(a) NSD force displacement relation (without GSA)



(b) GSA force displacement relation



(c) Combined force displacement relation of NSD with GSA

Figure 2-5: Qualitative force-displacement relations of NSD

The NSD without the GSA force-displacement relation is elastic nonlinear and it is characterized by the initial negative stiffness, the maximum force and the stiffening displacement limit shown in Figure 2-5(a). The negative stiffness generated at zero displacement is the maximum stiffness that can be generated by the NSD. The stiffening displacement is the displacement at which the stiffness becomes zero and thereafter the stiffness is positive. At some large displacement, the NSD output force becomes zero and tension initiates in the spring of the NSD.

Point E has the same displacement as the one imposed on the device so that the GSA deforms by the same amount and exerts a force on the NSD that depends on the displacement imposed. The GSA has a bilinear elastic force-displacement relation as shown in Figure 2-5(b).

Figure 2-5(c) shows the NSD plus GSA force-displacement relation. For displacements less than u'_y the NSD is essentially inactive.

2.2 Gap Spring Assembly Description and Operation

A schematic of the GSA is shown in Figure 2-6 and a photograph is shown in Figure 2-7.

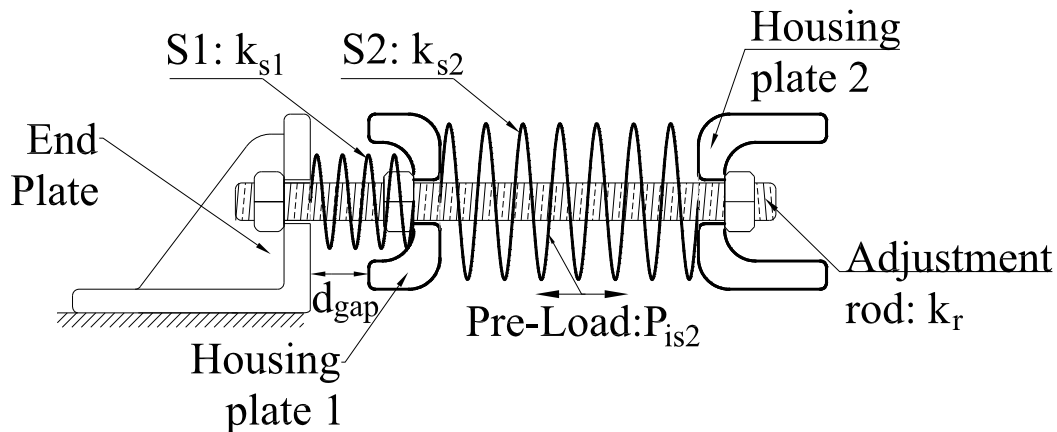


Figure 2-6: Detailed view of Gap Spring Assembly

Two GSA are located at the bottom of the NSD, each operating in compression. A GSA is connected on one side to the bottom of the NSD (through the end plate as shown in Figure 2-6). The other side of the GSA bears against the head of the top chevron brace of the NSD (point E in Figure 2-3) so that it can only transfer compressive forces. Accordingly, each of the two GSA devices operates in one direction but together they provide forces in both directions.

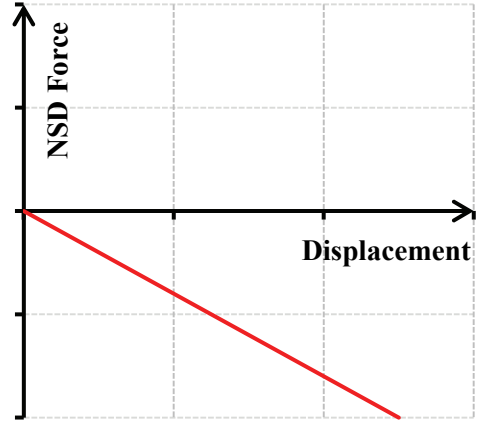
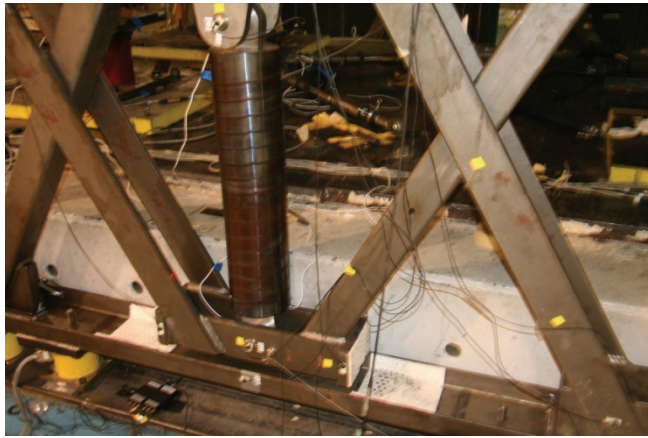


Figure 2-7: Photograph of un-deformed GSA installed at the NSD

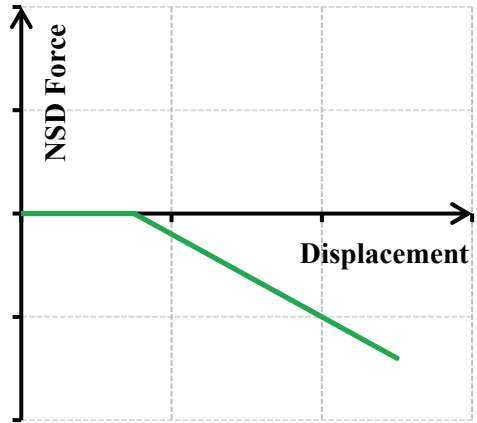
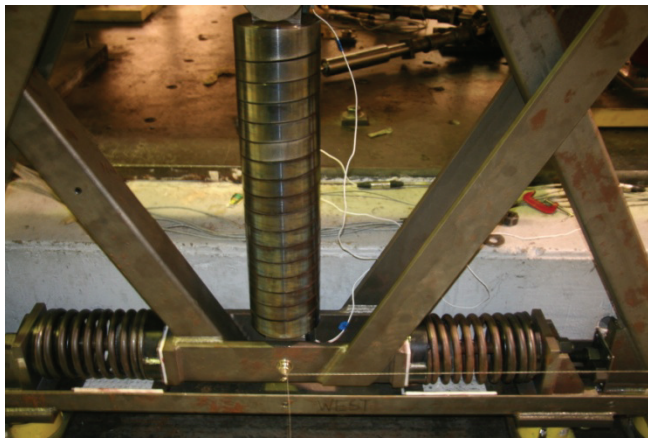
The GSA is comprised of two springs, two spring housing plates, the end plate and an adjustment rod with three nuts. There is a gap between the end plate and housing plate 1. Spring S2 is pre-compressed (by a force P_{is2} quantified in Section 3.3) and held in place by the rod and the two nuts in contact with the two housing plates.

Consider that an external load is applied to the un-deformed GSA of Figure 2-6 acting from right to left on housing plate 2. The assembly of the two housing plates and the pre-compressed spring S2 move as a rigid body compressing spring S1. The assembly exhibits the stiffness of spring S1, which is high. This operation continues for displacements less than the limit u'_y -see Figure 2-5(b). As the external force increases, the displacement eventually becomes equal to the limit u'_y and the housing plate 2 moves with respect to the rod resulting in compression of spring S2. The combined system of springs S1 and S2 in series (the latter of low stiffness) has very low stiffness. Displacement u'_y depends entirely on the properties of the two springs. The gap opening d_{gap} must be larger than u'_y for proper operation of the assembly.

The NSD has been tested with and without the GSA. These two NSD configurations are shown in Figure 2-8(a) and Figure 2-8(b) together with idealized force-displacement relations for the two configurations. An NSD without the GSA is only a special case of the case with GSA (when the engagement displacement of the latter is almost zero).



a) NSD without the Gap Spring Assembly and idealized force-displacement relation



b) NSD with Gap Spring Assembly and idealized force-displacement relation

Figure 2-8: Views of NSD and idealized force-displacement relations with and without the gap spring assembly

SECTION 3

BASIC FORCE-DISPLACEMENT RELATIONS OF NEGATIVE STIFFNESS DEVICE

3.1 Introduction

In this section basic force-displacement relations for the negative stiffness device are derived. These equations of the device are valid for certain conditions or assumptions so that the resulting algebraic equations are simple enough for use in analysis and design. The following assumptions are made:

- Frame members are rigid
- All elements are mass-less
- Hysteresis in the joints of the device is negligible

The effect of these assumptions is investigated later in Section 4 where complex models of behavior of the device are developed and compared to the simpler model of this section. In general, the basic model of this section is sufficient for most practical purposes.

3.2 Analysis of Negative Stiffness Device

Analysis of the NSD requires consideration of kinematics and equilibrium of forces in the deformed configuration. Consider that the device is installed in a structure and its top is subject to a known lateral displacement u as shown in Figure 2-4. The following is a derivation of the force produced by the device in the direction of the imposed displacement.

Consider the free body diagram of the pivot plate shown in Figure 3-1. The forces acting on the pivot plate (F_B , F_C and F_s) are shown. The figure also shows the GSA force F_g which does not act on the pivot plate. The free body diagram of the bottom chevron is given in Figure 3-2. Additional information on the NSD deformed shape is provided in Figure 2-4.

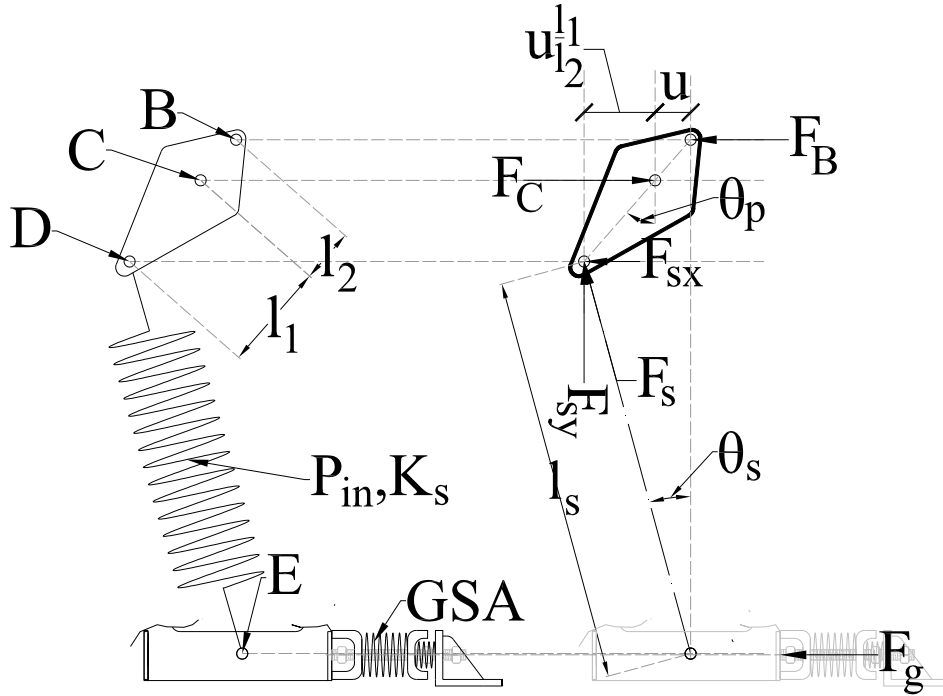


Figure 3-1: Forces acting on pivot plate

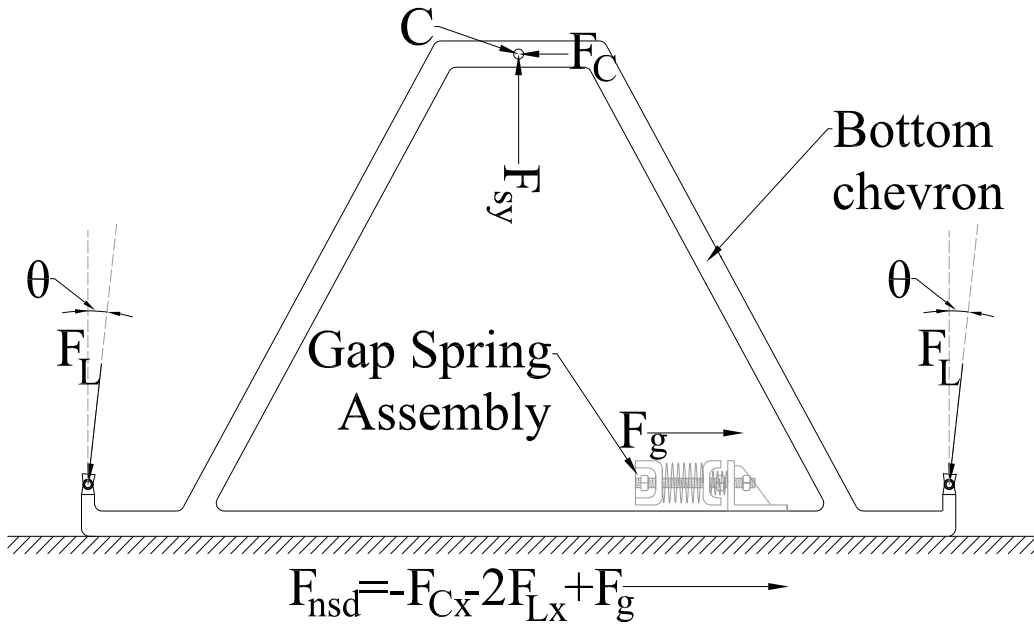


Figure 3-2: Free body diagram of bottom chevron

In addition to the main assumptions listed above, the following assumptions are made:

- The lever is assumed to have zero rotation and, therefore, the lever force acts in the horizontal direction. This assumption also leads to points B and A having the same

displacement. In reality, the lever rotates; the rotation being very small when the lever is long.

- The height loss of the device due to its inverted pendulum motion is ignored. This height loss, however small, results in small vertical displacement of point E, additional small lever rotation and some small loss in the spring pre-load.

When a displacement u is imposed on the top of the device, the lever causes the pivot plate to rotate and point B moves horizontally by the same amount as the imposed displacement. Moreover, point E, which is rigidly connected to the top channel through the top chevron, undergoes the imposed displacement u . Point D moves horizontally in the direction opposing u . These three conditions are written:

$$\begin{aligned} u_B &= u \\ u_E &= u \\ u_D &= -u \frac{l_1}{l_2} \end{aligned} \quad (3-1)$$

where l_2 is the distance from point C to point B and l_1 is the distance from point C to point D in Figure 3-1.

Points B and D move down and up, respectively, by:

$$\begin{aligned} v_B &= l_2 - \sqrt{l_2^2 - u^2} \\ v_D &= l_1 - \sqrt{l_1^2 - \left(u \frac{l_1}{l_2}\right)^2} \end{aligned} \quad (3-2)$$

The vertical distance between points E and D is:

$$v_{DE} = l_p + v_D = l_p + l_1 - \sqrt{l_1^2 - \left(u \frac{l_1}{l_2}\right)^2} \quad (3-3)$$

where l_p is the length of the pre-compressed spring in the un-deformed configuration (the installed length shown in Figure 2-3).

The spring length in the deformed configuration is obtained by using Equations(3-1), (3-2) and (3-3):

$$l_s = \sqrt{\left(l_p + l_1 - l_1 \sqrt{1 - \left(\frac{u}{l_2}\right)^2} \right)^2 + u^2 \left(1 + \frac{l_1}{l_2}\right)^2} \quad (3-4)$$

Taking moments about point C of the pivot plate in Figure 3-1, one can calculate the force at B (this is the axial force in the lever):

$$F_B = \frac{F_s}{\sqrt{l_2^2 - u^2}} \left[\cos \theta_s \left(u \frac{l_1}{l_2} \right) + F_s \sin \theta_s \left(\sqrt{1 - \left(\frac{u}{l_2} \right)^2} \right) l_1 \right] \quad (3-5)$$

where θ_s is the inclination angle of the spring and F_s is the force of the pre-compressed spring. This force varies with displacement and is given by:

$$F_s = P_{in} - K_s (l_s - l_p) \quad (3-6)$$

where P_{in} is the pre-compression force of the spring (a positive value) and K_s is the stiffness of the pre-compressed spring. Note that the force in the spring maximizes when the lateral displacement is zero.

The sine and cosine of the spring inclination angle are given by:

$$\begin{aligned} \sin \theta_s &= \frac{u}{l_s} \left(1 + \frac{l_1}{l_2} \right) \\ \cos \theta_s &= \frac{1}{l_s} \left(l_p + l_1 - \sqrt{l_1^2 - \left(u \frac{l_1}{l_2} \right)^2} \right) \end{aligned} \quad (3-7)$$

The total force produced by the device, exclusive of the GSA force, is the force acting on point C plus the horizontal component of forces in the double hinged columns. From vertical equilibrium in Figure 3-2, the vertical component of the axial load in the double hinged columns is equal to the vertical component of the spring force. The horizontal component of the axial load in the double hinged columns is given by:

$$F_{Lx} = \frac{1}{2} F_s \cos \theta_s \tan \theta \approx \frac{1}{2} F_s \cos \theta_s \frac{u}{h} \quad (3-8)$$

where θ is the inclination angle of the double hinged columns as shown in Figure 3-2 and Figure 2-4. This angle is assumed to be small (so that $\sin \theta \approx \theta$) when height h (height of the double hinged columns in Figure 2-3) is properly selected. From the free body diagram of Figure 3-2, the total force exerted by the NSD, inclusive of the GSA force, is given by:

$$F_{NSD} = -F_C - 2F_{Lx} + F_g \quad (3-9)$$

where F_g is the GSA force and F_C is the horizontal force at point C as calculated from horizontal equilibrium of the pivot plate and given by:

$$F_C = F_B + F_s \sin \theta_s \quad (3-10)$$

Substitutions of Equations (3-5) to (3-8) and (3-10) into (3-9) and after some algebra yields the total NSD force as:

$$F_{NSD} = -\left(\frac{P_{in} + K_s l_p}{l_s} - K_s\right) \left(\frac{l_1}{l_2}\right) \left(2 + \frac{l_p + l_1}{\sqrt{l_2^2 - u^2}} + \frac{l_2}{l_1} \frac{h + l_p + l_1 - (l_1/l_2)\sqrt{l_2^2 - u^2}}{h}\right) u + F_g \quad (3-11)$$

The effective stiffness of the NSD, exclusive of the GSA effects, can be obtained by dividing force F_{NSD} by the displacement u and letting $F_g=0$.

$$K_{NSD}^{eff} = -\left(\frac{P_{in} + K_s l_p}{l_s} - K_s\right) \left(\frac{l_1}{l_2}\right) \left(2 + \frac{l_p + l_1}{\sqrt{l_2^2 - u^2}} + \frac{l_2}{l_1} \frac{h + l_p + l_1 - (l_1/l_2)\sqrt{l_2^2 - u^2}}{h}\right) \quad (3-12)$$

The force-displacement of the gap spring assembly (GSA) is derived in Section 3.3. In its simplest form (elastic bilinear relation) it is given for a desired apparent yield displacement u'_y by:

$$F_g = \begin{cases} k_{s1}u, & 0 \leq u \leq u'_y \\ k_{s1}u'_y + \frac{k_{s2}k_{s1}}{k_{s2} + k_{s1}}(u - u'_y) & u > u'_y \end{cases} \quad (3-13)$$

$$P_{is2} = k_{s1}u'_y$$

where k_{s1} is the stiffness of the inner spring S1 in Figure 2-2 and Figure 2-6, k_{s2} is the stiffness of the outer spring S2 in Figure 2-2 and Figure 2-6, u'_y is the displacement at which the assembly exhibits change in stiffness and P_{is2} is the pre-load in spring S2 of the GSA.

As an example, Table 3-1 presents the nominal properties of the NSD used in the experiments of this report. Using these properties, calculations were performed and results are presented as follows: Figure 3-3 shows: a) the GSA force-displacement relation based on Equation (3-13), b) the NSD force-displacement relation without the GSA based on Equation (3-11) with $F_g=0$ and c) the NSD force-displacement relation with the GSA based on Equations (3-11) and (3-13).

Table 3-1: Nominal NSD properties used in the experimental study

Quantity	Symbol	Value	Units
Length BC of pivot plate	l_1	25.4	cm
Length CD of pivot plate	l_2	12.7	cm
NSD spring length	l_p	76.2	cm
NSD spring stiffness	K_s	1.4	kN/cm
NSD spring preload	P_{in}	16.5	kN
Double hinged column height	h	124.5	cm
Lever length	l_{lv}	67.3	cm
NSD engagement displacement	u'_y	1.65	cm
GSA spring S1 stiffness	k_{s1}	4.9	kN/cm
GSA spring S2 stiffness	k_{s2}	0.3	kN/cm
GSA spring S2 preload	P_{is2}	8.1	kN

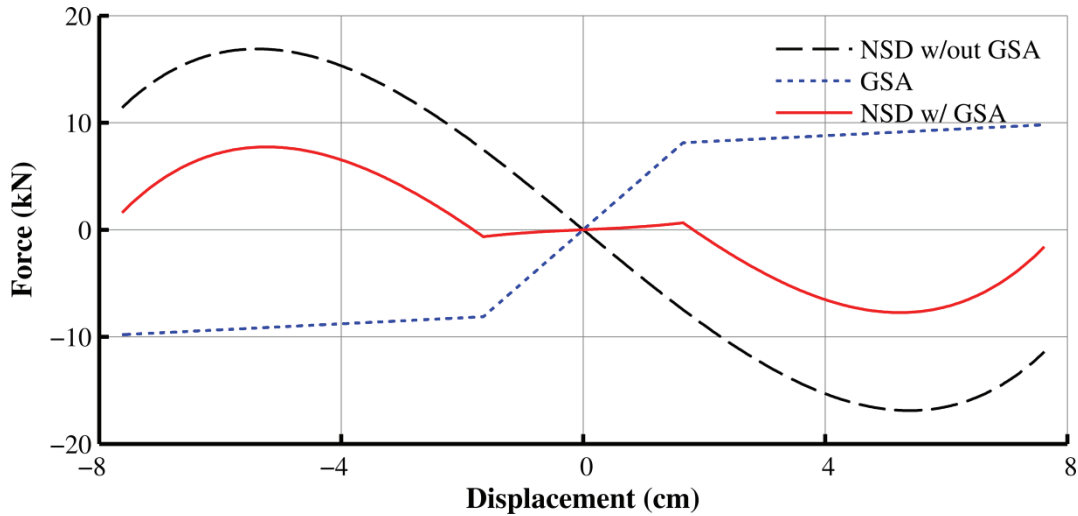


Figure 3-3: Force-displacement relations of GSA and of NSD with and without the GSA for the properties of Table 3-1

Figure 3-4 presents graphs of the effective stiffness versus lateral displacement of a) the GSA based on Equation (3-13) divided by displacement (i.e., F_g/u), b) the NSD without the GSA based on Equation (3-12) and c) the NSD with the GSA obtained by adding the results of a) and b).

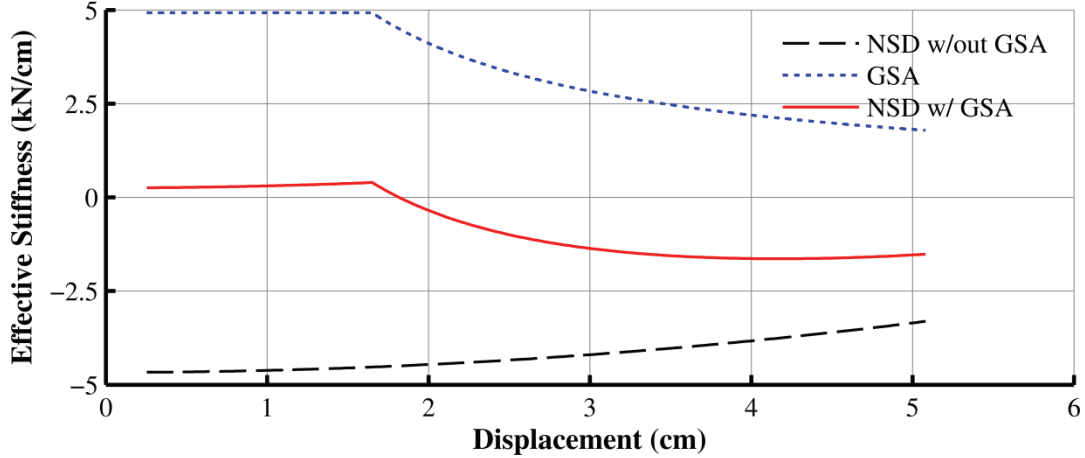


Figure 3-4: Effective stiffness as function of displacement for GSA and NSD with and without the GSA for the properties of Table 3-1

The instantaneous stiffness of the NSD is the slope of the force-displacement curve and is derived as the derivative of the NSD force with respect to the displacement. The stiffening displacement (NSD stiffness becomes zero) can be calculated by setting this derivative to zero, however the resulting equation cannot be solved explicitly for the stiffening displacement and a numerical procedure needs to be employed. Equation (3-14) presents expressions and Figure 3-5 presents graphs of the instantaneous stiffness of a) the GSA (dF_g/du) and b) the NSD with and without the effect of GSA for the device of the properties in Table 3-1.

$$\begin{aligned}
 K_{NSD}^{inst} &= \frac{dF_{NSD}}{du} = -\left(\frac{l_1}{l_2}\right) \left[\frac{d\tilde{F}}{du} \tilde{A}u + \tilde{F} \frac{d\tilde{A}}{du} u + \tilde{F}\tilde{A} \right] + \frac{dF_g}{du} \\
 \frac{dF_g}{du} &= \begin{cases} k_{s1}, & 0 \leq u < u'_y \\ \frac{k_{s2}k_{s1}}{k_{s2} + k_{s1}}, & u > u'_y \end{cases} \\
 \tilde{A} &= \left(2 + \frac{l_p + l_1}{\sqrt{l_2^2 - u^2}} + \frac{l_2}{l_1} \frac{h + l_p + l_1 - (l_1/l_2)\sqrt{l_2^2 - u^2}}{h} \right) \\
 \tilde{F} &= (P_{in} + K_s l_p / l_s) - K_s \\
 \frac{d\tilde{A}}{du} &= u \left(\frac{1}{(l_2^2 - u^2)^{3/2}} + \frac{1}{h\sqrt{l_2^2 - u^2}} \right) \\
 \frac{d\tilde{F}}{du} &= -\frac{dl_s}{du} \frac{P_{in} + K_s l_p}{l_s^2} \\
 \frac{dl_s}{du} &= \frac{u}{l_2 l_s} \left(l_2 + l_1 \frac{l_1 + l_p + 2\sqrt{l_2^2 - u^2}}{\sqrt{l_2^2 - u^2}} \right)
 \end{aligned} \tag{3-14}$$

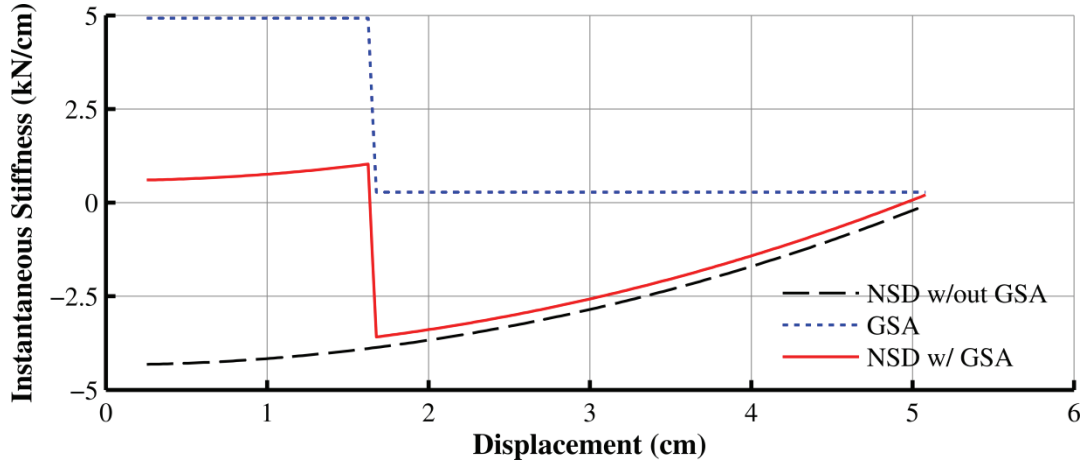


Figure 3-5: Instantaneous stiffness as function of displacement for GSA and for NSD with and without the GSA for the properties of Table 3-1

Equation (3-11) for the NSD force includes the contribution of the horizontal component of the axial force in the double hinged columns, which typically is very small. When this contribution is ignored, Equation (3-11) simplifies into:

$$F_{NSD} = -\left(\frac{P_{in} + K_s l_p}{l_s} - K_s\right) \left(\frac{l_1}{l_2}\right) \left(2 + \frac{l_2}{l_1} + \frac{l_p + l_1}{\sqrt{l_2^2 - u^2}}\right) u + F_g \quad (3-15)$$

Note that the GSA force F_g is given by Equation (3-13). Comparison of the force-displacement of the NSD without the GSA ($F_g=0$) and with due consideration of the NSD double-hinged column load effect (Equation (3-11)) or without due consideration of the column load effect (Equation (3-15)) is presented in Figure 3-7 for the parameters of Table 3-1. The comparison demonstrates that ignoring the NSD column axial load effects is sufficiently accurate for practical purposes.

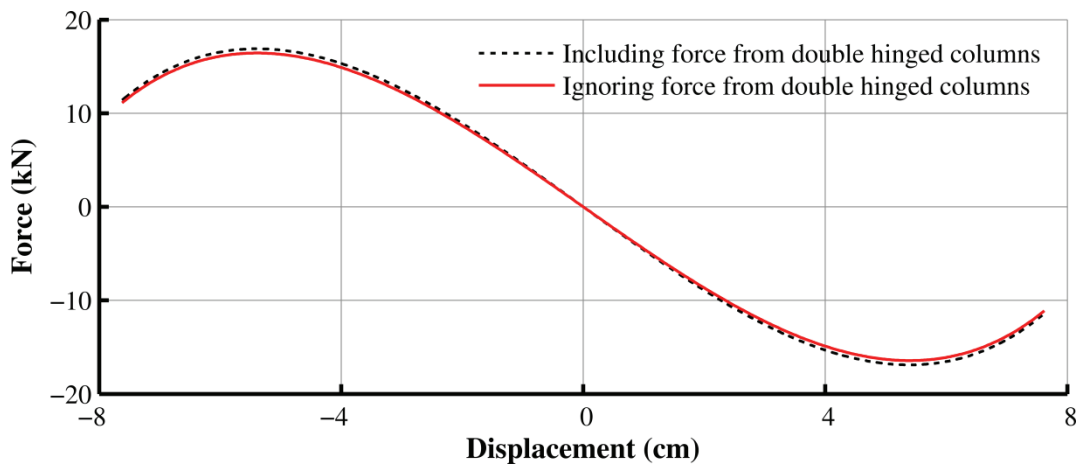


Figure 3-6: Effect of the double hinged column axial load on the NSD force-displacement relation without the GSA and for the properties of Table 3-1

An important property of the NSD is the magnification of the negative stiffness. Equation (3-11) or the simpler Equation (3-15) reveals the two mechanisms by which this magnification is achieved: (a) the lever ratio l_1/l_2 and (b) a factor that results from the use of the double inverted chevron brace system and the way the components of the device connect to the braces.

In order to better understand the significance of stiffness magnification in the NSD, consider a simplified negative stiffness device that only consists of a pre-compressed spring without the magnification mechanisms and the GSA, as shown in Figure 3-7. This basically is the original idea for the vibration isolation systems of Molyneaux (1957) but with the addition of the double hinged columns so that the system is in self-equilibrium in the vertical direction. Once the top of the system in Figure 3-7 displaces by u , the spring exerts a horizontal force component in the direction of displacement, thus generating negative stiffness. If the height loss due to the pendulum motion of the assembly is neglected, the horizontal force-displacement relation of this system is given by:

$$F = - \left(\frac{P_{in} + K_s l_p}{\sqrt{l_p^2 + u^2}} - K_s \right) \left(\frac{h - l_p}{h} \right) u \quad (3-16)$$

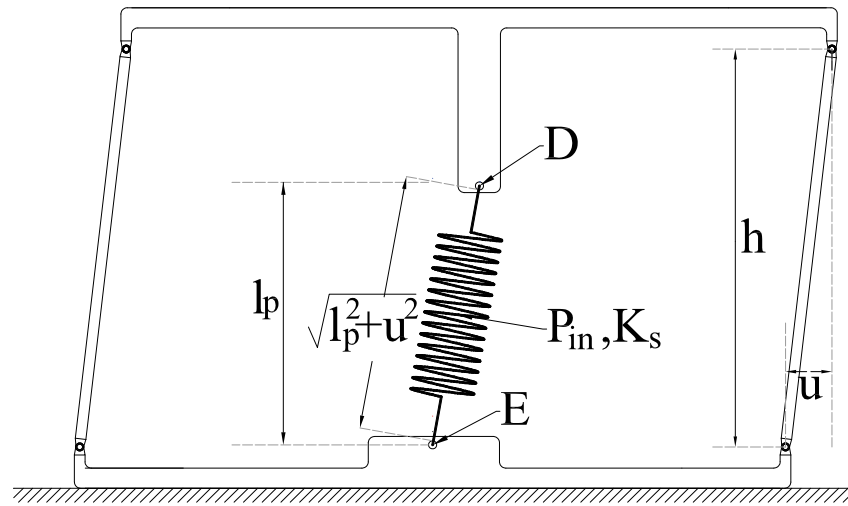
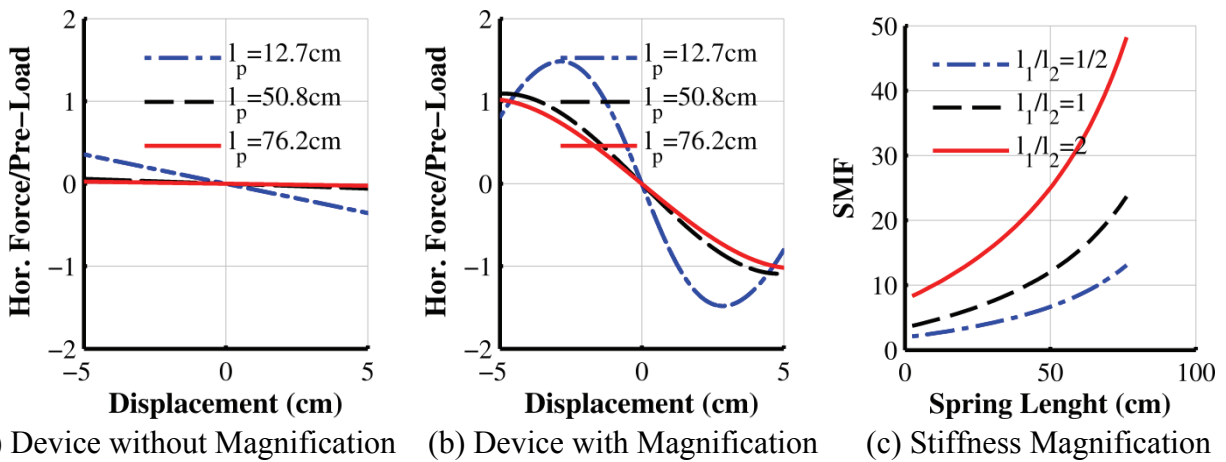


Figure 3-7: Simple negative stiffness device without magnification

A comparison of the force-displacement relation generated by Equations (3-15) and (3-16) is shown in Figure 3-8(a) and (b). The NSD force is normalized by the spring preload, the length of the spring in the un-deformed position l_p varies in the range 12.7 to 76.4cm (5 to 30inch) and other parameters for the NSD with magnification are as in Table 3-1. The efficiency of the NSD with magnification is apparent. To better illustrate the magnification, the stiffness magnification factor (SMF) at zero displacement is defined as the force given by Equation (3-15) for $F_g = 0$ divided by the force given by Equation (3-16), in the limit $u = 0$. The result is:

$$SMF = \frac{l_1}{l_2} \left(2 + \frac{l_2}{l_1} \frac{h+l_p}{h} + \frac{l_p+l_1}{l_2} \right) \frac{h}{h-l_p} \quad (3-17)$$

Figure 3-8(c) presents values of the stiffness magnification factor for various values of the lever ratio (l_1/l_2) by varying the value of length l_1 while all other parameters are as presented in Table 3-1. Evidently there is significant magnification of stiffness even when the lever ratio is less than unity. Also, the SMF increases with increasing spring length. Note that the tested device has $l_1/l_2 = 2$ resulting in a value of SMF at zero displacement equal to 48. This significant magnification has a desired major consequence: a proportional reduction in the requirement for NSD spring preload.



(a) Device without Magnification (b) Device with Magnification (c) Stiffness Magnification
Figure 3-8: Comparison of normalized force-displacement relations of NSD and negative stiffness magnification factor

The tested prototype of NSD had a provision for adjustment of length l_2 so that the magnification factor could be modified by approximately ± 3 cm. This was achieved by connecting the pivot plate and the lever with a bolt through a slotted hole as shown in Figure 3-9.

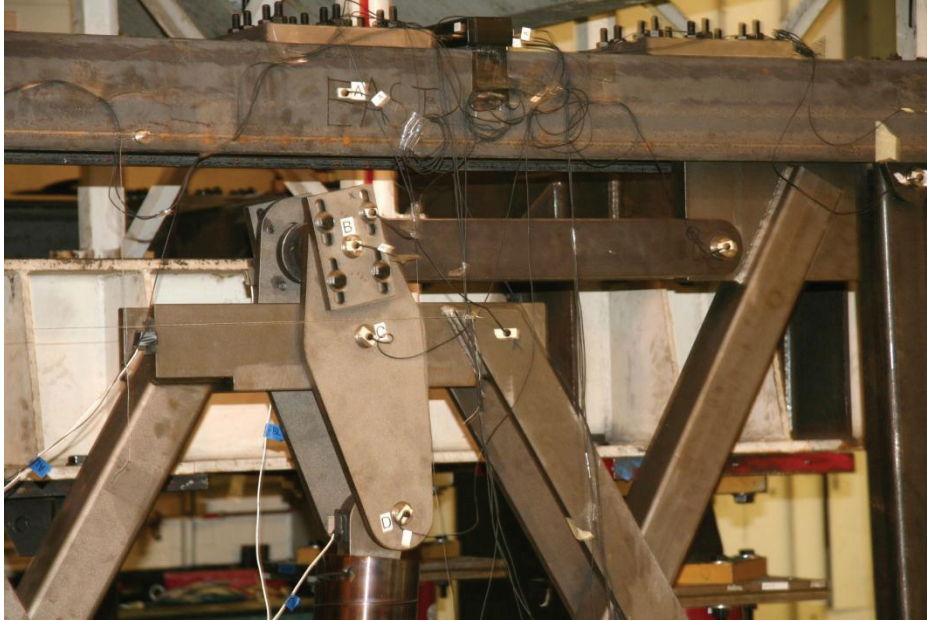


Figure 3-9: Adjustable lever arm connection used for negative stiffness magnification

Figure 3-10 shows the force-displacement relation of the NSD without the GSA as predicted by Equation (3-11) with $F_g=0$ and for the properties of Table 3-1 when length l_2 is varied from the actual value of 12.7cm (5inch) by ± 3.2 cm (1.25inch). It may be observed in Figure 3-10 that reduction of the lever length (increase in lever ratio l_1/l_2) results in magnification of negative stiffness but also more rapid loss of negative stiffness with increasing displacement.

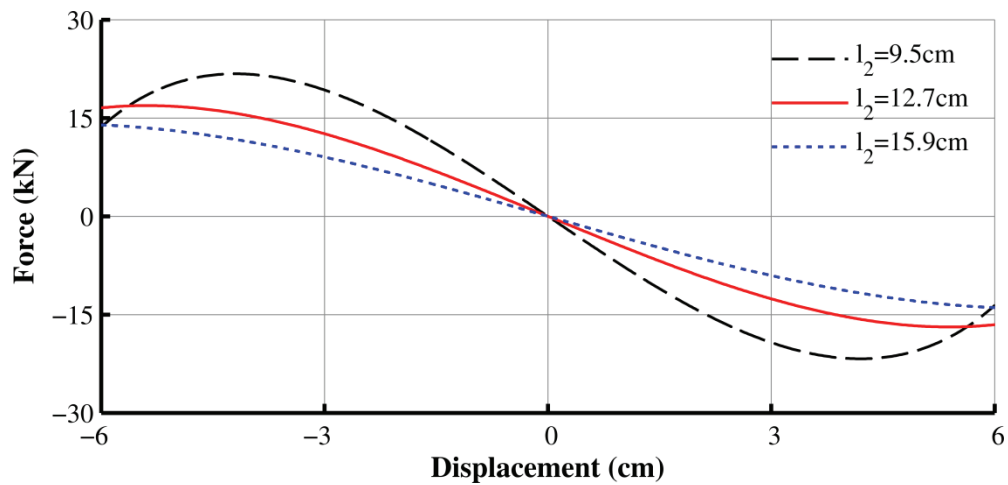


Figure 3-10: Force-displacement relations of NSD without GSA for various values of length l_2

3.3 Basic Force-Displacement Relations for Gap Spring Assembly

This section presents the derivation of Equation (3-13) used in the NSD force-displacement relation. The principle of operation of the GSA (gap spring assembly) is shown in Figure 3-11. The GSA works only in compression and therefore two GSA are needed for each NSD.

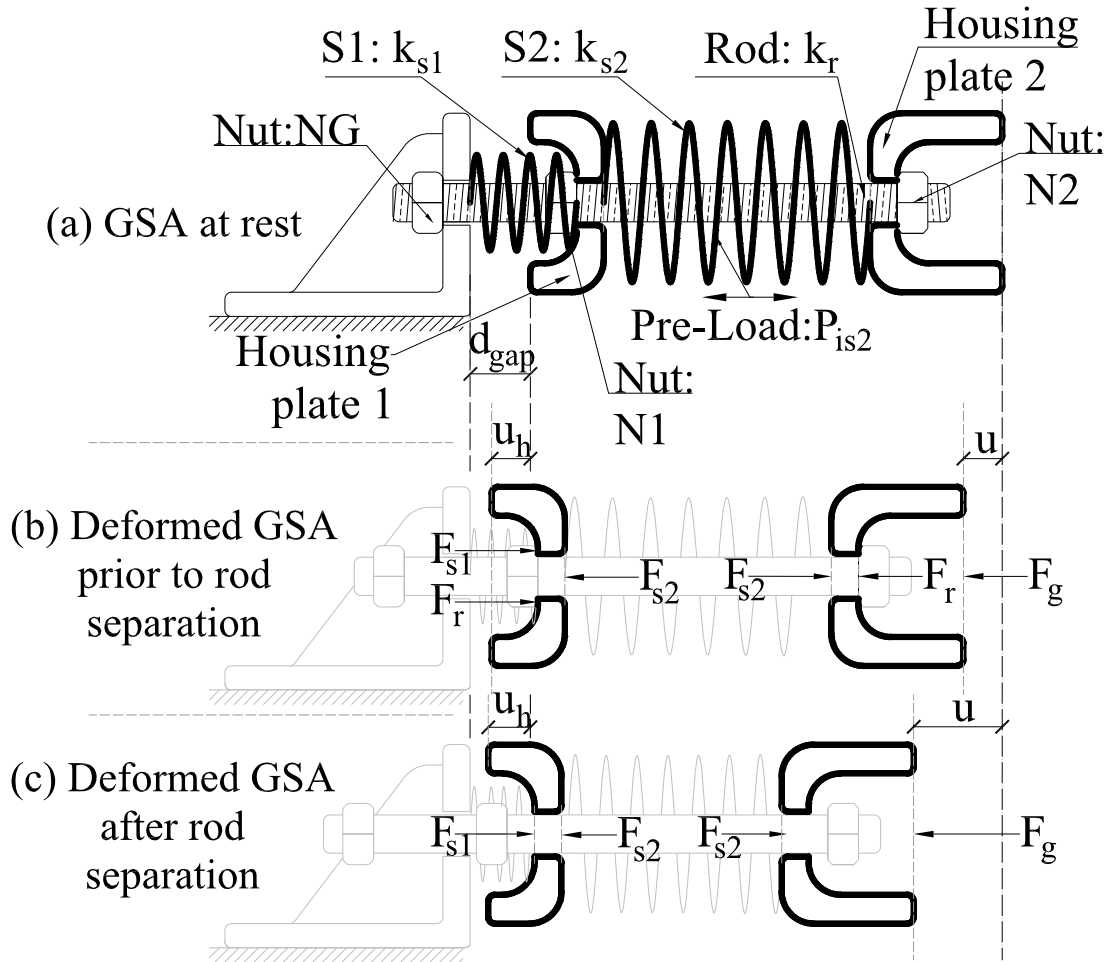


Figure 3-11: Free body diagrams of housing plates of gap spring assembly at three deformed stages

Consider the GSA as shown in Figure 3-11(a) in the un-deformed configuration. Note that d_{gap} is the gap between housing plate 1 and the reaction plate of spring $S1$ in the un-deformed configuration (the value of d_{gap} should be large enough so that the gap does not close during the operation of the assembly). Spring $S2$ of stiffness k_{s2} is pre-compressed by an initial force P_{is2} (positive) and held in place by nuts $N1$ and $N2$ attached to a rod passing through housing plates 1 and 2. Spring $S1$ of stiffness k_{s1} is initially unstressed.

Consider that an external force F_g is applied to the GSA as shown in Figure 3-11(b) resulting in displacement u of the assembly. This displacement is equal to the displacement of housing plate

2. Moreover, u_h is the displacement of housing plate 1, F_{s1} is the force of spring $S1$, F_{s2} is the force of spring $S2$, F_r is the force in the rod connecting housing plates 1 and 2 (note that the force in the rod between housing plate 1 and the reaction plate of spring $S1$ is zero as the rod is freely allowed to move through the reaction plate) and k_r is the stiffness of the rod. Note that the value of k_r is orders of magnitude larger than the stiffness of springs $S1$ and $S2$ so that its exact value is not important for calculating the GSA force. Also, the stiffness of spring $S1$ is much larger than the stiffness of spring $S2$ -typically 10 to 100 times larger.

Once installed spring $S2$ is held in place by nuts N1 and N2 of the rod passing through the housing plates. Under the action of preload, the rod deforms and the spring pre-load is slightly reduced. Although the loss in preload is very small and the preload value effectively still is P_{is2} , the initial rod deformation given by $u_{in} = P_{is2}/k_r$ is important in the behavior of the assembly. From the free body diagrams of housing plates 1 and 2 of Figure 3-11(b) and (c), the spring and rod forces can be expressed as:

$$F_{s1} = k_{s1}u_h \quad (3-18)$$

$$F_{s2} = P_{is2} + k_{s2}(u - u_h) \quad (3-19)$$

$$F_r = \begin{cases} k_r(P_{is2}/k_r - u + u_h), & u \leq P_{is2}/k_r + u_h \\ 0 & u > P_{is2}/k_r + u_h \end{cases} \quad (3-20)$$

The two parts of Equation (3-20) correspond to two stages of operation of the gap spring assembly depicted in Figure 3-11(b) when $F_r \neq 0$ and Figure 3-11(c) when $F_r = 0$. The first stage is defined when the force of the rod is nonzero and therefore nuts N1 and N2 are still in contact with housing plates 1 and 2. The second stage initiates when the nuts separate from housing plates 1 and 2 and the force of the rod becomes zero. From the free body diagrams of Figure 3-11, equilibrium of housing plates 1 and 2 requires that:

$$F_g + F_r - F_{s2} = 0 \quad (3-21)$$

$$F_{s1} + F_r - F_{s2} = 0 \quad (3-22)$$

Solution of Equations (3-18) to (3-22) results in the force-displacement relation of the gap spring assembly for the first stage:

$$u = \left(1 + \frac{k_{s1}}{k_r + k_{s2}}\right)u_h \approx u_h \quad (3-23)$$

$$F_g = \frac{k_{s1}(k_r + k_{s2})}{k_r + k_{s2} + k_{s1}}u \approx k_{s1}u \quad (3-24)$$

Equation (3-23) shows that the total displacement of the assembly is effectively (due to the very large value of stiffness k_r by comparison to k_{s1} and k_{s2}) equal to the deformation of spring $S1$ - therefore, spring $S2$ moves almost as a rigid body. This is also evident in Equation (3-24) where the stiffness of the assembly depends almost entirely on the stiffness of spring $S1$.

The second stage of operation of the GSA (shown in Figure 3-11(c)) initiates when the rod and nuts N1 and N2 separate from housing plates 1 and 2. The displacement and force at which this occurs can be calculated using Equations (3-18) to (3-22) by setting $F_r = 0$ and $u = u'_y$. The result is:

$$\begin{aligned} F_g^{u=u'_y} &= \left[1 + (k_{s2}/k_r)\right] P_{is2} \approx P_{is2} \\ u'_y &= \frac{P_{is2}}{k_{s1}} \left(1 + \frac{k_{s1}}{k_r} + \frac{k_{s2}}{k_r}\right) \approx \frac{P_{is2}}{k_{s1}} \end{aligned} \quad (3-25)$$

Solution of Equations (3-18) to (3-22) for $F_r = 0$ results in the force-displacement relation of the GSA during the stage when $u > u'_y$. The displacement of housing plate 1 is given by:

$$u_h = \frac{P_{is2} + k_{s2}u}{k_{s1} + k_{s2}} \quad (3-26)$$

The force-displacement relation is given by:

$$F_g = \frac{k_{s1}}{k_{s1} + k_{s2}} P_{is2} + \frac{k_{s1}k_{s2}}{k_{s1} + k_{s2}} u \quad (3-27)$$

Equations (3-27) and (3-24) can be cast into the form of Equation (3-13) that was used in the NSD force-displacement derivation.

A typical design of the GSA would call for the stiffness of the GSA for displacement less than u'_y (equal to the force given by Equation (3-24) divided by displacement u) to be equal to the negative stiffness generated by the NSD without the GSA (equal to the force given by Equation (3-11) for $F_g=0$ divided by u at the limit $u = 0$). This yields the following expression for the required stiffness of spring $S1$:

$$k_{s1} = -\frac{P_{in}}{l_p} \frac{l_1}{l_2} \left(2 + \frac{l_p + l_1}{l_2} + \frac{l_2}{l_1} \frac{h + l_p}{h}\right) \quad (3-28)$$

The pre-load of spring $S2$ is then calculated using the stiffness of spring $S1$ above and the apparent yield displacement u'_y as $P_{is2} = k_{s1}u'_y$. In doing so, the stiffness of the NSD (with the GSA) is zero at zero displacement and remains nearly so until displacement u'_y is reached.

Proper design of the GSA requires that the physical gap opening d_{gap} in Figure 3-11 remains open for all displacements of the NSD. Implications in the GSA behavior arise when the physical gap is closed at a displacement $u \approx u_h$ equal to or less than the displacement limit u'_y . A detailed investigation of this case is presented later in Section 4.6. If, however, the physical gap closes at a displacement larger than the limit u'_y , the GSA force-displacement relation is minimally affected with some minor increase in stiffness. This is due to the fact that when this phenomenon occurs, spring S1 stops deforming and only spring S2 is active.

Therefore for proper behavior, and based on Equation (3-26), d_{gap} should be selected such that:

$$d_{gap} > \frac{P_{s2} + k_{s2}u_{max}}{k_{s1} + k_{s2}} \quad (3-29)$$

In Equation (3-29), u_{max} is the maximum NSD expected displacement.

3.4 Modeling of Negative Stiffness Device in General Purpose Analysis Programs

The NSD can be modeled in general purpose dynamic analysis programs by (a) direct modeling of the geometry of the device and its components and performing large displacement analysis, or (b) activating user-defined elements that emulate the force-displacement relations described by Equations (3-11) and (3-13) without the need for large displacement analysis. The former approach is described in Section 4.7 herein. The latter and simpler approach is described in this section and implemented in program SAP2000 (Computers and Structures Inc., 2007).

Program SAP2000 contains the “nonlinear elastic link” element that can replicate any random elastic behavior as shown in Figure 3-12. The element requires data on force and displacement without any restriction other than the behavior has to be elastic.

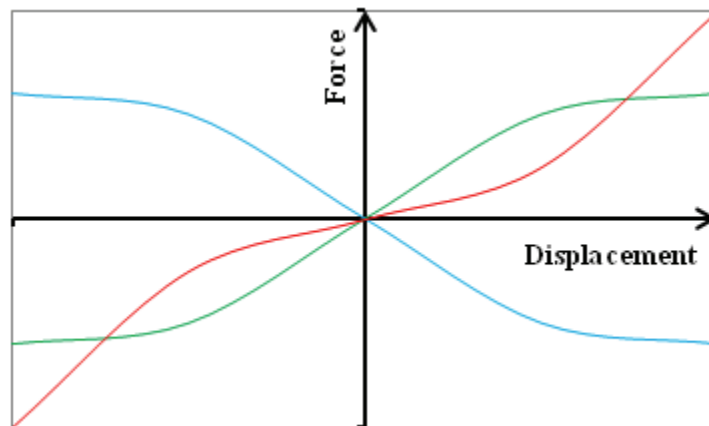


Figure 3-12: Force-displacement loops that can be produced using the nonlinear elastic element in program SAP2000

The NSD model in program SAP2000 requires the use of two elements sharing two nodes in a parallel arrangement as shown in Figure 3-13. These elements are:

- A nonlinear elastic element ML1 representing the NSD without the GSA and having a force-displacement relation given by Equation (3-11) with $F_g=0$.
- A nonlinear elastic element ML2 representing the GSA and having a force-displacement relation given by Equation (3-13).

The use of two elements is not necessary (the NSD with GSA is completely described by Equation (3-11)) but is convenient for performing studies with and without the effect of the GSA.

The two elements, ML1 and ML2, overlap and share the same joints on top (J1) and bottom (J2) in order to avoid any additional moments that might be introduced if they were to be placed apart. Table 3-2 summarizes some secondary properties that need to be used in SAP2000.

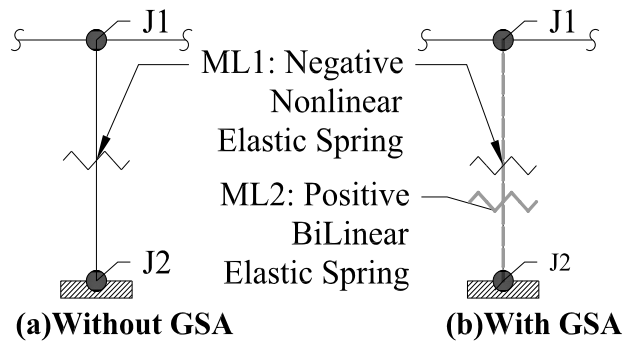


Figure 3-13: SAP2000 NSD element with and without GSA

Table 3-2: SAP2000 NSD element parameters

	ML1	ML2
Non-Linear (U2)	Equation (3-11)	Equation (3-13)
Rotational Stiffness(R1,R2,R3)	0	0
Effective Stiffness	0	0
Vertical Stiffness (U1)	0	0

The model has been implemented in SAP2000 for the parameters of Table 3-1 and subjected to a known displacement history at joint J1. Results are compared with the results of Equations (3-11) and (3-13) in Figure 3-14. The results produced by SAP2000 are identical to the analytical results.

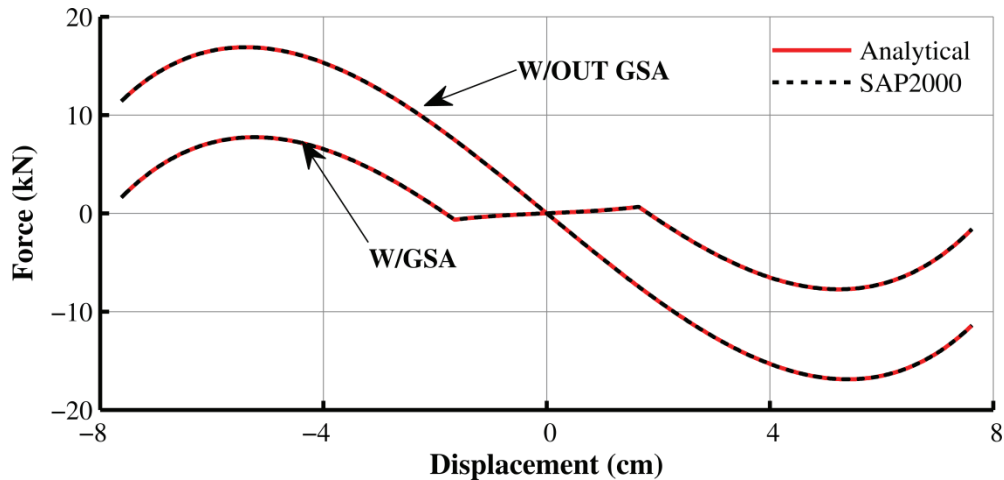


Figure 3-14: Comparison of results of program SAP2000 to analytical results for NSD with properties of Table 3-1

3.5 Considerations in the Implementation of NSD in Structures

Negative stiffness devices are inherently unstable systems. When added to a structure it is apparent that the total stiffness in each principal direction (contributed by the structure and the NSD) must be positive and sufficiently large to avoid serviceability problems. Moreover, the placement of the NSD must be such that the structure is torsionally stable. It is intuitively obvious that when positive stiffness elements are added to a structure, the torsional stiffness is increased by placing these elements far away from the center of rotation. The opposite is true for negative stiffness elements. Placing NSD far away from the center of rotation reduces the torsional stiffness.

Consider the plan view of a floor or base of a structure shown in Figure 3-15. Elements with instantaneous stiffness K_p denote elements with positive stiffness. These elements may be elastomeric bearings or columns with linear or non-linear behavior. Typically these elements provide stiffness in both principal directions. Elements with instantaneous stiffness K_n denote elements with negative stiffness. Their force-displacement relation may be linear or non-linear.

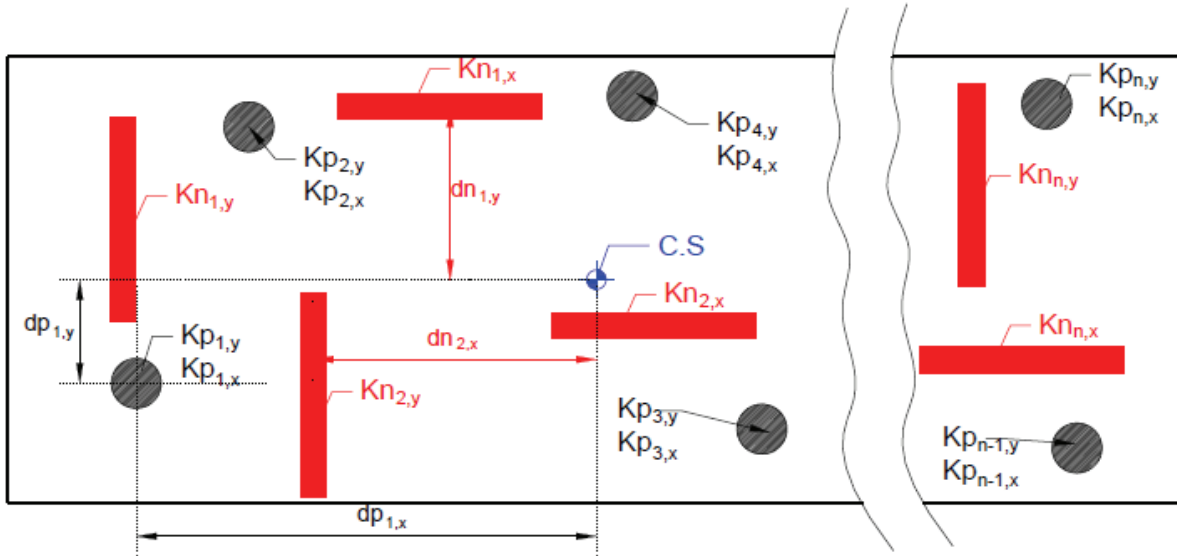


Figure 3-15: Plan view of a structure with positive and negative stiffness elements

In order for the structure to be stable, the following conditions must apply at every time instant:

$$\begin{aligned}
 K_{TOT,X} &= \sum_1^n K_{p,x} - \sum_1^n K_{n,x} > 0 \\
 K_{TOT,Y} &= \sum_1^n K_{p,y} - \sum_1^n K_{n,y} > 0 \\
 K_{TOT,\theta} &= \sum_1^n K_{p,x} d_{p,y}^2 + \sum_1^n K_{p,y} d_{p,x}^2 - \sum_1^n K_{n,y} d_{n,x}^2 - \sum_1^n K_{n,x} d_{n,y}^2 > 0
 \end{aligned}
 \tag{3-30}$$

SECTION 4

ADVANCED FORCE-DISPLACEMENT RELATIONS OF NEGATIVE STIFFNESS DEVICE

4.1 Introduction

In this section the assumptions of Section 3 are relaxed to arrive at advanced force-displacement relations for the NSD. The resulting relations are too complex for use in design. However, these advanced relations are used to demonstrate that the simpler force-displacement relations presented in Section 3 are sufficiently accurate for design and analysis purposes.

Models of behavior of the NSD with due consideration for the following effects are independently developed and studied:

1. Large deformations. The formulations account for NSD height loss, lever rotation and double-hinged column rotation.
2. Inertia effects. Mass and moment of inertia of the NSD components are considered. Also, P- Δ effects resulting from the weight of the device are accounted for.
3. Hysteresis of the device. Friction in the joints is considered.
4. Flexibility in the elements of the device. Flexibility of the top and bottom beams connecting the device to the structure and ground is considered.

4.2 NSD Relations Considering Large Deformation Effects

The assumptions made in Section 3.2 are relaxed and the force-displacement relations of the NSD are re-derived by accounting for the lever rotation, NSD height loss of the device and double-hinged column rotation. Figure 4-1 shows the deformed shape of the device, Figure 4-2 shows the free body diagram of the pivot plate and Figure 4-3 shows the free body diagram of the bottom chevron, all with consideration of large deformation effects. Note that on lateral displacement of the NSD, the lever rotates so that the displacements of points A and B are not equal. Specifically, $u = u_A = u_E \neq u_B$. The displacement of point D is now related to the displacement of point B rather than to point A.

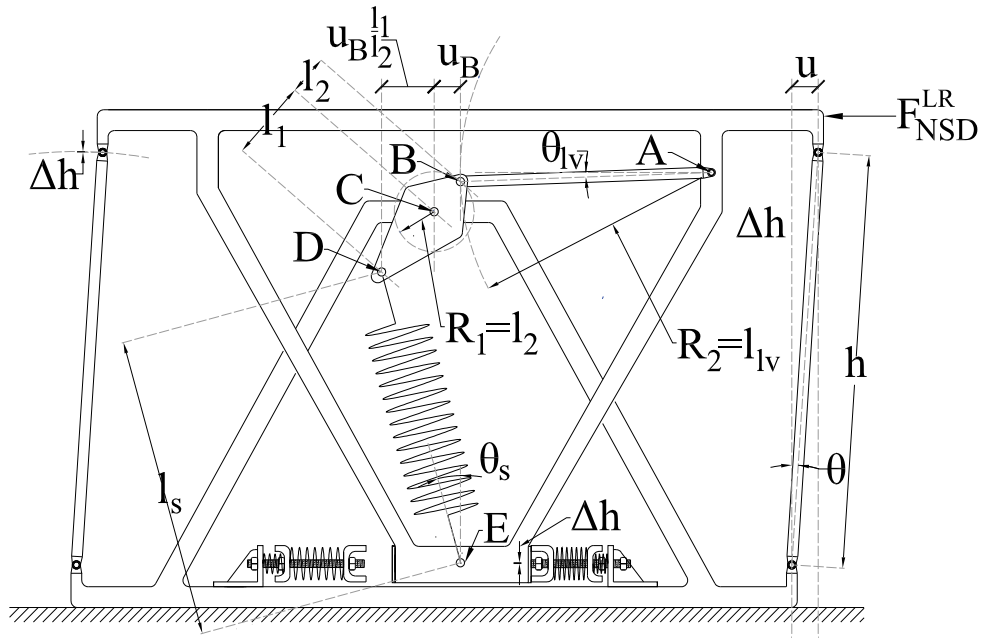


Figure 4-1: Deformed NSD when considering large deformation effects

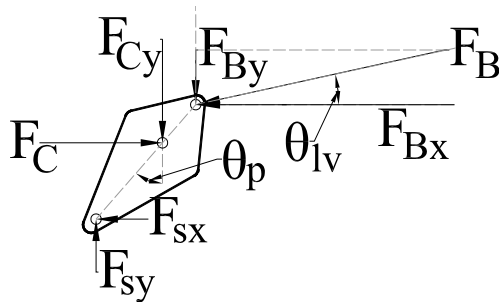


Figure 4-2: Free body diagram of pivot plate

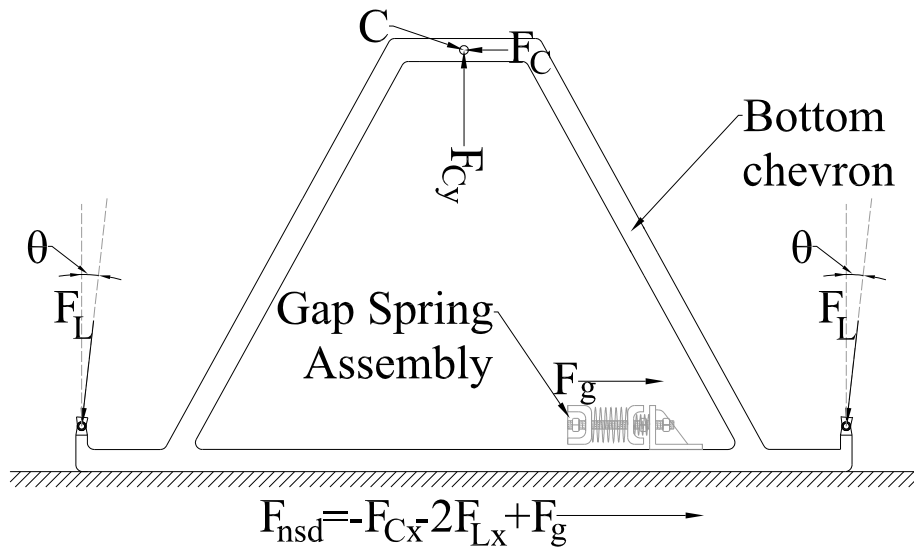


Figure 4-3: Free body diagram of bottom chevron

The height loss of the device is:

$$\Delta h = h - \sqrt{h^2 - u^2} \quad (4-1)$$

Note that h is the distance between the top and bottom pins of the double-hinged column.

In order to derive the relation between the displacements of points A and B, consider a reference coordinate system centered at point C. Point B moves around a circle which is centered at C and has radius l_2 . Point B follows a trajectory that lies always on the circle R1 shown in Figure 4-1. The equation describing R1 is given by:

$$x_1^2 + y_1^2 = l_2^2 \quad (4-2)$$

Moreover, point B moves in a circle centered at A with radius l_{lv} (R2 in Figure 4-1). Due to the imposed displacement u and the height loss of the device, the center of this circle (point A) moves resulting in the following expression to describe circle R2:

$$(x_2 - l_{lv} - u)^2 + (y_2 - l_2 + \Delta h)^2 = l_{lv}^2 \quad (4-3)$$

where l_{lv} is the length of the lever from pin A to pin B.

In order to find the relation between the horizontal displacements of point A and B, the intersection point of the two circles needs to be determined. This point satisfies Equations (4-2) and (4-3) with $y_1 = y_2 > 0$. Note that the coordinates are positive since point B cannot move below point C. These conditions are given by:

$$\begin{aligned} x_1 &= x_2 = u_B \\ y_1 &= y_2 \end{aligned} \quad (4-4)$$

Use of Equations (4-2), (4-3) and (4-4) results in:

$$u_B = \frac{1}{2} \frac{(l_{lv} + u)(2l_2^2 + \tilde{Q}) - (l_2 - \Delta h)\sqrt{(2l_2l_{lv})^2 - \tilde{Q}^2}}{(l_2 - \Delta h)^2 + (l_{lv} + u)^2} \quad (4-5)$$

$$\tilde{Q} = \Delta h^2 - 2\Delta h l_2 + u(2l_{lv} + u) \quad (4-6)$$

The horizontal displacement of point D is related to the displacement of point B by:

$$u_D = -u_B \frac{l_1}{l_2} \quad (4-7)$$

The angle of rotation of the lever θ_{lv} can then be calculated from any of the following two equations:

$$\begin{aligned}\sin \theta_{lv} &= \frac{l_2 - \sqrt{l_2^2 - u_B^2} - \Delta h}{l_{lv}} \\ \cos \theta_{lv} &= \frac{l_{lv} + u - u_B}{l_{lv}}\end{aligned}\quad (4-8)$$

The height loss of the device affects the length of the spring. This length is given by:

$$l_s = \sqrt{\left(l_p + l_1 - l_1 \sqrt{1 - (u_B/l_2)^2} + \Delta h\right)^2 + \left(u + u_B \frac{l_1}{l_2}\right)^2} \quad (4-9)$$

The sine and cosine of the spring angle θ_s (see Figure 4-1) are then given by:

$$\begin{aligned}\cos \theta_s &= \frac{l_p + l_1 - \sqrt{l_1^2 - (u_B l_1/l_2)^2} + \Delta h}{l_s} \\ \sin \theta_s &= \frac{1}{l_s} \left(u + u_B \frac{l_1}{l_2}\right)\end{aligned}\quad (4-10)$$

Employing moment equilibrium of the pivot plate in Figure 4-2, the axial force in the lever is:

$$F_b = F_s \frac{\cos \theta_s u_B l_1/l_2 + \sin \theta_s l_1 \sqrt{1 - (u_B/l_2)^2}}{\cos \theta_{lv} \sqrt{l_2^2 - u_B^2} - u_B \sin \theta_{lv}} \quad (4-11)$$

where F_s is given by Equation (3-6).

Using vertical force equilibrium of the pivot plate in Figure 4-2, the vertical force at point C is determined to be $F_{Cy} = F_{sy} - F_{by}$. The axial load in each double hinged column is then determined from the free body diagram of Figure 4-3:

$$F_L = \frac{F_s \cos \theta_s - F_b \sin \theta_{lev}}{2 \cos \theta} \quad (4-12)$$

where θ is the inclination angle of the double hinged columns as shown in Figure 4-3. This angle is given by:

$$\theta = \arcsin(u/h) \quad (4-13)$$

The horizontal force at point C is determined from horizontal equilibrium of the pivot plate as $F_C = F_b \cos \theta_{lv} + F_s \sin \theta_s$ and the total NSD force is then determined as $F_{NSD}^{LR} = -F_C - 2F_L \sin \theta + F_g$ to yield the final expression for the NSD force:

$$F_{NSD}^{LR} = -F_b (\cos \theta_{lv} - \sin \theta_{lv} \tan \theta) - F_s (\sin \theta_s + \cos \theta_s \tan \theta) + F_g \quad (4-14)$$

A comparison of the NSD force-displacement relation of the device with the properties of Table 3-1 with due (Equation (4-14)) and without due (Equation(3-11)) consideration of large deformation effects is presented in Figure 4-4 for the case $F_g=0$ (without GSA). There is very small difference between the two relations so that one can conclude that large deformation effects are insignificant for practical purposes. The reason for this behavior is that the selected lever length and column height are large enough to cancel out any large deformation effects.

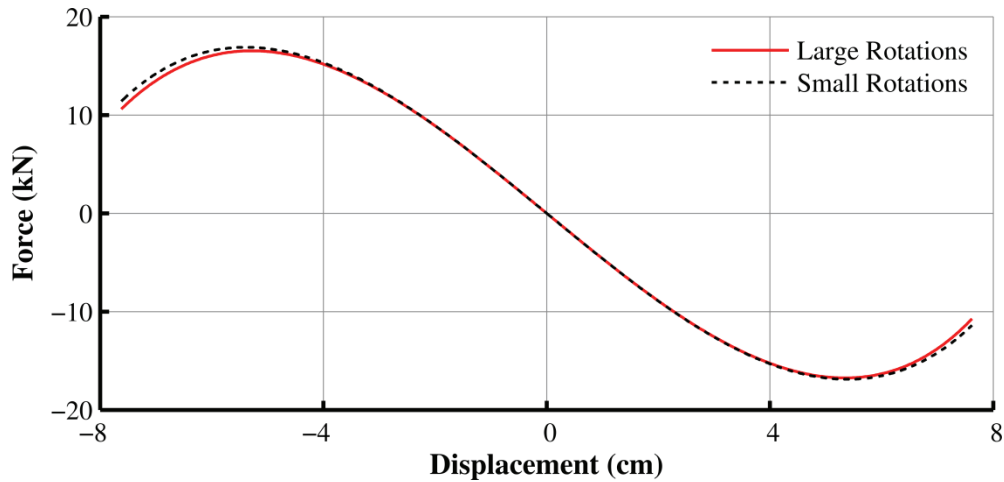


Figure 4-4: Comparisons of NSD force without the GSA predicted without due (small rotations) and with due (large rotations) consideration of large deformation effects for the device with properties of Table 3-1

Figure 4-5 presents comparisons of force-displacement relations for devices with the properties of Table 3-1 but for the lever length varied whereas the column height is set to a large value. This combination of parameters explores the effect of lever length while removing any effect of the column height. Evidently, large deformations have insignificant effect even at small lever lengths.

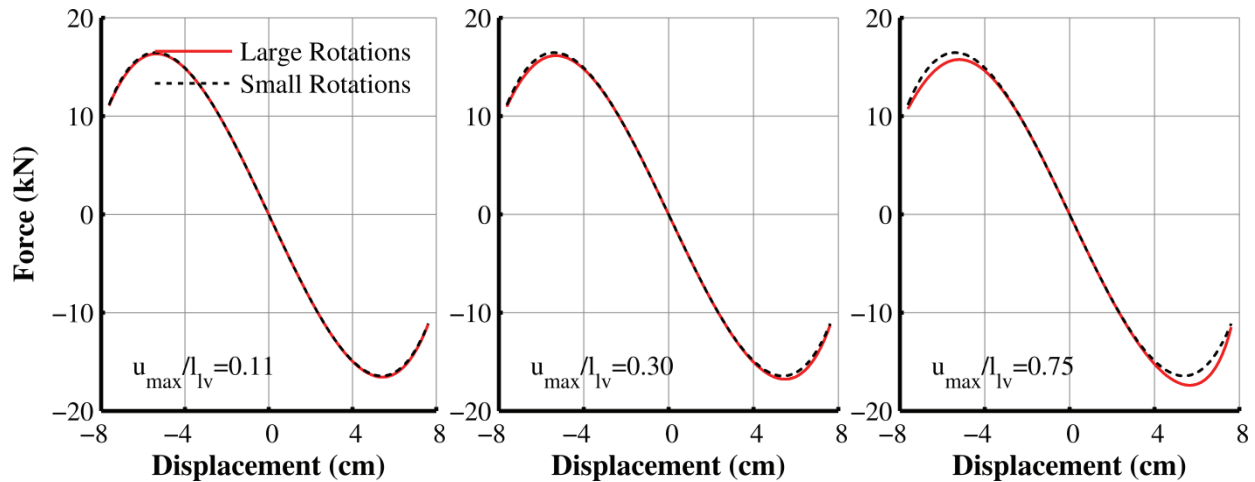


Figure 4-5: Force-displacement relations of NSD without GSA for varied lever length and for very large column height

Similarly, Figure 4-6 presents comparisons of force-displacement relations for NSD devices without the GSA and with the properties of Table 3-1 when the column height is varied whereas the lever length is set to a large value. This combination of parameters explores the effect of column height while removing any effect of the lever length. Again the large deformation effects are small but for very small heights where the effects are pronounced. For the studied device, the effects were important when the height was about equal or less than twice the amplitude of the imposed displacement (angle θ equal to about 25°), an obviously very small height.

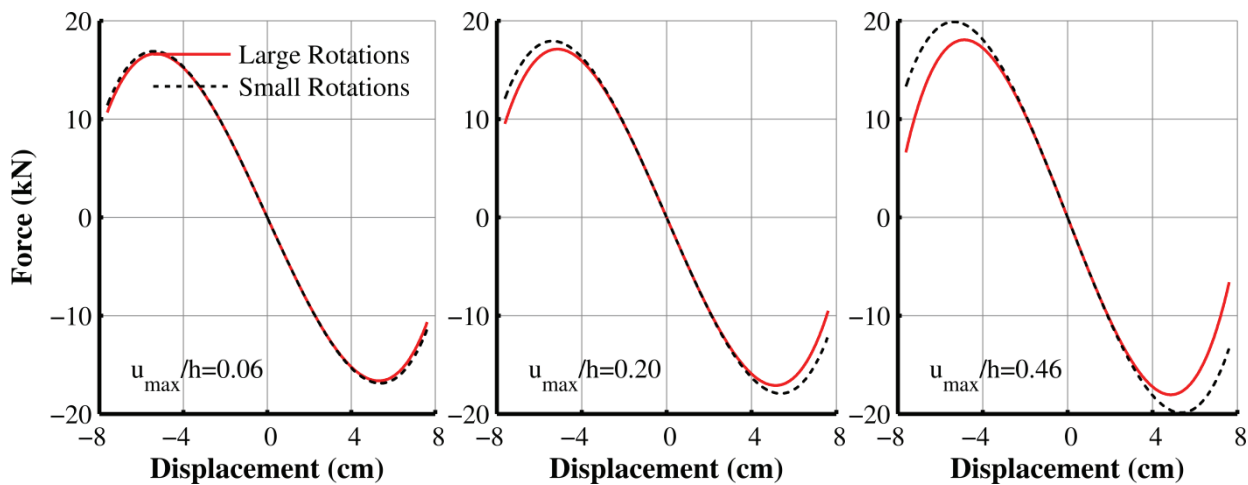


Figure 4-6: Force-displacement relations of NSD without GSA for varied column height and for very large lever length

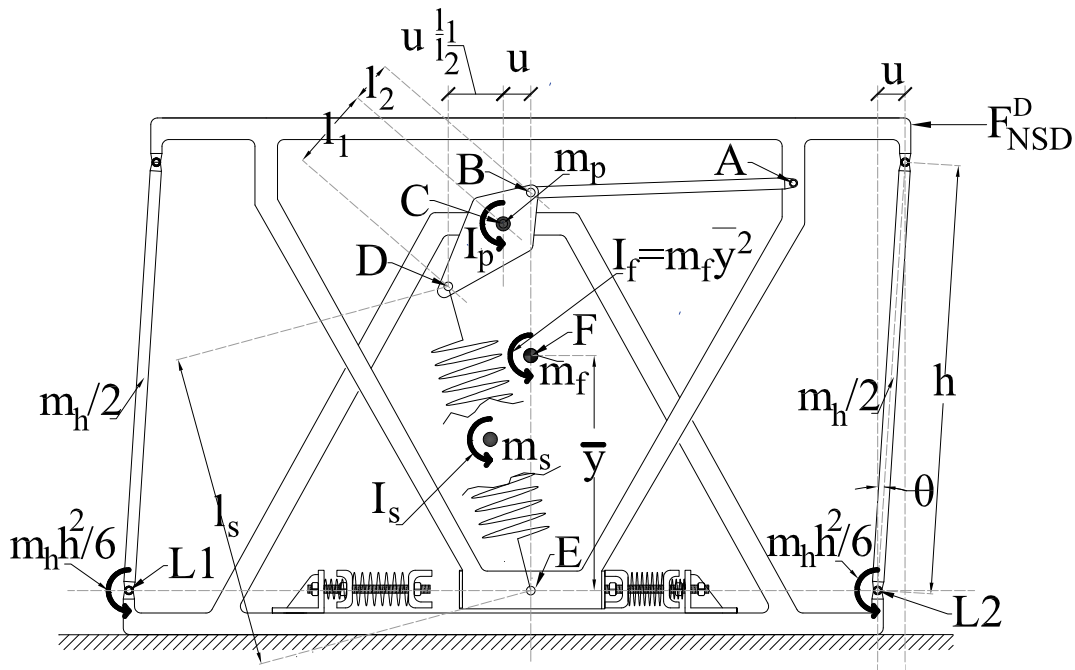
The behavior of the GSA is not affected by large deformations so that the equations of Section 3 are valid. Moreover, the SAP2000 model described in Section 3.4 can be implemented with the large deformation effects included by simply specifying for element ML1 the force-displacement relation given by Equation (4-14) instead of Equation (3-11). The GSA force, represented by element ML2, is still described by Equation (3-13). In this way, large deformation effects for the

NSD are accounted for in program SAP2000 without having to execute large deformation analysis.

4.3 NSD Relations Considering Inertia Effects

In the derivation that follows large deformations are ignored, members are assumed rigid, friction in the joints is disregarded and only the mass and mass moment of inertia effects are considered.

The rigid body dynamics of the NSD are derived using the Lagrangian formulation. Figure 4-7 shows the location of the center of mass, the mass and the mass moment of inertia of the components of the NSD. Frame elements connected to the top channel have mass m_f . These elements undergo an inverted pendulum motion around the base and their moment of inertia I_f is lumped at point F (that is, the center of mass of the moving elements is located at distance \bar{y} from point E-see Figure 4-7). The double-hinged columns have total mass m_h and mass moment of inertia for rotation about L1 and L2 equal to I_h . Mass m_p and moment of inertia I_p of the pivot plate are lumped at point C. The center of mass of the vertical spring undergoes both translation and rotation. Its mass m_s is lumped at its center of mass.



$$I_s = m_s l_s^2 / 12 \quad (4-15)$$

The angles of rotation of the pivot plate θ_p and of the spring θ_s are given by:

$$\begin{aligned} \theta_p &= \arcsin \frac{u}{l_2} \\ \theta_s &= \arcsin \left[\frac{u}{l_s} \left(1 + \frac{l_1}{l_2} \right) \right] \end{aligned} \quad (4-16)$$

where l_s is given by Equation (3-4). The horizontal and vertical displacements of the spring's center of mass are given by:

$$\begin{aligned} u_{CMs} &= \frac{u - u l_1 / l_2}{2} \\ v_{CMs} &= \frac{l_1 - \sqrt{l_1^2 - (u l_1 / l_2)^2}}{2} \end{aligned} \quad (4-17)$$

The Euler-Lagrange equation for the NSD is then derived as follows:

$$\begin{aligned} \frac{d}{dt} \left(\frac{\partial L}{\partial \dot{u}} \right) - \frac{\partial L}{\partial u} &= F_{NSD}^D \\ L &= K - V \end{aligned} \quad (4-18)$$

In Equation (4-18), K is the total kinetic energy of the system, V is the total potential energy of the system with respect to a reference coordinate system and F_{NSD}^D is the force generated by the NSD as shown in Figure 4-7. The total kinetic and potential energies (with reference to point L1) are given by:

$$K = (1/2) \left(I_p \dot{\theta}_p^2 + m_s \dot{u}_s^2 + m_s \dot{v}_s^2 + I_s \dot{\theta}_s^2 + I_h \dot{\theta}^2 + I_f \dot{\theta}^2 \right) \quad (4-19)$$

$$V = (1/2) g \left[2m_f \bar{y} \cos \theta + m_s \left(l_p + l_1 - l_1 \sqrt{1 - (u/l_2)^2} \right) + m_h (h \cos \theta) + 2m_p (l_p + l_1) \right] + U_s \quad (4-20)$$

In (4-20), U_s is the strain energy of the pre-compressed spring which is given by:

$$U_s = (1/2) K_s \left(l_s - l_p - P_{in} / K_s \right)^2 \quad (4-21)$$

In order to include the effects of the horizontal component of force in the double-hinged columns, the spring length l_s in Equation (4-21) is calculated using Equations (4-9) for $u_B = u$ and Equation (4-1). This results in the following expression for the spring length:

$$l_s = \sqrt{\left(l_p + l_1 - l_1 \sqrt{1 - (u/l_2)^2} + \Delta h\right)^2 + u^2 \left(1 + \frac{l_1}{l_2}\right)^2} \quad (4-22)$$

Using Equations (4-15) to (4-22), the following expression for the NSD force is derived:

$$\begin{aligned} F_{NSD}^D &= M_a \ddot{u} + M_v \dot{u}^2 + M_u u + F_g \\ M_a &= \frac{m_f \bar{y}^2}{h^2 - u^2} + \frac{m_h h^2}{3(h^2 - u^2)} + m_s \left(\frac{1}{4} - \frac{l_1}{2l_2} + \frac{l_1^2}{4(l_2^2 - u^2)} + \frac{l_t^2 q^2}{12r^4} \right) + \frac{I_p}{l_2^2 - u^2} \\ M_v &= \frac{3m_f \bar{y}^2 + m_h h^2}{3(h^2 - u^2)^2} u + \frac{4I_p + m_s l_1^2}{4(l_2^2 - u^2)^2} u - \frac{m_s l_t^2 q}{12r^4 l_s} \left(q \frac{dl_s}{du} + u \cdot l_s \cdot \frac{d^2 l_s}{du^2} \right) + \frac{m_s l_t^4 q^3}{12l_s r^8} u \\ M_u &= K_{NSD}^{eff} - \left(\frac{m_f \bar{y}}{h^2} + \frac{m_h}{2h} - \frac{m_s}{4\sqrt{l_2^2 - u^2}} \frac{l_1}{l_2} \right) g \\ q &= l_s - u \frac{dl_s}{du}; \quad r^4 = l_2^2 l_s^2 - l_t^2 u^2; \quad l_t = l_1 + l_2 \end{aligned} \quad (4-23)$$

For simplicity, the simpler expression of Equation (3-4) can be used in Equations (4-23) for the spring length l_s and its derivatives dl_s/du and $d^2 l_s/du^2$. Moreover, Equations (4-23) may be further simplified by using the approximation $\sqrt{h^2 - u^2} \approx h$. Finally, term K_{NSD}^{eff} in Equation (4-23) is given by Equation (3-12).

Comparisons of force-displacement relations of the NSD with the geometric and other properties of Table 3-1 and the mass properties of Table 4-1 are presented in Figure 4-8. Harmonic motion of the top of the NSD is imposed with amplitude equal to 8cm and varying frequency. Evidently, there are effects of inertia forces on the calculated force-displacement relations but these effects are of importance for frequencies of 2Hz or larger. Such frequencies are a characteristic of very stiff structures.

Table 4-1: Masses and mass moment of inertia of elements of NSD with properties of Table 3-1

Quantity	Symbol	Value	Units
Spring mass	m_s	54.4	kg
Mass moment of inertia of pivot plate	I_p	0.35	$Kg-cm^2$
Mass of lever, top chevron and channel	m_f	227	kg
Mass of double-hinged column	m_h	44	kg
Location of center of mass of elements translating by displacement u^1	\bar{y}	83.1	cm
1. These elements consist of the top chevron, the top channel, the lever and all rigid blocks connected to the top channel			

Additional results are presented in Figure 4-9 where the history of NSD force is presented for the case of 1Hz frequency analysis. Finally, Figure 4-10 compares NSD force-displacement relations and force histories for NSD displacement input being the history of the NSD displacement measured in shake table testing of the analyzed device. Evidently, the inertia effects in these cases of realistic NSD motion are insignificant.

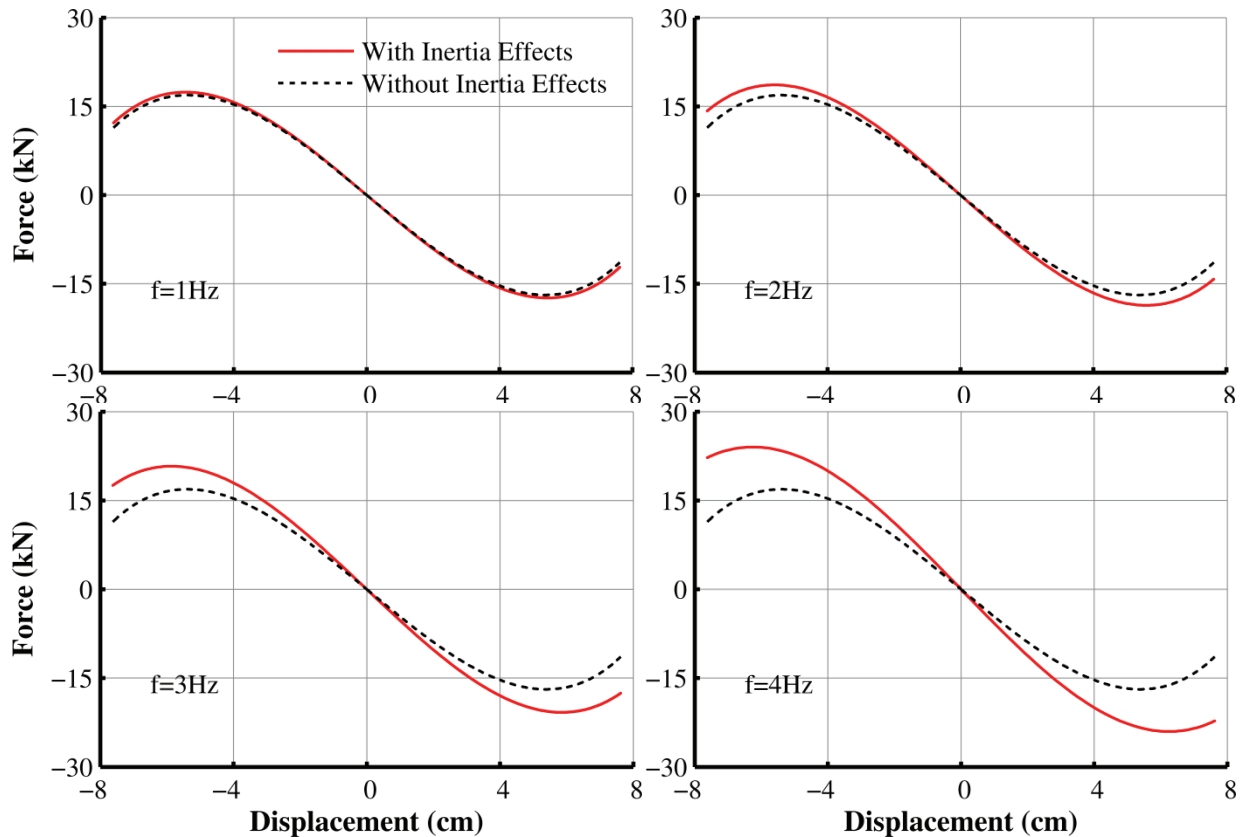


Figure 4-8: Force-displacement relations of NSD without GSA with due and without due consideration of inertia effects

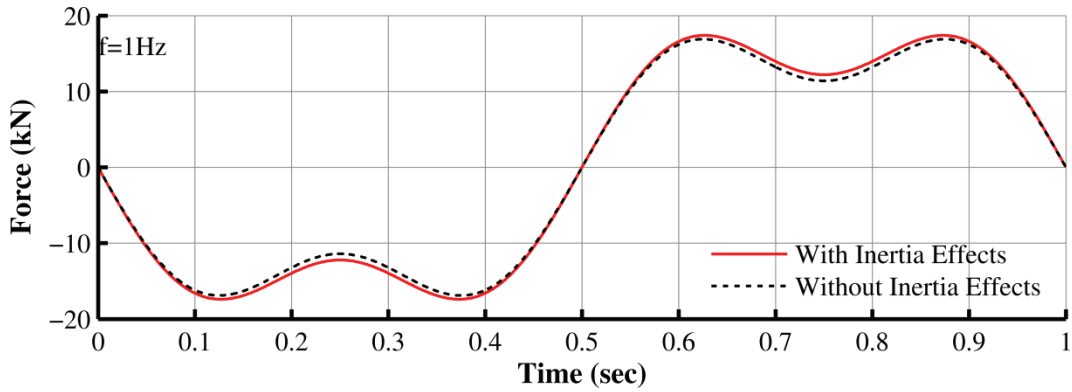


Figure 4-9: Comparison of force histories of NSD without GSA with due and without due consideration of inertia effects

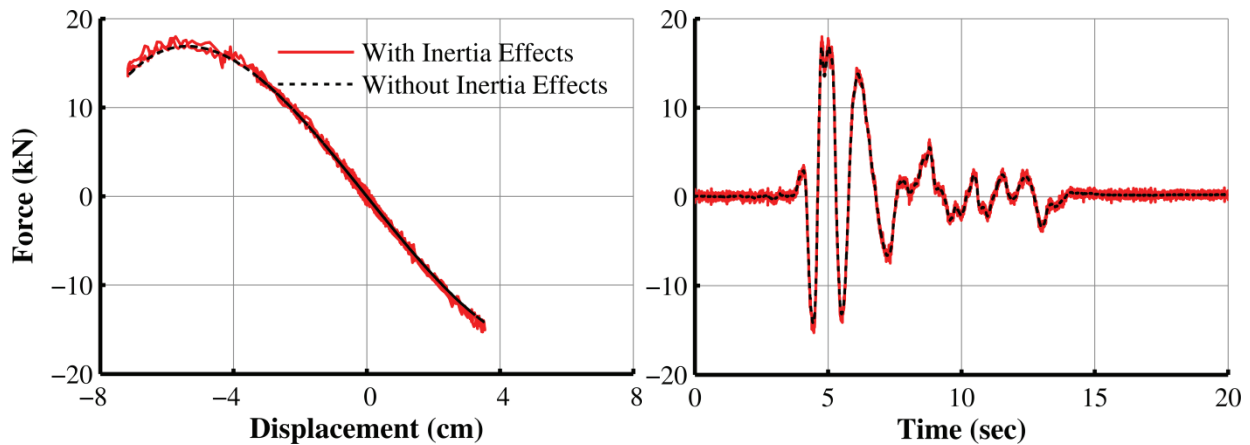


Figure 4-10: Comparison of force-displacement relations and force histories of NSD without GSA with due and without due consideration of inertia effects for random motion measured in shake table test

The simple two element model of the NSD in program SAP2000 described in Section 3.4 may be extended to approximately include inertia effects by assigning mass to element ML1 that represents the NSD exclusive of the GSA. To do so, Equation (4-23) is inspected to realize that the NSD force includes a component that is velocity dependent ($M_v \dot{u}^2$), which cannot be accounted for in the simple SAP2000 model. However, this term turns out to be small by comparison to the acceleration-related term so it is justifiable to neglect it. For demonstration, Figure 4-11 compares the two contributors to the NSD force in Equation (4-23) for the device of the properties in Table 3-1 and Table 4-1 subjected to high frequency motion. The figure presents time histories of the terms $M_a \ddot{u}$ (acceleration term) and $M_v \dot{u}^2$ (velocity term) where it is apparent that the acceleration term dominates over the velocity term. Accordingly, the velocity term in Equation (4-23) is ignored ($M_v = 0$) and u is set equal to zero in the expression for term M_a . The resulting value of M_a is used as a mass \bar{m} assigned only to link element ML1 (see Figure 3-13):

$$\bar{m} = \frac{m_f \bar{y}^2}{h^2} + \frac{m_h h^2}{3h^2} + m_s \left(\frac{1}{4} - \frac{l_1}{2l_2} + \frac{l_1^2}{4l_2^2} + \frac{(l_1 + l_2)^2}{12l_2^2} \right) + \frac{I_p}{l_2^2} \quad (4-24)$$

To assess the accuracy of this representation, Equation (4-23) is used to predict the exact force-displacement relation of the NSD for the case of motion of 4Hz frequency in Figure 4-12 and compare it to an approximate expression using the same equation but without the contribution of term $M_v \dot{u}^2$ and the approximate expression for term M_a . The comparison is good but the stiffening behavior of the NSD is not captured well.

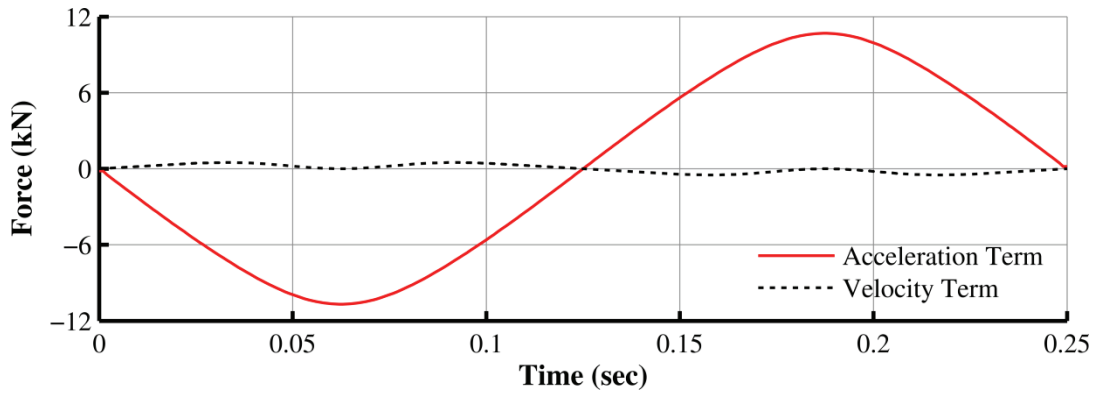


Figure 4-11: Comparison of contributions of acceleration ($M_a \ddot{u}$) and velocity ($M_v \dot{u}^2$) terms in NSD force

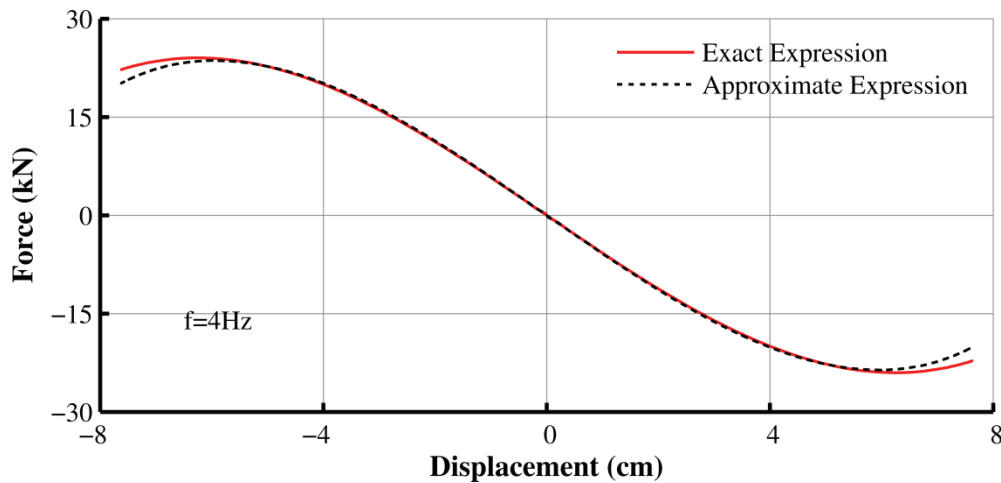


Figure 4-12: Comparison of exact and approximate expressions for NSD force-displacement relation for case of motion with 4Hz frequency

4.4 NSD Relations Considering Friction

4.4.1 Hysteresis due to pin friction

Pins are not frictionless. Moreover, pins have finite dimensions. Consider the assembly shown in Figure 4-13. Let assume that the breakaway force between the pin and the connecting part 2 has not been exceeded. Rotation of the pin occurs because connecting part 1 rotates relatively to the pin. Equivalently the reverse could have been assumed. Independently of exactly how the rotation of the connection takes place, the resultant force acting on the pin is:

$$P_p = \sqrt{P_{px}^2 + P_{py}^2} \quad (4-25)$$

where P_{px} is the horizontal force and P_{py} is the vertical force exerted by the pin on the rotating parts.

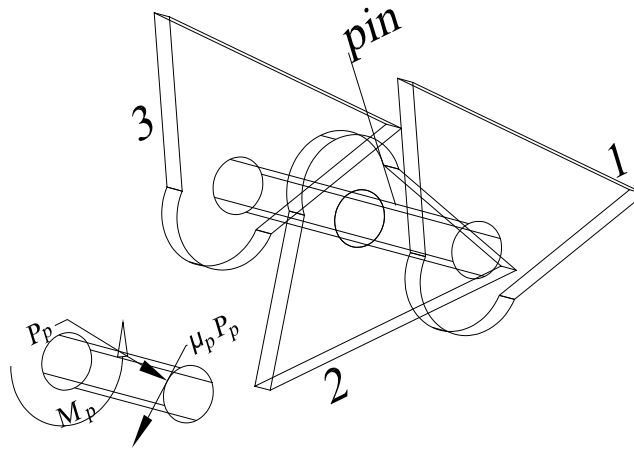


Figure 4-13: Pin friction model

The tangential friction force acting on the perimeter of the pin is given by the following expression, where μ_p is the friction coefficient:

$$S_p \approx \mu_p P_p \quad (4-26)$$

This force always acts tangentially at the perimeter of the pin. Its point of application is of no interest. Rather important is that, regardless of its location, it causes a moment with respect to the center of the pin:

$$M_p = r \mu_p P_p \quad (4-27)$$

where r is the radius of the pin.

In order to model hysteresis in the device one needs to include the friction moments described by Equation (4-27) (acting on every pin) in the equilibrium equations for the NSD. In doing so we consider that the friction coefficient is constant (Coulomb model) and the same for all pins of the device. Moreover, we assume that rotations are small.

The NSD force-displacement relations with the effects of joint friction are derived from the free body diagrams of Figure 4-14 (free bodies of pivot plate and double-hinged columns are shown in bold in Figure 4-14). Note that these diagrams are the same as those used in Section 3.2 with the addition of joint friction moments and an additional force as described below.

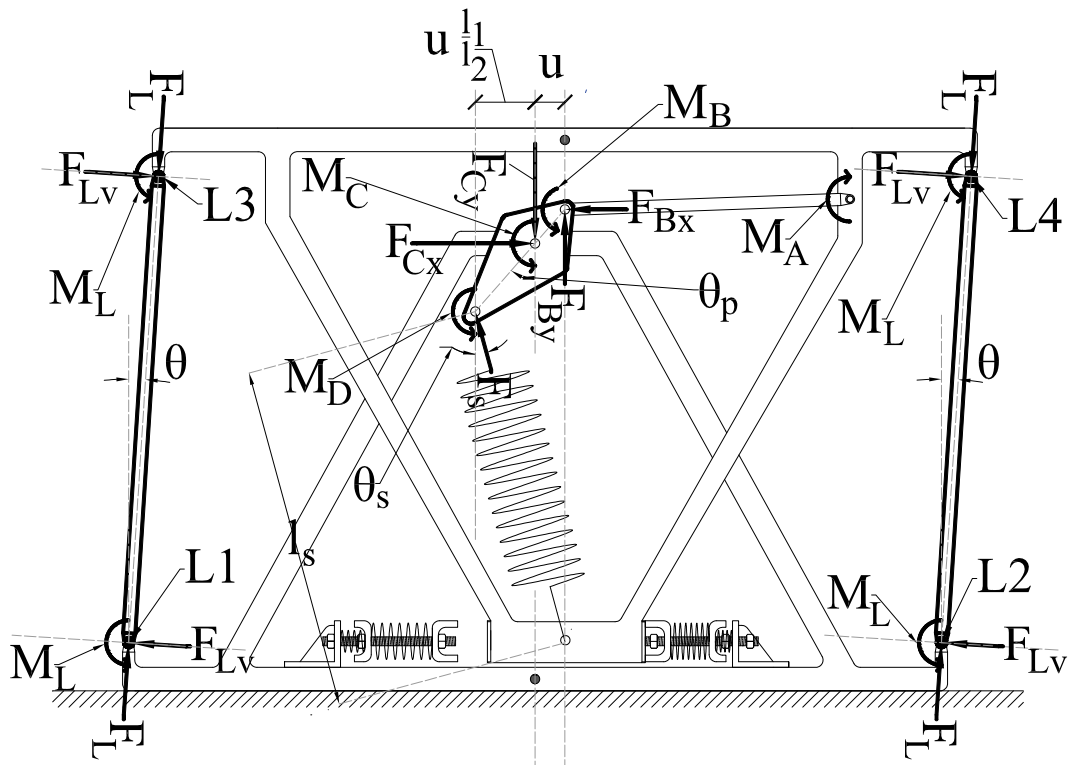


Figure 4-14: Free body diagrams (bodies in bold) used for deriving NSD force-displacement relations with effects of joint friction

At point B, in addition to the lever's axial force, a vertical force is acting on the pivot plate. This force is the shear in the lever caused by the pin friction and is given by:

$$F_{By} = \frac{M_B + M_A}{l_v} \quad (4-28)$$

This force acts in the vertical direction as the rotation of the lever is assumed very small so the lever is essentially horizontal. Accordingly, the lever axial force is in the horizontal direction. From moment equilibrium of the pivot plate in Figure 4-14 around point C, the horizontal force at point B (this is the axial force in the lever) is derived as:

$$F_{Bx} = \frac{F_s \sin \theta_s \sqrt{l_1^2 - (u l_1 / l_2)^2} + F_s \cos \theta_s u l_1 / l_2}{\sqrt{l_2^2 - u^2}} - \frac{M_D + M_B + M_C + u(M_B + M_A) / l_v}{\sqrt{l_2^2 - u^2}} \quad (4-29)$$

M_B, M_C and M_D are the friction moments at points B, C and D, respectively, and F_s and θ_s are given by Equations (3-6) and (3-7), respectively. From horizontal equilibrium of the pivot plate, the horizontal force at point C is obtained as:

$$F_{Cx} = F_{Bx} + F_s \sin \theta_s \quad (4-30)$$

From vertical equilibrium of the pivot plate, the vertical force at point C is:

$$F_{Cy} = F_s \cos \theta_s + F_{By} \quad (4-31)$$

In the derivations of Sections 3.2, 4.2 and 4.3, the shear in the columns of the NSD was assumed zero ($V_L = 0$) since the columns are double-hinged and joint friction was neglected. In the current derivation, there are friction moments at the column joints as shown in Figure 4-14. Accordingly, there is shear in the columns. This shear is constant throughout the height of the column and given by:

$$F_{Lv} = \frac{2M_L}{h} \quad (4-32)$$

F_{Lv} is considered to be acting in the horizontal direction since the angle of rotation of the columns is assumed to be small.

The force of the NSD is derived from horizontal equilibrium of the bottom chevron. This diagram is the same as that of Figure 3-2 with the addition of the shear force from the double-hinged columns:

$$F_{NSD}^{FR} = -F_{Cx} - 2F_L (u/h) + 2F_{Lv} + F_g \quad (4-33)$$

where F_L is the axial force of the double-hinged columns. Assuming small angle of rotation of the double-hinged columns, this force is given by:

$$F_L = F_{Cy} / 2 \quad (4-34)$$

The total force of the NSD is finally obtained by substituting Equations (4-34), (4-32), (4-30) and (4-29) into (4-33) and simplifying:

$$F_{NSD}^{FR} = \{F_{NSD}\} + \left\{ \frac{M_D + M_C + M_B}{\sqrt{l_2^2 - u^2}} + \frac{(M_B + M_A)}{l_v} \left(\frac{u}{\sqrt{l_2^2 - u^2}} + \frac{u}{h} \right) + \frac{4M_L}{h} \right\} \quad (4-35)$$

In this equation, force F_{NSD} is given by Equation (3-11). The equation above can be decomposed into a nonlinear elastic part and a hysteretic part:

$$F = F_{el} + F_{pl} \quad (4-36)$$

F_{el} is given by the first term in the curly brackets and F_{pl} is given by the second term in the curly brackets of Equation (4-35). This decomposition leads to the observation that hysteresis in the NSD will always develop around an elastic baseline that is described by component F_{el} (given by Equation (3-11)). When sliding occurs at all pins, the magnitude of the moments is given by:

$$\begin{aligned} M_{yA} &= M_{yB} = r\mu|P_A| \\ M_{yD} &= r\mu|P_D| \\ M_{yC} &= r\mu|P_C| \\ M_{yL} &= r\mu|P_L| \end{aligned} \quad (4-37)$$

The resultant forces in the pins are given by:

$$\begin{aligned} P_B &= P_A = \sqrt{F_{Bx}^2 + F_{By}^2} \\ P_D &= F_s \\ P_C &= \sqrt{F_{Cx}^2 + F_{Cy}^2} \\ P_L &= \sqrt{F_{Lv}^2 + F_L^2} \end{aligned} \quad (4-38)$$

The hysteretic moment is approximated using the Sivaselvan and Reinhorn (2001) hysteretic model:

$$\delta M = k_o \left\{ 1 - \left| \frac{M}{M_y} \right|^2 \text{sign}(M) \text{sign}(\delta u) \right\} \delta \theta \quad (4-39)$$

In Equation (4-39), $\delta \theta$ is the rotation increment of the pin, δu is the increment of the imposed displacement on the NSD, k_o is the elastic stiffness of the pin prior to slipping and M_y is the magnitude of the moment given by Equation (4-37).

The rotations of the pins are:

$$\begin{aligned} \theta_A &= \arcsin \frac{l_2 - \sqrt{l_2^2 - u^2}}{l_{lv}} \approx \frac{l_2 - \sqrt{l_2^2 - u^2}}{l_{lv}} \\ \theta_B &= \arcsin \frac{u}{l_2} + \theta_A \end{aligned}$$

$$\begin{aligned}\theta_C &= \arcsin \frac{u}{l_2} \\ \theta_D &= \theta_C + \theta_s = \arcsin \frac{u}{l_2} + \arcsin \left[\frac{u}{l_s} \left(1 + \frac{l_1}{l_2} \right) \right] \\ \theta_L &= \arcsin \frac{u}{h} \approx \frac{u}{h}\end{aligned}\tag{4-40}$$

Equation (4-39) requires the calculation of pin rotation increments which can be done by a) calculating the derivatives $d\theta/du$ of the angles in Equations (4-40) with respect to the displacement, b) solving for the rotation differential, and c) approximating the rotation increment $\delta\theta$ with the rotation differential $d\theta$. For example, the rotation increment for joint C is given by the equation below (the process repeats for the rest of the pins):

$$\delta\theta_C = \frac{1}{\sqrt{l_2^2 - u^2}} \delta u\tag{4-41}$$

The result is 27 equations with 27 unknowns. These are Equations (4-28) to (4-32), (4-34), (4-35), (4-37), (4-38), five more equations for the rotation increments (using Equations (4-40) and the procedure described above) and five more equations obtained from Equation (4-39) written for each pin.

Assuming that initially the device is un-deformed, the initial forces and moments are:

$$\begin{aligned}F_{Bx} &= 0; F_{By} = 0; F_{Cx} = 0; F_{Cy} = P_{in}; F_{Lx} = 0; F_{Ly} = P_{in} / 2 \\ P_B &= 0; P_D = P_C = P_{in}; P_L = P_{in} / 2 \\ M_A &= 0; M_B = 0; M_C = 0; M_D = 0; M_L = 0\end{aligned}\tag{4-42}$$

Solution is obtained by an incremental approach in which a very small displacement increment δu is applied, increment rotations $\delta\theta$ are calculated using Equation (4-41) and the like for the other angles, Equation (4-39) is then used to calculate the increment in moment δM for each pin and the moments at each pin for the next step are finally calculated using:

$$M^{n+1} = M^n + \delta M\tag{4-43}$$

The updated moments from Equation (4-43) and the displacement at the next step $u^{n+1} = u^n + \delta u$, are used in Equation (4-35) to calculate the NSD force at step $n+1$. Then, Equations (4-28) to (4-32), (4-34) are used to calculate various quantities, which when used in Equations (4-38) result in the pin forces. These are then substituted in Equations (4-37) to obtain the yield moments at step $n+1$.

Figure 4-15 compares force-displacement loops of the NSD without the GSA force ($F_g=0$) for the properties of Table 3-1 for a cycle of motion (frequency is not relevant as inertia effects are neglected) and for various values of the friction coefficient. The pin radius is $r=1.43\text{cm}$ —the actual value in the tested device. The top graphs compare loops of the NSD with and without friction. The bottom graphs only show the hysteretic component of the loops. The results show a complex hysteretic component of force, which however, is negligible for pin friction coefficient of 0.1. Noting that friction in the pins typically is about 0.2, the effects of friction should generally be small but not necessarily negligible.

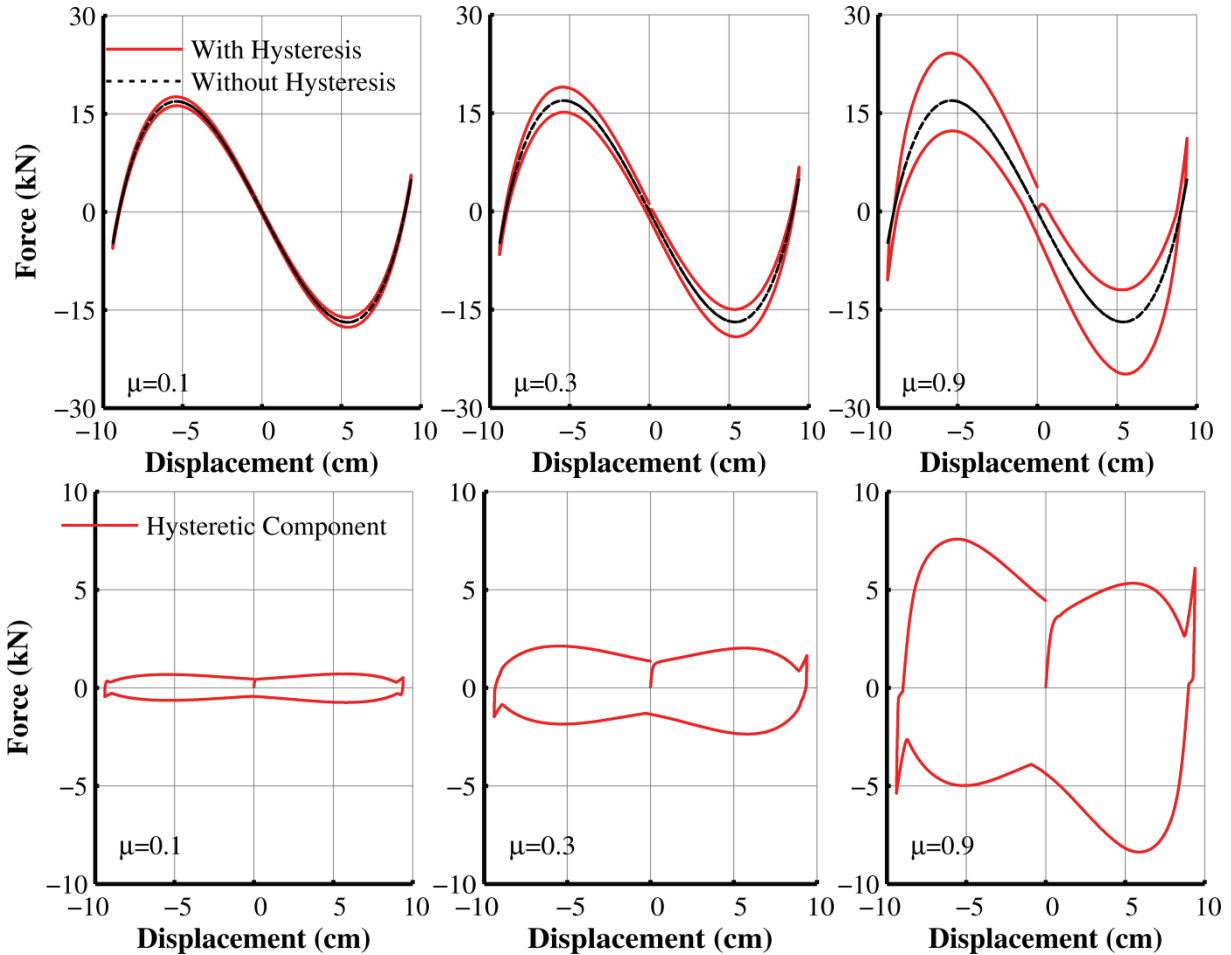


Figure 4-15: Force-displacement loops of NSD without GSA with properties of Table 3-1 and various values of pin friction coefficient

4.4.2 Hysteresis in SAP2000 model of NSD

The hysteretic behavior of the NSD is complex and the various contributors to hysteresis cannot be isolated and measured in experiments. This suggests that an attempt to model the hysteretic behavior (and other effects) of the NSD by explicitly modeling every detail in a finite element model would still require testing of the device so that the model is calibrated (details of friction in the joints still need to be assumed) so that the behavior of the analyzed NSD matches the one

observed in experiments. Alternatively and in much simpler way, hysteresis may be introduced in the previously described SAP2000 model of the NSD by introducing a single hysteretic element that captures either the exact hysteresis observed in experiments, or a simple constant hysteresis produced by a Coulomb friction model that approximates the experimentally observed behavior. Approximately, the NSD hysteresis can be captured by assuming that the hysteretic force is constant and independent of displacement (equivalent to constant or Coulomb friction). This behavior can be easily modeled by adding a hysteretic element in parallel to the element assembly described in Section 3.4 and shown in Figure 3-13. A link element (Wen element in SAP2000) needs to be added between joints J1 and J2 and overlapping with elements ML1 and ML2 in Figure 3-13. Results comparing the analytical derivations that assume non-constant hysteresis versus the SAP2000 results with constant hysteresis are shown in Figure 4-16. The SAP2000 element was subjected to a prescribed displacement history at joint J1. The analytical model was based on the theory of Section 4.4.1 and the NSD had the parameters of Table 3-1. The friction coefficient for the pins was set equal to 0.2. The resulting force-displacement loops with these parameters were in good agreement with the NSD experimental response. The SAP2000 model followed the description in Section 3.4 with an added hysteretic element with yield force equal to 0.73kN. This value is the zero displacement force intercept in the analytical model. Evidently, the simple SAP2000 with hysteresis produces results in good agreement with the analytical model.

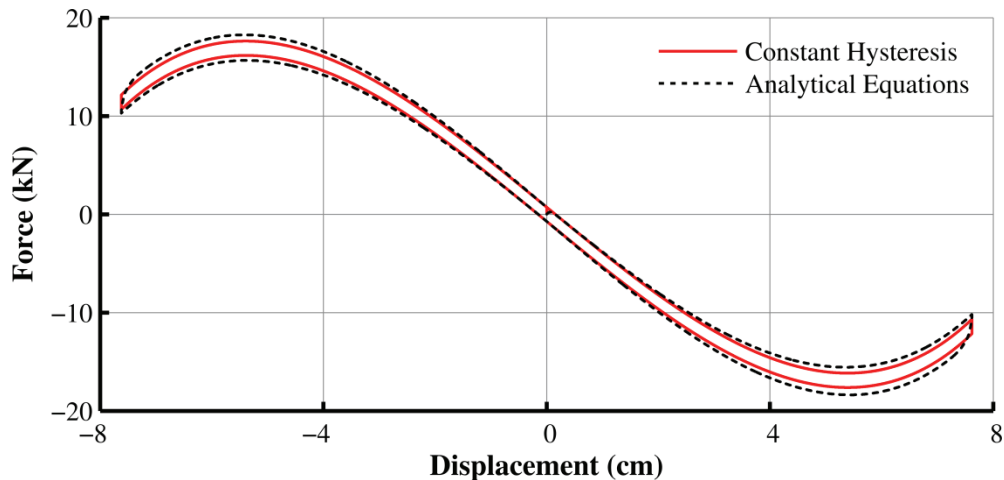


Figure 4-16: Comparison of force-displacement loops of NSD without GSA produced by analytical model and by SAP2000 constant friction model

A more complex model in SAP2000 employs an assembly of elements as shown in Figure 4-17 that can generate a hysteretic force proportional to the NSD force. A description and some properties of the link elements of the model are presented in Table 4-2. Figure 4-18 shows experimental results for the force-displacement relation of the tested NSD (properties of Table 3-1) without the GSA and identifies quantities that are needed for the model calibration. Note that the red line in the figure shows the measured force-displacement relation and the black line represents the calculated elastic relation (baseline) of the NSD. This baseline relation was

calculated from the measured force-displacement relation after averaging the force values in the ascending and descending branches of the loops within sequential windows of displacement.

The element depicted in Figure 4-17 consists of:

- 1) Seven joints of which J1 represent the top of the NSD, J2, J6 and J7 represent the bottom of the NSD and J3, J4 and J5 are intermediate joints.
- 2) Multi-linear elastic element ML1 that simulates the NSD without GSA force exclusive of hysteresis. The force-displacement relation is calculated using the analytical model of Section 3.2 for the NSD without the GSA and imported to program SAP2000. The shear deformation location of ML1 is at its bottom joint J2 so that the overturning moment is transferred at the top joint J3. The vertical stiffness of ML1 is zero.
- 3) Rigid elements FRL and FRR (beam elements of high stiffness) to connect the top of the NSD and element ML1 to flat sliders FPL and FPR located at distance $b/2$ on each side of element ML1. Rigid element FRT to connect the top of the NSD to the superstructure. Frame element FRT must have releases in the axial, torsional and in plane bending deformations at joint J3 so that only a horizontal shear force is developed by element FRT at joint J3. FRT must not have releases for out of plane bending in order to provide stability of the assembly below; however it needs to be ensured that none of the elements below generate forces in the out-of-plane direction of the NSD. Also, the in-plane bending moment that is introduced by the assembly and applied to the superstructure at joint J1 is dependent on the length of element FRT. This length should be selected such that the NSD force develops at the correct location.
- 4) Flat sliders FPL and FPR. Due to the configuration of the sliders with respect to element ML1, the overturning moment created by the NSD force in element ML1 results in axial compressive forces on either slider FPL or slider FPR depending on the direction of the force (e.g., when the force points towards the right, slider FPR is compressed whereas slider FPL uplifts and has zero axial force). This enables the generation of displacement-dependent friction force with a zero value at zero displacement of NSD. Elements FPL and FPR should be active only in the vertical and horizontal degrees of freedom. The two elements must have the same vertical stiffness (effective and “nonlinear stiffness” in SAP2000) and their elastic stiffness should be large enough compared to the negative stiffness of the NSD for small displacements as given by the right hand side of Equation (3-28). The two elements are flat sliders so that their radius of curvature should be infinite (specified as zero in SAP2000). They should have the same friction coefficient given by Equation (4-44) of which the terms have been defined in Figure 4-18.

$$\bar{\mu} = \frac{F_{\max} - F_{el\max} - F_y}{F_{el\max}} \quad (4-44)$$

- 5) Element WEN to supplement the displacement-dependent friction force generated by elements FPL and FPR. This is necessary as elements FPL and FPR do not produce a hysteretic force at zero displacement as the actual NSD. Element WEN is connected directly to joint J1 so that it does not affect the axial loads on FPL and FPR. WEN generates a hysteretic force in the horizontal direction with yield force value equal to force F_y identified in Figure 4-18 (zero displacement intercept of NSD force).
- 6) Elements LINL and LINR which are multi-linear elastic elements that overlap with FPL and FPR, respectively. Their purpose is to provide the assembly with constant vertical stiffness when the FPL and FPR elements uplift and also to avoid numerical problems. The elements generate force only in the vertical direction, have zero stiffness (and force) in compression, and their tensile stiffness is constant and equal to the vertical stiffness of elements FPL and FPR.
- 7) Element ML2 that simulates the GSA force. It is connected between joints J1 and J2 so that it does not affect the axial (overturning) loads on elements FPL and FPR and, therefore, it does not contribute to hysteresis (whereas element ML1 is connected to joints J2 and J3 in order to cause axial loads on the slider elements and generate hysteresis). The force-displacement relation is calculated using the analytical model of Section 3.3 for the GSA and imported into program SAP2000.

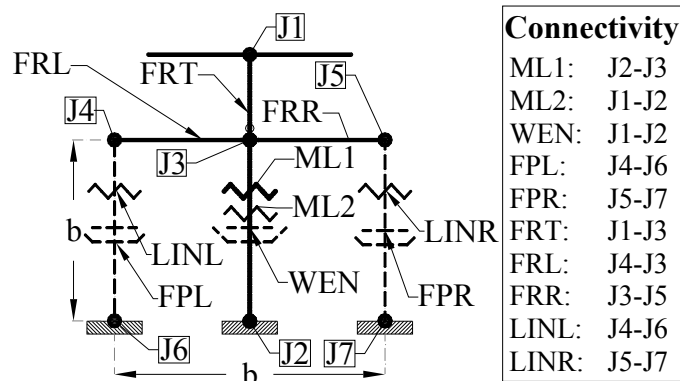


Figure 4-17: SAP2000 model of NSD capable of generating complex hysteresis

Table 4-2: Description of elements of SAP2000 model of NSD with complex hysteresis

Element ID	Type of Link Element	Simulates	Releases ² / Inactive DOF's	Shear Deformation Location	Properties
ML1	ML ¹	NSD	U1,U3,R2,R3	J2	U2 ³
ML2	ML ¹	GSA	U1,U3,R1,R2,R3	J1	U2 ³
FPL	FS ¹	Hysteresis	U3,R1,R2,R3	J4	
FPR				J5	
WEN	Wen	Hysteresis	U1,U3,R1,R2,R3	J1	U2
FRT	Frame	N/A	At J3:P,T,M3	N/A	Rigid
FRL	Frame	N/A	None	N/A	Rigid
FRR	Frame	N/A	None	N/A	Rigid
LINL	ML ¹	N/A	U2,U3,R1,R2,R3	Any location as it does not affect	U1
LINR					U1

1. ML=Multi-Linear Elastic, FS: Flat Slider
 2. The releases for the link elements are applied by not activating the DOF's in the link element definitions
 3. The force displacement is calculated based on section 3.2 and pasted into the link element definition

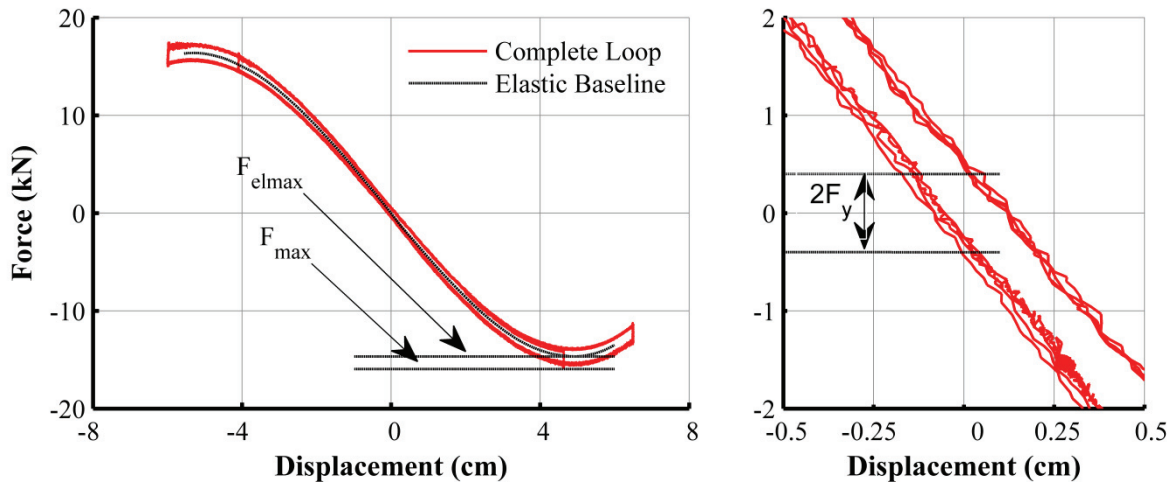


Figure 4-18: Experimental force-displacement relation of NSD without GSA and quantities for model calibration

The masses of the link elements in this model need to be very small so that they do not affect the analysis results. Incorporating mass to capture inertia effects as described in Section 4.3 will produce incorrect results as any mass assigned to element ML1 (based on Equation 4-24) will result in friction at zero displacement to elements FPL and FPR, which will alter the behavior of the assembly.

Results for the force-displacement loop of the NSD without GSA with the properties of Table 3-1 obtained by this element are compared in Figure 4-19 to results obtained by the analytical model of Section 4.4.1. Results are in good agreement but not identical due to the artificial nature of the SAP2000 model.

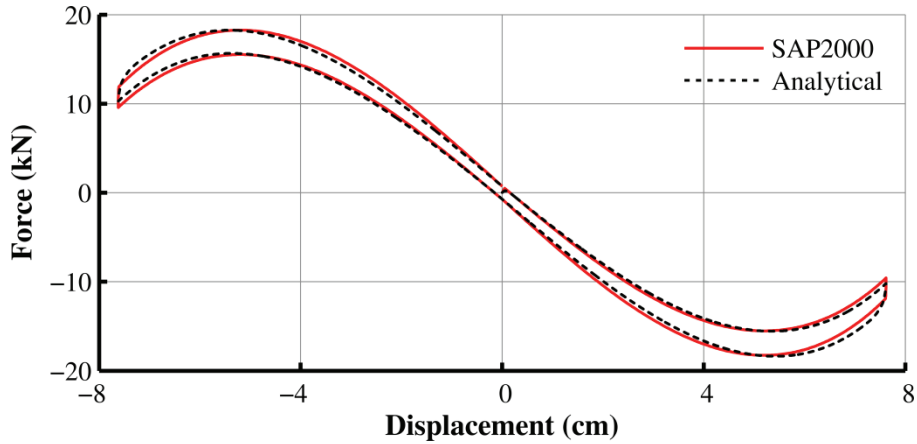


Figure 4-19: Comparison of force displacement loops of NSD without GSA produced by the analytical model with hysteresis and the SAP2000 force-proportional hysteresis model

4.5 NSD Relations Considering Member Flexibility

In this section, flexibilities in the top and bottom frame elements of the NSD assembly are considered. When these elements are considered rigid, as done in the formulation presented so far, point C (see Figure 2-3 and Figure 2-4) is motionless (or fixed) with respect to the bottom of the device and point E undergoes the motion of the top of the device with respect to the bottom. This is only true if the top and bottom chevrons were rigid. The bottom chevron could be considered rigid if it was fixed to the ground and the top chevron was connected to a rigid beam. The tested device had the top and bottom beams made of channels with their weak axis in the direction perpendicular to the plane of the device. Moreover, the channels were not continuously supported so that some flexure could occur in the channel sections. This introduced some limited flexibility in the assembly which is investigated herein.

Figure 4-20 illustrates the model used for consideration of flexibilities. A spring with stiffness k_b is introduced connecting point C to the ground to represent the combined flexibilities of the bottom chevron and its bottom beam (channel). A spring with stiffness k_t is introduced at the midpoint of the top beam in order to represent the combined flexibilities of top chevron and its top beam (channel).

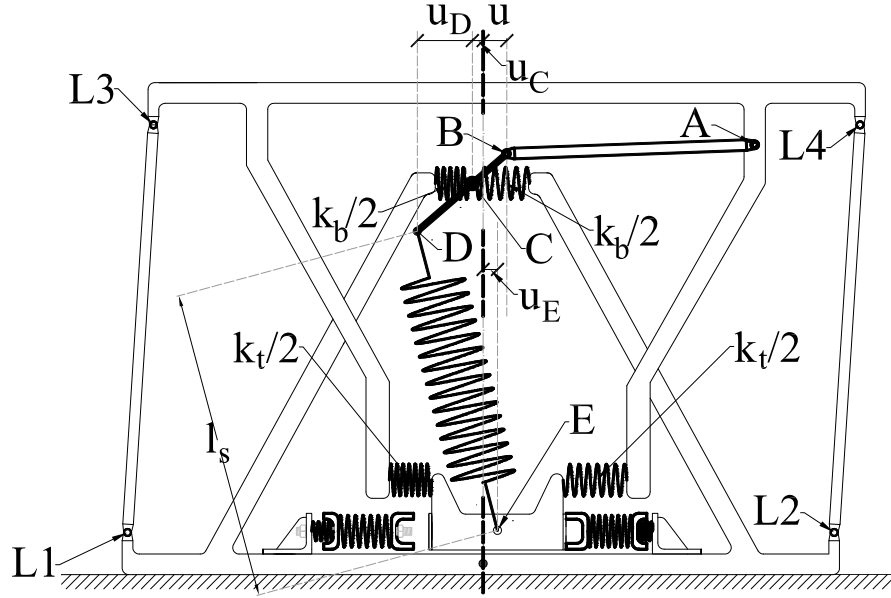


Figure 4-20: Model of NSD with top and bottom chevron flexibility

Two additional degrees of freedom are introduced: the horizontal displacement of point C and the horizontal displacement of point E. Note that previously $u_E = u$ but now the two displacements differ so that:

$$u_{fE} = u_E - u \quad (4-45)$$

Where u_{fE} is the deformation of spring with stiffness k_t . The rotation of the pivot plate is:

$$\theta_p = \arcsin\left(\frac{u - u_C}{l_2}\right) \quad (4-46)$$

The vertical displacement of point B is:

$$v_B = l_2 - \sqrt{l_2^2 - (u - u_C)^2} \quad (4-47)$$

Also point D moves horizontally in the opposite direction than displacement $(u - u_C)$ by amount u_D and vertically by an amount v_D :

$$\begin{aligned} u_D &= -(u - u_C)(l_1/l_2) + u_C \\ v_D &= l_1 - \sqrt{l_1^2 - (u - u_C)^2 (l_1/l_2)^2} \end{aligned} \quad (4-48)$$

The length of the spring is now given from Equation (4-49) instead of Equation (3-4):

$$l_s = \sqrt{\left(l_p + l_1 - \sqrt{l_1^2 - \left((u - u_C)(l_1/l_2)\right)^2}\right)^2 + \left[(u - u_C)(l_1/l_2) - u_C + u_E\right]^2} \quad (4-49)$$

Considering equilibrium of moments about point C for the pivot plate (free body diagram of Figure 3-1) the force at B is calculated as:

$$F_B = \frac{F_s}{\sqrt{l_2^2 - (u - u_C)^2}} \left[\cos \theta_s (u - u_C) \frac{l_1}{l_2} + \sin \theta_s \left(\sqrt{l_1^2 - \left((u - u_C) \frac{l_1}{l_2}\right)^2} \right) \right] \quad (4-50)$$

The sine and cosine of the spring inclination angle are now given by:

$$\begin{aligned} \sin \theta_s &= \frac{(u - u_C)(l_1/l_2) - u_C + u_E}{l_s} \\ \cos \theta_s &= \frac{\left(l_p + l_1 - \sqrt{l_1^2 - \left((u - u_C)(l_1/l_2)\right)^2}\right)}{l_s} \end{aligned} \quad (4-51)$$

The horizontal reaction at point C is obtained from horizontal equilibrium of forces acting on the pivot plate as shown in Figure 3-1 and using Equations (4-50), (4-51) and (3-6) for the spring force:

$$F_{Cx} = \left(\frac{P_{in} + K_s l_p}{l_s} - K_s \right) \frac{l_1}{l_2} \left\{ \left[\frac{(l_p + l_1)}{\sqrt{l_2^2 - (u - u_C)^2}} + 1 \right] (u - u_C) + (u_E - u_C) \left(1 + \frac{l_2}{l_1} \right) \right\} \quad (4-52)$$

Moreover:

$$F_{Cx} = k_b u_C \quad (4-53)$$

Also, the force acting at point E in the horizontal direction is related to the displacement of point E relative to the top beam by:

$$-\left(\frac{P_{in} + K_s l_p}{l_s} - K_s \right) \frac{(u - u_C)(l_1/l_2) - u_C + u_E}{l_s} + F_g = k_t (u - u_E) \quad (4-54)$$

The force-displacement relation of the GSA is related to the total displacement of point E and is given by:

$$F_g = \begin{cases} k_{s1}u_E, & 0 \leq u_E \leq u'_y \\ k_{s1}u'_y + \frac{k_{s2}k_{s1}}{k_{s2} + k_{s1}}(u_E - u'_y) & u_E > u'_y \end{cases} \quad (4-55)$$

$$u'_y = \frac{P_{is2}}{k_{s1}}$$

Finally, the total NSD force can be obtained from the free body diagram in Figure 3-2:

$$F_{NSD} = -F_{Cx} - \left(\frac{P_{in} + K_s l_p}{l_s} - K_s \right) \left(l_p + l_1 - \sqrt{l_1^2 - ((u - u_C)(l_1/l_2))^2} \right) (u/h) + F_g \quad (4-56)$$

The second term in the equation above is the horizontal component of the axial load of the double hinged columns. Equations (4-56), (4-55), (4-54), (4-53) and (4-52) represent a system of five nonlinear equations with five unknowns ($F_{Cx}, F_g, F_{NSD}, u_C, u_E$), which cannot be explicitly solved. The unknowns are collected in a vector \mathbf{x} and the equations are arranged in the following form:

$$\mathbf{x} = \begin{bmatrix} F_{Cx} & F_g & F_{NSD} & u_C & u_E \end{bmatrix}^T \quad (4-57)$$

$$\mathbf{f}(\mathbf{x}) = \mathbf{0}$$

In Equation (4-57), \mathbf{f} is a function of vector \mathbf{x} . The initial conditions at $t=0$ (or equivalently at $u=0$) are \mathbf{x}_0 and the solution of Equations (4-57) is obtained for each increment of displacement u by iteration:

$$\mathbf{x}_{n+1}^{(j+1)} = \mathbf{x}_{n+1}^{(j)} - D\mathbf{f}^{-1}(\mathbf{x}_{n+1}^{(j)})\mathbf{f}(\mathbf{x}_{n+1}^{(j)}) \quad (4-58)$$

The matrix derivative $D\mathbf{f}^{-1}$ in (4-58) is given in Equation (4-59) and can be calculated either analytically or numerically.

$$D\mathbf{f}^{-1}(\mathbf{x}) = \begin{bmatrix} \frac{\partial f_1(x)}{\partial F_{cx}} & \dots & \dots & \dots & \frac{\partial f_1(x)}{\partial u_E} \\ \cdot & \cdot & & & \cdot \\ \cdot & & \cdot & & \cdot \\ \cdot & & & \cdot & \cdot \\ \frac{\partial f_5(x)}{\partial F_{cx}} & \dots & \dots & \dots & \frac{\partial f_5(x)}{\partial u_E} \end{bmatrix} \quad (4-59)$$

where f_i is the i -th component of vector \mathbf{f} . For each value of displacement u considered, Equation (4-58) is employed repeatedly until the following condition is satisfied, where ε is a specified truncation error parameter:

$$\|\mathbf{x}_{n+1}^{(j+1)} - \mathbf{x}_{n+1}^{(j)}\| \leq \varepsilon_{\mathbf{x}=\mathbf{x}_{n+1}^{(j)}} \quad (4-60)$$

Using the NSD properties of Table 3-1, calculations were performed for the NSD force-displacement relation without the GSA and results are presented in Figure 4-21 for the case without flexibilities and three cases with only flexibility for the bottom chevron and beam, specified by three values of stiffness k_b . Similarly, Figure 4-22 compares results for the NSD with GSA when only the top chevron and beam are assumed flexible with three values of stiffness k_t .

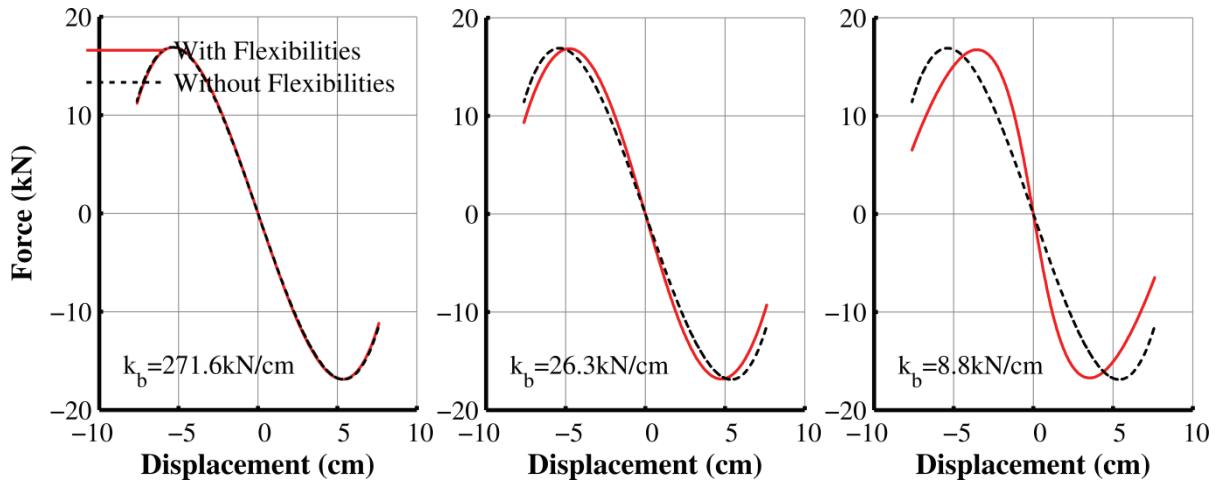


Figure 4-21: Force-displacement relations of NSD without GSA for rigid top and for flexible bottom chevron

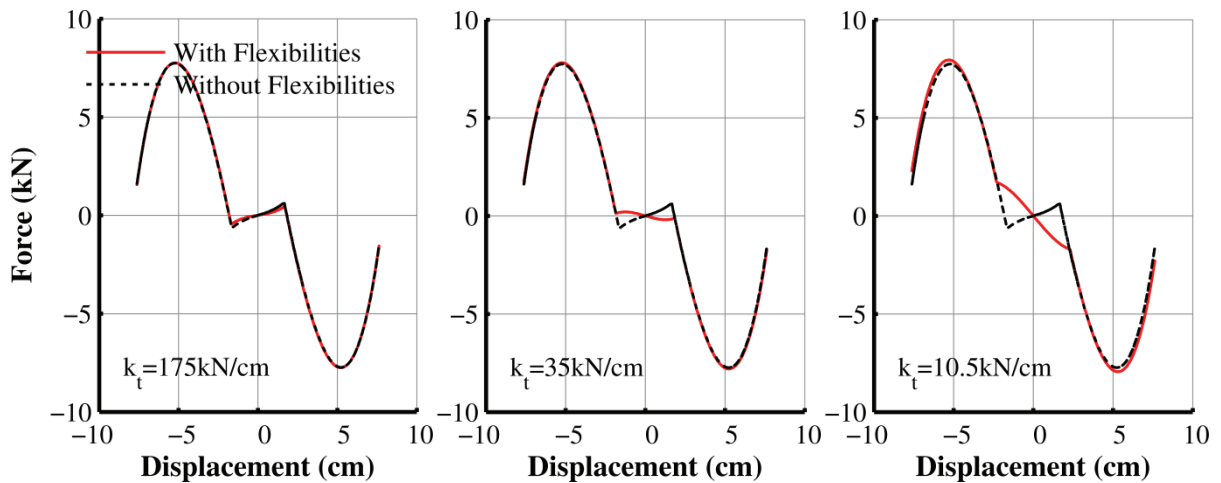


Figure 4-22: Force-displacement relations of NSD with GSA for flexible top and for rigid bottom chevron

It can be seen that a flexible bottom chevron (Figure 4-21) increases the negative stiffness generated by the device. This is due to the fact that point C now moves and therefore for the same imposed displacement on the NSD the pivot plate-spring mechanism rotates more than if the frame elements were rigid. However, it should be noted that this requires unrealistically high flexibility.

In the case of a flexible top chevron in Figure 4-22, only the NSD with GSA behavior is affected (comparisons not shown here demonstrated that when the NSD without GSA is studied there is insignificant effect of the top chevron flexibility on the NSD force).

In general, the top and bottom beams connecting the chevrons to the structure above and below the NSD will have very large stiffness eliminating any effects of the type shown in Figure 4-21 and Figure 4-22. However, in the tested device there was requirement to measure the force transmitted by the NSD so that the NSD was mounted on two load cells. This, coupled with the use of channels bent about their weak axis (required due to space limitations) resulted in some flexibility with undesirable behavior. This was mitigated by installing the device on four load cells as shown in Figure 2-1. The top chevron for the current device properties was sufficiently stiff so that it did not affect the device behavior.

4.6 Advanced Force-Displacement Relation of Gap Spring Assembly

The GSA should have the gap clearance (see Figure 2-6 and Figure 4-23) large enough such that $d_{gap} > P_{is2}/k_{s1}$. This ensures that the gap is open during operation of the GSA. This section investigates the case when the gap closes. Particularly, the following cases are investigated: (a) the case $d_{gap} < P_{is2}/k_{s1}$ that results in closing of the gap, and (b) the case in which the gap is reduced by adjustment of nut NG in Figure 4-23 so that spring S1 is pre-loaded. It is shown that in both cases the behavior of the GSA is abnormal and should be avoided. Both of these cases were also experimentally investigated and the analysis presented herein explains the undesirable observed behavior.

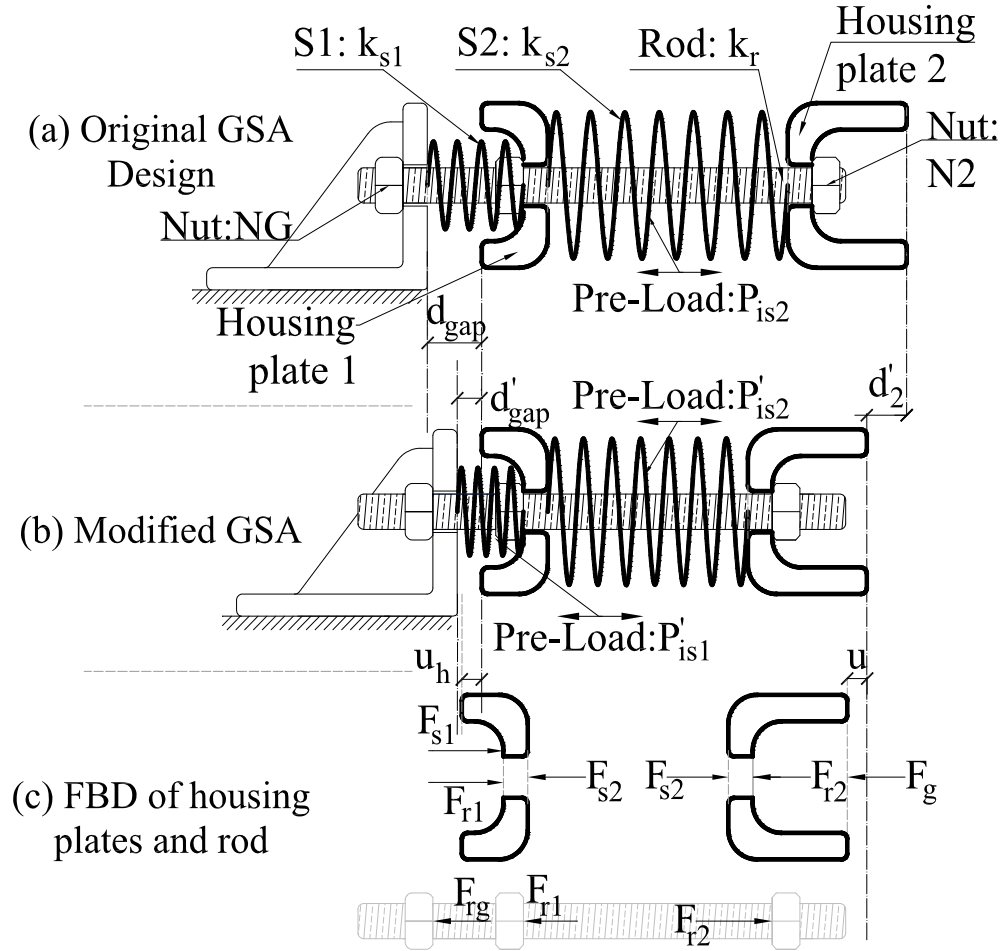


Figure 4-23: Free body diagrams of housing plates 1 and 2 and rod of GSA

Assume a case where the GSA (shown in Figure 4-23(a) in the original configuration prior to any modifications) is subjected to the following modifications: (a) Nut N2 is adjusted (tightened) by a distance d'_2 as shown in Figure 4-23(b) so that the pre-load of spring S2 is increased from value P_{is2} to value P'_{is2} , such that $d_{gap} < P'_{is2}/k_{s1}$ and (b) Nut NG is adjusted so that the physical gap opening is reduced from d_{gap} to d'_{gap} as shown on the left in Figure 4-23(b) so that the pre-load in spring S1 is now given by $P_{is1} = k_{s1}(d_{gap} - d'_{gap})$. The modified GSA in its un-deformed shape is shown in Figure 4-23(b). The forces acting on its components are shown in Figure 4-23(c) when the GSA deforms by amount u due to the action of force F_g and prior to the gap closing. These forces are related to displacements by:

$$\begin{aligned}
F_{s1} &= k_{s1} (d_{gap} - d'_{gap}) + k_{s1} u_h \\
F_{s2} &= P'_{is2} + k_{s2} (u - u_h) \\
F_{rg} &= \begin{cases} k_r (P_{is1}/k_r - u_h), & u_h \leq P_{is1}/k_r \\ 0 & u_h > P_{is1}/k_r \end{cases} \\
F_{r2} &= \begin{cases} k_r (P'_{is2}/k_r - u + u_h), & u \leq P'_{is2}/k_r + u_h \\ 0 & u > P'_{is2}/k_r + u_h \end{cases}
\end{aligned} \tag{4-61}$$

In the equations above, the term P'_{is2}/k_r is the initial deformation of the rod due to force P'_{is2} and P_{is1}/k_r is the initial deformation of the rod due to force P_{is1} (where for simplicity the length of the two segments of the rod passing through S1 and S2 are assumed equal). The expressions for forces F_{rg} and F_{r2} in the equations above give rise to a variety of behaviors depending on the properties of the springs. From the free body diagrams of Figure 4-23(c), the equilibrium equations of housing plates 1 (valid prior to the gap closing) and 2 and the rod are given by:

$$\begin{aligned}
F_{s1} + F_{r1} - F_{s2} &= 0 \\
F_{r2} + F_g - F_{s2} &= 0 \\
F_{r1} &= F_{r2} - F_{rg}
\end{aligned} \tag{4-62}$$

Substituting Equations (4-61) into Equations (4-62), and considering $F_{rg} > 0$ and $F_{r2} > 0$, results in the force-displacement relation of the GSA:

$$\begin{aligned}
F_g &= \frac{(k_{s1} + k_r)(k_{s2} + k_r)}{2k_r + k_{s1} + k_{s2}} u \\
u_h &= \frac{k_{s2} + k_r}{2k_r + k_{s1} + k_{s2}} u
\end{aligned} \tag{4-63}$$

Equation (4-63) is valid until $u_h = P_{is1}/k_r$. The first transition in stiffness occurs when $u_h = P_{is1}/k_r$ and the corresponding transition force and displacement can be readily calculated from Equation (4-63) by using $u_h = P_{is1}/k_r$. The result is:

$$\begin{aligned}
F_g &= \frac{k_{s1} + k_r}{k_r} P_{is1} \\
u &= \frac{P_{is1}}{k_r} \frac{2k_r + k_{s1} + k_{s2}}{k_{s2} + k_r}
\end{aligned} \tag{4-64}$$

Substituting Equations (4-61) into Equations (4-62), and considering $F_{rg} = 0$ and $F_{r2} > 0$ leads to the force-displacement relation following the first transition:

$$\begin{aligned}
F_g &= P_{is1} \frac{k_{s2} + k_r}{k_{s2} + k_r + k_{s1}} + k_{s1} \frac{k_{s2} + k_r}{k_{s2} + k_r + k_{s1}} u \\
u &= \frac{k_{s2} + k_r + k_{s1}}{k_{s2} + k_r} u_h + \frac{P_{is1}}{k_{s2} + k_r}
\end{aligned} \tag{4-65}$$

The gap will close prior to the rod separating from housing plates 1 and 2 if the displacement given by Equation (4-65) for $u_h = d'_{gap}$ is smaller than $u = P'_{is2}/k_r + d'_{gap}$ and force F_{r2} will still have a nonzero force ($F_{r2} > 0$). This leads to the following condition:

$$d_{gap} < \frac{P'_{is2}}{k_r} \frac{k_r + k_{s2}}{k_{s1}} \approx \frac{P'_{is2}}{k_{s1}} \tag{4-66}$$

If the condition above is violated, the GSA will exhibit a behavior similar to the one described in Section 3.3. If the condition of Equation (4-66) is satisfied, the next transition in the force-displacement relation will occur when the gap closes. Note that the above condition is independent of the modification to the physical gap opening. The force and displacement at which the gap closes are calculated by substituting $u_h = d'_{gap}$ into Equation (4-65). The result is:

$$\begin{aligned}
F_g &= k_{s1} d_{gap} \\
u &= \frac{k_{s2} + k_r + k_{s1}}{k_{s2} + k_r} d'_{gap} + \frac{P_{is1}}{k_{s2} + k_r}
\end{aligned} \tag{4-67}$$

After the gap closes, the force-displacement relation of the GSA is determined by solving the second of Equations (4-62) for force F_g and using Equation (4-61) for $u_h = d'_{gap}$ and $u \leq P'_{is2}/k_r + d'_{gap}$ ($F_{rg}=0$ and $F_{r2} > 0$). The result is:

$$F_g = (k_{s2} + k_r)(u - d'_{gap}) \tag{4-68}$$

The next transition in the force-displacement relation of the GSA occurs when $F_{r2}=0$ (or equivalently $u - d'_{gap} = P'_{is2}/k_r$) which leads to $F_g = (k_{s2} + k_r)(P'_{is2}/k_r)$. Following this transition point, the force-displacement relation of the GSA is determined by combining the second expression in Equation (4-62) (the first expression is not valid after the gap closes) with Equation (4-61) for $F_{rg}=0$ and $F_{r2}=0$. The result is:

$$F_g = P'_{is2} + k_{s2}(u - d'_{gap}) \tag{4-69}$$

Figure 4-24 illustrates the force-displacement relation of the GSA as described by Equations (4-63) to (4-69) and by considering that the stiffness of the rod is much larger than the stiffness of springs S1 and S2 ($k_r \gg k_{s1} > k_{s2}$).

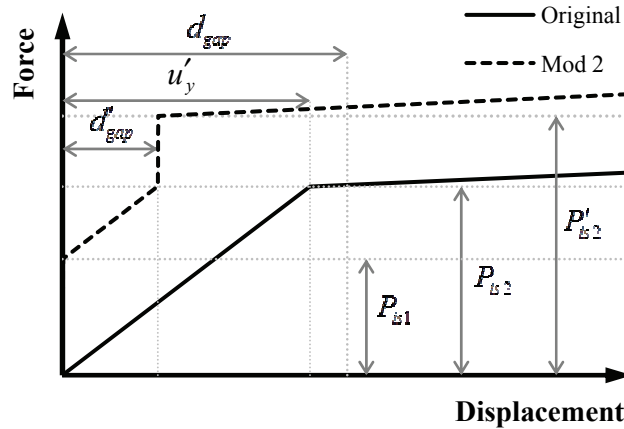


Figure 4-24: Force-displacement relation of modified GSA

The behavior depicted by the dashed line in Figure 4-24 was actually observed for the GSA in the shake table testing. The abrupt increase of force at zero displacement of the tested device occurred because nut NG was erroneously adjusted in the laboratory so that the physical gap was reduced from its original value d_{gap} to d'_{gap} . The abrupt increase of GSA force seen in at displacement equal to d'_{gap} was also observed in testing and was the result of the gap closing (due to spring S2 having a preload different than specified and due to spring S1 having a stiffness different than specified leading to $d_{gap} < P'_{is2} / k_{s1}$).

4.7 Detailed Model of NSD in Program SAP2000

A detailed, explicit model of the NSD was developed in program SAP2000 to further validate the analytical models developed earlier. The model is illustrated in Figure 4-25.

The pre-compressed spring is modeled as a frame element (member DE in Figure 4-25) with a cross section area calculated so that it yields the stiffness of the spring in the axial direction. The moment of inertia of the spring should be very small but non zero. Frame elements that are perpendicular to the spring axis are connected at joints D and E and shown as $D - D''$ and $E - E''$ ($E - E''$ is not connected to the top chevron) respectively in Figure 4-25. These elements are used for the application of the preload. The preload is applied as external point element load (not joint load) in the local coordinate system of the frame elements directly at joints D and E without any eccentricity. The reason for using this procedure is that SAP2000 rotates the element loads together with the frame elements but it does not rotate joint loads together with the joints in large displacement analysis.

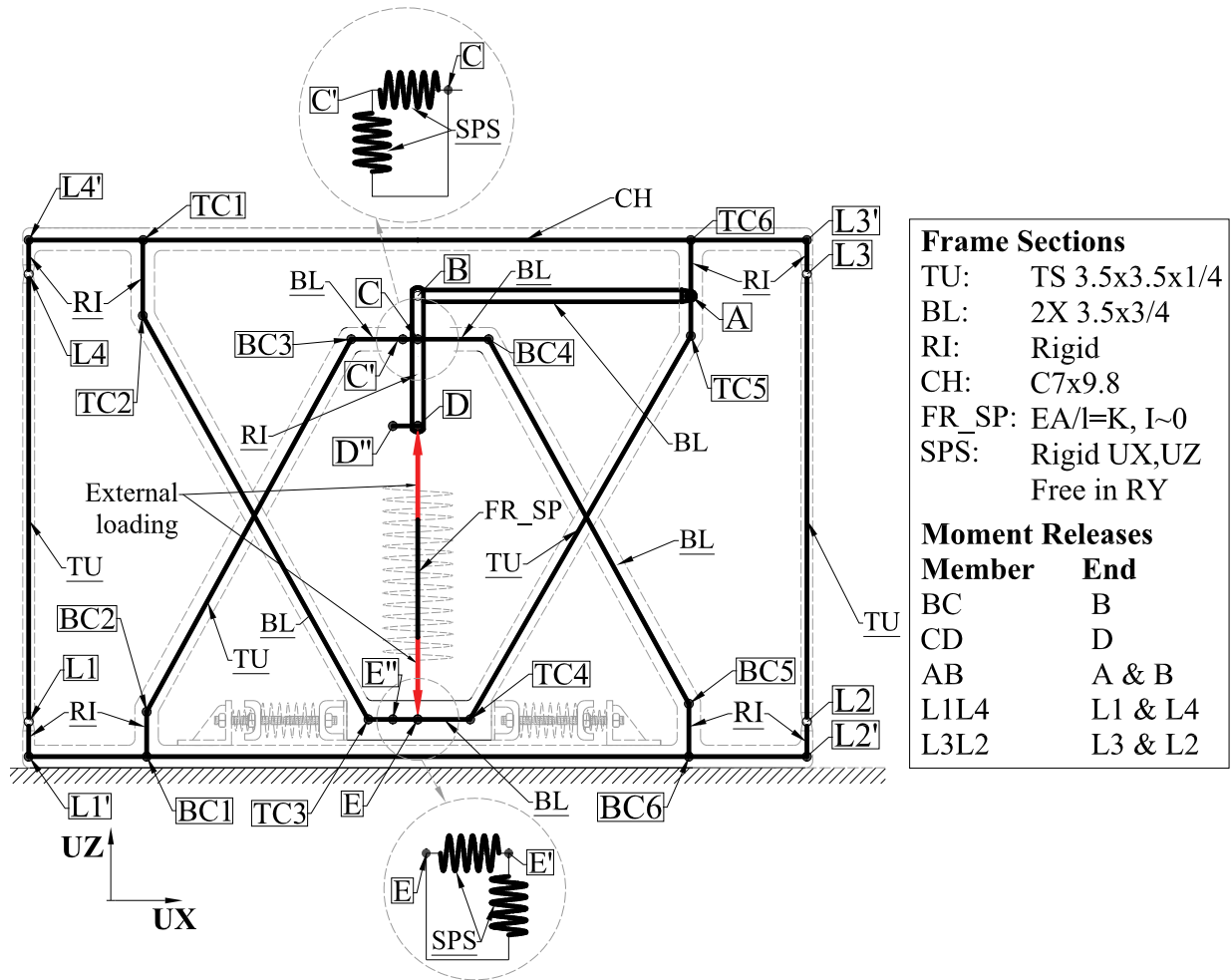


Figure 4-25: Detailed model of NSD in program SAP2000

The frame element assembly $D''-D-E-E''$ needs to deform as a rigid body with the rotations at all joints being calculated as the rigid body rotation of the spring. In order to achieve zero relative rotation between the spring and the supplemental frame elements ($D-D''$ and $E-E''$), the supplemental frame elements need to be rigid. Moreover, the spring frame element must have small but non-zero bending stiffness so that it allows for unrestricted rotation of the supplemental frame elements ($D-D''$ and $E-E''$). To ensure that the joint rotations are equal to the rigid body rotation of the spring, special detailing must take place at the connections of the spring on top and bottom. At point D free rotation between member CD and member DE must be allowed and the rotation at point D must be equal to the rigid body rotation of the spring (member DE). In order to achieve this, a moment release must be specified at joint D for member CD but not for member DE. The situation is complicated at the bottom of the spring since the spring should also be free to rotate with respect to its surrounding elements. This problem cannot be solved by specifying moment releases since the frame element is continuous and applying a moment release on the spring would make member $E-E''$ unstable. In order to resolve this problem, two joints are introduced at point E (joints E and E') which coincide but for clarity are shown in

different positions in the window at the bottom of Figure 4-25. The two joints are connected using zero length springs that have sufficiently large stiffness in order to prevent any relative translation between the two joints. Free rotation is allowed between the two joints.

The pivot plate is modeled as two rigid beam elements that merge into point C. In order to model the connection between the pivot plate and the bottom chevron at point C, an additional joint C' is introduced at the location of joint C (the two joints are shown for clarity in different locations at the top of Figure 4-25). The two joints are connected with stiff axial springs in order to ensure equal translations but independent rotations while the continuity of the bottom chevron is maintained.

In a sample analysis, the model was subjected to a prescribed displacement history at the top channel and solution in program SAP2000 was obtained by the direct integration method and by activating large displacements capability. The preload was applied as a separate static nonlinear load case and the results were used as the initial conditions for the displacement history analysis. Joint friction was neglected. Results obtained for the NSD without the GSA are compared in Figure 4-26 to the analytical solution with large rotation effects that was presented in Section 4.2. The two sets of results are nearly identical. The very small differences seen in Figure 4-26 are due to the fact that the SAP2000 model accounts for flexibility effects whereas the analytical solution neglects flexibility. Evidently, the analytical model in Section 4.2 is very accurate in describing the behavior of the NSD.

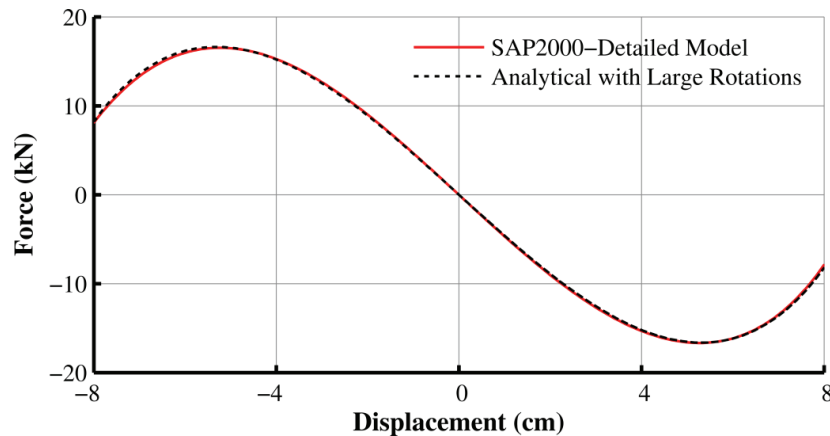


Figure 4-26: Comparison of force-displacement relations of the NSD without GSA produced by the analytical model with due consideration of large rotation effects and by the detailed model in SAP2000

The complexity of the detailed SAP2000 model and the requirement for large displacement analysis and use of direct integration resulted in unacceptably large execution times. This demonstrates that while possible to develop accurate and highly detailed models of the NSD in commercial software, the much simpler models presented in Sections 3.4 and 4.4.2 are sufficiently accurate and preferred.

SECTION 5 EXPERIMENTAL SETUP

5.1 Introduction

The NSD was tested in displacement-controlled experiments and as part of a structural system on the shake table. This section describes in detail the experimental setup for both tests. Moreover, results are presented that verify the validity of the experimental data by comparing measured quantities obtained by different instruments.

5.2 Specimen Description

The model structure used in the shake table testing is shown in the photographs of Figure 5-1 and Figure 5-2, whereas Figure 5-3 shows schematics of the model structure on the shake table. The model structure is a quarter length scale three-story steel model. It is a portion of the 6-story legacy model last used by Fenz and Constantinou (2008b) in the testing of a seismic isolation system. The 3-story model is supported on four low damping elastomeric bearings (same as those used by Wolff and Constantinou, 2004). The superstructure is a moment resisting frame in the longitudinal and braced frame in the transverse direction. Five concrete blocks, each weighing 8.9kN, were installed at each floor and two more at the base in order to achieve mass similitude. The total weight of the model (frame, base and added weight) on top of the isolators was 196kN (distributed as 53.2kN at the base and 47.6kN at each floor) in the tests without the NSD and it was 201kN in the tests with the NSD (the added 5kN was due to the weight of the NSD connection components). All beams and columns are S3×5.7 (SI designation S75×8.5) and all braces are L1½×1½×¼ (SI designation L38×38×6.4). The beam to column connections are fully welded and stiffened so that they are rigid. Horizontal bracing of all floors at all bays achieves, together with the concrete blocks, rigid diaphragm behavior. The 3-story structure seats on a base-mat that consists of a grid of two longitudinal W14x90 beams (SI designation W360x134) and four transverse W12x35 beams (SI designation W310x52), which are located at the superstructure's column locations. Also, the model features two HSS16x8x5/16 (SI designation HSS406.4x203.2x7.9) beams in the transverse direction that are connected on the top of the W14x90 beams. These beams were used to connect two NSD to the superstructure at the base-mat and to the shake table.

Four isolators were placed below the W14x90 beams on a 122cmx244cm footprint as shown in Figure 5-3 and Figure 5-4. The yellow plates seen at the bottom of the isolator-load cell assembly in Figure 5-1 and Figure 5-4 were used to level the bearings and to raise them so that the gravity loads on each isolator were approximately equal.

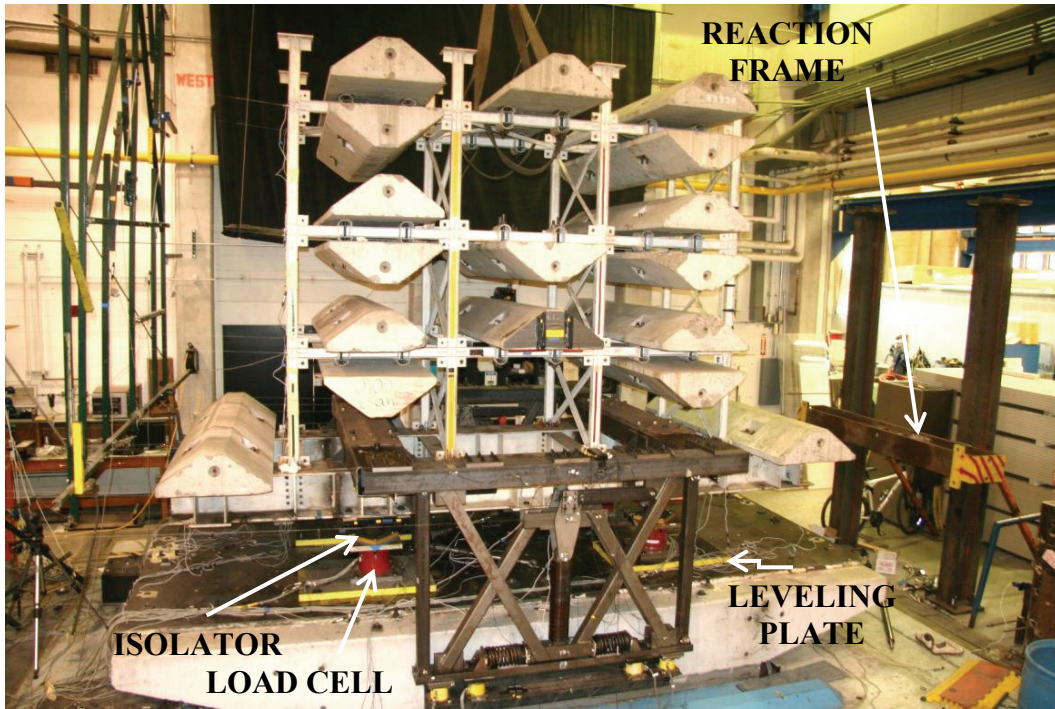


Figure 5-1: East view of model structure with NSD on shake table



Figure 5-2: North-West view of model structure with NSD on shake table

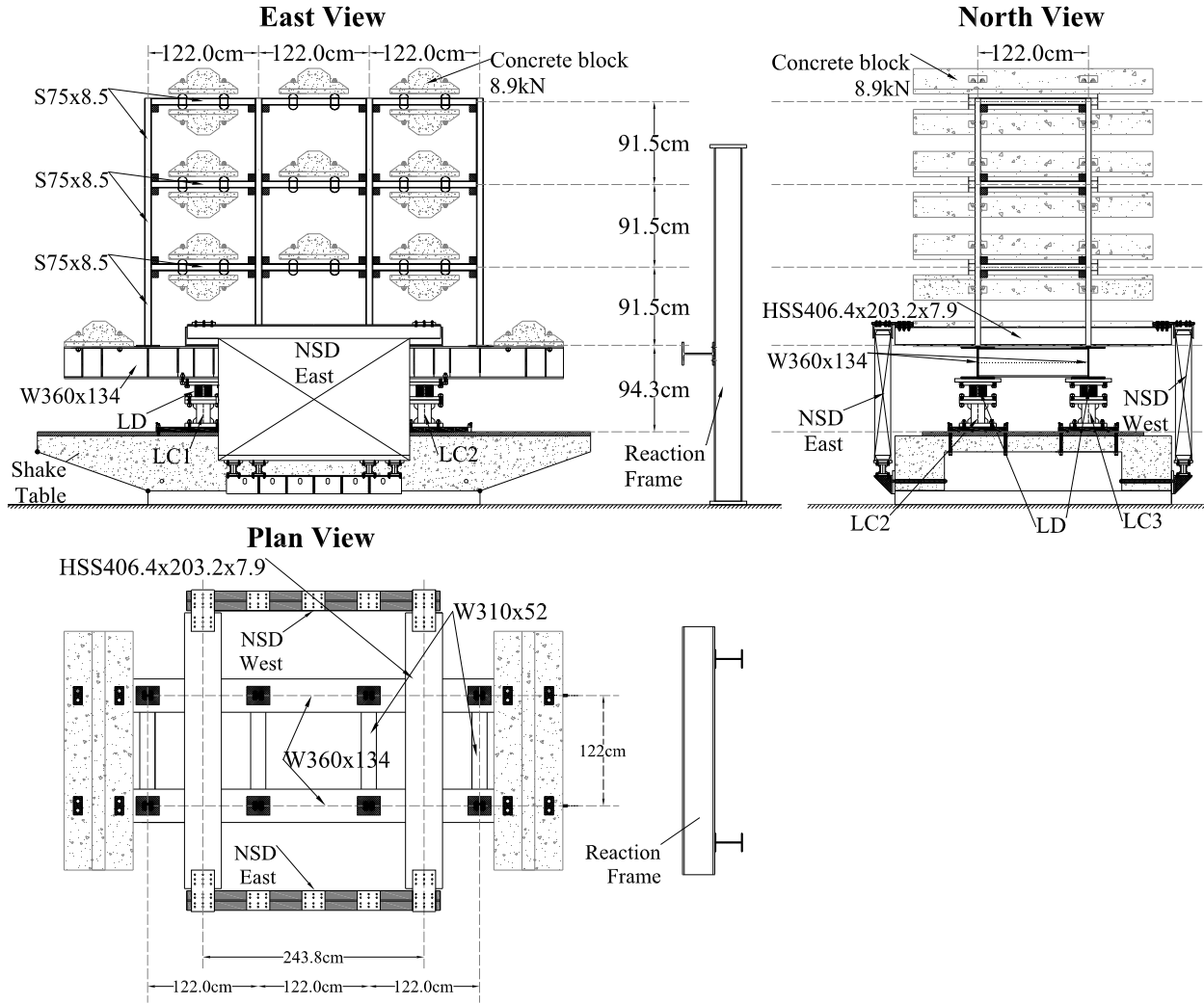


Figure 5-3: Schematics of 3-story base-isolated structure used in testing

Two linear viscous dampers were installed in the isolation system between the shake table and the base of the structure inclined at 36° with respect to the horizontal plane and 28° with respect to a vertical plane as shown in Figure 5-4. The dampers could be easily connected and disconnected during testing. Each damper assembly consisted of the damper, a load cell and a coupler as illustrated in Figure 5-5.

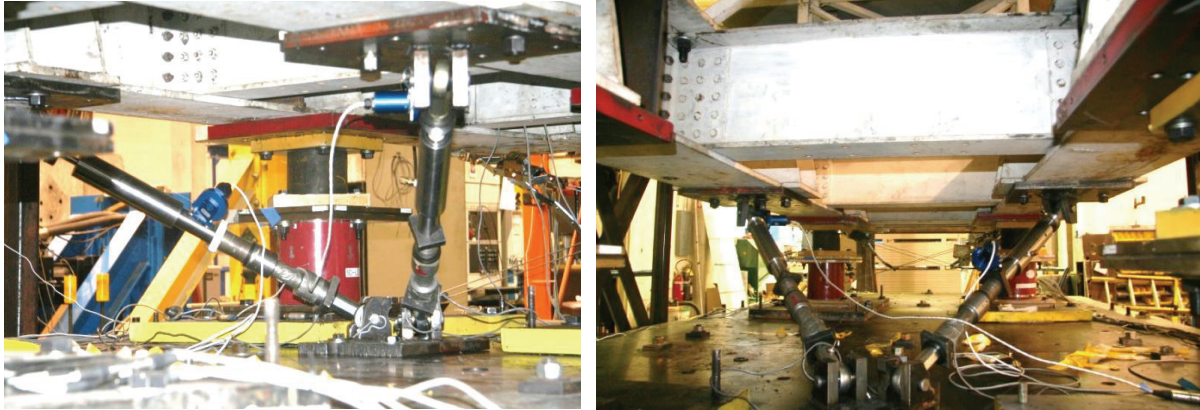


Figure 5-4: Views of viscous dampers and elastomeric bearings in isolation system

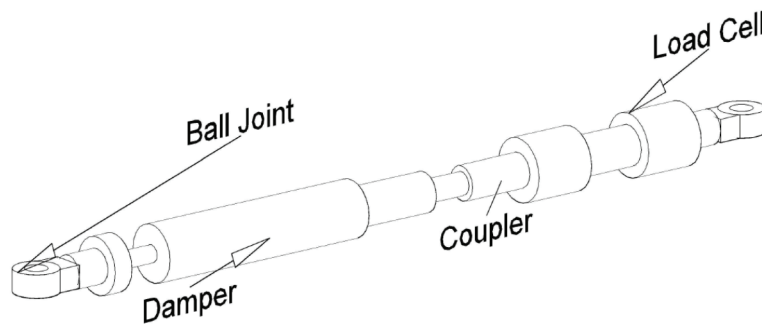


Figure 5-5: Viscous damper assembly

Two NSD were connected to the shake table and to the HSS16x8x5/16 beams of the base-mat. The connection to the shake table was through an angle on the side of the table as shown in Figure 5-6 and Figure 5-7. Stiffeners were welded to the angle in order to prevent bending deformations. Four load cells between the NSD and the angle were used to measure the force of the NSD.

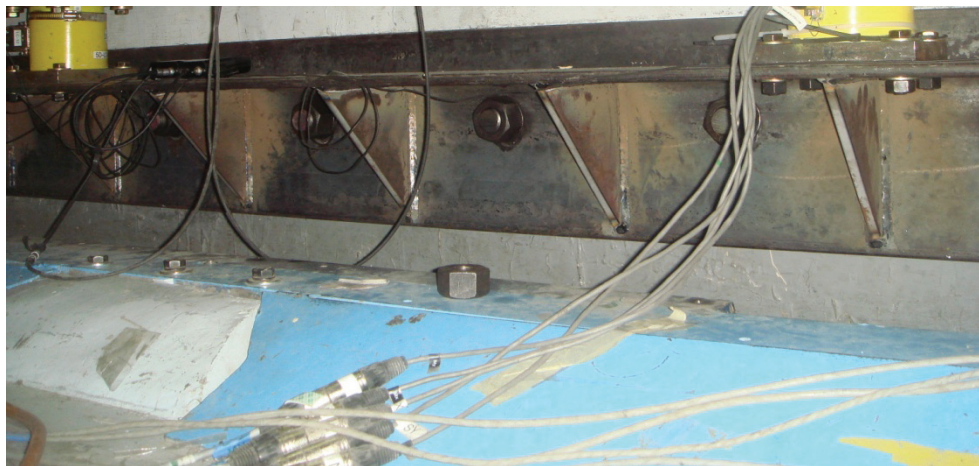


Figure 5-6: Angle used to connect the bottom of the NSD to the shake table

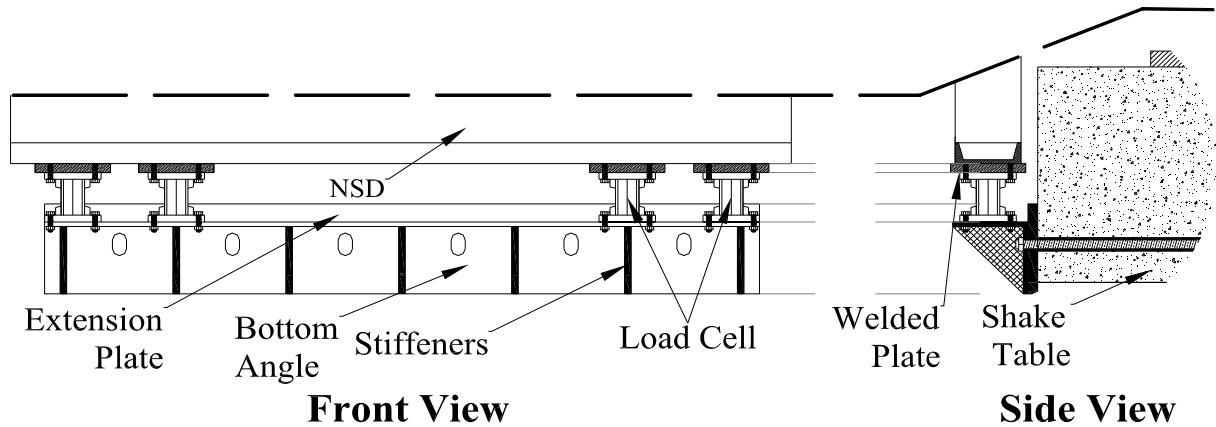


Figure 5-7: Schematic of connection of bottom of NSD to shake table

The connection of the NSD to the structure above was complicated as it needed to accommodate height loss that the NSD exhibits during lateral deformation. Details of the connection are shown in Figure 5-8 and Figure 5-9. The connection allowed motion of the NSD relative to the structure in the vertical direction. Also and since the device is unidirectional, the connection allowed for unrestricted relative motion between the structure and the device in the transverse direction.

The top connection was formed by bolting two angles side by side in order to create a channel that surrounds the device without being in direct contact. This assembly was designed so that a gap of 0.63cm (0.25inch) existed between the NSD and the angles. The assembly also had two side plates for connecting the angle to the HSS tubes located at the base of the structure. The NSD force was transferred by four rollers to four triangular reaction blocks (formed by angles and stiffeners) which were bolted to the side plates as shown in Figure 5-8. The use of rollers allowed for vertical and transverse movement of the NSD as they only transfer force in the longitudinal direction of the NSD.

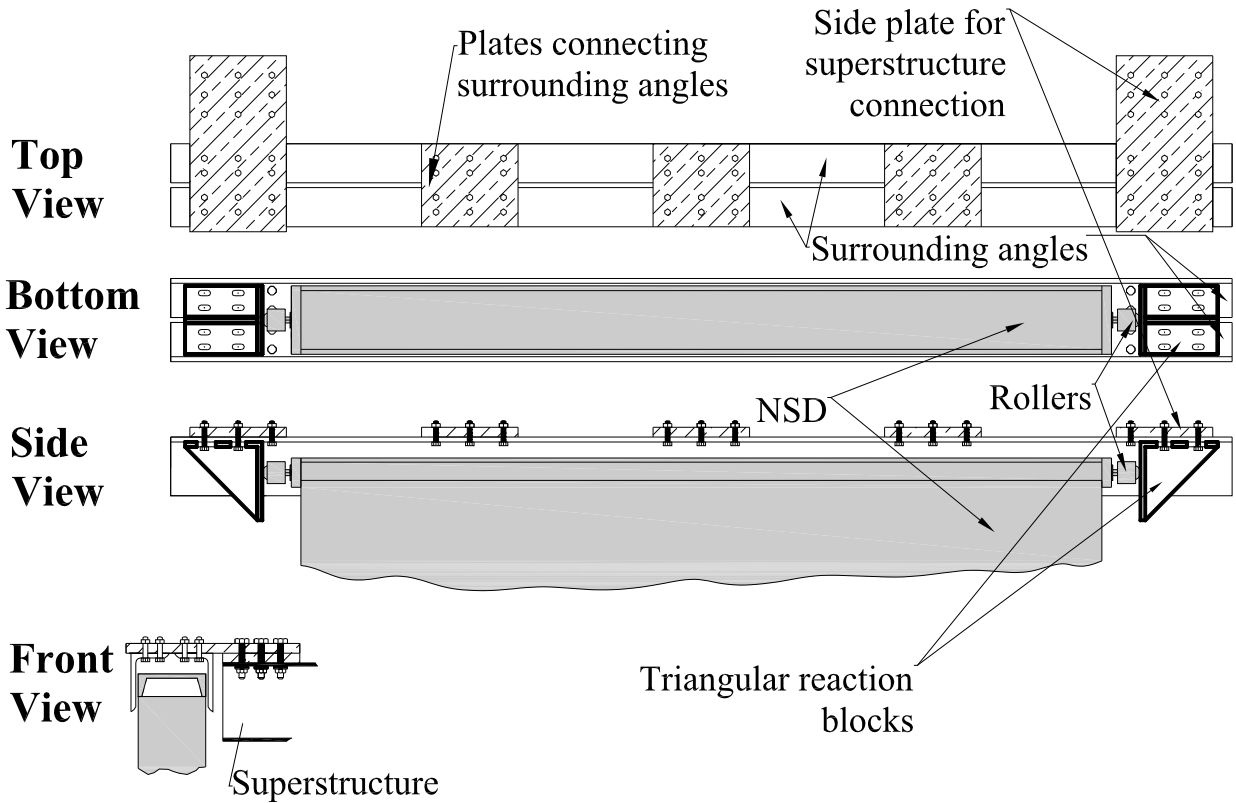


Figure 5-8: Schematic of connection of NSD to superstructure

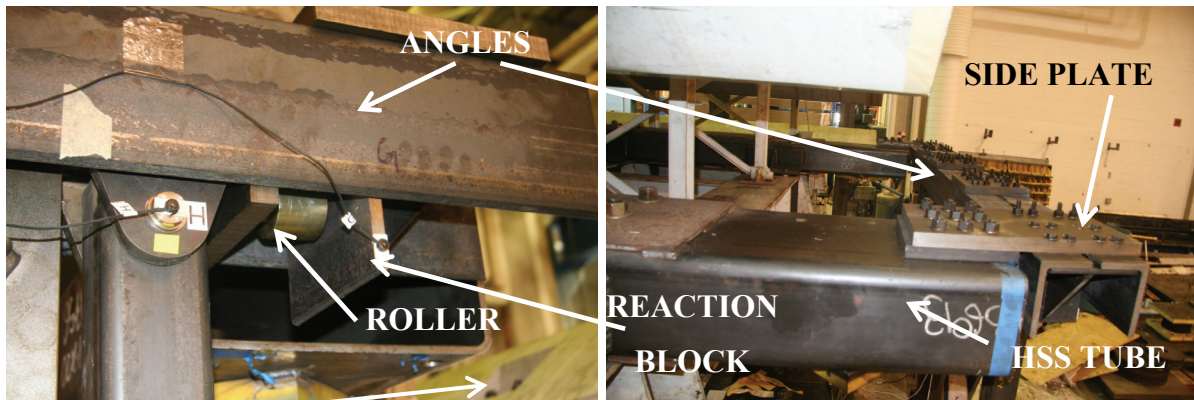


Figure 5-9: Photographs of NSD connection to superstructure

The location of the NSD on the perimeter of the model created unstable torsional behavior (for small rotations around the un-deformed position of the structure) for the configuration of the NSD without the GSA (see Section 3.5). Ideally the devices should be located as close to the center of rotation as possible but space limitations did not allow it. The model was stabilized by bracing it in the transverse direction (testing was only conducted with motion in the longitudinal direction) using cables that acted as diagonal bracing. Figure 5-10 shows the bracing.



Figure 5-10: View of transverse cables used for torsional stability in tests of NSD without the GSA

The NSD displacement-controlled tests were conducted on the shake table by connecting the base-mat of the isolated model to a reaction frame adjacent to the shake table so that the top of the NSD was motionless while the shake table (and, thus, the bottom of the NSD) was subjected to prescribed motion. This enabled the determination of the force-displacement relations of the NSD including the effects of the actual conditions of installation in the model.

The reaction frame is shown in the schematics of Figure 5-3 and is visible on the right in the photograph of Figure 5-1. The connection of the model base-mat to the reaction frame consisted of high strength rods within tubes and compression only washer load cells as shown in Figure 5-11 and Figure 5-12. Since the washer load cells could only measure compression, the connectors had to be pre-stressed after connecting them to the structure and the frame by tying the bolts on the back of the reaction frame until a load larger than the expected base shear was achieved.

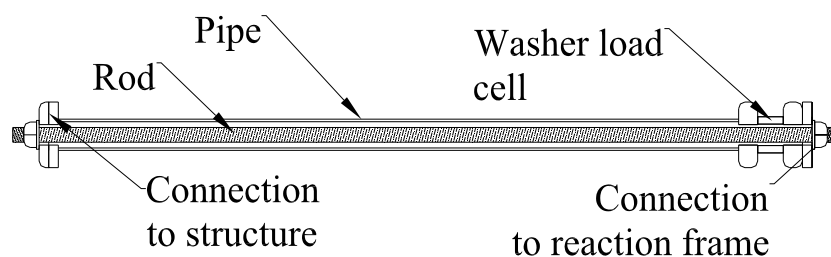


Figure 5-11: Connectors of model base-mat to reaction frame



Figure 5-12: Reaction frame and connector view

5.3 Instrumentation

Figure 5-13 and Figure 5-14 show a list of the potentiometers (displacement transducers) and accelerometers installed on the superstructure and shake table. Two accelerometers and two potentiometers were installed at each floor, base and the shake table in order to have redundancy in the measurements and to measure torsional motion. Vertical accelerometers were installed on the shake table and the base at four opposite corners. Transverse accelerometers were also installed on the 1st and 3rd floor and the base at the NE and SW corners of the model.

The elastomeric bearings were installed on top of four 5-component load cells. The load cells measured axial force in the vertical direction, shear force in the two orthogonal horizontal directions and moments about the two horizontal axes. Details on the load cells and how they are calibrated can be found in Bracci et al. (1992). The list of all the measured components (channels) for load cell 4 is shown in Figure 5-15. Fifteen more components were measured for the other three load cells. A view of loads cells below the elastomeric bearings is shown in Figure 5-16.

The NSD instrumentation included the Krypton advanced camera system. The camera tracked and recorded the coordinates of Light Emitting Diodes (LED) that were installed at selected points on the NSD. Figure 5-17 shows a photograph of LED installed at six points of one NSD.

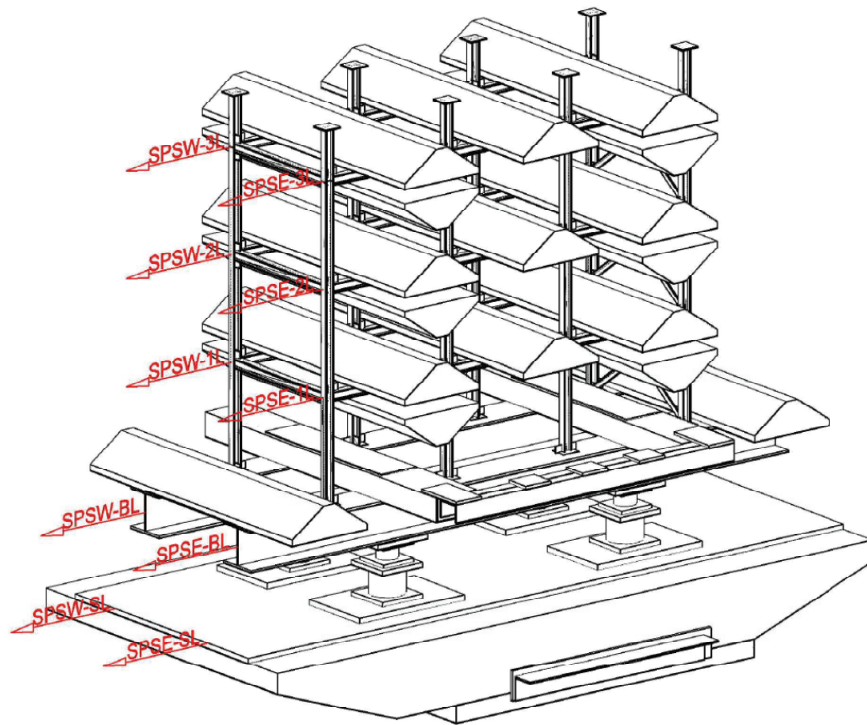


Figure 5-13: List of potentiometers for superstructure and shake table

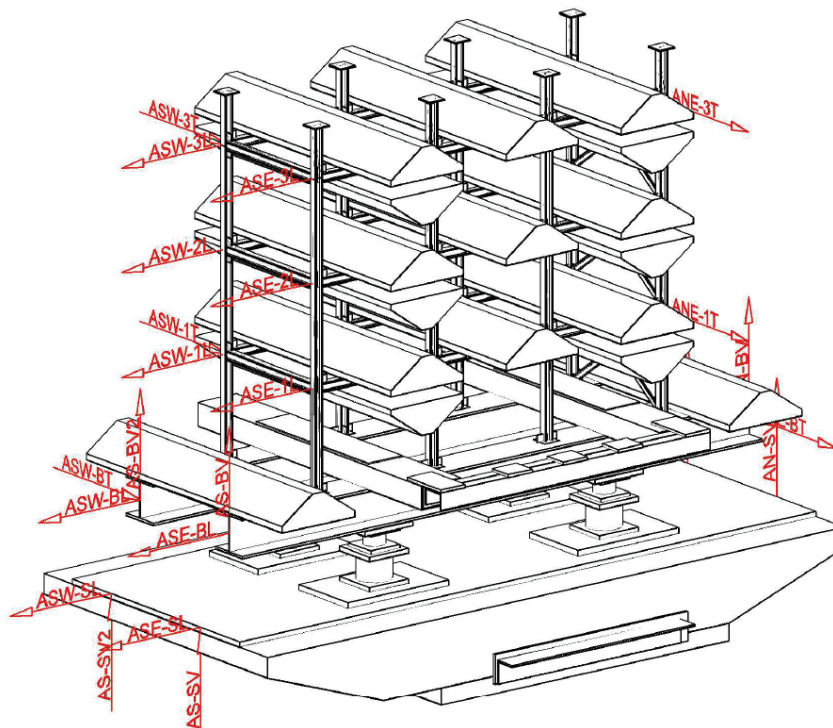


Figure 5-14: List of accelerometers for superstructure and shake table

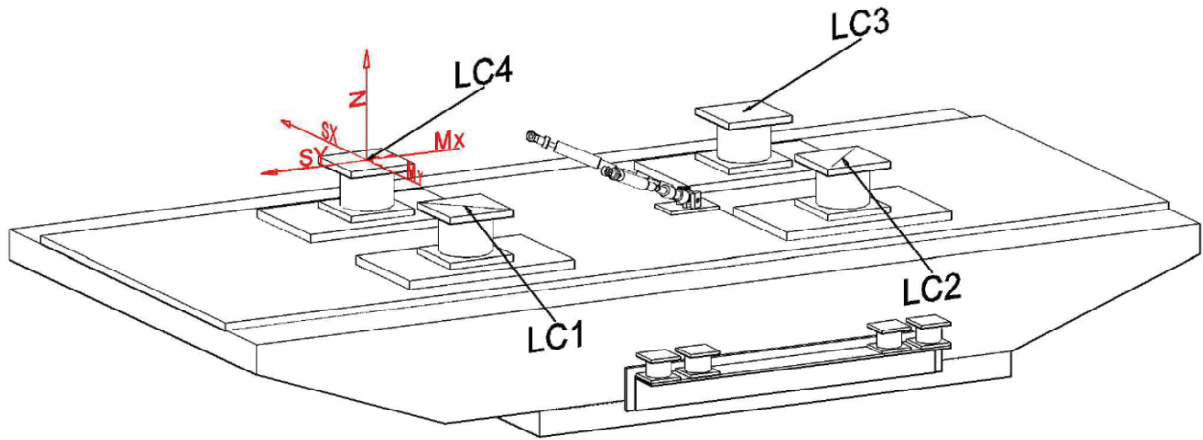


Figure 5-15: Five-component load cell channels



Figure 5-16: View of load cells below elastomeric bearings

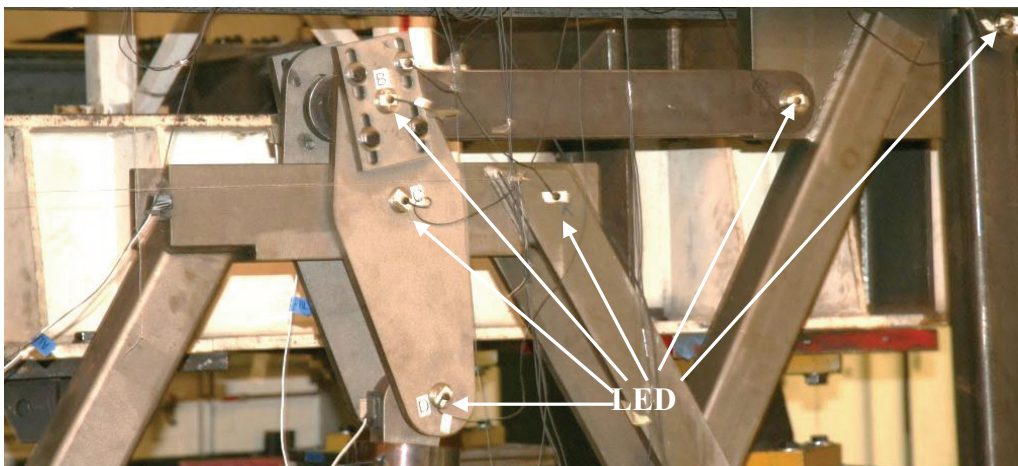


Figure 5-17: LED installed at four points of the East NSD

Figure 5-18 shows the location of all LED installed on the NSD at the East side of the model. Each point shown in Figure 5-18 (A, B, C, D, E, K, B1, L1, L2, L3, L4, JL, JR, FLB, FRB, GR1, GR2, GL1, GL2, CHB, LC1, LC2, ANL and ANR) were monitored by the Krypton camera and their displacement, velocity and acceleration histories could be obtained in all three directions.

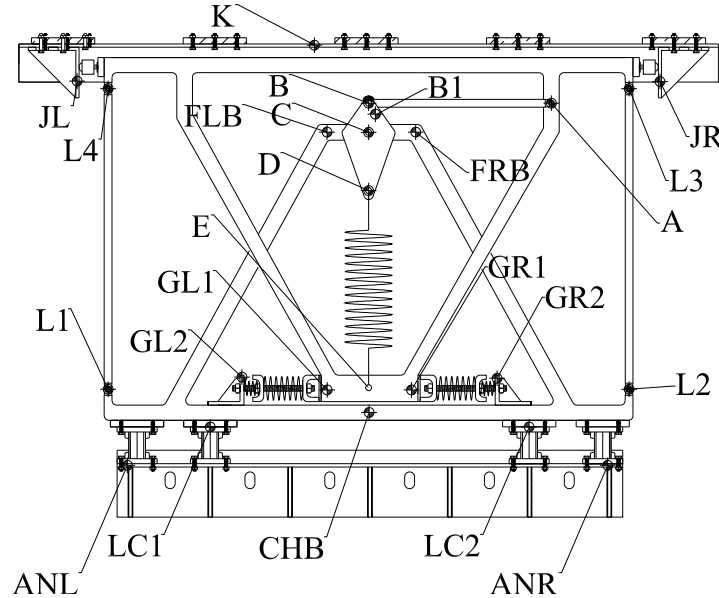


Figure 5-18: Complete LED instrumentation of NSD on East side

The forces of each NSD were measured using four 5-component load cells installed at the bottom of each NSD as shown in Figure 5-19 and Figure 5-20. These load cells were small size replicas of the load cells used under each elastomeric bearing. Initially only load cells LC1 and LC2 on the East and load cells LC3 and LC4 on the West were used. However, flexibility problems in the supporting channels of the NSD affected the behavior of the NSD so that additional load cells LC5 and LC6 on the East and LC7 and LC8 on the West were added for stiffening.

Accelerometers and displacement transducers (string pots) were also installed on the NSD in order to obtain additional data on the NSD motion. A complete list of string pots and accelerometers installed on both devices is shown in Figure 5-19 (NSD East) and Figure 5-20 (NSD West) together with the designation, location and measurement direction of the instruments. Note that the direction of measurement is either the tangential to a point's trajectory or the longitudinal direction. Figure 5-21 shows an accelerometer installed at the NSD pre-compressed spring top pin that measures the tangential acceleration of the trajectory of point D and a string pot installed at the head of the top chevron that measures the displacement of point E in the model longitudinal direction.

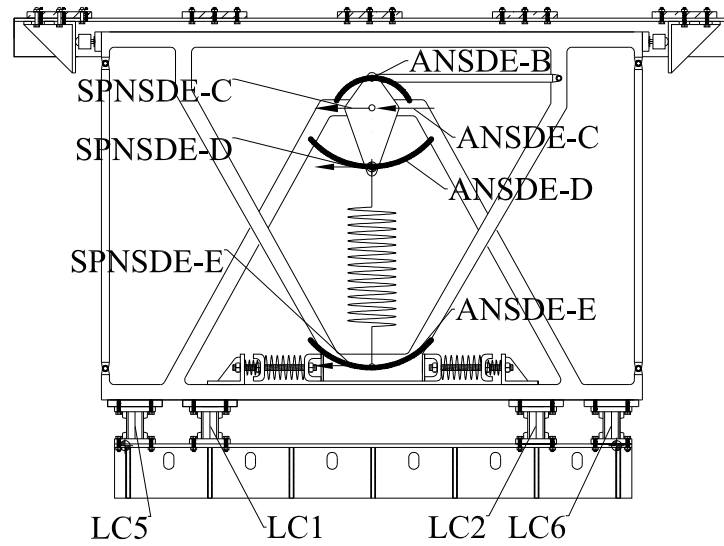


Figure 5-19: String pot, accelerometer and load cell instrumentation of NSD East

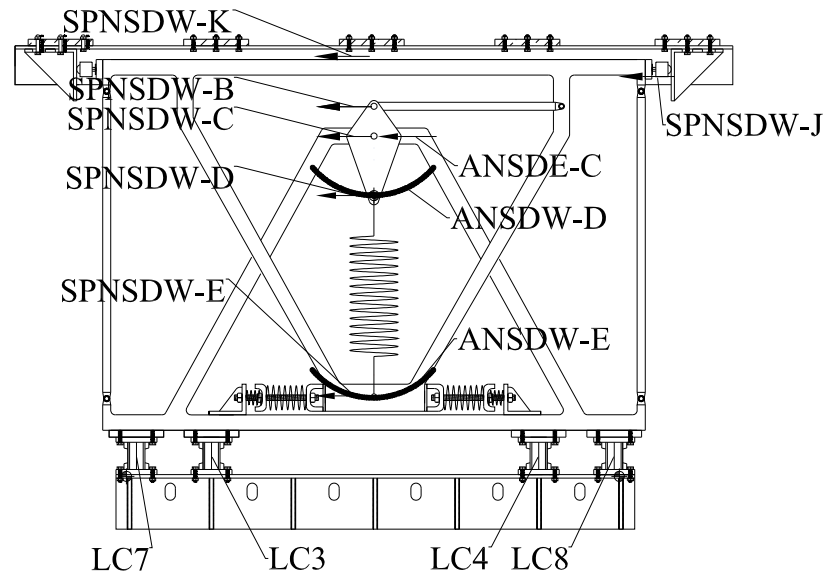


Figure 5-20: String pot, accelerometer and load cell instrumentation of NSD West

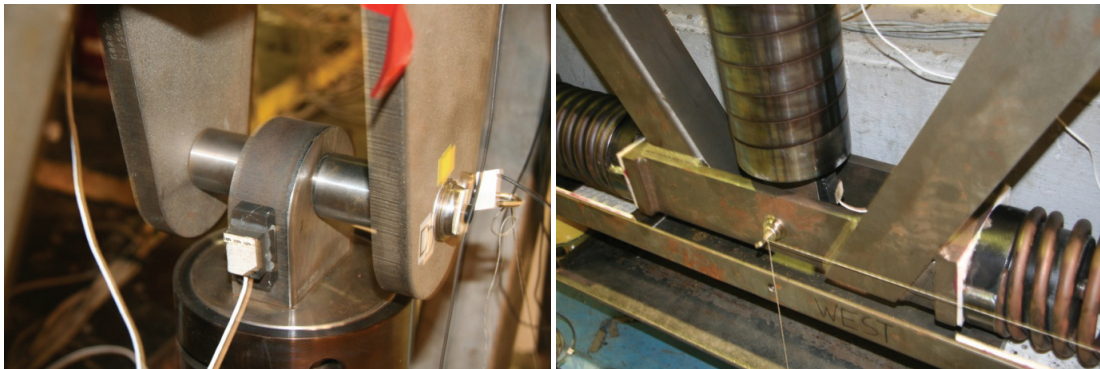


Figure 5-21: Views of accelerometer and string pot installed on NSD

Each damper was instrumented with a load cell and a displacement transducer to measure the damper change of length as shown in Figure 5-22.

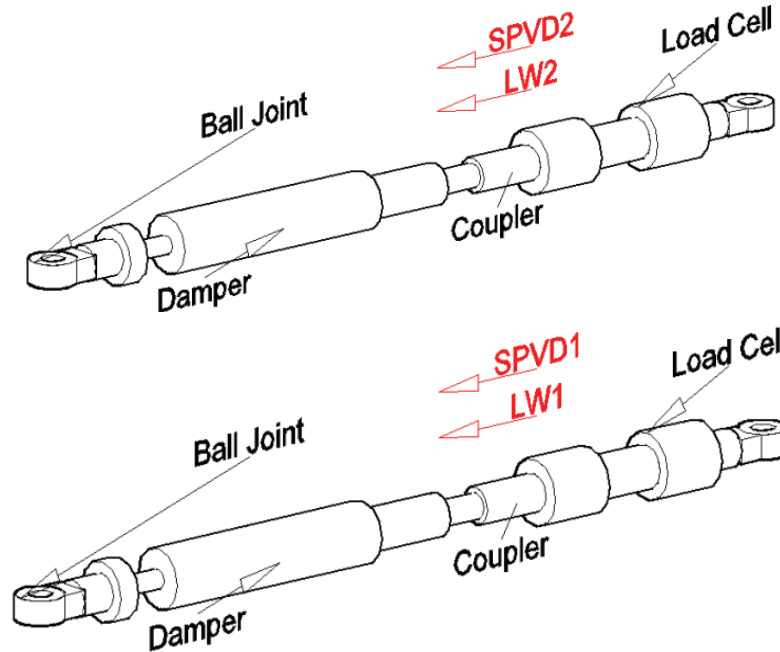


Figure 5-22: Damper instrumentation

An important part of any experimental study is to have redundancy in the measurements so that (a) the accuracy of measurements can be checked, and (b) sufficient data are acquired in case of failure of instrumentation. Although rarely reported, load cells often have measurement errors due to calibration errors (particularly for complex multichannel cells in which there is channel “cross-talk”), manufacturing errors (e.g., due imperfect placement of strain gages), installation errors in the test arrangement (e.g., leveling), condition of other supporting equipment (e.g., conditioners) and effects of the environmental conditions (e.g., temperature and humidity). Deviations of measured force of up to 20% of the actual forces are not uncommon. Figure 5-23 compares results for the base shear in a shake table test of the isolated model without the NSD (only elastomeric bearings) obtained by direct measurement of the shear force (force F_{ld}) and by processing of the accelerations obtained at each floor and the base-mat of the structure (force F_{acc}). Force F_{ld} was obtained as the sum of the shear forces recorded by all load cells supporting the isolators (sum of 1SY+2SY+3SY+4SY in Figure 5-15) and force F_{acc} was calculated as the sum of the floor and base-mat inertia forces:

$$F_{acc} = m_b \ddot{u}_b + m_f (\ddot{u}_1 + \ddot{u}_2 + \ddot{u}_3) \quad (5-1)$$

where m_b is the mass of the base-mat (weight equal to 53.2kN for tests without NSD and 58.2kN for tests with NSD), m_f is the mass of one floor (weight equal to 47.6kN), \ddot{u}_b is the longitudinal acceleration of the center of mass of the base-mat and \ddot{u}_1, \ddot{u}_2 and \ddot{u}_3 are the accelerations of center

of mass of the 1st, 2nd and 3rd floors, respectively. The center of mass accelerations were calculated as the average of the two accelerometer recordings on each floor. For example, \ddot{u}_b is the average of the recordings of instruments ASEBL and ASWBL (see Figure 5-14), \ddot{u}_1 is the average of the recordings of instruments ASE-1L and ASW-1L, etc. The data in Figure 5-23 were obtained in a test designated as E-PS10317 with the isolation system consisting of elastomeric bearings only in a test with ground motion PS10317.

The two sets of results in Figure 5-23 are in very good agreement. However, to obtain this good agreement, the load cell measurement was multiplied by factor of 1.055- a factor found to be systematically needed as the load cell measurements were lower than the results obtained from processing of acceleration records. It was discovered that the difference was due to load cell calibration errors so that the correction could be made for the load cell measurement. The load cell calibration procedure is described in Bracci et al. (1992) and utilizes the fixture shown in Figure 5-24. The load cells are bolted together and placed on top of two rollers at the edges of the two outermost load cells. A loading beam is placed on top of the load cells supported by two rollers placed on two of the load cells. A reference load cell is placed at the center and on top of the loading beam and load is applied on top of the reference load cell. The two outermost load cells are calibrated based on having half the load measured from the reference load cell. This however ignores the weight of the loading beam and the weight of the load cells. Each load cell with features weighs around 1.8kN and the loading beam, reference load cell and other features also weigh around 1.8kN for a total of about $5 \times 1.8 = 9\text{kN}$ additional unaccountable load. The distribution of this load gives rise to shear forces of 4.5kN for the two outer cells which are calibrated for the shear force. Given that load cells were calibrated to a shear of about 90kN, this leads to a calibration error of the order of 5%.

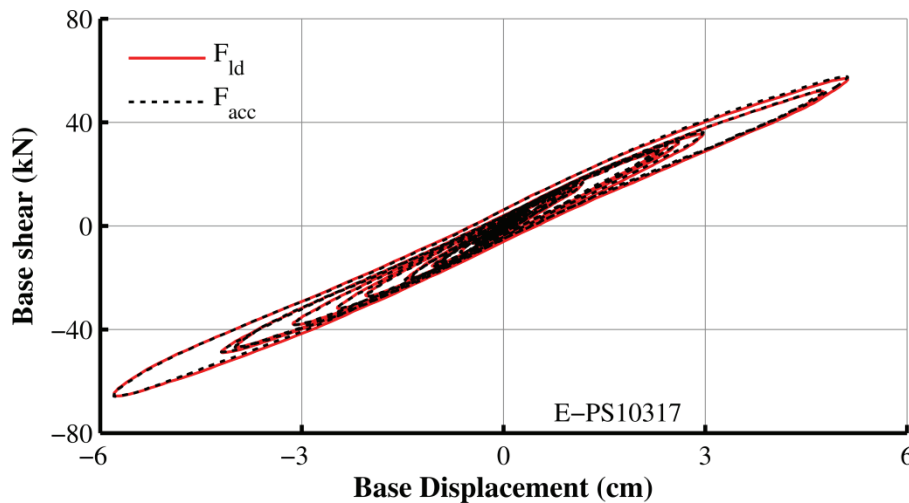


Figure 5-23: Comparison of base shear-base displacement loops obtained from processing of acceleration records (force F_{acc}) and directly measured by load cells (force F_{ld}) in structure on elastomeric bearings

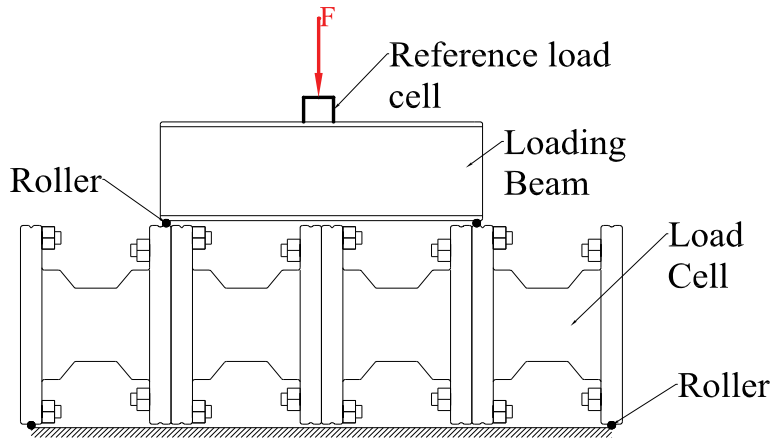


Figure 5-24: Load cell calibration fixture

In another comparison of measured quantities, Figure 5-25 compares the damper force directly measured by the damper load cells to forces obtained as the difference of the base shear force measured by processing of the acceleration records (force transmitted through the isolation system consisting of bearings and dampers, F_{acc} given by Equation (5-1)) and the force measured by the isolator load cells (force transmitted through the isolators only, F_{ld}). The measurements were made in a test designated as ED-PS10317 with the isolation system consisting of elastomeric bearings and dampers in a test with ground motion PS10317. To compare the two quantities, the sum of the damper load cell forces was multiplied by the direction cosines in order to obtain the horizontal component of the damper forces. Again, the agreement between the two independent measurements is very good. However, the damper load cell forces have been corrected by factor found only after comparisons like the one shown in Figure 5-25. Further investigation showed that the source of the problem was incorrect calibration factors for the damper load cells.

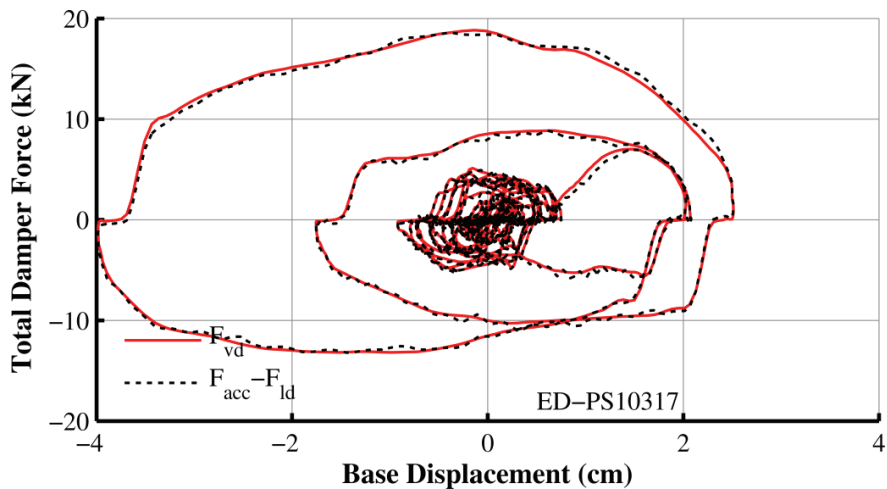


Figure 5-25: Comparison of viscous damper horizontal force obtained from processing of acceleration records and isolator load cells ($F_{acc}-F_{ld}$) and from damper load cells (F_{vd})

Finally, the NSD load cell measurements are compared to acceleration-based measurements in a test designated as ENB-PS10317 with the isolation system consisting of elastomeric bearings and NSD without GSA in a test with ground motion PS10317. The sum of the NSD load cell direct measurement (F_{nsd}) was compared to the force obtained by subtracting the isolator load cell measurement (force transmitted through the bearings) from the base shear force obtained from processing of the floor and base-mat acceleration records F_{acc} given by Equation (5-1). Results are presented in Figure 5-26. Evidently, there is some difference in the two independent measurements. Accepting that the acceleration-based measurements (dashed dark line) is correct, there must be some error originating in the load cell of the NSD. Further investigation determined the NSD West load cells had output nonlinearly dependent on the displacement of the device and could not be corrected by use of a single correction factor that applies for all situations. The load cells were re-calibrated at the conclusion of testing when it was discovered that one load cell had cross-coupling of channels and nonlinear behavior. This behavior was exacerbated by large out of plane shear forces, axial forces and moments transferred by the NSD. Further evidence of problematic measurement of force by the NSD West load cells is provided in Figure 5-27 where the NSD East force is compared to the NSD West force for a test conducted in displacement control at frequency of 0.02Hz. The NSD was tested without the GSA for which the two devices should have identical behavior due to the high precision of manufacturing of the assembly and the machined springs (this was not the case for the GSA which were made of helical springs). Also, the two NSD were later disassembled and the two machined springs were tested to find that they had identical stiffness. Yet, the results of Figure 5-27 show the NSD West having an output force about 15% lower than the NSD East force. Moreover, analytical investigations based on the models presented in Section 4 cannot explain such differences. That is, studies have shown that hysteresis of any kind will not affect the NSD elastic baseline (average of loading and unloading branches), that even large flexibilities only lead to increase in stiffness without effect on the peak forces (when GSA is not present) and that large rotation effects only result in a minor reduction in the peak NSD.

As an example, a comparison of experimental results to analytical results for the NSD without the GSA and for the properties of Table 3-1 is presented in Figure 5-28. Testing was performed in displacement-controlled mode. The analytical model was the one presented in Section 3.2 that excluded any flexibility, hysteresis and inertia effects. It is apparent that the experimental NSD East force is in good agreement with analytical predictions with a difference between the two of not more than 5%. Such difference is easily explained by considering standard load cell error and physical reasons such as tolerances in pre-loading of the machined spring, minor variations in length l_2 (which was adjusted many times during testing), minor flexing of pins when pre-load is released, etc. However, the large differences between experimental and analytical results for the NSD West force cannot be explained except by considering gross load cell errors. This conclusion is reinforced by verification of the accuracy of the analytical model presented in Figure 5-29 for shake table test ENB-PS10317. The force from two NSD (without GSA) was measured by processing of acceleration records and use of isolator load cell force measurements.

For this, the sum of the elastomeric bearing load cell recordings (F_{ld}) was subtracted from the acceleration based base shear force (F_{acc}). The experimental results were then further processed to remove hysteresis by averaging the force values in the ascending and descending branches of the loops within sequential windows of displacement. The analytical results are in excellent agreement with experimental results.

Concluding, the NSD force measurement contains errors which are attributed to one load cell for NSD West. These errors do not significantly affect global results. For this reason, for the remainder of this report, results from NSD West will be shown for the displacement-controlled tests with the understanding that they contain some error. However, results for the shake table tests will be based on acceleration-based data so that they are considered accurate.

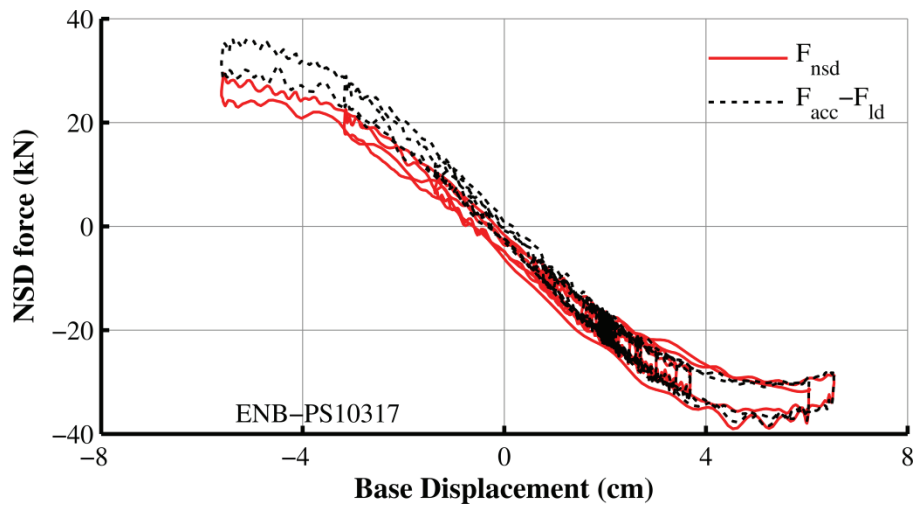


Figure 5-26: Comparison of NSD force-displacement loops (two devices) obtained from NSD load cells (F_{nsd}) and from records of base shear (acceleration-based) and isolator load cells ($F_{acc}-F_{ld}$)

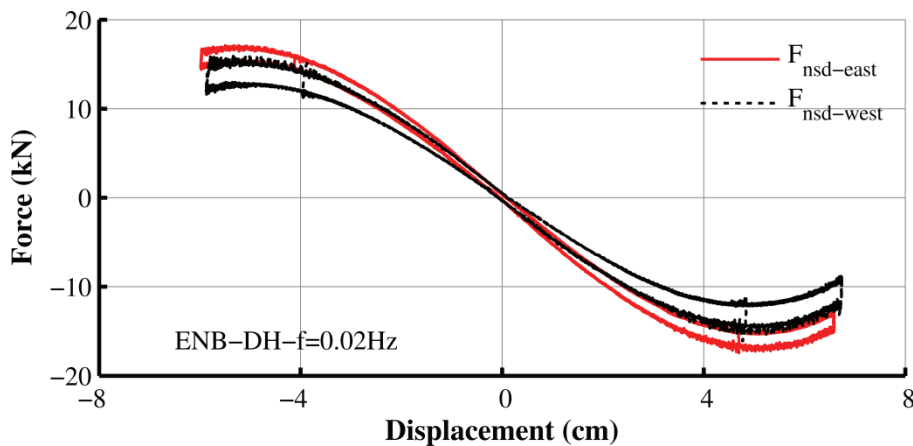


Figure 5-27: Comparison of measured NSD East to NSD West force-displacement loops

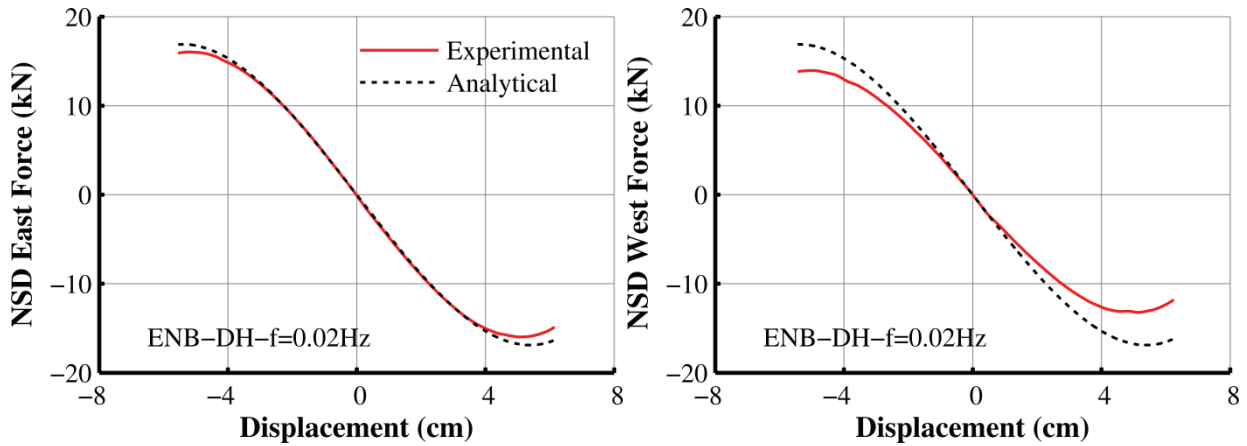


Figure 5-28: Comparison of NSD East (left) and West (right) force-displacement relations based on measurement by the NSD load cells and predicted by analysis for the nominal NSD properties of Table 3-1

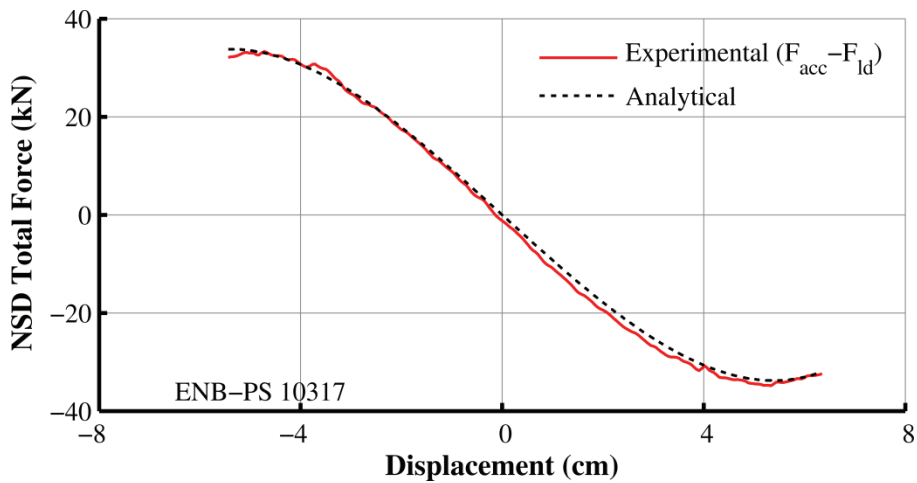


Figure 5-29: Comparison of experimental and analytical total NSD force-displacement relations

SECTION 6 EXPERIMENTAL RESULTS

6.1 Introduction

This section presents the following experimental results:

1. Force-displacement relations of the elastomeric bearings obtained in testing of the bearings in bearing testing machine.
2. Dynamic response of the fixed-base structure in the shake table testing.
3. Force-displacement relations of the GSA obtained in testing of each device after removal from the NSD.
4. Force-displacement relations of the isolation system in various configurations obtained in displacement-controlled tests on the shake table.
5. Dynamic response of the isolated structure in various configurations in the shake table testing.

6.2 Experiment Outline

Two different experimental setups were utilized for the following two phases of testing: displacement-controlled tests and shake table tests.

Some description of the displacement-controlled testing was provided in Sections 5.2 and 5.3. In the displacement-controlled tests, the structure was externally restrained at the base as shown in Figure 5-11 and Figure 5-12 and sinusoidal motion was imposed by the shake table with various combinations of amplitude and frequency of excitation.

Various configurations were tested in the displacement-controlled and in the shake table tests. These configurations are listed in Table 6-1. Two basic groups of tests were conducted: without viscous dampers (designation E) and with viscous dampers (designation ED). Three different NSD configurations were tested: NSD-A (NSD without the GSA), NSD-B (NSD with lever at center and with GSA) and NSD-BLA (NSD with lever at upper position and with GSA). Also, tests were conducted without the NSD.

Table 6-1: Notation and tested configurations

Device	Without dampers				With Dampers			
	E	ENA	ENB	ENB-LA	ED	EDNA	EDNB	EDNB-LA
LD	✓	✓	✓	✓	✓	✓	✓	✓
VD					✓	✓	✓	✓
NSD-B			✓				✓	
NSD-BLA				✓				✓
NSD-A		✓				✓		

LD=Low Damping Elastomeric Bearings, VD=Linear Viscous Dampers, NSD-A=NSD with GSA, NSD-B=NSD w/out GSA and lever at center ($l_2=12.7\text{cm}$), NSD-BLA= NSD w/out GSA and lever at upper position ($l_2=15.2\text{cm}$).

Table 6-2 presents information on the earthquake motions used in the shake table testing. Note that only one-directional excitation was used. For similitude requirements, the original earthquake motions were compressed in time by a factor of 2 in consistency with the length scale factor of 4. Table 6-3 identifies which earthquake motions were used for each isolation system and NSD configuration.

Table 6-2: Earthquake motions used for shake table testing

Earthquake/ Date	Station	Component Notation	Moment Magnitude	PGA (g)	PGV (cm/sec)	PGD (cm)
Denali, Alaska 3/2002	Alyeska Ps10 TAPS Pump Station #10	PS-10317	7.9	0.32	96.1	100.5
San Fernando 2/1971	CDMG 279 Pacoima Dam, Upper Left Abutment)	PUL-254	6.6	1.16	75.6	18.1
Loma Prieta 10/1989	CDMG Station 47125, Capitola	CAP-000	6.9	0.48	34.5	7.1
Northridge-01 1/1994	USGS/VA 637 LA - Sepulveda VA Hospital	0637-270	6.7	0.80	74.1	16.3
Chi-Chi, Taiwan 9/1999	CWB 9999936 TCU129	TCU-129-E	7.6	0.79	47.3	38.7
Kobe 1/1995	JMA 99999 KJMA	KJM-090	6.9	0.71	77.8	18.9
Northridge-01 1/1994	CDMG 24279 Newhall - Fire Station	NWH-090	6.7	0.70	81.8	26.1
Kocaeli, Turkey 8/1999	ERD 99999 Duzce	DZC-270	7.5	0.33	55.3	29.6

Table 6-3: Earthquake motions and tested configurations

Ground Motion	Testing Configuration							
	Without Dampers				With Dampers			
	E	ENA	ENB	ENB-LA	ED	EDNA	EDNB	EDNB-LA
PS-10317	✓	✓	✓	✓	✓	✓	✓	✓
PUL-254	✓	✓	✓	✓	✓	✓	✓	✓
CAP-000	✓	✓	✓	✓	✓	✓	✓	✓
0637-270	✓	✓		✓	✓	✓		✓
TCU-129-E	✓		✓	✓	✓		✓	✓
KJM-090	✓	✓	✓	✓	✓	✓		✓
NWH-090	✓		✓	✓	✓	✓	✓	✓
DZC-270	✓		✓	✓	✓		✓	✓

6.3 Testing of Elastomeric Bearings

The four elastomeric bearings used in the isolation system of the model structure were the bearings used in Wolff and Constantinou (2004). The geometry of the elastomeric bearings is shown in Figure 6-1. The bearings were individually tested in the bearing testing machine of Figure 6-2 (described in Kasalanati and Constantinou, 1999) prior to their installation on the shake table. The four bearings were tested at various frequencies and amplitudes of harmonic motion.

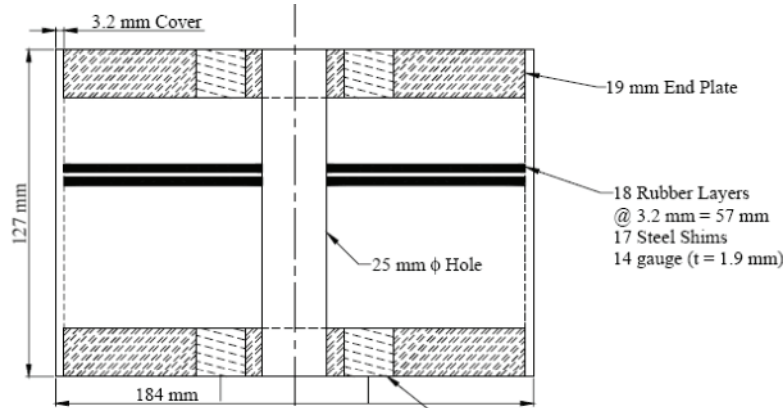


Figure 6-1: Section of elastomeric bearing (Wolff and Constantinou, 2004)

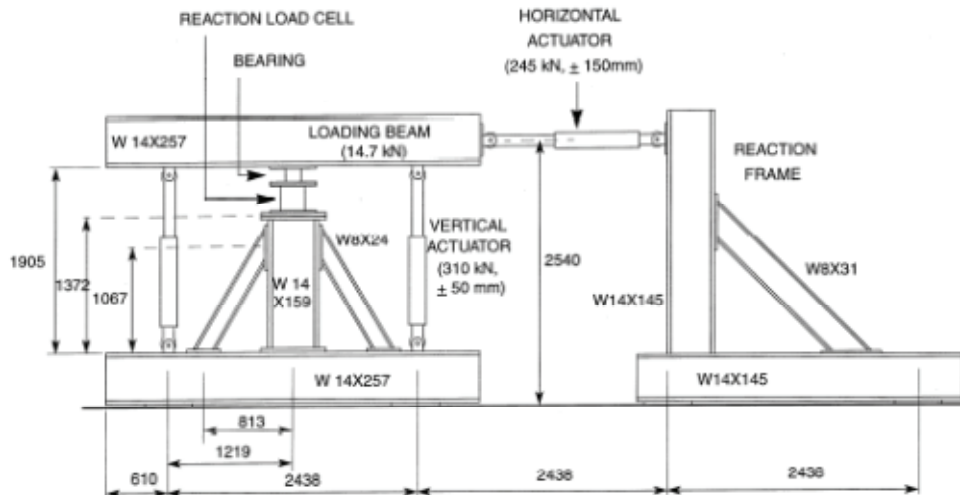


Figure 6-2: Schematic of single bearing testing machine (Kasalanati et al, 1999)

Sample force-displacement loops for the four elastomeric bearings are shown in Figure 6-3 and Figure 6-4 for two different frequencies, compressive load of 50kN and shear strain amplitude of 140%. The results are in good agreement with those reported in Wolff and Constantinou (2004) for tests conducted nearly 10 years ago. While the four bearings have nearly identical properties, the bearings were placed as follows to minimize eccentricities: bearing LD4 was placed on top of load cell LC1, bearing LD1 on top of load cell LC2, bearing LD3 on top of load cell LC3 and bearing LD2 on top of load cell LC4 (see Figure 5-15).

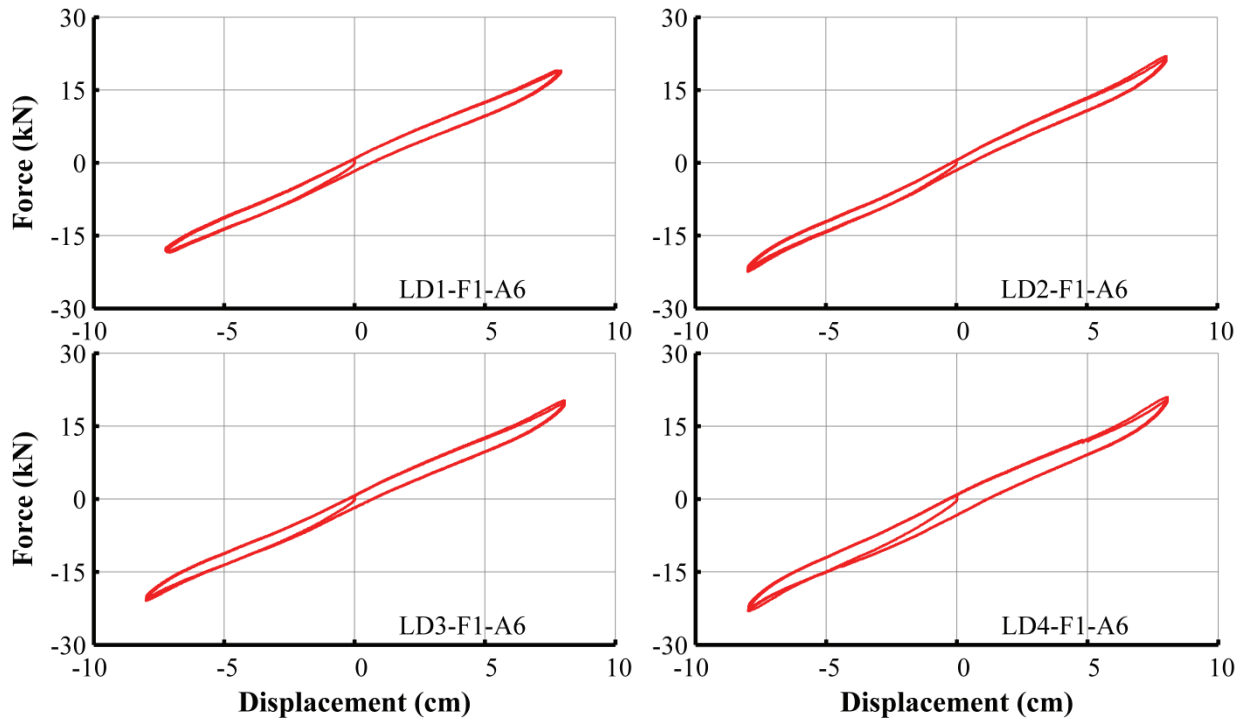


Figure 6-3: Recorded force-displacement loops of elastomeric bearings at shear strain of 145%, compressive load of 50kN and frequency of 0.01Hz

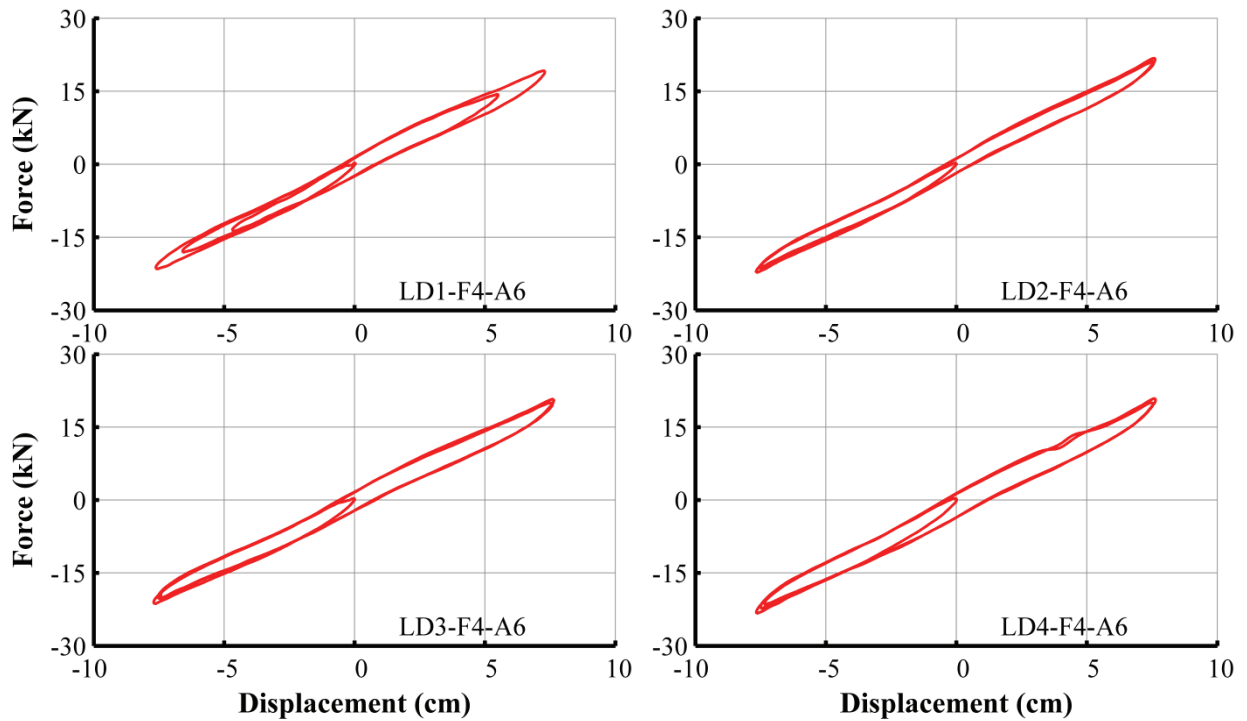


Figure 6-4: Recorded force-displacement loops of elastomeric bearings at shear strain of 145%, compressive load of 50kN and frequency of 1Hz

6.4 Testing of GSA

The four GSA units were removed from the two NSD and tested in compression as shown in Figure 6-5. This was done after the shake table testing was concluded in order to investigate features of behavior observed in the shake table testing. A compressive load F was applied to a washer load cell that was placed on top of the GSA and a potentiometer measured the GSA deformation.

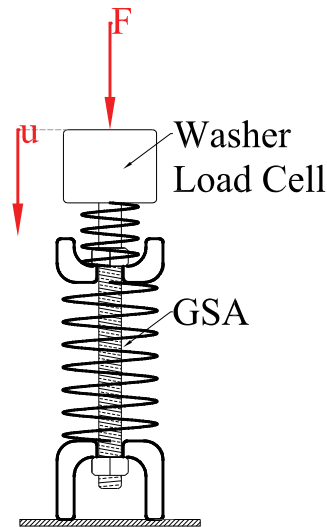


Figure 6-5: Testing arrangement for GSA

Recorded force-displacement relations for the four GSA are shown in Figure 6-6. The GSA designated NE and SE were extracted from the East NSD and the GSA designated NW and SW were extracted from the West NSD. Evidently, the devices exhibit bilinear behavior with small hysteresis. The GSA NW, SW and NE have nearly identical behavior but the properties of pre-engagement stiffness (stiffness for displacement less than the NSD engagement displacement) and the engagement displacement differ from the nominal properties of Table 3-1 and Figure 3-3. Specifically in Table 3-1, the engagement displacement is 1.65cm and the pre-engagement stiffness is 4.9kN/cm. The experimental values are about 2.0cm for the displacement and 3.5kN/cm for the pre-engagement stiffness. GSA SE has correct pre-engagement stiffness, but has larger than nominal engagement displacement and post-engagement stiffness.

The differences are due to differences in the properties of the coil springs used in the GSA. Unlike the machined pre-loaded springs of the NSD, these springs can have differences in behavior of the order observed due to small differences in geometry (particularly the diameter of wire, d , and the mean winding diameter, D -where the spring stiffness, K , is related to these quantities by $K \sim d^4 / D^3$).

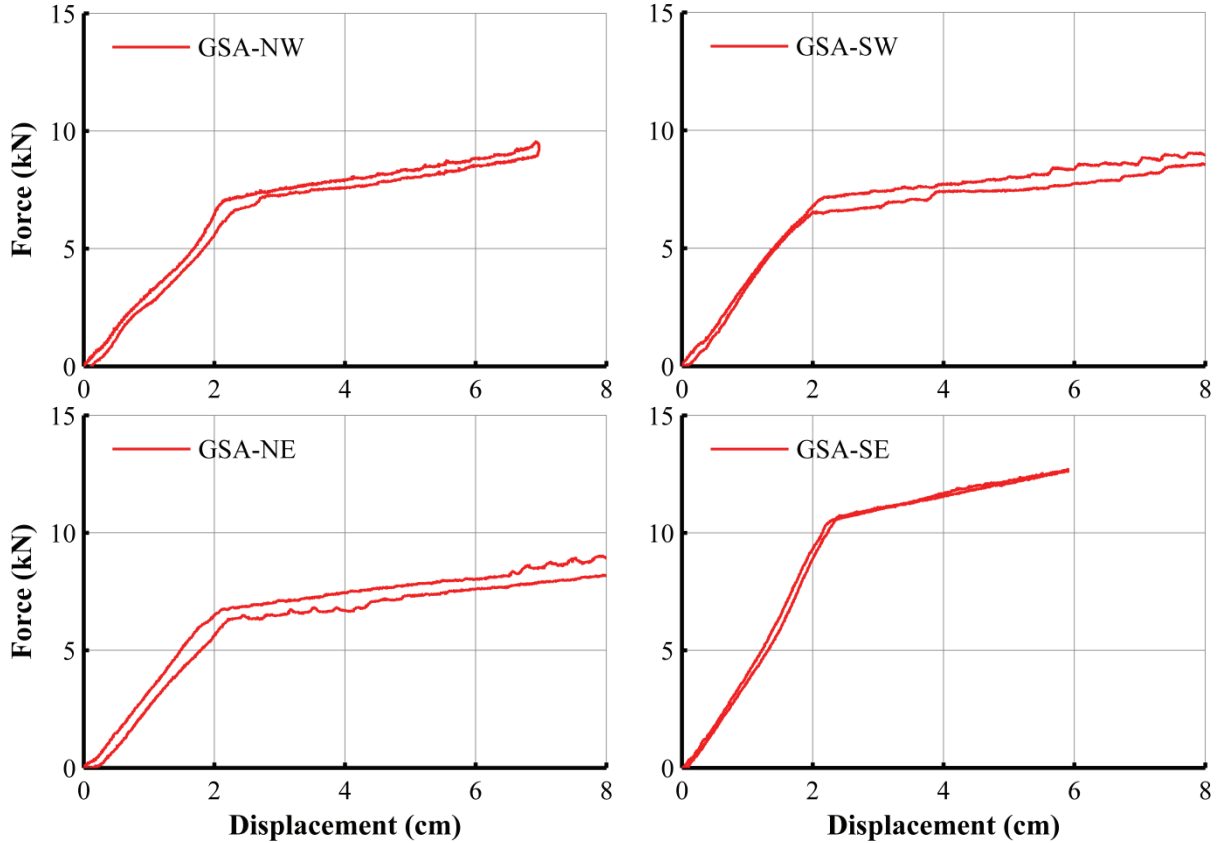


Figure 6-6: Experimental force-displacement relations of GSA

Note that the GSA, as tested, did not have the end angle plates (Figure 3-11) so, effectively, the physical gap opening d_{gap} was large. Accordingly, the testing of the GSA did not reveal the implications of the variability in the stiffness and engagement displacement properties. Furthermore, spring S1 (see Figure 3-11) was free of any pre-load in the GSA testing (as it should have been in the NSD). However, when it was installed in the NSD, it was accidentally compressed and therefore the behavior changed. Accordingly, the testing of individual GSA did not reveal the behavior of the devices observed when tested within the NSD. Nevertheless, the testing revealed differences in GSA spring stiffness that are important in understanding the behavior of the NSD as observed in the shake table testing and in designing an improved version of the GSA. Observations of the GSA behavior in this experimental study led to a revision in the design of the GSA which was implemented in a modification of the device for the second phase of the research project. The revised design is shown in Figure 6-7 where the rod running through the springs (see Figure 2-6) was replaced by a tube surrounding spring S2. The behavior of the revised GSA of Figure 6-7 is still described by the basic theory of Section 3.3 where now quantity k_r is the axial stiffness of the tube rather than the axial stiffness of the rod.

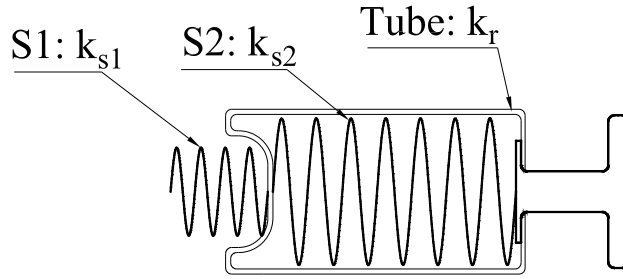


Figure 6-7: Schematic of revised GSA

The revised GSA design also corrected for additional problems observed in the original design. Specifically, the coils of spring S2 were observed to rub against the housing plate as shown in the photographs of Figure 6-8 and Figure 6-9. In Figure 6-8, the spring coils are seen deformed non-uniformly as a result of friction between the coils and the housing plate. In Figure 6-9, wear marks on the housing plate due to the rubbing of parts are evident. Also, the revised GSA did not have the additional friction problem described in the sequel.

The original GSA experienced some motion perpendicular to its axis so that the threaded rod could rub against the hole of the housing plate. To reduce this problem in the original GSA, the device was fitted with Teflon sheets where the GSA contacted the NSD and a guide was installed as shown in Figure 6-8. Nevertheless, the GSA contributed a friction force to the NSD force that could be modeled as:

$$F_{fr} = \mu_f^2 F_g \quad (6-1)$$

In Equation (6-1), F_g is the force of the GSA and μ_f is the friction coefficient between steel and Teflon. The equation arises from the fact that the friction coefficient multiplied by the GSA force is equal to the normal load on the Teflon-steel interface of the guide. This normal load multiplied by the friction coefficient of the Teflon-steel (guide) interface results in the force in the NSD direction. Simple calculations (e.g., $\mu_f = 0.05$, $F_{g,max} = 10kN$, the added friction force is 0.025kN) reveal that this force is very small and can be ignored.

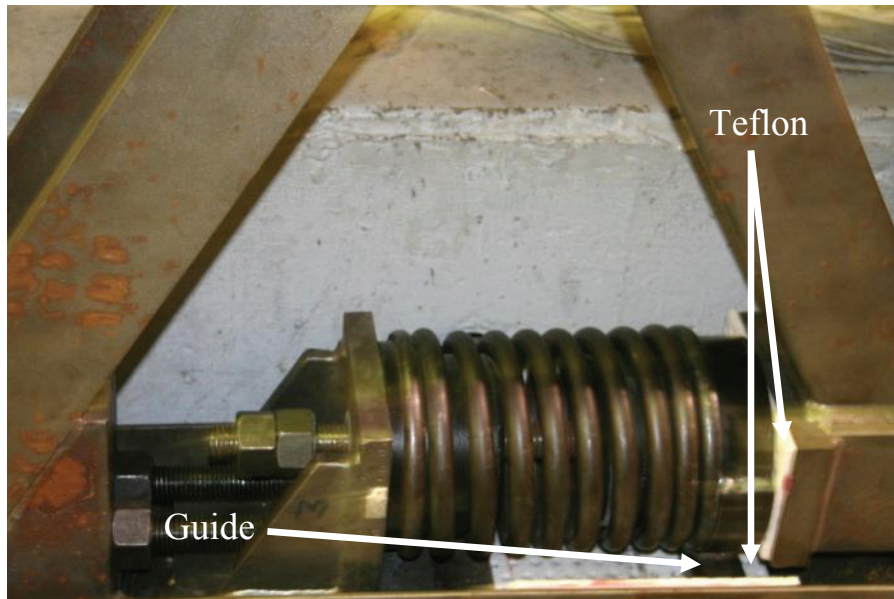


Figure 6-8: Deformed GSA of West NSD in displacement-controlled test at 2.5in amplitude and 0.02Hz frequency (observe uneven coil movement)

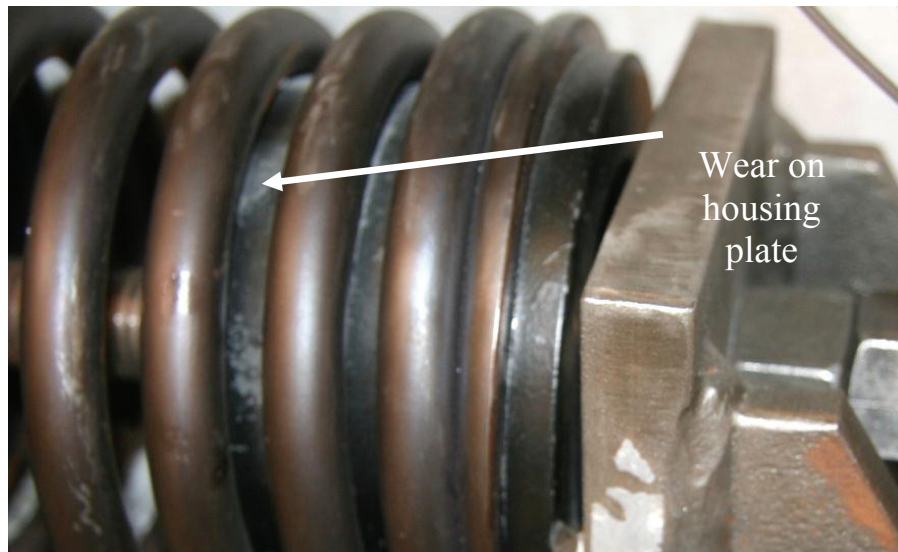


Figure 6-9: Wear on housing plate due to friction between housing plate and spring

6.5 Testing of Linear Viscous Dampers

The dampers were tested in displacement-controlled tests on the shake table together with the NSD. The dampers are linear viscous and have been previously extensively used in shake table testing by Kasalanati and Constantinou (1999) and Wolff and Constantinou (2004). The devices were sent back to the manufacturer to be re-pressurized prior to the testing for this project.

In the shake table testing the devices were installed at an angle with respect to the axis of shake table motion, referred to here as the horizontal direction. Using the installation geometry described in Section 5.2, the horizontal component of each damper force is given by:

$$F_{vd,x} = F_{vd} \cos \theta_x \cos \theta_z \quad (6-2)$$

Angles θ_x and θ_y are equal to 36 and 28 degrees, respectively, resulting in $\cos \theta_x \cos \theta_z = 0.71$. However, during seismic testing there was some repositioning of the dampers so that the angles slightly changed so that $\cos \theta_x \cos \theta_z = 0.69$. The damper deformation is related to the isolation system (or base) displacement by:

$$u_{vd} = u_b \cos \theta_x \cos \theta_z \quad (6-3)$$

Note that F_{vd} is the force of each damper measured by the load cell on each damper and u_{vd} is the damper relative displacement (deformation) obtained from potentiometers SPVD1 and SPVD2 (see Figure 5-22). The isolation system or base displacement u_b is obtained as the average relative displacement of the base of the model and the shake table using measurements from potentiometers SPSESL, SPSWSL, SPSEBL, SPSWBL as shown in Figure 5-13.

Figure 6-10(a) compares experimental results for the relation between the damper deformation and base displacement for a harmonic test at 0.5Hz frequency and 6.58cm amplitude of the shake table. Figure 6-10(b) shows the average damper force obtained as the average of load cells LW1 and LW2 (Figure 5-22) plotted against the average damper deformation obtained as the average of the recordings of potentiometers SPVD1 and SPVD2. The total (from two dampers) horizontal damper force component versus the base displacement is shown in Figure 6-10(c). It was obtained as the sum of recordings of load cells LW1 and LW2 multiplied by factor 0.71 (for $\cos \theta_x \cos \theta_z$).

It can be seen in Figure 6-10(a) that the damper deformation shows some “hysteresis” with respect to the base displacement. This was the result of some small rigid body motion between the pins and the holes of the damper connections. The test results reveal linear viscous behavior with a damping constant for individual dampers equal to 0.63kN-sec/cm, which is essentially the same as that reported in Wolff and Constantinou (2004). The effective damping constant in the longitudinal direction for the two inclined dampers is then equal to $2 \times 0.63 \times (0.69)^2 = 0.60$ kN-sec/cm, where 0.69 is the direction cosine for the dampers. Note that the same result is directly obtained from the loops in Figure 6-10(c).

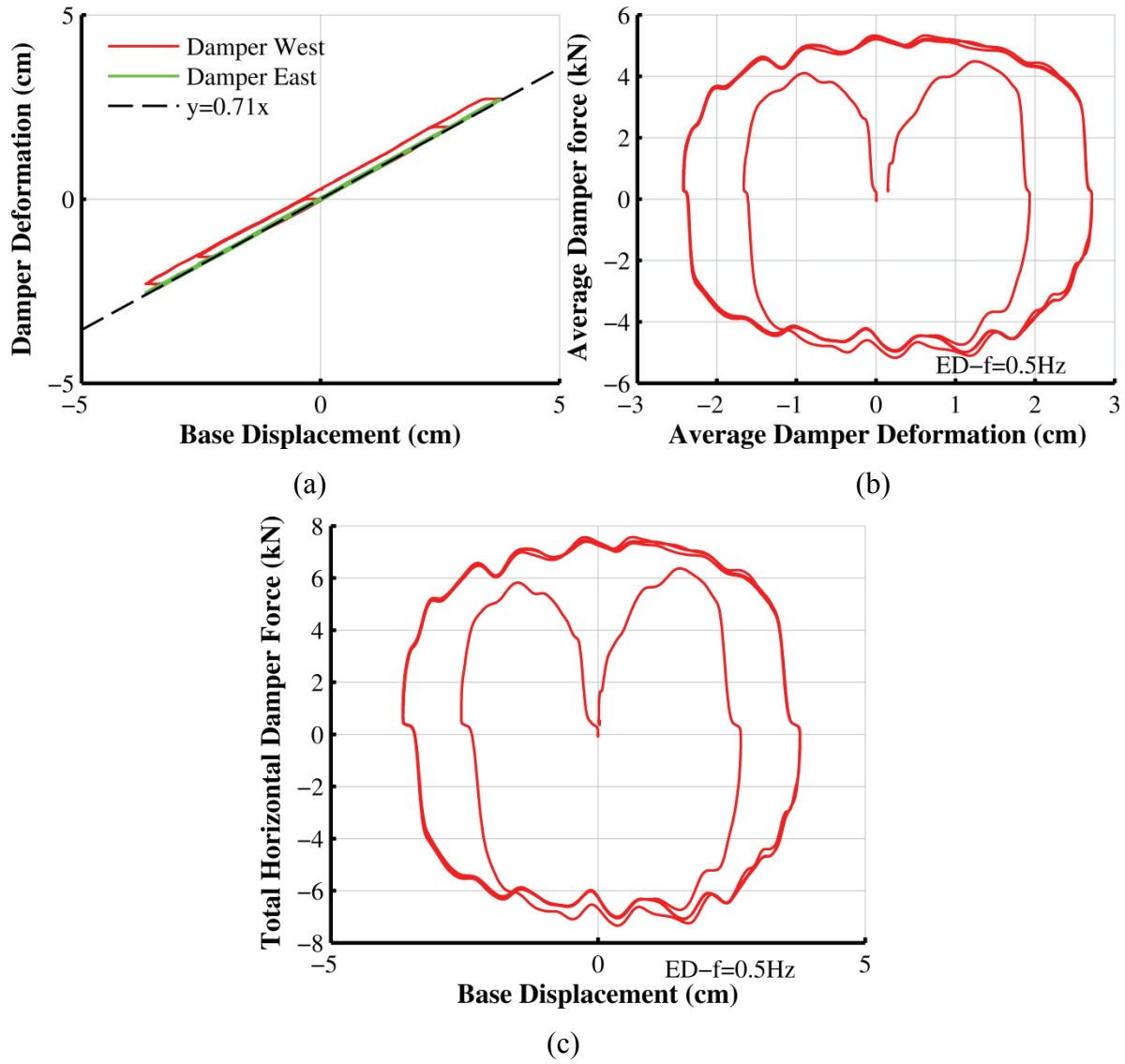


Figure 6-10: Experimental results for dampers obtained in displacement-controlled tests at frequency of 0.5Hz

6.6 Testing of NSD

Figure 6-11 shows photographs of the deformed NSD during a displacement-controlled test on the shake table.

Figure 6-12 to Figure 6-18 show results on the histories of motion of points of the NSD obtained by the Krypton camera tracking system (see Figure 2-3, Figure 3-1 and Figure 5-18) for the cases with and without the GSA (note that configurations ENA, etc. are described in Table 6-1).



Figure 6-11: Deformed NSD West (left) and NSD East (right) during displacement-controlled test at 6.4cm amplitude and 0.02Hz frequency

The results in Figure 6-12 to Figure 6-18 verify the validity of the assumptions made on the kinematics of the NSD for the development of the analytical model in Section 3. Specifically, the displacements of points A, B and E are essentially equal and the displacement of C is essentially zero (when assuming rigid members). Also point D has a displacement almost double the displacement of point B (same as the ratio l_1/l_2 for the device). Also, the motion of the points is essentially unaffected by the frequency of testing so that, indeed, the inertia effects have insignificant effects on the kinematics of the device.

The small deviations from perfect behavior are due to a) imperfect positioning of the lever (the lever was frequently adjusted up and down and exact re-positioning was impossible), b) the LED of the Krypton were not exactly positioned at the center of each pin, and c) large rotation effects of the lever that cause small differences in the motion of points A and B. Moreover, it is observed that point E has the same displacement as point A in the case without the GSA (configuration ENB) but the two points have slightly different displacements when the GSA is added (configuration ENA). The reason is that the GSA causes small deformation of the top channel of the NSD (see Section 4.5). Differences are however small as seen, for example, in Figure 6-13, and do not affect the device behavior.

Note that the displacement of point C is nonzero but small. The theory of Section 4.5 where the NSD flexibility is accounted for predicts some small motion of point C as observed in the experiments. Nevertheless, this displacement is too small by comparison to that of point A to have any effect.

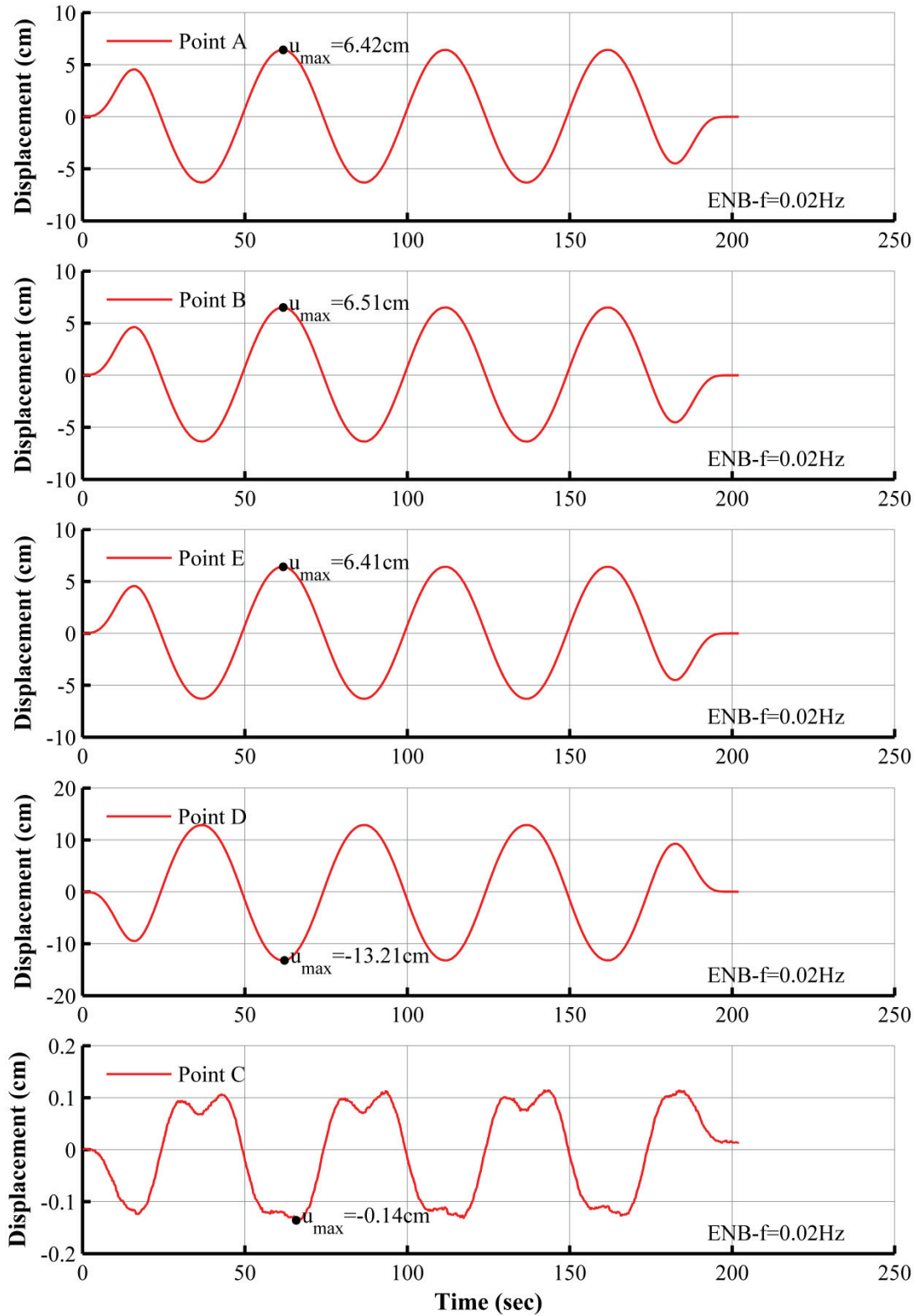


Figure 6-12: Displacement histories of points on NSD for configuration ENB (without GSA) in test at 0.02 Hz frequency

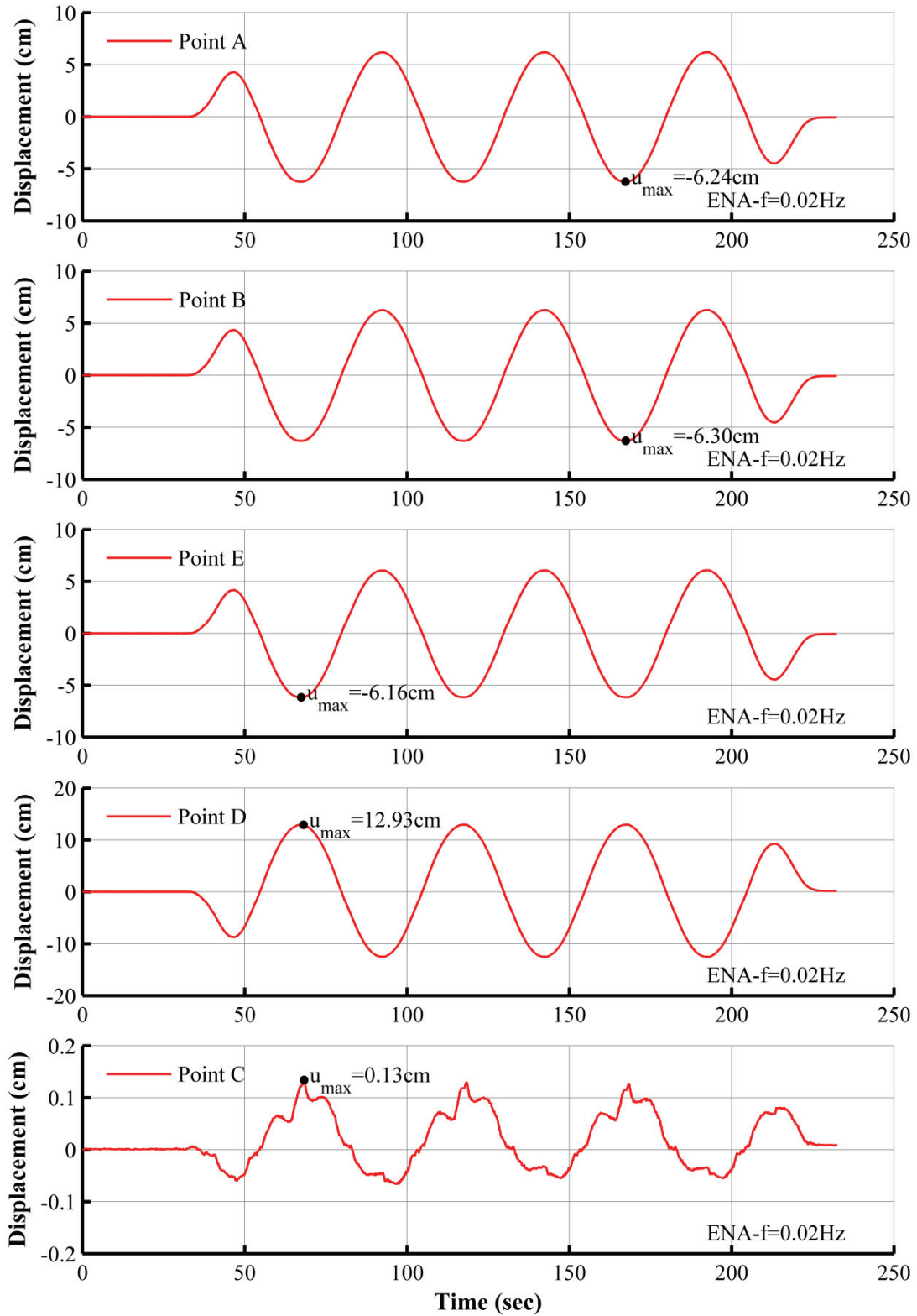


Figure 6-13: Displacement histories of points on NSD for configuration ENA (with GSA) in test at 0.02 Hz frequency

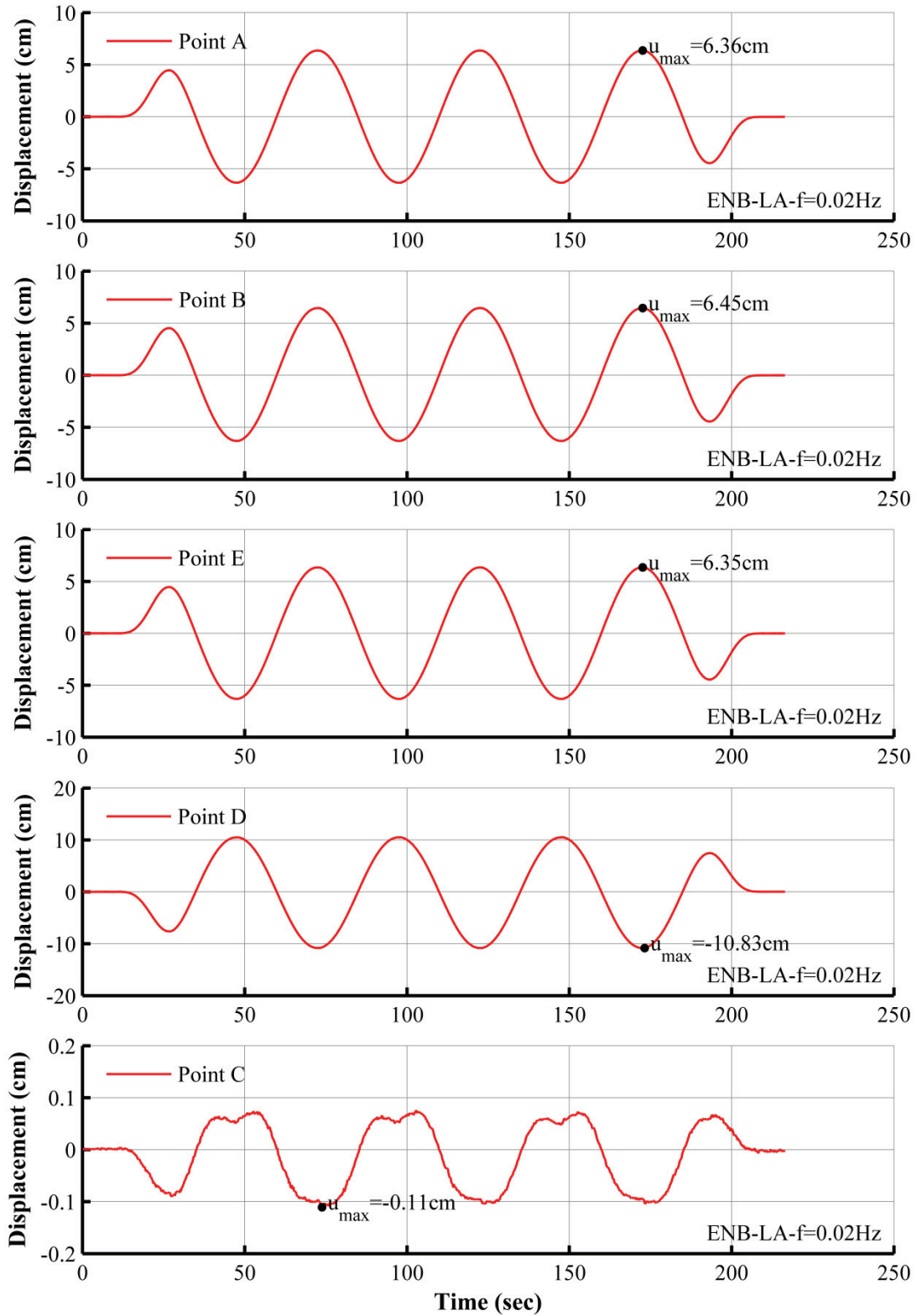


Figure 6-14: Displacement histories of points on NSD for configuration ENB-LA (with GSA) in test at 0.02 Hz frequency

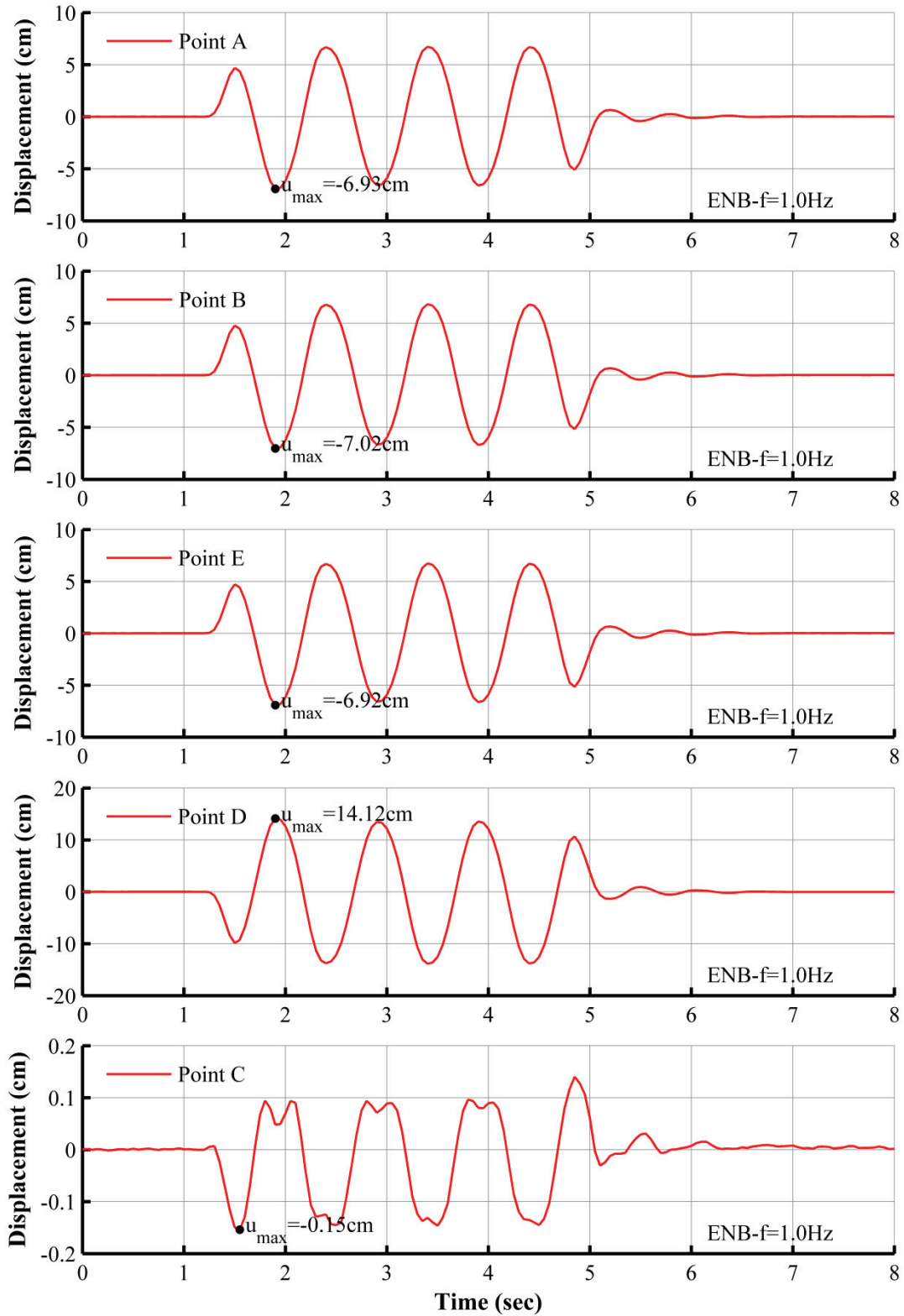


Figure 6-15: Displacement histories of points on NSD for configuration ENB (with GSA) in test at 1 Hz frequency

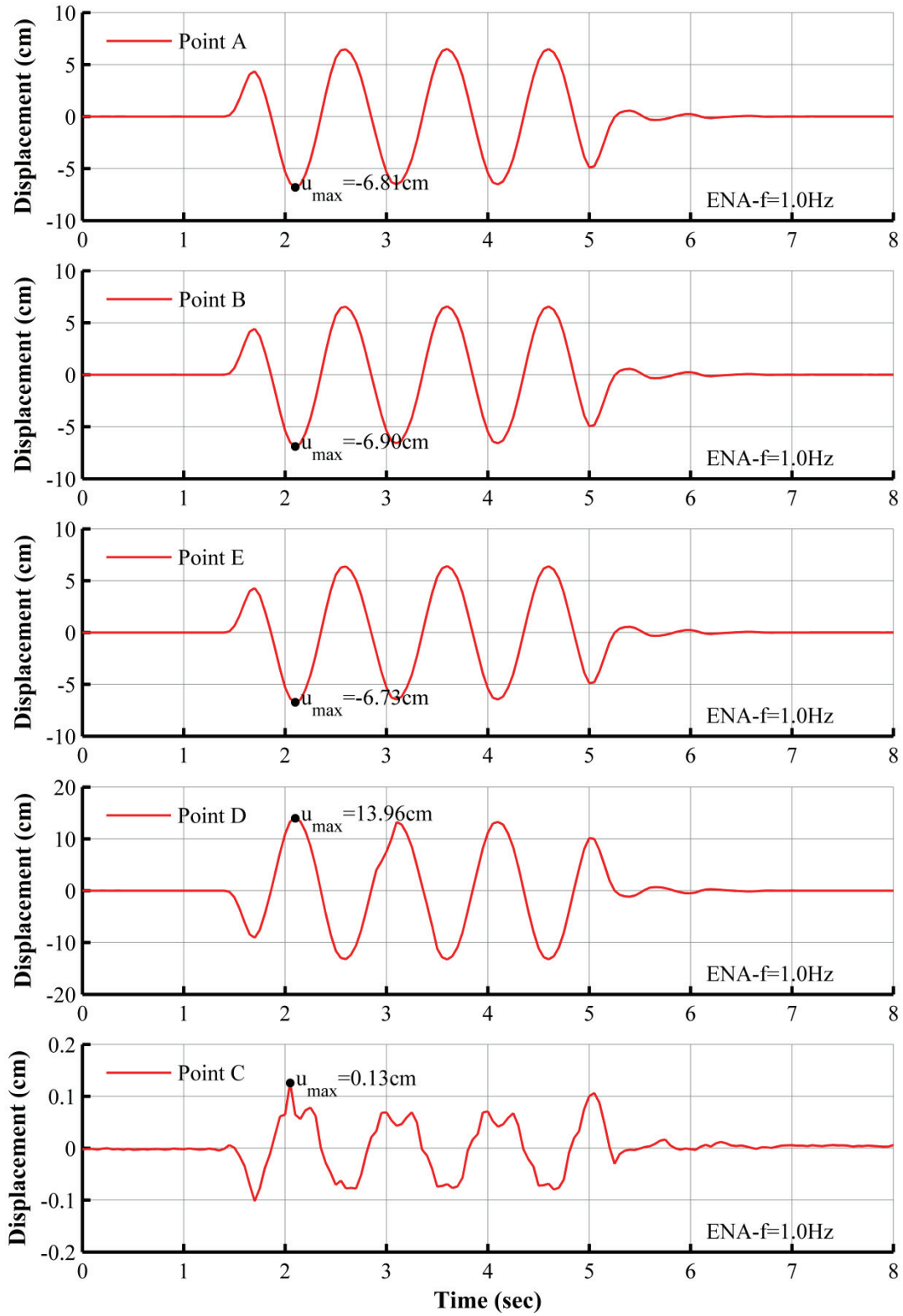


Figure 6-16: Displacement histories of points on NSD for configuration ENA (with GSA) in test at 1 Hz frequency

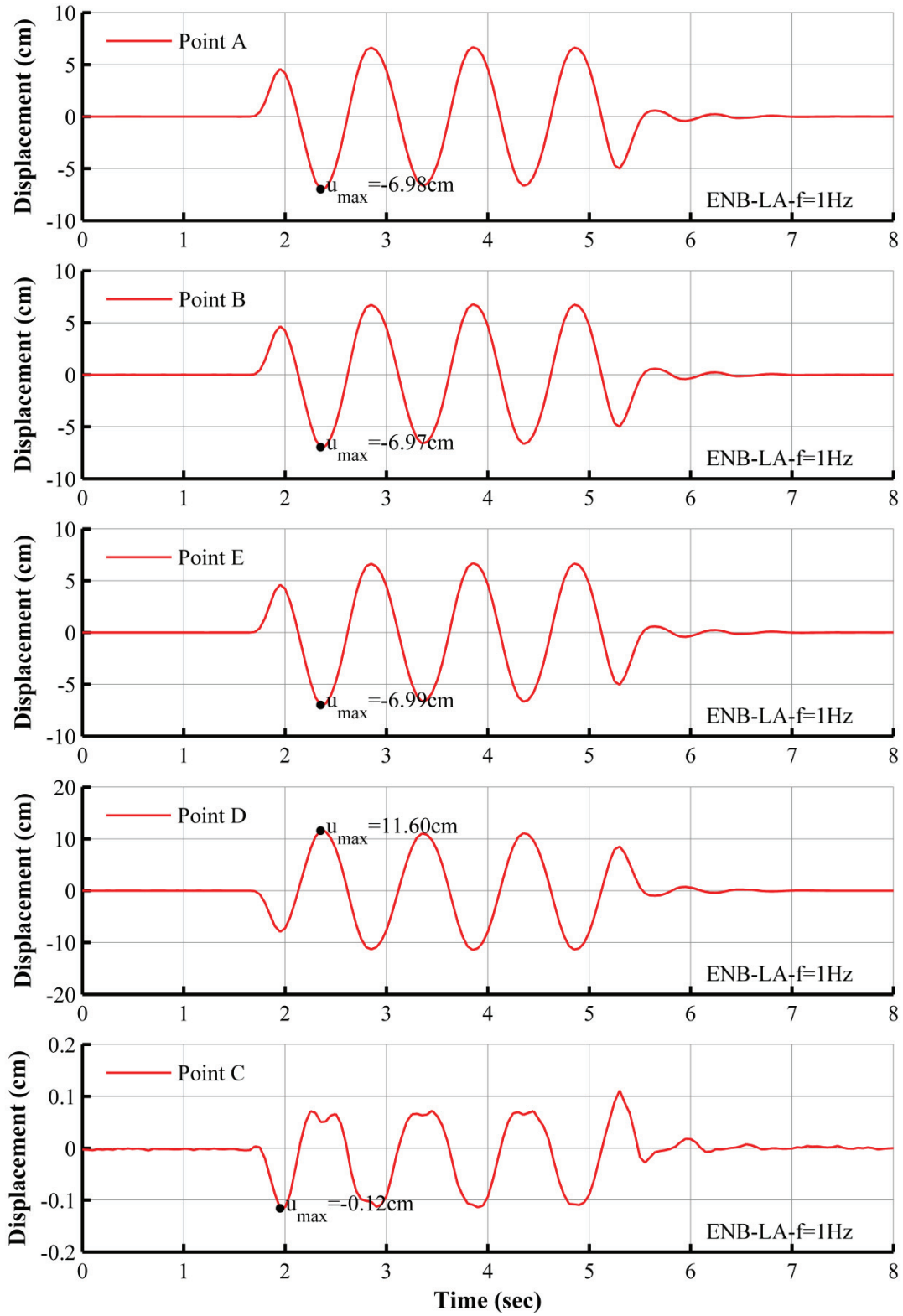


Figure 6-17: Displacement histories of points on NSD for configuration ENB-LA (with GSA) in test at 1 Hz frequency

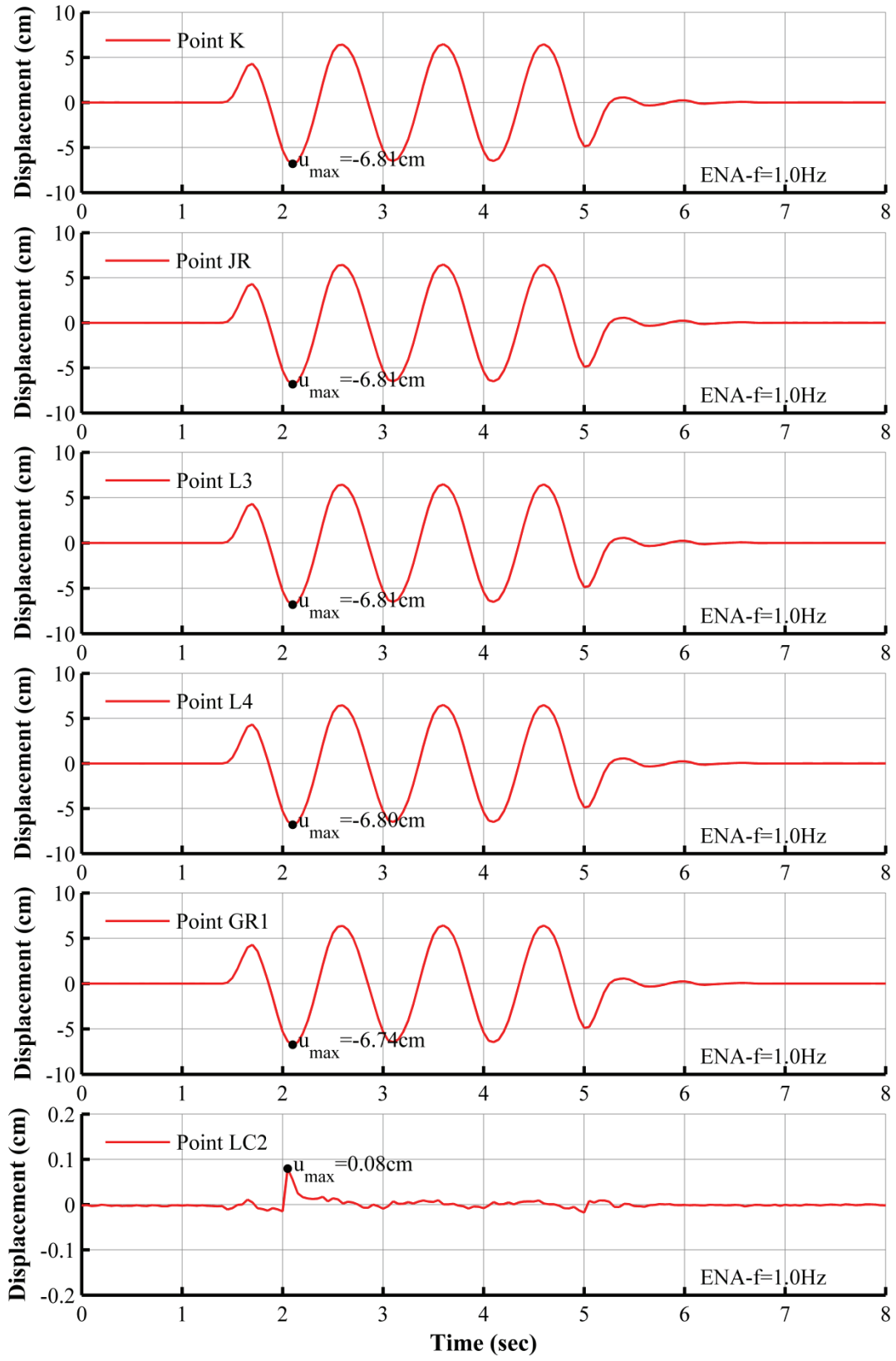


Figure 6-18: Displacement histories of additional points on NSD for configuration ENA (with GSA) in test at 1 Hz frequency

Figure 6-19 presents recorded force-displacement relations of the NSD East and NSD West in displacement-controlled tests at the frequency of 0.02Hz for configurations ENB (NSD without GSA), ENA (NSD with GSA) and ENB-LA (NSD without GSA and the lever arm modified). The latter shows the different behavior generated by the NSD when the lever arm is modified by moving the pin in the slotted connection (point B in Figure 3-9) by about 2.5cm. When compared to configuration ENB (centered pin), the peak NSD force in the ENB-LA (modified lever arm) is reduced and the stiffening displacement is increased.

Figure 6-20 presents recorded force-displacement relations of the isolation system obtained in the tests of which the individual NSD relations are shown in Figure 6-19. The column of graphs on the left in Figure 6-20 show loops of force-displacement for the elastomeric bearings as directly measured by the load cells (marked LD) and for the NSD (from the data of Figure 6-19 (marked NSD Total). The graphs on the right of Figure 6-20 show the loops of total force (LD plus NSD) denoted as “Base Shear”. The following should be noted in the results of Figure 6-19 and Figure 6-20:

1. For cases ENB and ENB-LA (without GSA), the NSD East has slightly larger forces than the NSD West. As explained in Section 5.3, there was a measurement error in the NSD West. Also, both devices show some hysteresis which is due to pin friction and dependent on the pre-loaded spring instantaneous force (see Section 4.4 for details). The NSD West shows more friction at large displacements than the NSD East which could, again, be due to measurement errors in the load cells.
2. The non-zero force at zero displacement observed in configuration ENA (with GSA) in the two bottom graphs of Figure 6-19 are due to abnormalities in the GSA as explained in Section 4.6 and, particularly, the reduction in the gap opening.

The effect of the frequency of motion is shown in the recorded force-displacement relations of the NSD East (without GSA) in Figure 6-21. There is a small effect of frequency in consistency with the theoretical predictions on the effect of inertia forces in Section 4.3. It should be noted that the results shown in Figure 6-21 were obtained from load cells which, during the testing, moved together with the shake table and, therefore, measured the inertia force of the parts attached to them in addition to the NSD force. That is, the measurement includes parasitic inertia effects that could not be corrected.

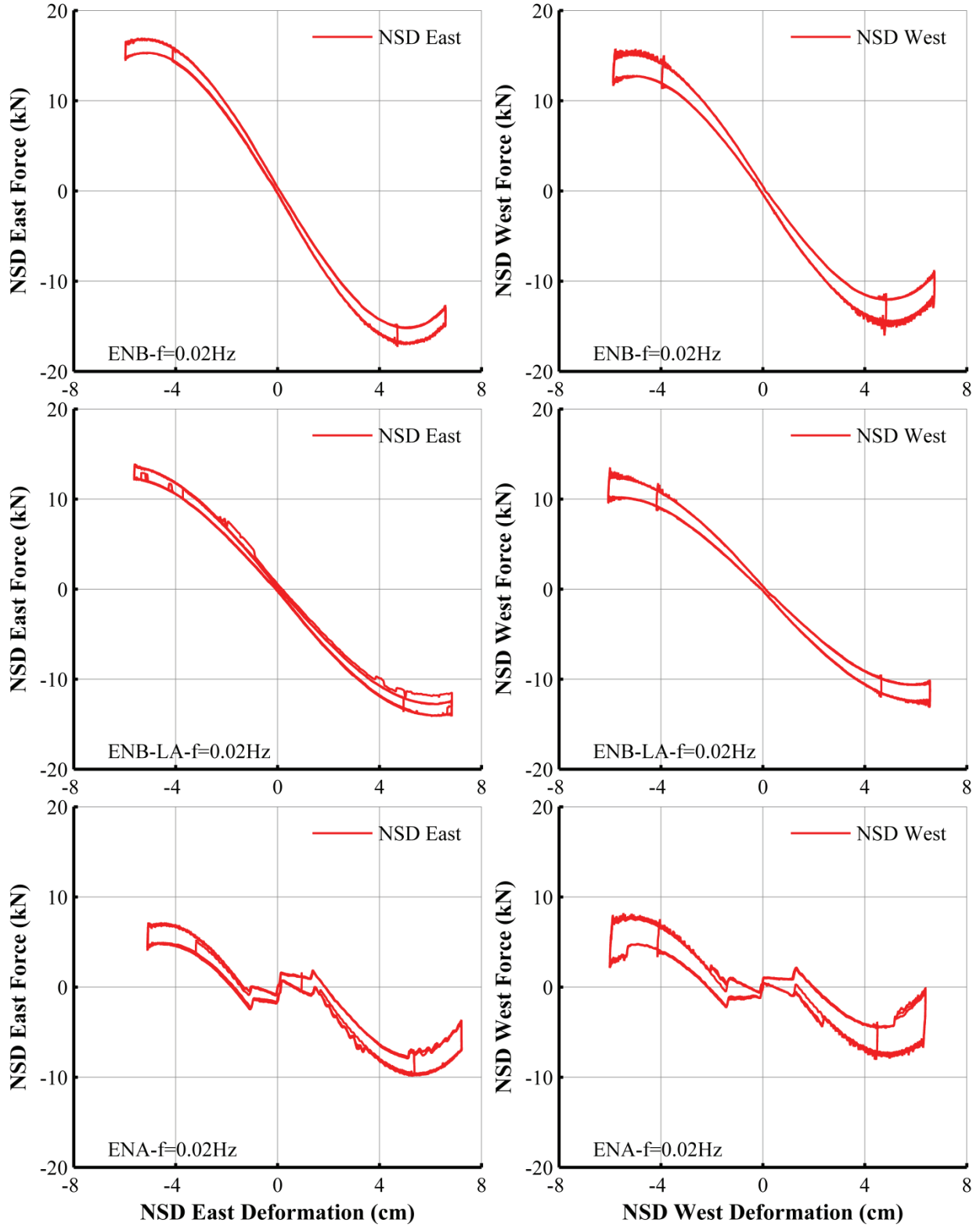


Figure 6-19: Force-displacement relations of NSD obtained in displacement-controlled test at 0.02Hz frequency for configurations ENB and ENB-LA (without GSA) and ENA (with GSA)

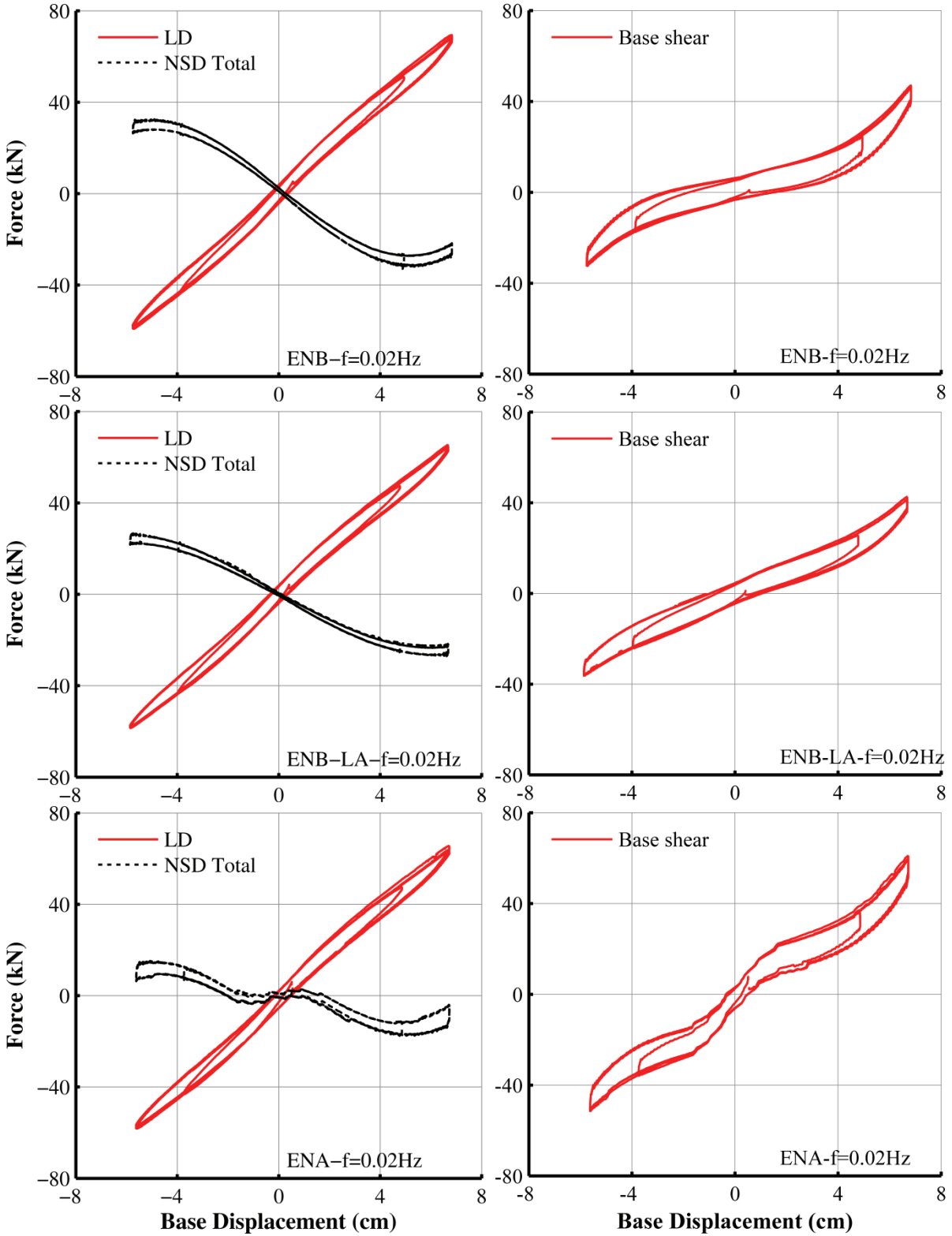


Figure 6-20: Force-displacement relations of isolation system (bearings-LD and NSD) obtained in displacement-controlled test at 0.02Hz frequency for configurations ENB and ENB-LA (without GSA) and ENA (with GSA)

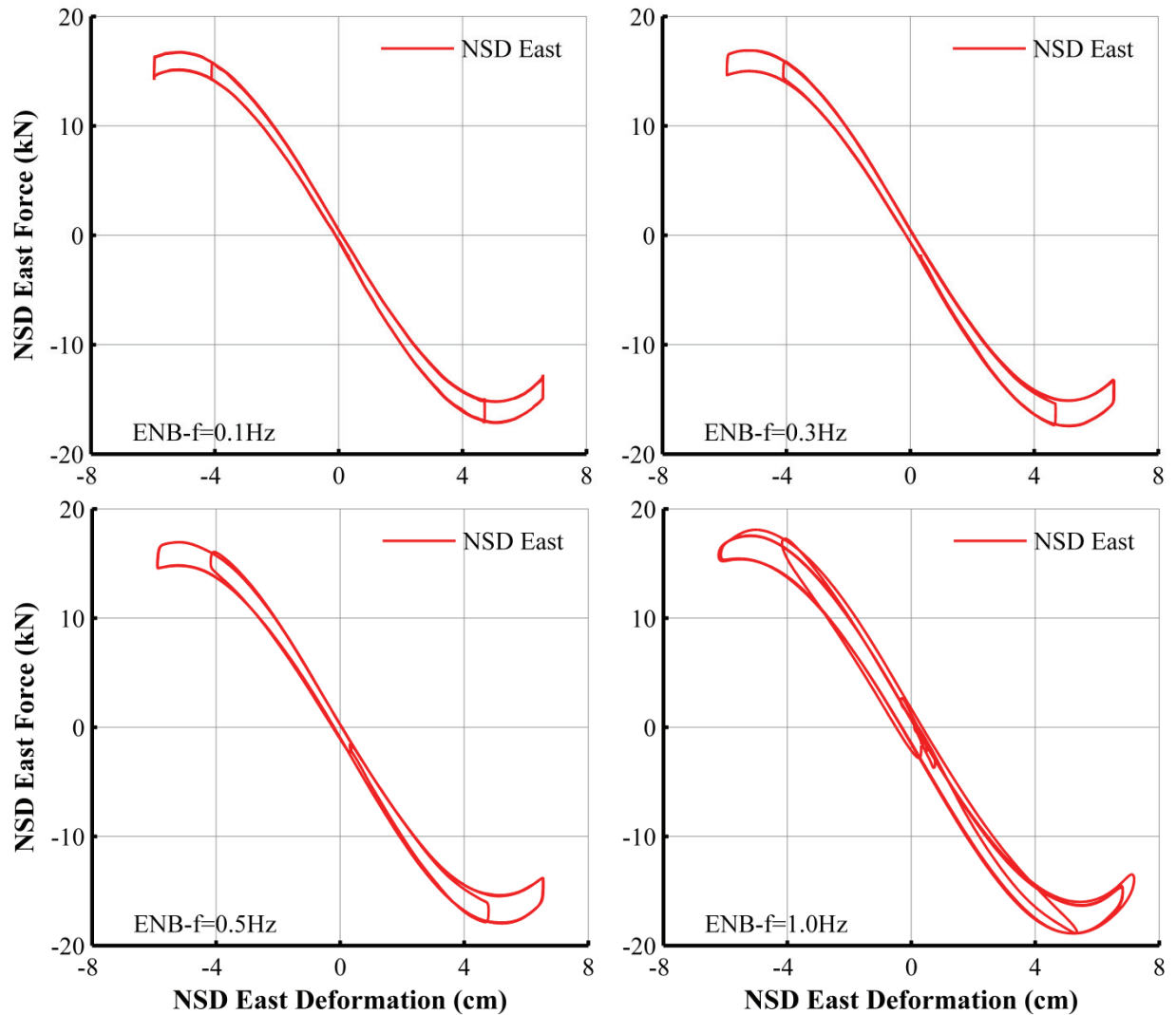


Figure 6-21: Effect of frequency on NSD East force-displacement relation

6.7 Identification of Properties of Fixed Superstructure

Prior to testing the isolated structure, the superstructure was identified by directly connecting the base, without the elastomeric bearings, on the load cells (see Figure 5-3) and subjecting it to shake table motion. For the identification of the superstructure properties, the shake table was driven in white noise motion with frequency content of 0 to 50Hz, amplitude of 0.1g and 60 second duration. The transfer functions were obtained (see Bracci et al., 1992 for description of process) using records of acceleration recorded at each floor and the shake table and shown in Figure 6-22. The mode shape, period and damping ratio of each of the three translational (testing direction) modes of the superstructure were derived from the transfer functions (see Bracci et al., 1992) and are presented in Table 6-4.

Table 6-4: Mode shape, period and damping ratio for three modes of vibration of superstructure obtained in low amplitude white noise testing

Mode No.	Period (sec)	Damping Ratio	Mode Shape		
			1 st floor	2 nd floor	3 rd floor
1 st	0.299	0.0862	0.415	0.753	1.000
2 nd	0.077	0.0137	-1.216	-0.816	1.000
3 rd	0.046	0.0078	2.364	-2.199	1.000

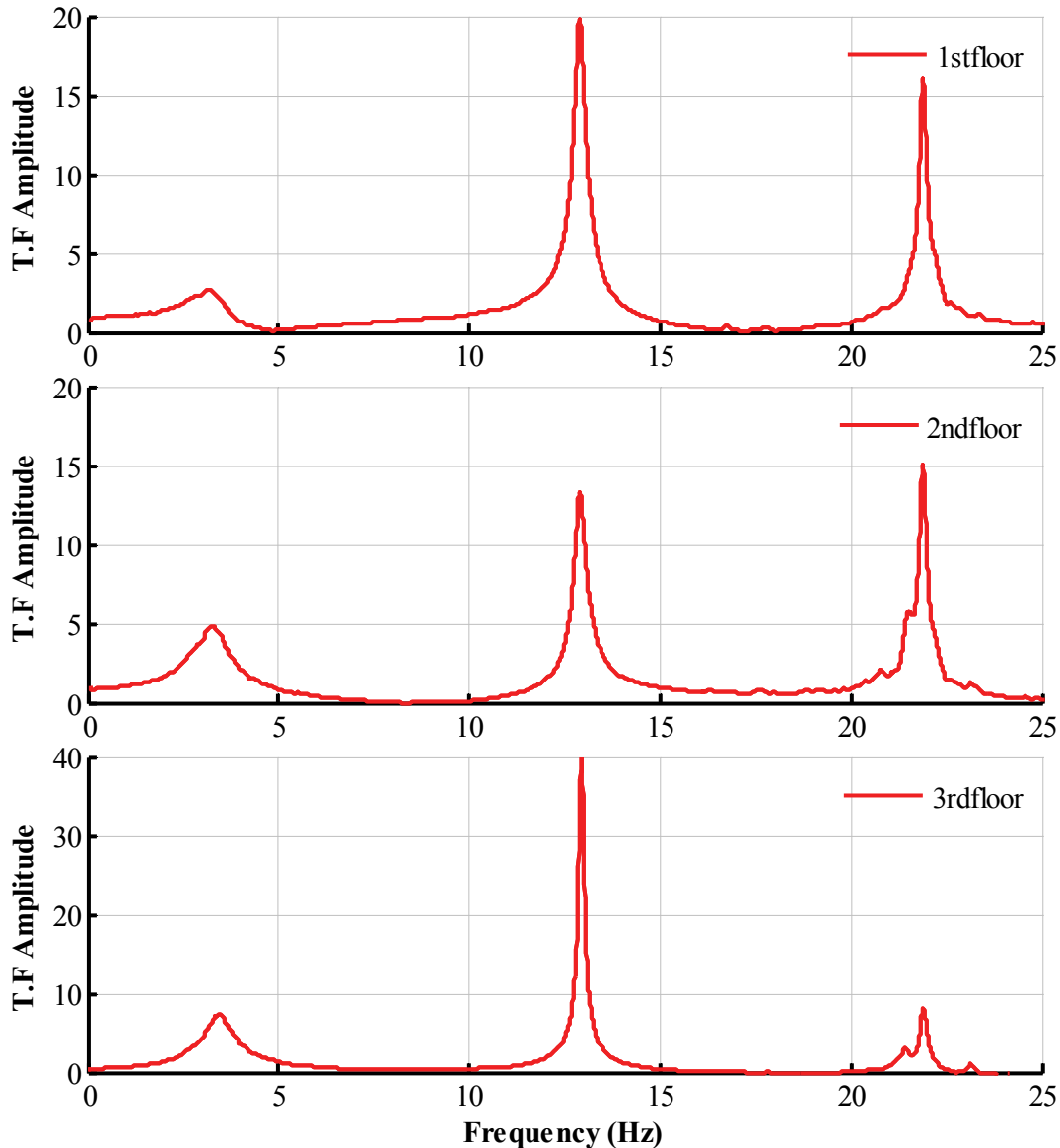


Figure 6-22: Amplitude of transfer functions (T.F.) of superstructure obtained in low amplitude white noise testing

The structure has a high damping ratio in the first mode, something also observed in previous identification of the complete 6-story model (Fenz and Constantinou, 2008b and Wolff and

Constantinou, 2004). This is attributed to slippage in the connections of the concrete blocks to the steel frame. The damping is dependent on the amplitude of motion, hence to the excitation too. It is largest at small amplitude vibration with rich frequency content. The structure was also identified in low amplitude (to prevent yielding) seismic excitation. Results are presented in Table 6-5 and Figure 6-23. Table 6-6 presents the stiffness and damping matrix of the structure as obtained from the data of Table 6-4 and Table 6-5 and using the procedures in Bracci et al. (1992). The degrees of freedom are the displacements of each floor with respect to the ground. There is some difference between the two sets of results, which are typical of the difficulties in the identification of models that are not exactly linear elastic and linear viscous.

Table 6-5: Mode shape, period and damping ratio for three modes of vibration of superstructure obtained in low amplitude seismic testing with motion ATL 270

Mode No.	Period (sec)	Damping Ratio	Mode Shape		
			1 st floor	2 nd floor	3 rd floor
1 st	0.277	0.0597	0.385	0.746	1.000
2 nd	0.077	0.0135	-1.217	-0.803	1.000
3 rd	0.045	0.0060	2.528	-2.328	1.000

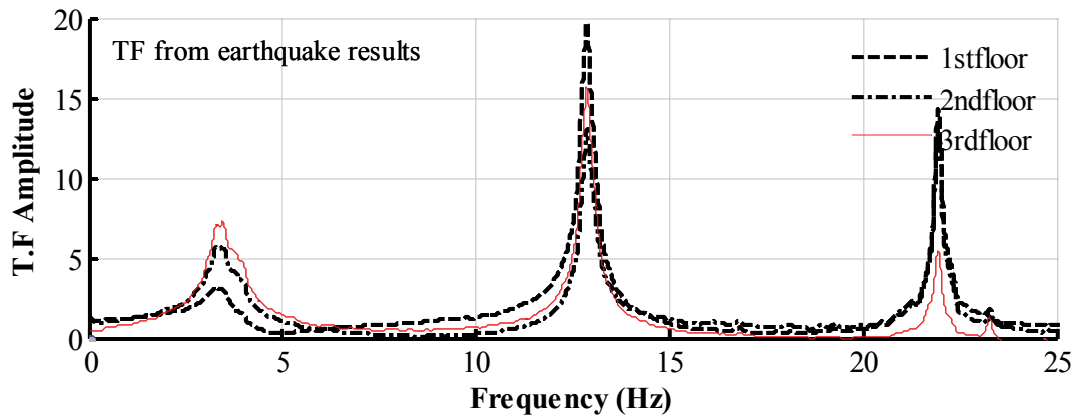


Figure 6-23: Amplitude of transfer functions of superstructure obtained in low amplitude seismic testing with motion ATL 270

Table 6-6: Stiffness and damping matrices of superstructure constructed from modal data in identification tests

Test	Stiffness matrix (kN/cm)	Damping Matrix ($kN\text{-}sec/cm$)
White noise	$K = \begin{bmatrix} 555.5 & -333.2 & 26.6 \\ -333.2 & 515.8 & -233.2 \\ 26.6 & -233.2 & 185.9 \end{bmatrix}$	$C = \begin{bmatrix} 0.118 & 0.018 & 0.021 \\ 0.018 & 0.123 & 0.028 \\ 0.021 & 0.028 & 0.143 \end{bmatrix}$
Seismic motion ATL-270	$K = \begin{bmatrix} 558.9 & -330.2 & 40.3 \\ -330.2 & 520.9 & -242.5 \\ 40.3 & -242.5 & 190.1 \end{bmatrix}$	$C = \begin{bmatrix} 0.101 & 0.018 & 0.004 \\ 0.018 & 0.097 & 0.015 \\ 0.004 & 0.015 & 0.116 \end{bmatrix}$

6.8 Shake Table Testing Results

This section presents results as follows:

1. A comparison of the 5%-damped acceleration response spectra for all ground motions as calculated from the recorded acceleration histories of the table in all tested configurations and as calculated from the target acceleration history in Figure 6-24. There are some differences in the spectra of the motions but they are sufficiently close to be able to compare experimental results for the various configurations.
2. Peak recorded inter-story drift ratio, floor accelerations, base displacements and base shear forces in tabular form in Table 6-7 to Table 6-9 for all tests.
3. Histories of recorded inter-story drift ratio, floor accelerations and bearing axial loads, and force-displacement loops in graphical form for all configurations tested but only for one seismic motion (PS10317) in Figure 6-25 to Figure 6-34. Results for all other tests are presented in Appendix A. Results in graphical form for floor response spectra of all floors and the base are presented in Figure 6-35 to Figure 6-38 for all ground motions and all configurations tested.
4. Comparisons of peak recorded inter-story drift ratio, floor acceleration, base displacement and base shear force for all tested configurations and all motions in graphical form in Figure 6-39 to Figure 6-41.

The following comments describe how the results in Table 6-7 to Table 6-9, Figure 6-25 to Figure 6-38 and Appendices A and B were obtained:

1. Displacements and accelerations were directly measured by string pots and accelerometers, respectively. Relative displacements were calculated by subtracting the records of displacements at two points.
2. For configurations without dampers (cases ENA, ENB and ENB-LA), the NSD forces were calculated as the difference of the base shear force calculated from records of acceleration after multiplication by the effective mass and addition over the height of the model (F_{acc} as given by Equation (5-1)) and the elastomeric bearing forces F_{ld} as directly measured by the load cells supporting the bearings (see Section 5.3). This approach resulted in the most accurate measurement of the NSD forces. The NSD forces were also measured by load cells directly connected to the NSD but their measurements contained some error as described in Section 5.3. Appendix B presents comparisons of NSD forces obtained by the two procedures.
3. For configurations with dampers, the NSD forces were directly measured by the NSD load cells. The measurement contains some small error.
4. The viscous damper force component in the longitudinal model direction was calculated as the sum of the load cell force measurements from the two dampers multiplied by the damper's direction cosine factor which equals 0.69. For some tests, the data stream from the load cell of the East damper was lost due to a loose connector. For those cases, the

total damper force was calculated as twice the value obtained from the single functional load cell on the West damper times the direction factor 0.69. Appendix A presents in Figures A-2 to A-17 comparisons of the viscous damper force component in the longitudinal direction obtained from two load cell measurements to the force obtained from one load cell and then doubled. The comparison is excellent so that the loss of data from the faulty connection did not result in any important loss of information.

The effect of the NSD is best observed in the peak response data of Table 6-7 to Table 6-9 and in graphical form in Figure 6-39 to Figure 6-41. In discussing the results, it is important to note that configuration E represents a seismically isolated structure with low damping elastomeric bearings. The effective period of the isolated structure in the scale of the model is about 0.8sec (or 1.6sec in the prototype scale) and its effective damping is about 5-percent. The period is relative low but realistic given the loads carried by the bearings and the limitations imposed by considerations of stability of the bearings. However, it may be regarded realistic for a light weight structure supported by elastomeric bearings. Also, damping is low so that another configuration with linear viscous dampers (configuration ED) was tested. Configuration ED had an effective period of about 0.8sec and effective damping of about 25-percent, of which 20-percent was contributed by the dampers and 5-percent by the elastomeric bearings. Moreover, configurations ENA and EDNA included the NSD with GSA, configurations ENB and EDNB included the NSD without GSA and configurations ENB-LA and EDNB-LA included the NSD with modified lever arm (negative stiffness reduced in absolute value-see Figure 6-19) and without the GSA. Direct observations in the results of Tables 6-9 to 6-11, Figure 6-35 to Figure 6-38 and Figure 6-39 to Figure 6-41 are:

1. The damped configuration ED outperforms the low-damped configuration E in all response measures. The isolation system (or base) displacement is reduced by 30 to 50-percent, base shear is less and inter-story drift is less in most cases, whereas the floor acceleration is about the same (with some cases a little more and some cases a little less). In general, the results are consistent with those of Wolff and Constantinou (2004) and confirm the widely accepted position that linear viscous damping offers important benefits in seismically isolated structures.
2. The addition of the NSD with GSA (configurations ENA and EDNA) resulted in some reduction of inter-story drift and floor acceleration in the majority of tested cases, and some reduction in base shear, which was significant in the case of the configurations without dampers. The floor spectra were reduced for all ground motions even in cases where the presence of the NSD increased the peak floor accelerations. As discussed earlier, the GSA had a larger engagement displacement than needed and especially for cases with dampers (where base displacement was smaller) peak quantities occurred prior to the NSD engaging. Moreover attempts to adjust the gap opening resulted in unwanted behavior and details of its construction (that were later corrected) resulted in parasitic

behavior. This behavior essentially reduced the efficiency that the GSA could have offered.

3. The addition of the NSD without the problematic GSA (configurations ENB, ENB-LA, EDNB and EDNB-LA) shows drastic reductions in base shear, floor accelerations and inter-story drift. The efficiency of the dampers in controlling base displacements is particularly demonstrated for ground motions PS10317, NWH-090 and DZC-270 were in their absence (configurations ENB and ENB-LA) displacements are significantly increased when compared to configuration E, however in their presence (EDNB and EDNB-LA) displacements are the same as those exhibited by configuration ED. Note that these configurations result in reduced effective stiffness. On the basis of the loops in Figure 6-20, the effective stiffness for systems ENB and ENB-LA is about 5kN/cm and 7kN/cm, respectively, for displacements less than 4cm. On the basis of this stiffness, the effective period is about 1.3sec and 1.1sec, respectively, instead of 0.8sec for the configuration without the NSD. Also, the effective damping is more.
4. In all configurations without the GSA (configurations ENB, ENB-LA, EDNB and EDNB-LA), permanent deformations occurred as depicted in the histories of base displacement in Figure 6-27 and Figure 6-28. No permanent deformations occurred in the configurations with GSA (ENA and EDNA). These permanent deformations could be eliminated at the conclusion of testing by disconnecting the NSD. The occurrence of permanent deformations for case ENB is explained by the force-displacement loops in Figure 6-25 for configurations E, ENA and ENB. It is apparent that the low effective stiffness of ENB leads to permanent deformations larger than those exhibited by configurations E and ENA.

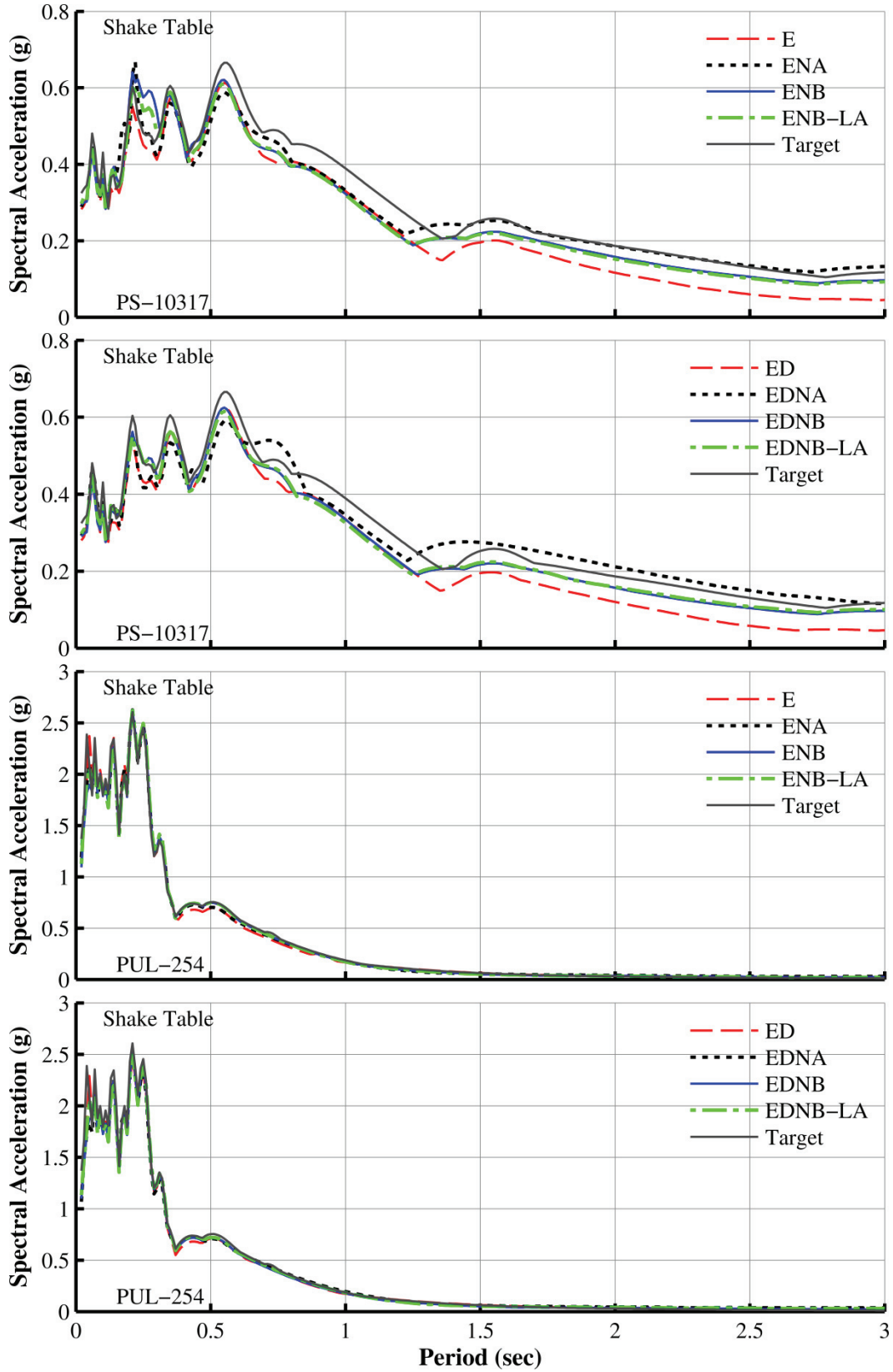


Figure 6-24: Target and table motion 5%-damped acceleration response spectra

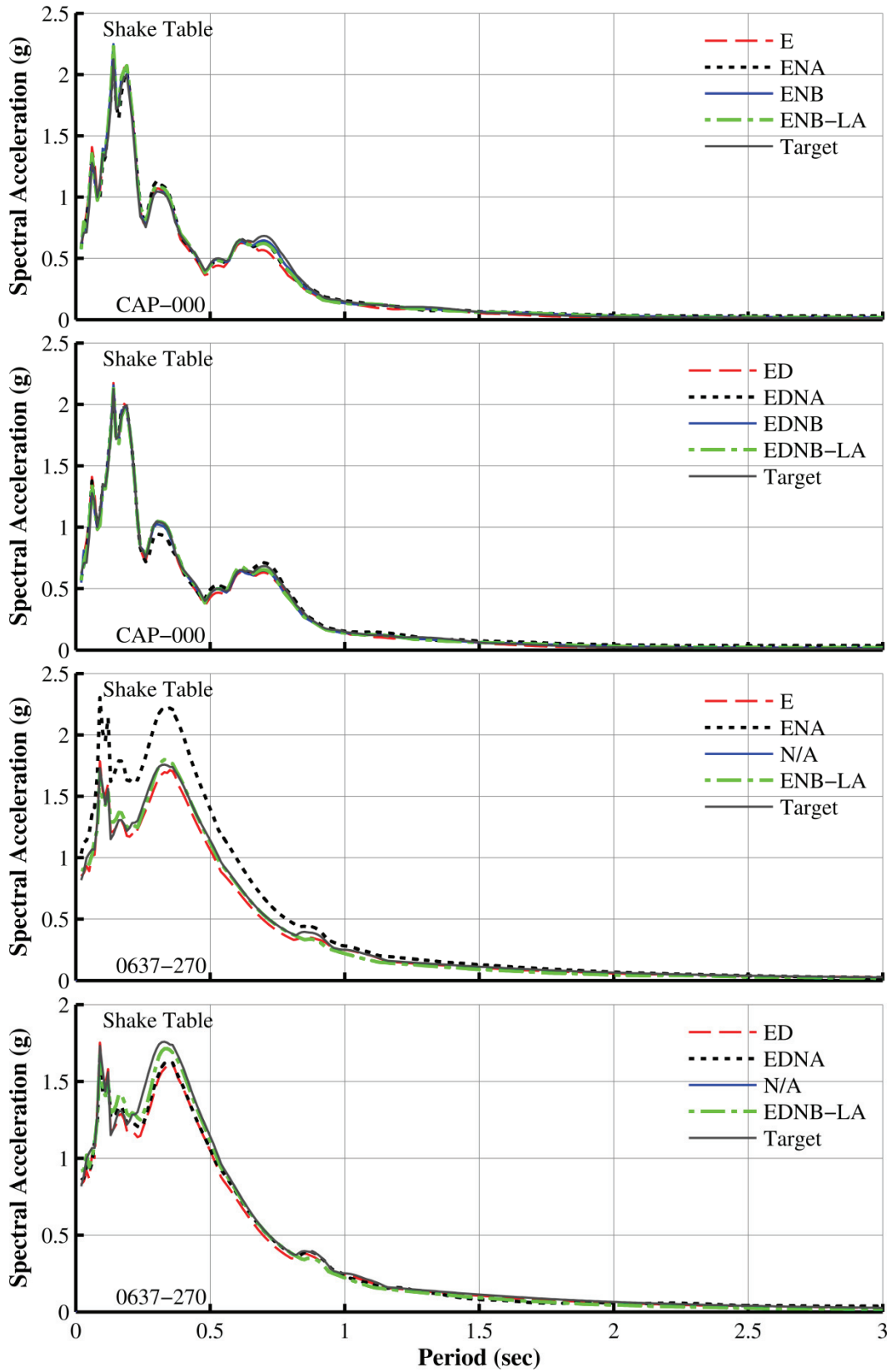


Figure 6-24 (cont'd): Target and table motion 5%-damped acceleration response spectra

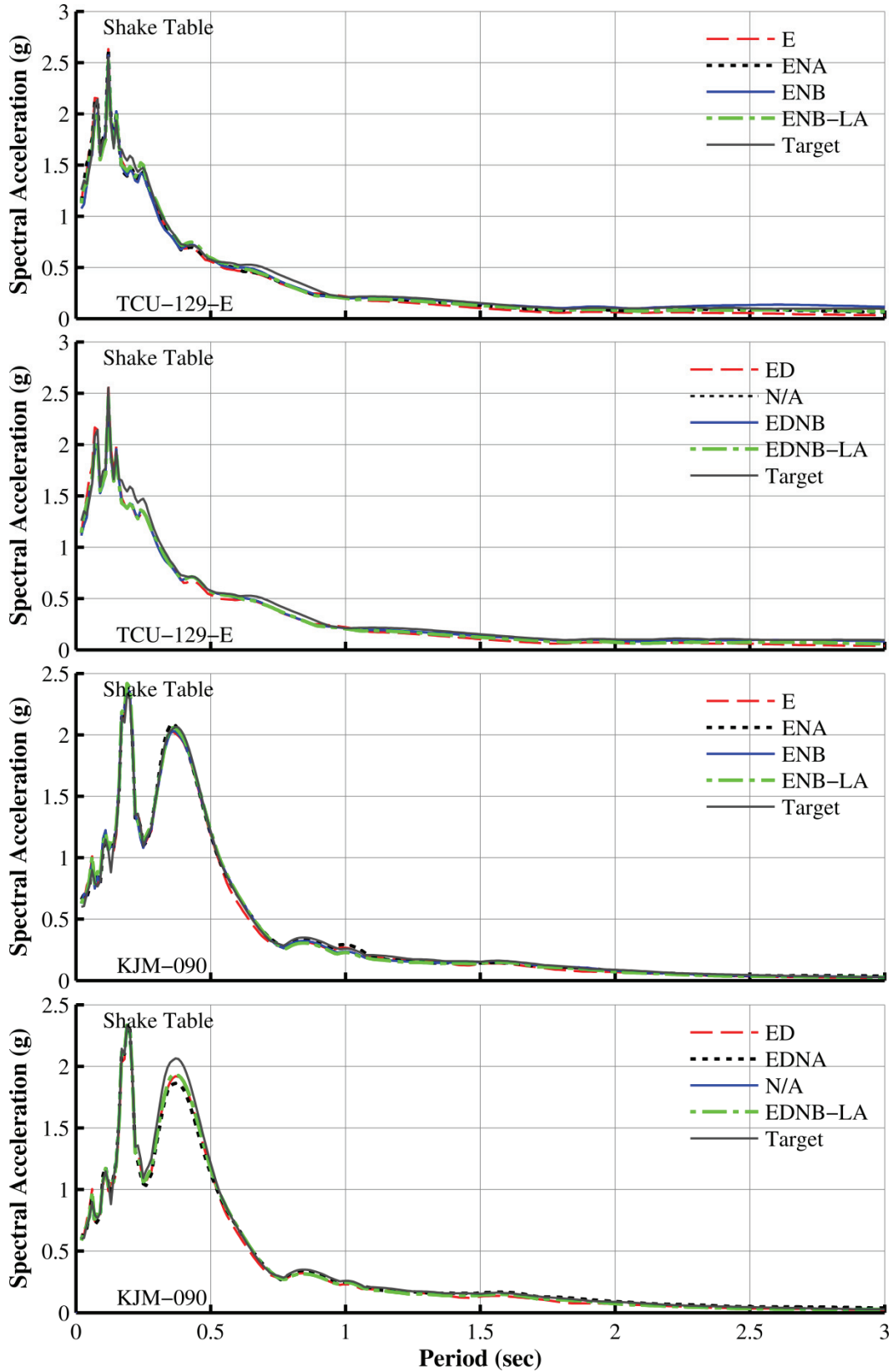


Figure 6-24 (cont'd): Target and table motion 5%-damped acceleration response spectra

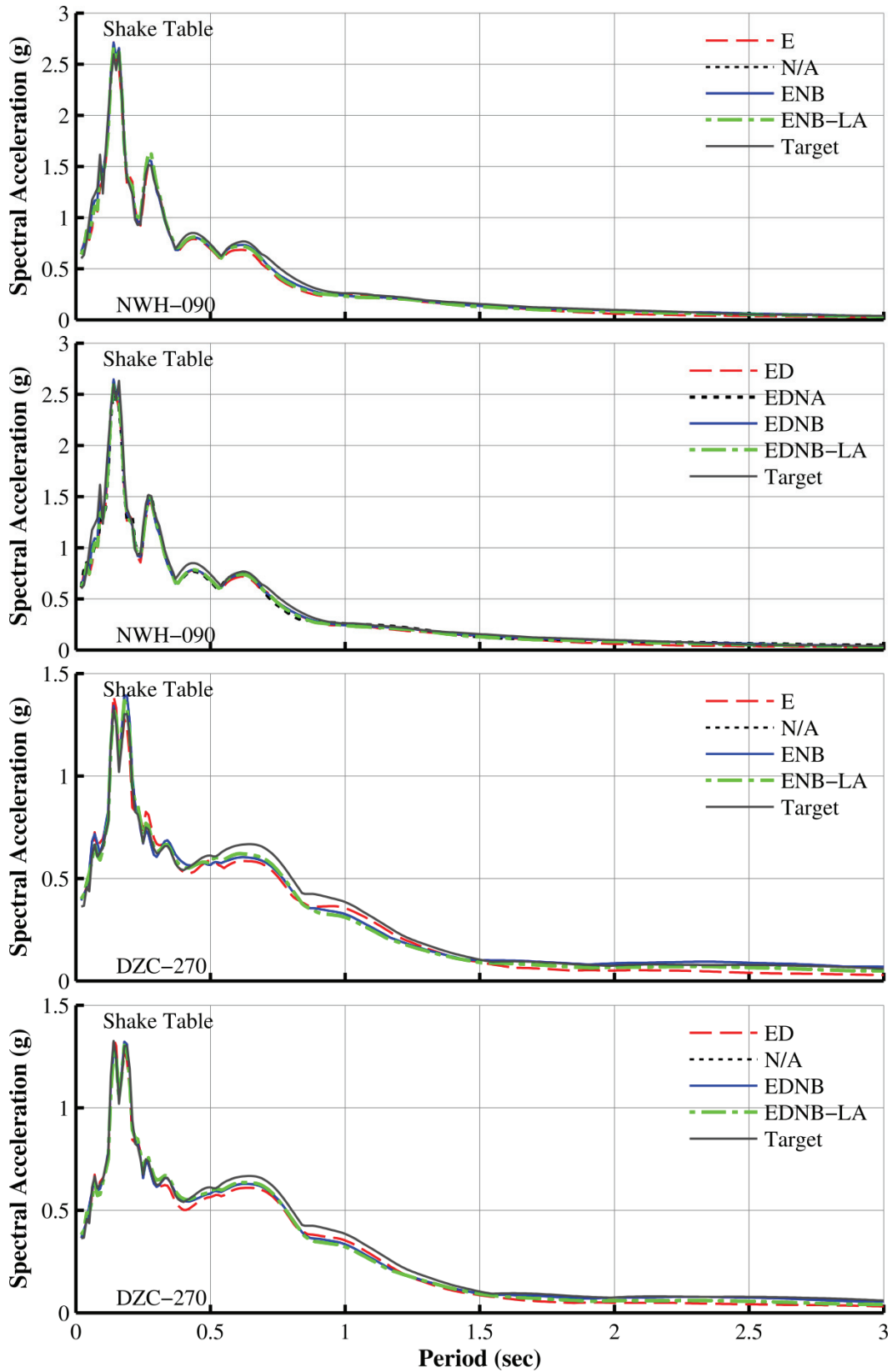


Figure 6-24 (cont'd): Target and table motion 5%-damped acceleration response spectra

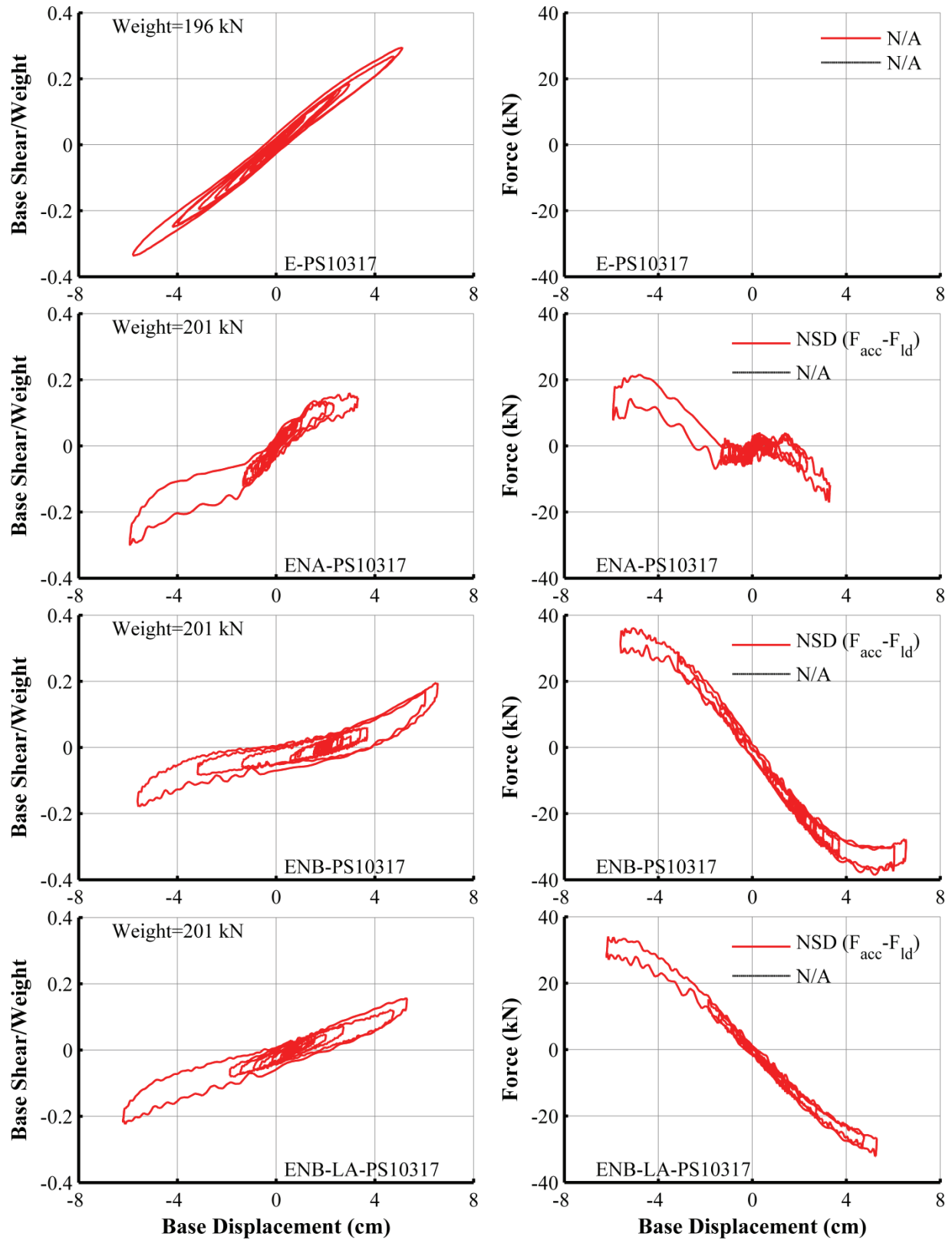


Figure 6-25: Base shear divided by weight and NSD force versus base displacement loops recorded for motion PS10317 and configurations without dampers

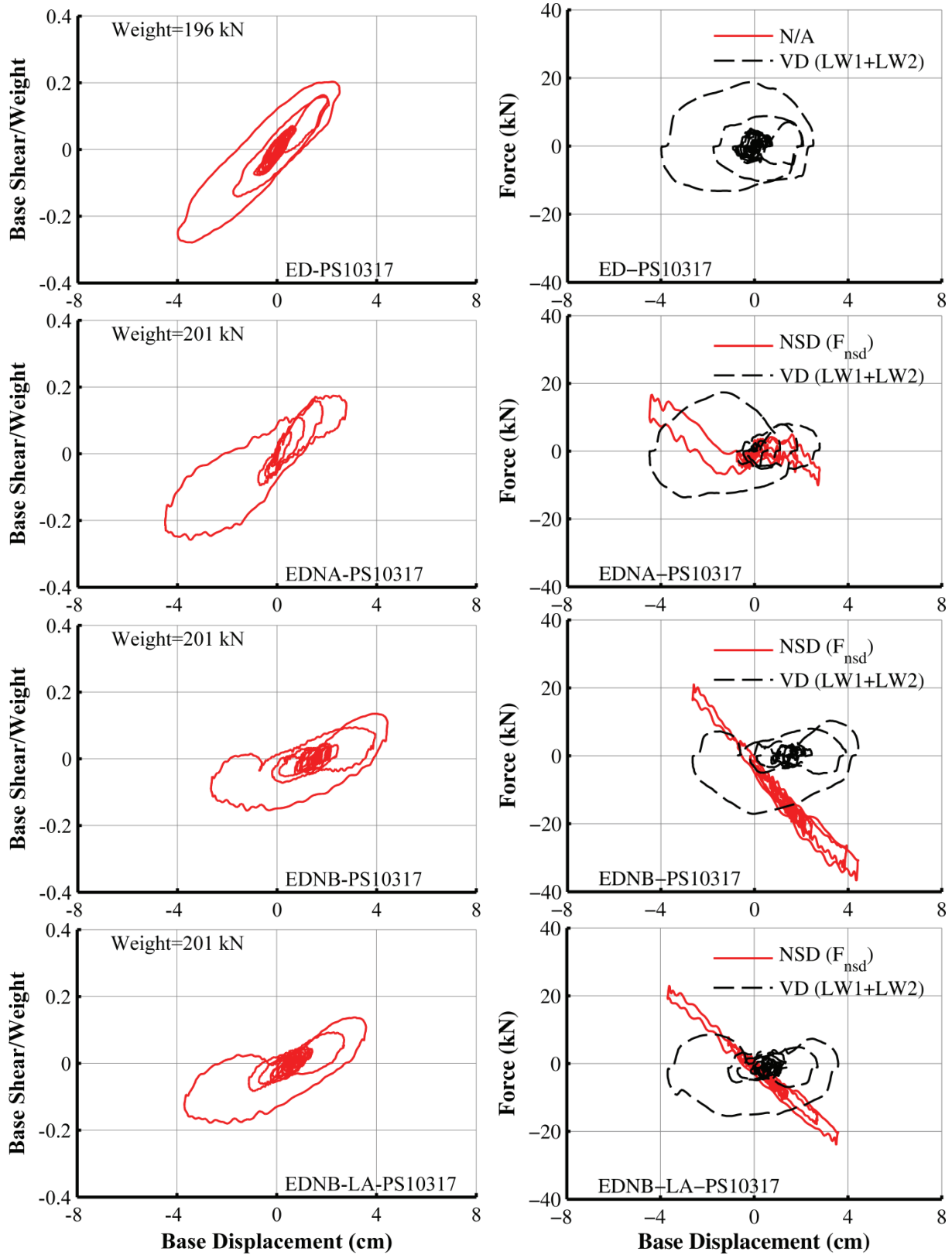


Figure 6-26: Base shear divided by weight, NSD force and viscous damper force versus base displacement loops recorded for motion PS10317 and configurations with dampers

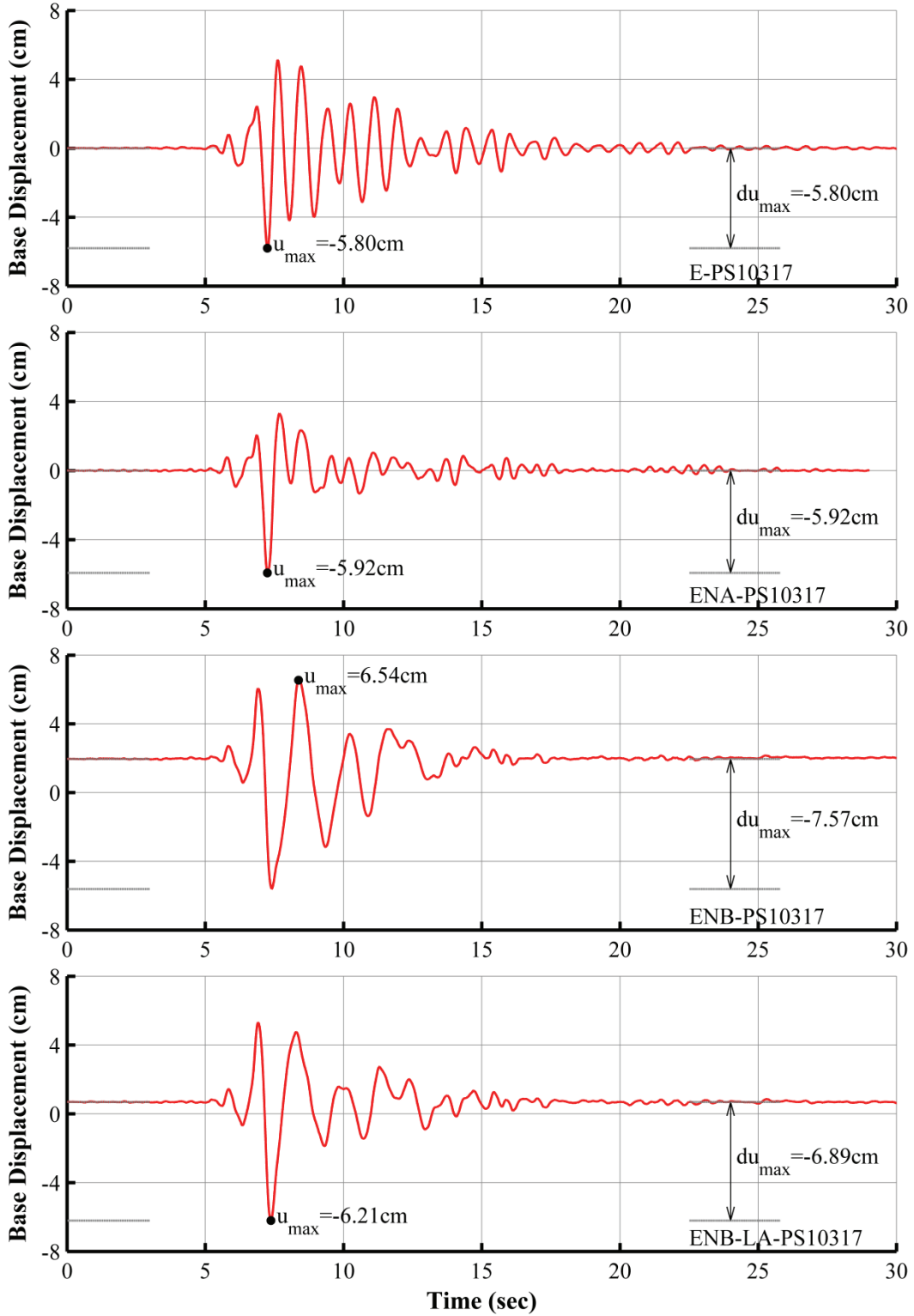


Figure 6-27: Base displacement histories recorded for motion PS10317 and configurations without dampers

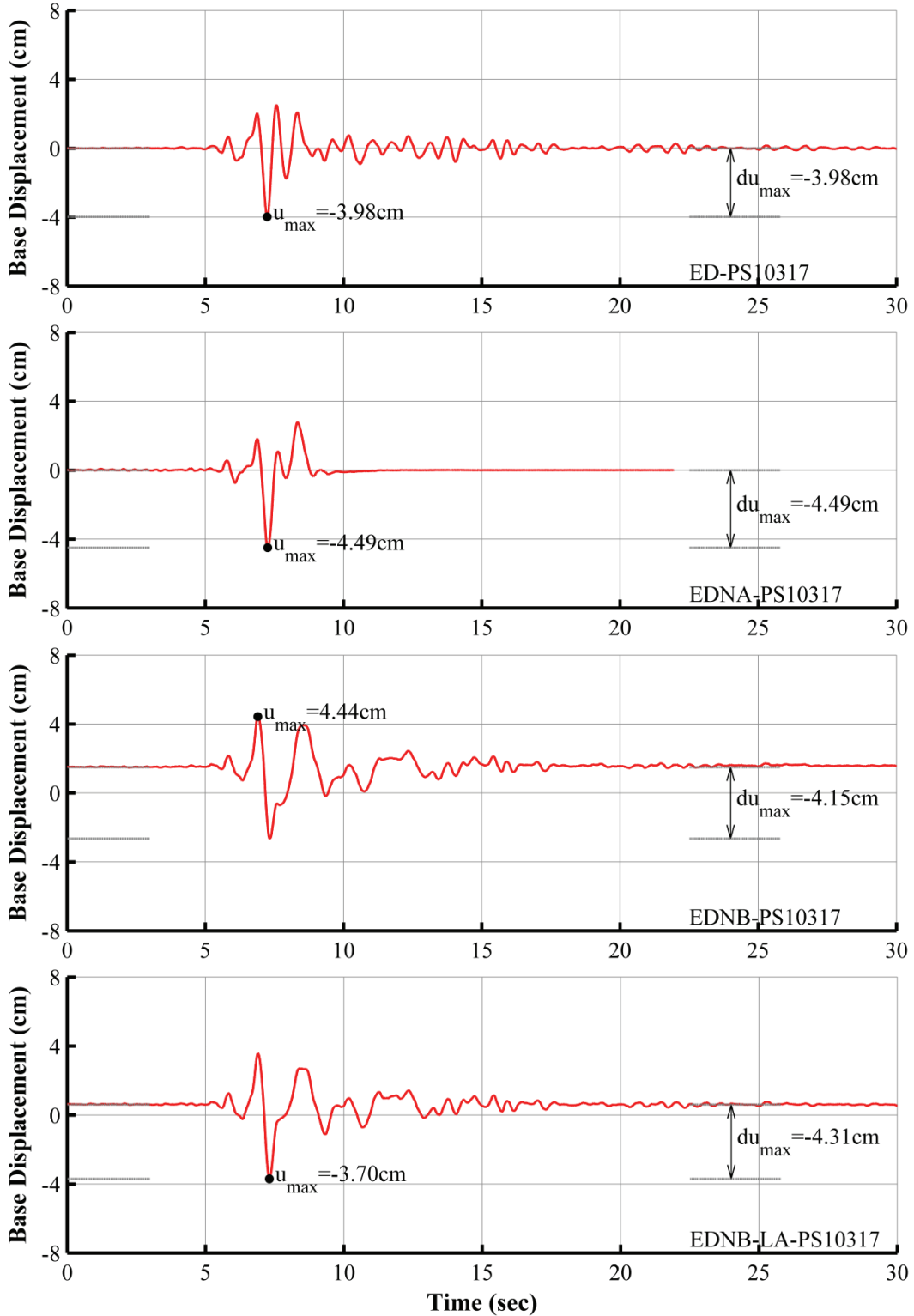


Figure 6-28: Base displacement histories recorded for motion PS10317 and configurations with dampers

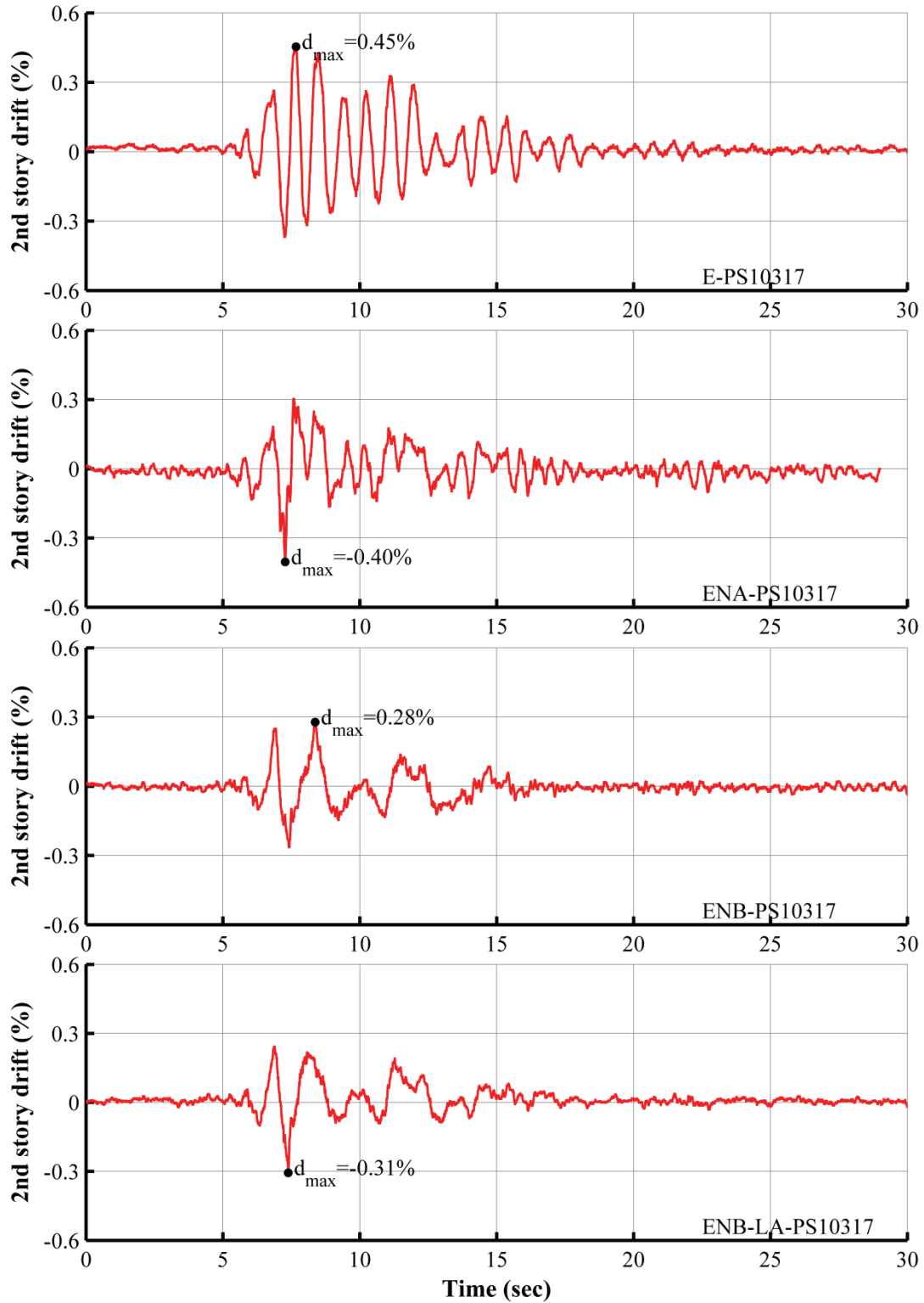


Figure 6-29: 2nd story drift ratio recorded for motion PS10317 and configurations without dampers

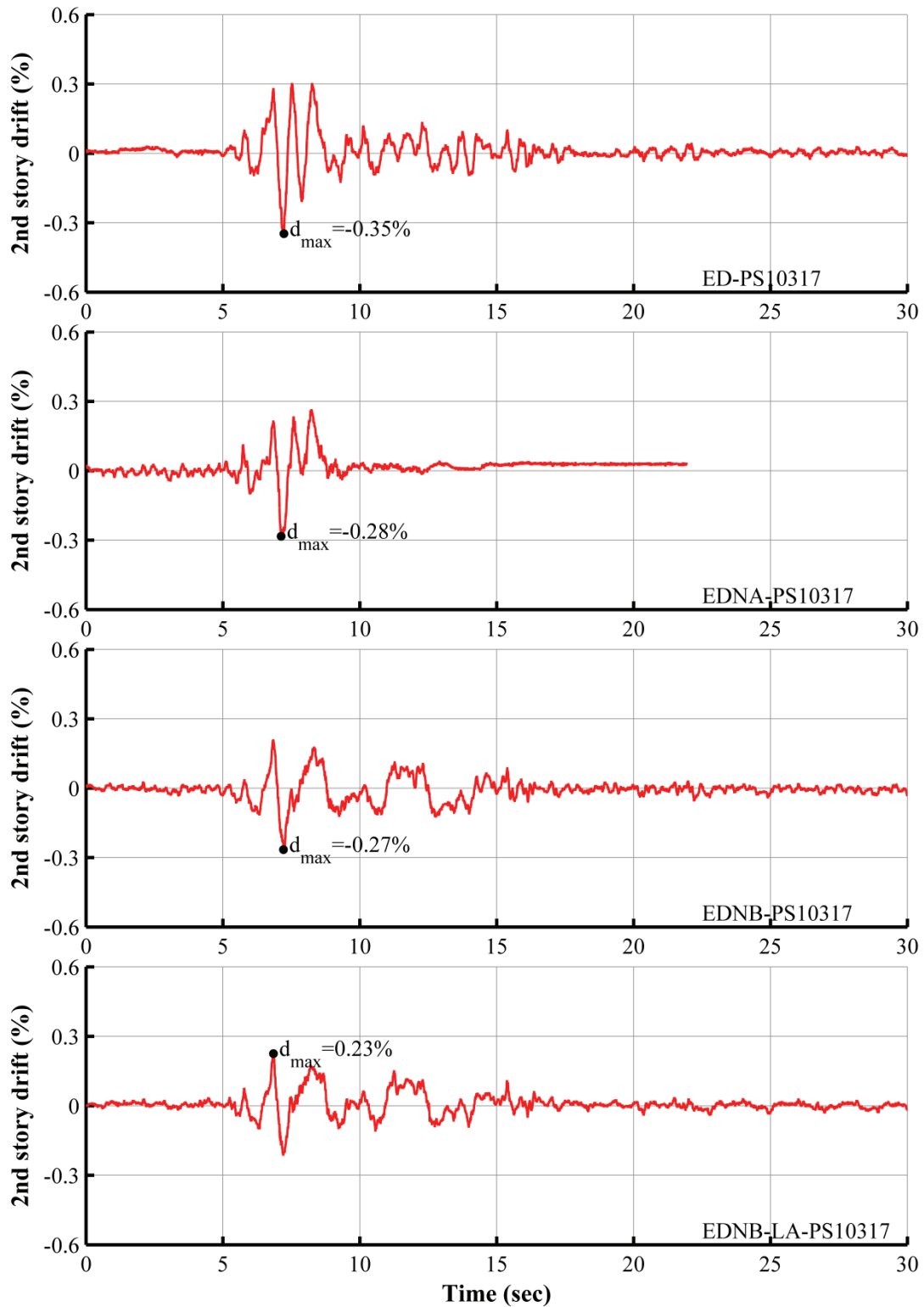


Figure 6-30: 2nd story drift ratio recorded for motion PS10317 and configurations with dampers

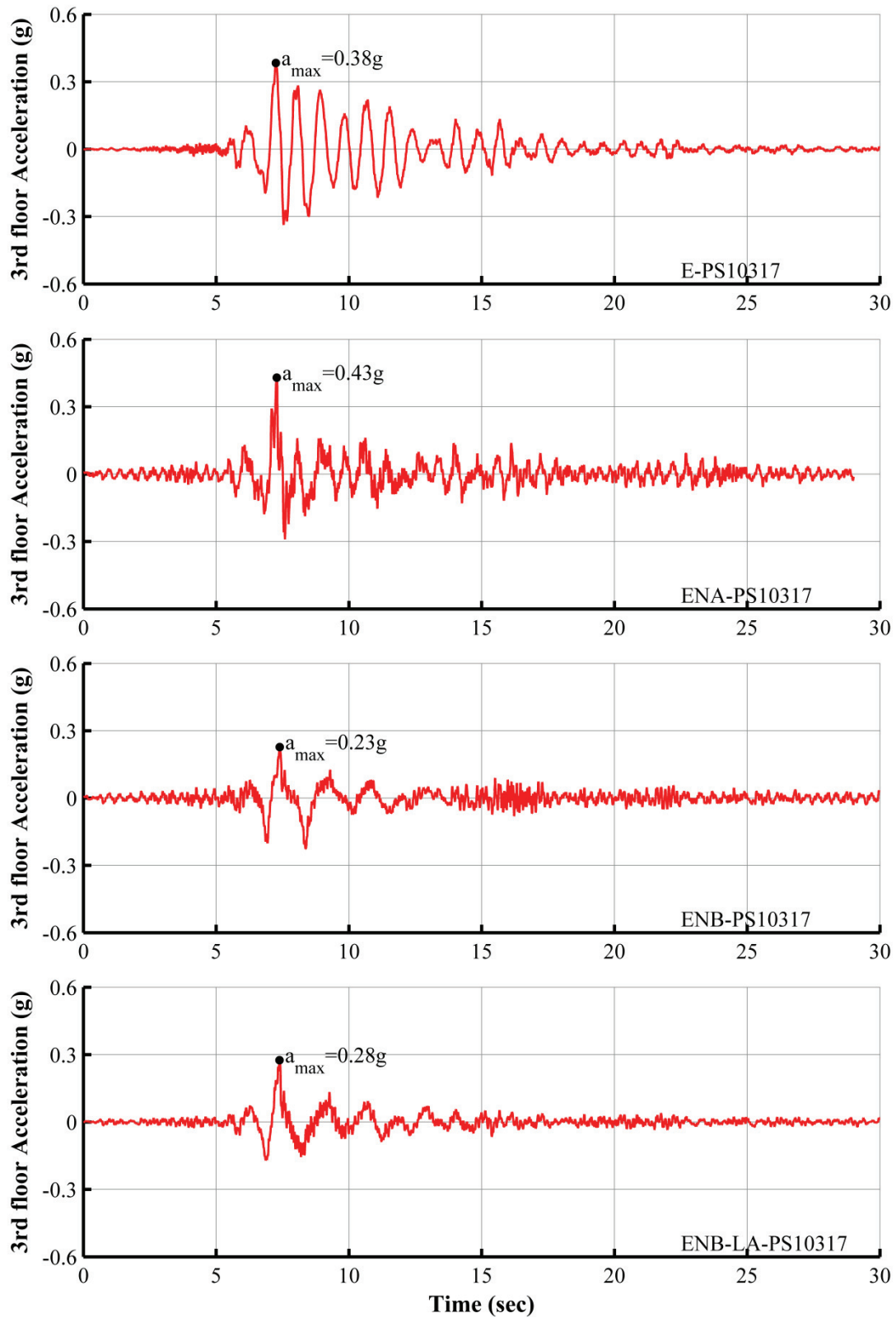


Figure 6-31: 3rd floor acceleration histories recorded for motion PS10317 and configurations without dampers

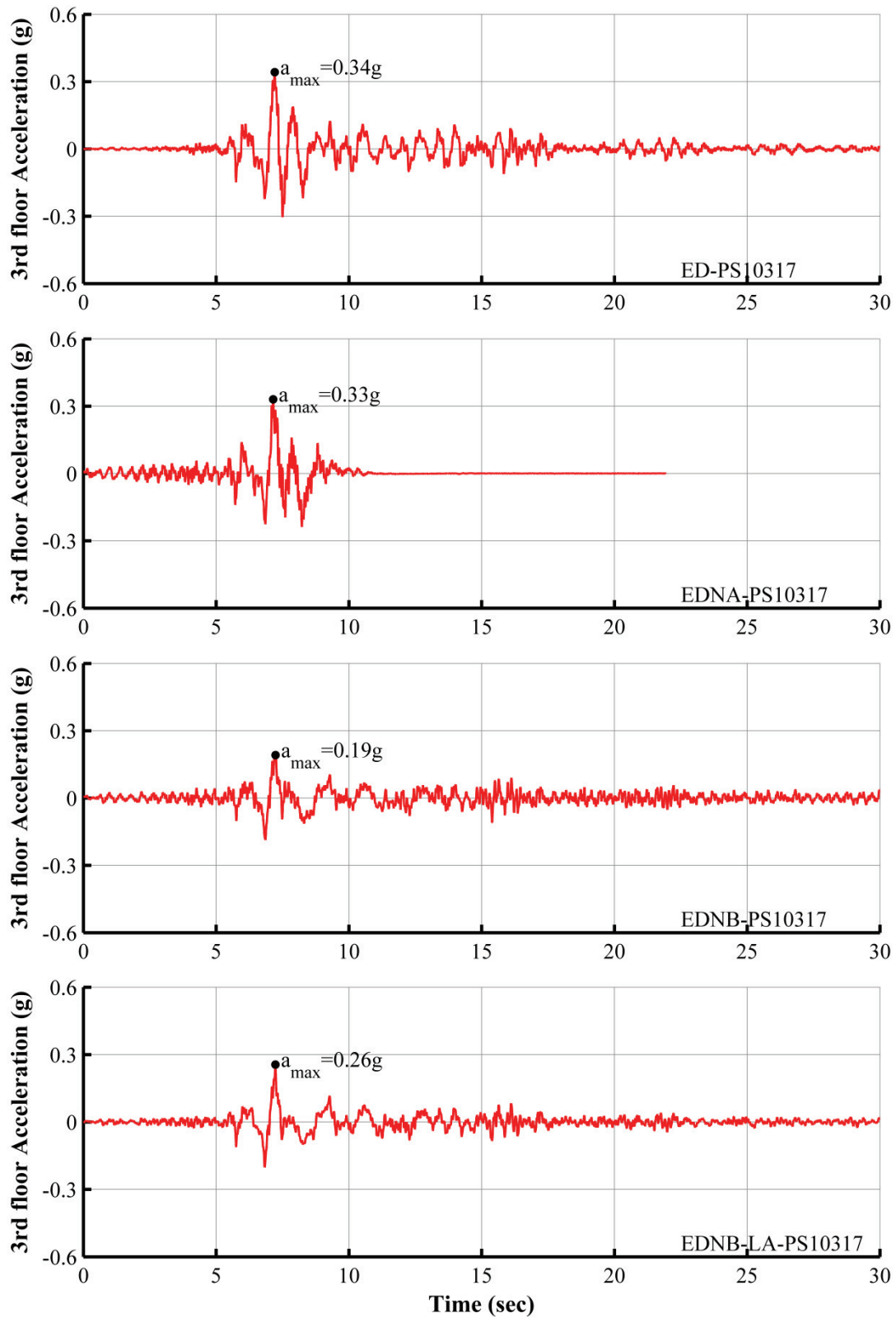


Figure 6-32: 3rd floor acceleration histories recorded for motion PS10317 and configurations with dampers

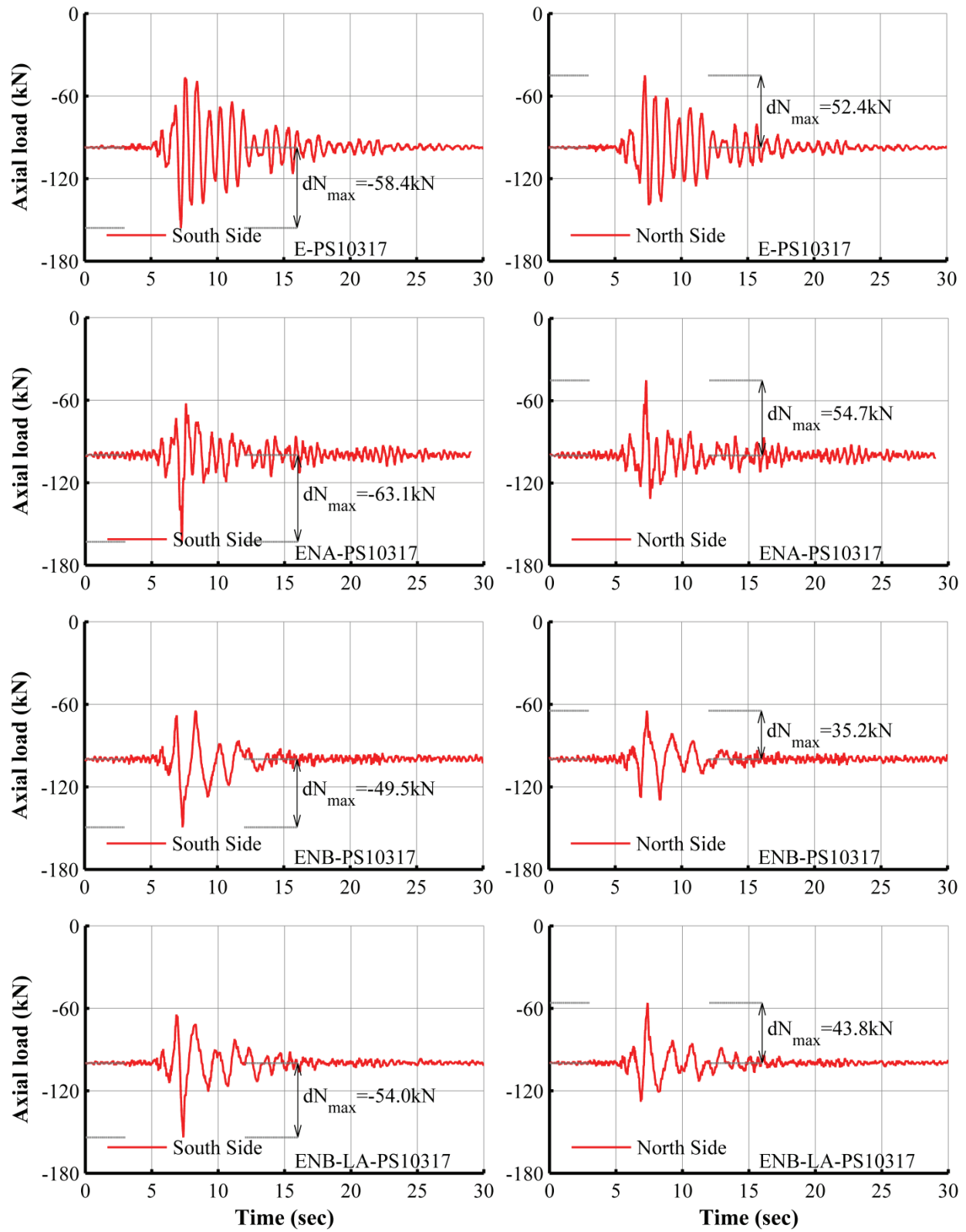


Figure 6-33: Axial load histories (for pair of load cells) for ground motion PS10317 for systems without dampers

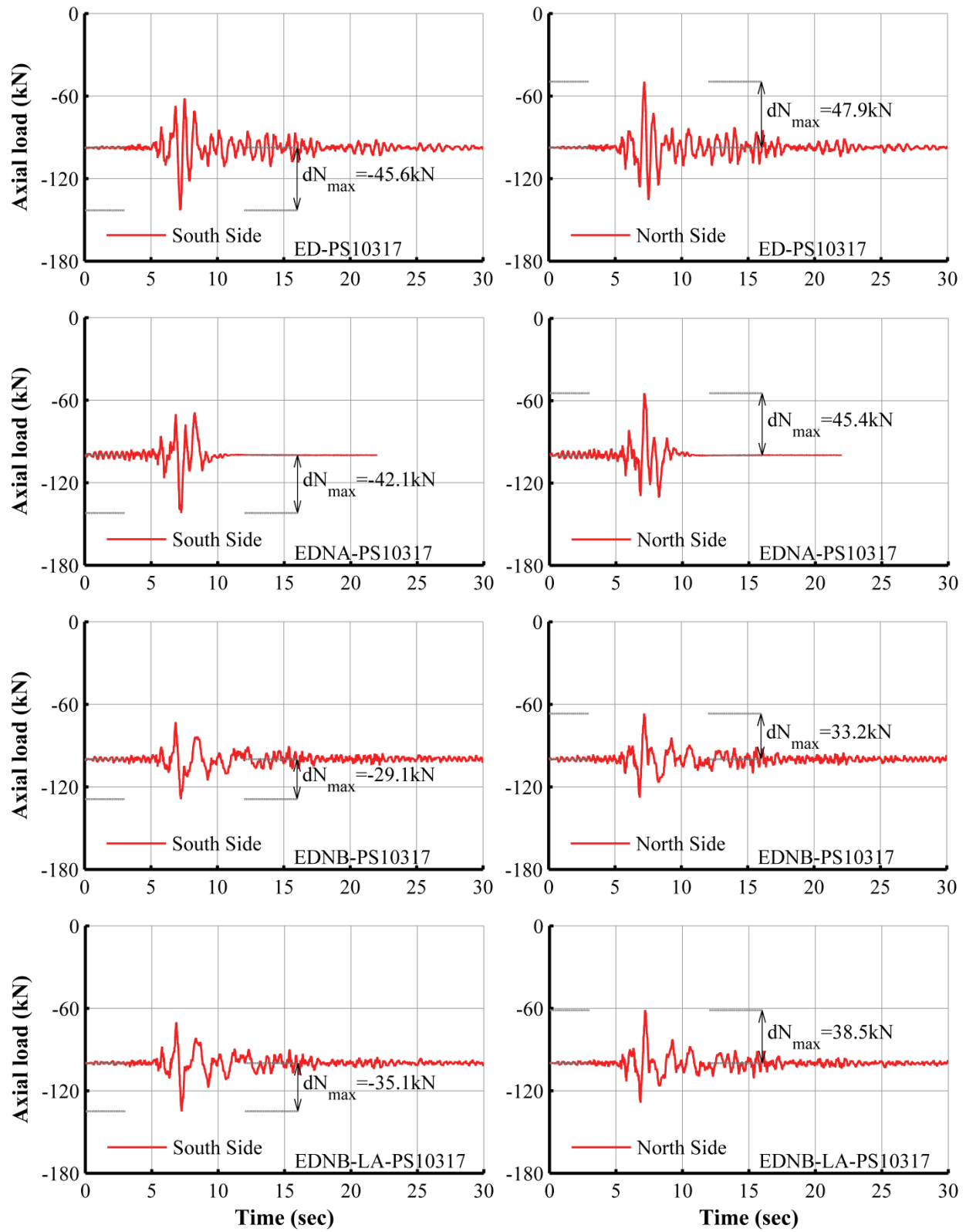


Figure 6-34: Axial load histories (for pair of load cells) for ground motion PS10317 for systems with dampers

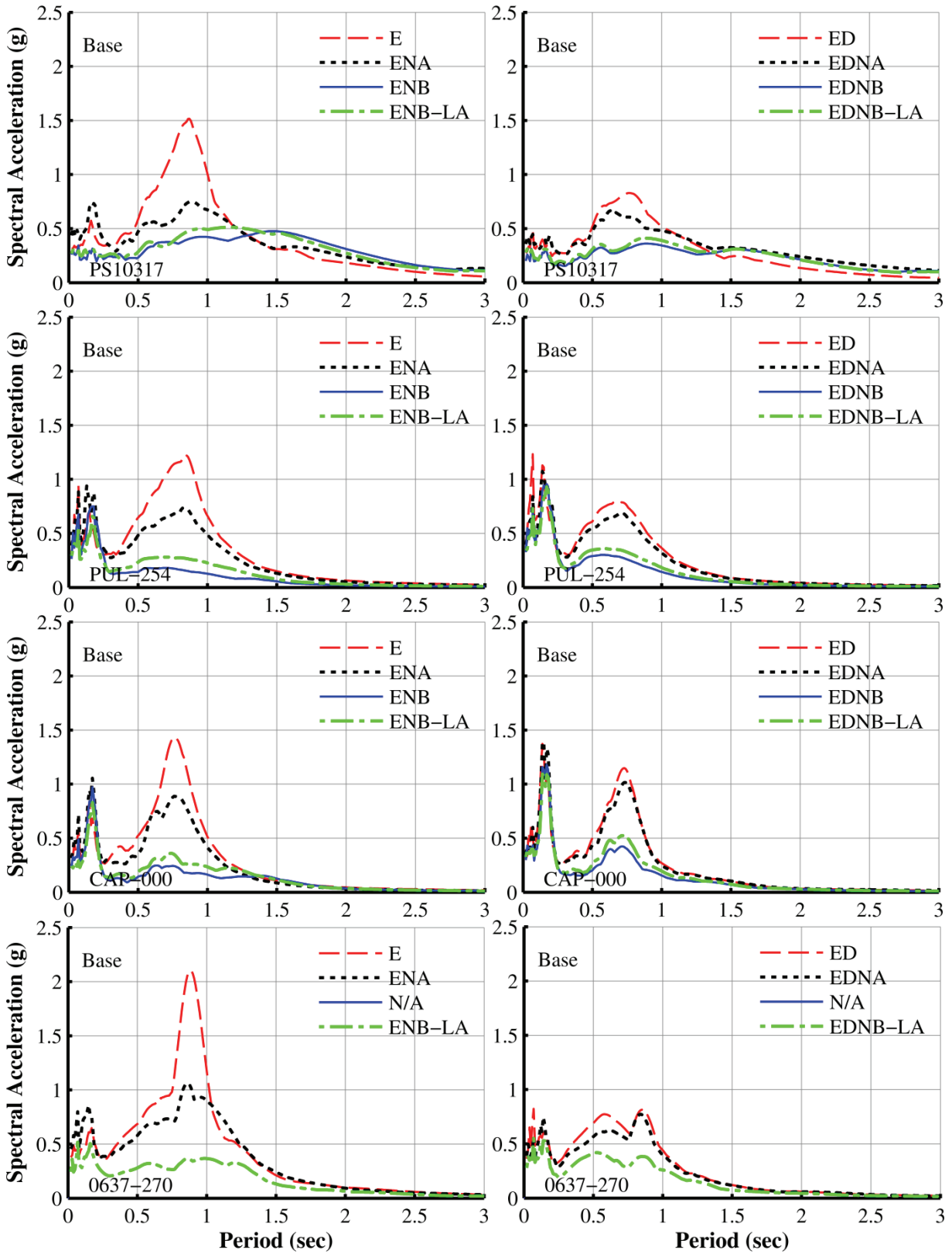


Figure 6-35: Base 5%-damped acceleration response spectra

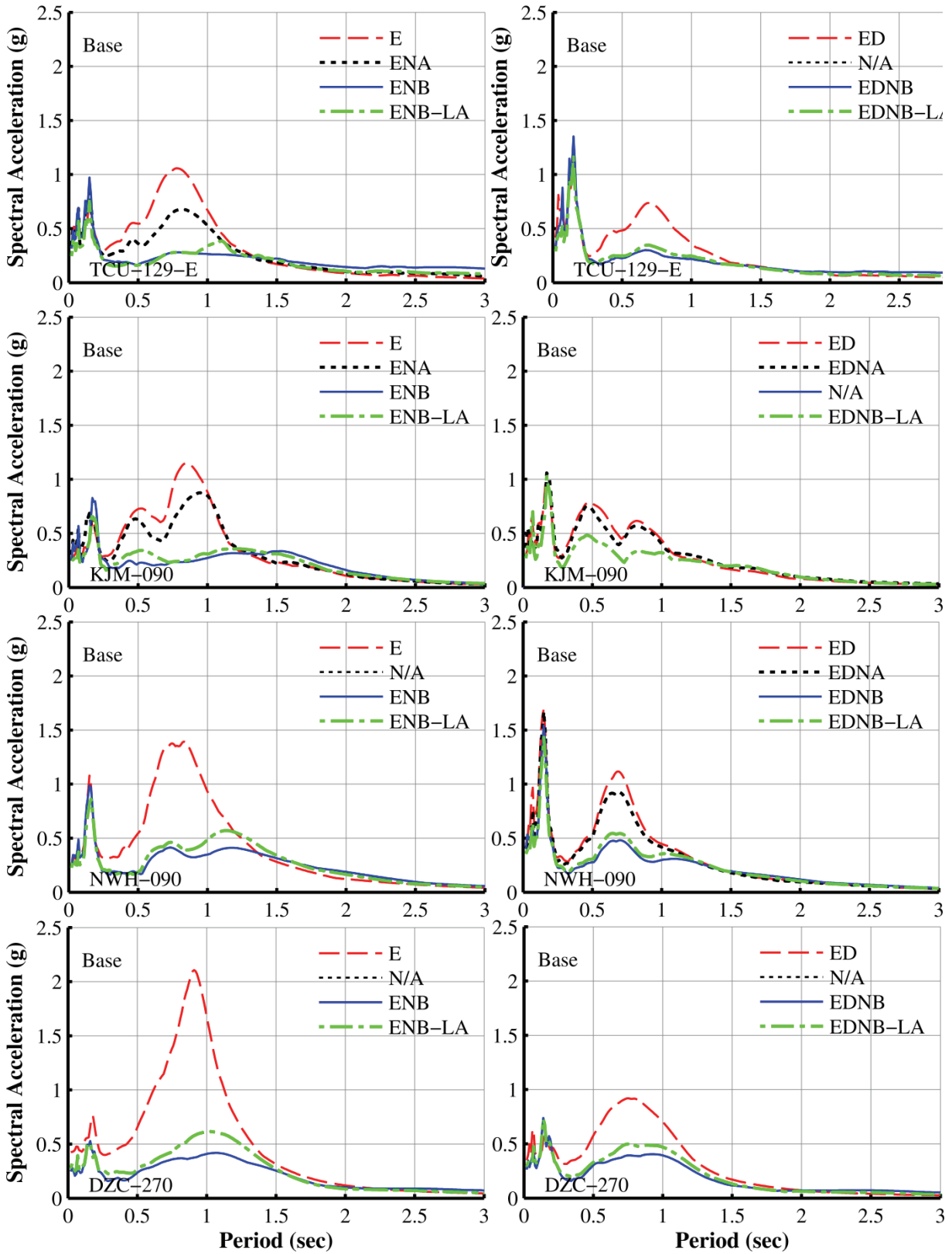


Figure 6-35 (cont'd): Base 5%-damped acceleration response spectra

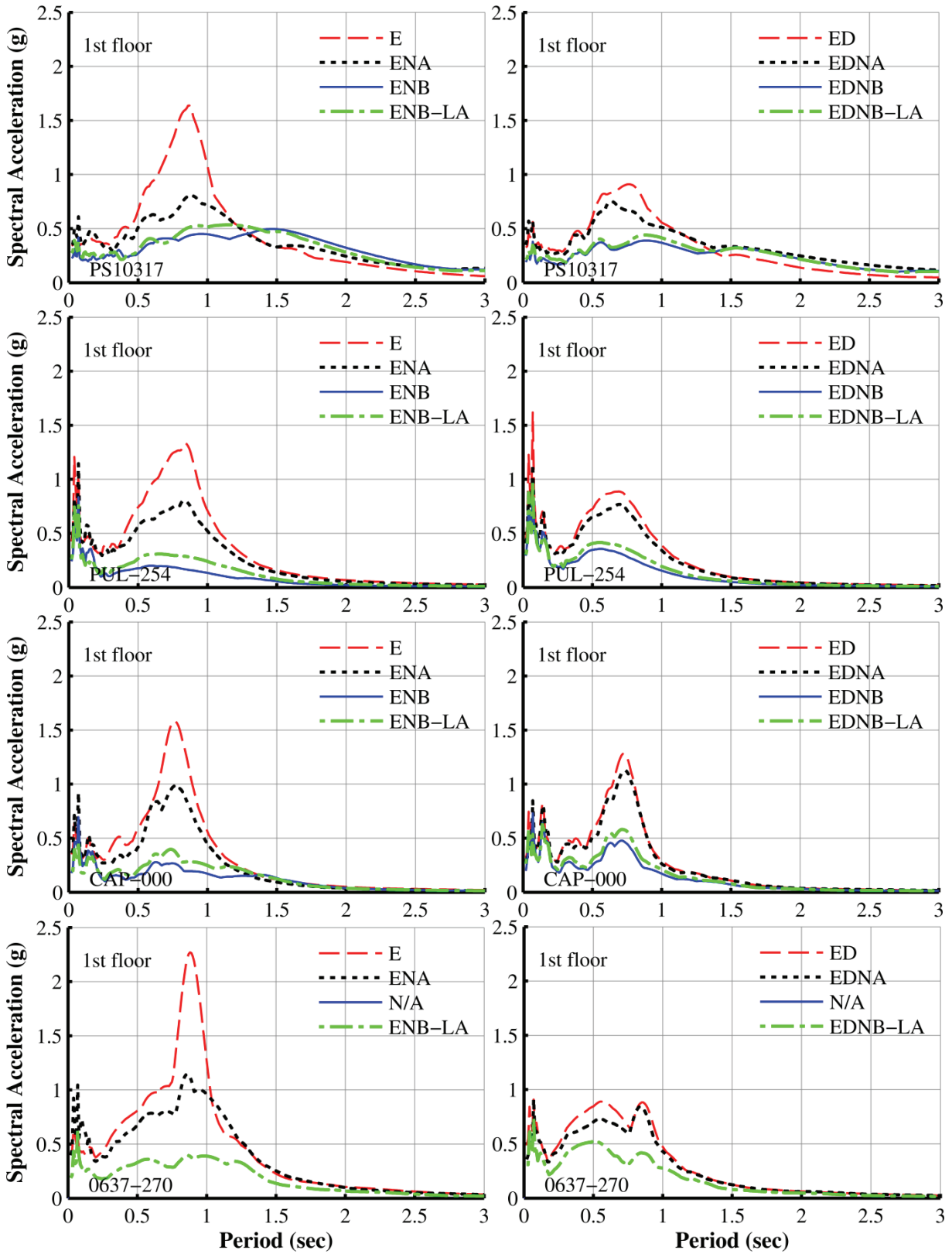


Figure 6-36: First floor 5%-damped acceleration response spectra

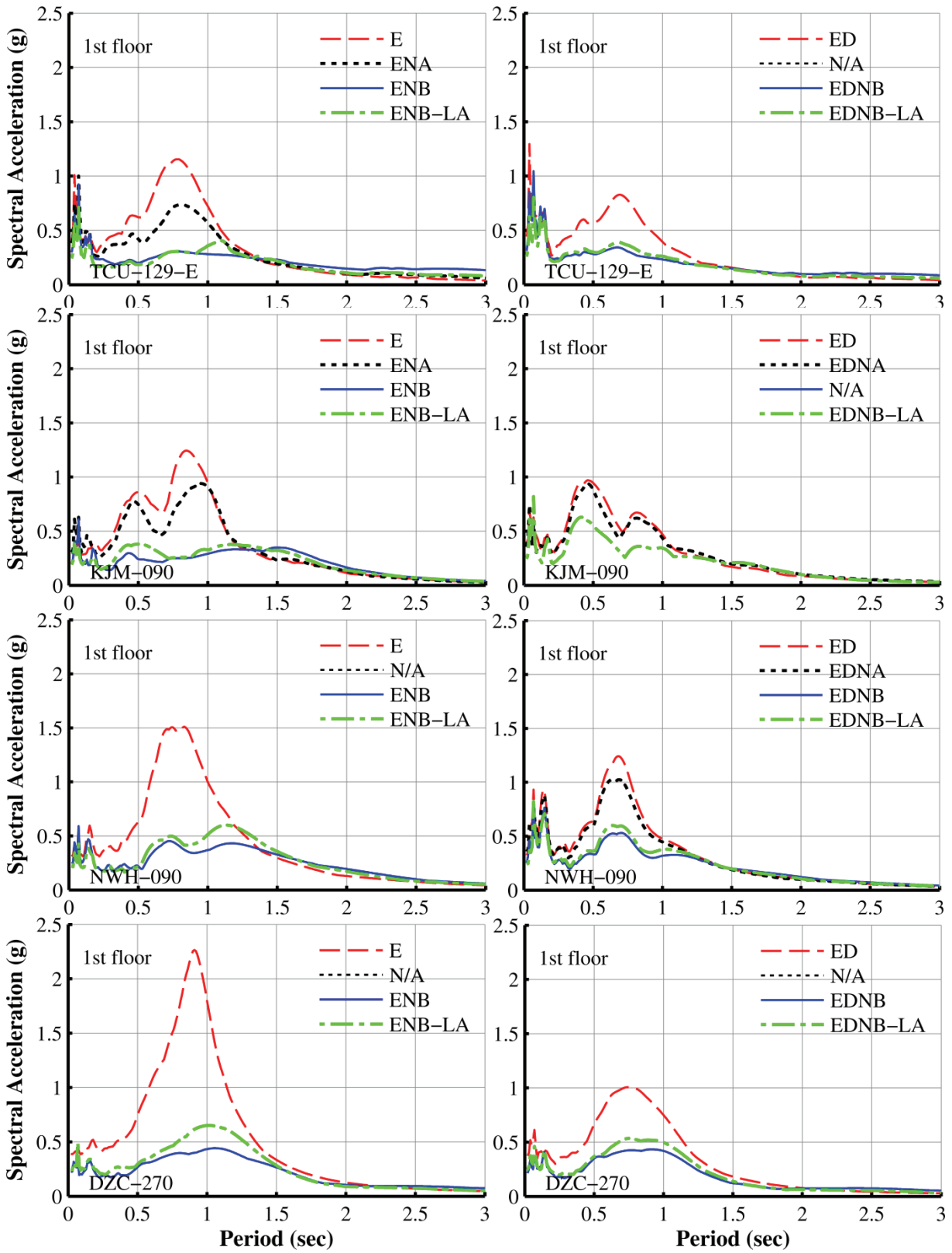


Figure 6-36 (cont'd): First floor 5%-damped acceleration response spectra

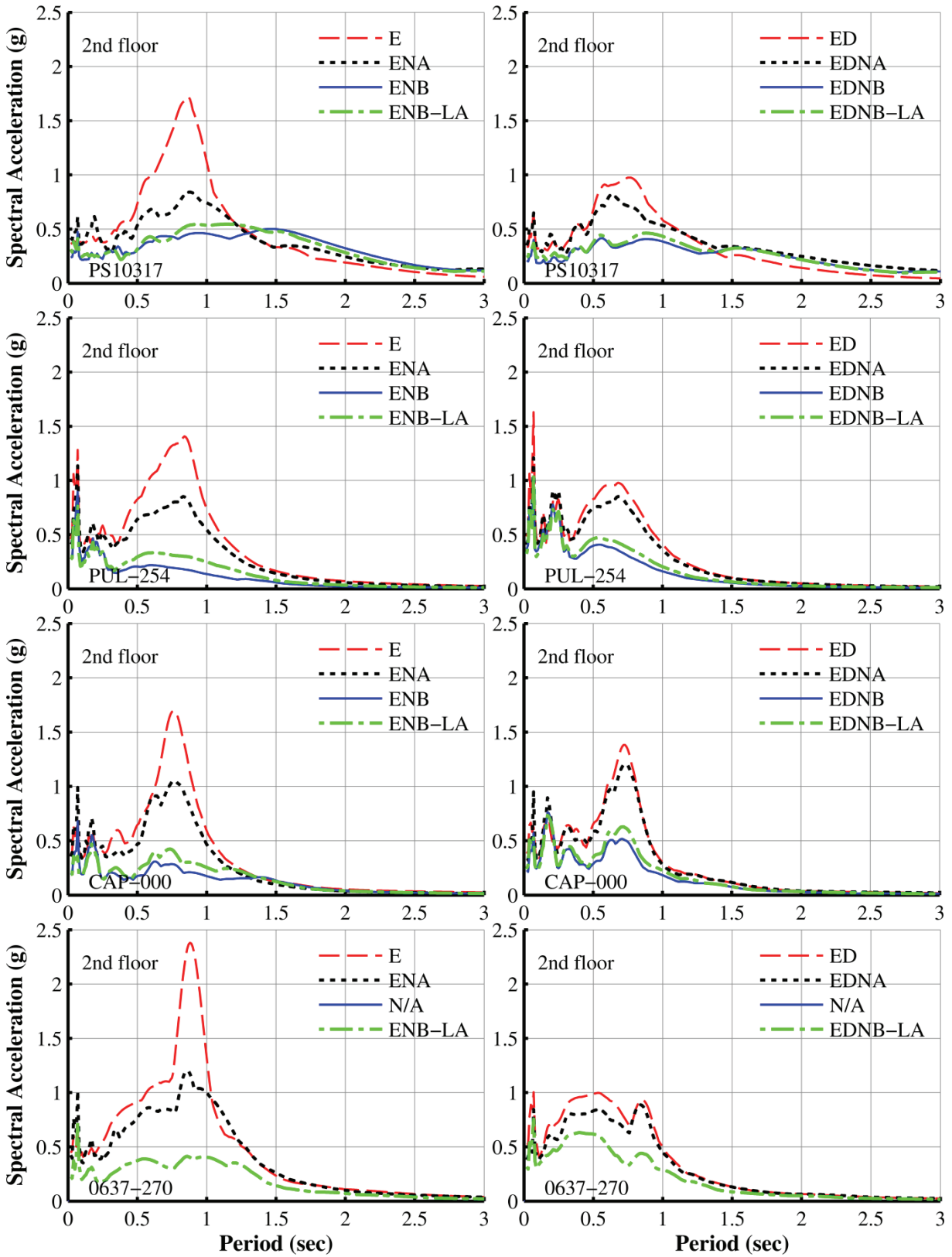


Figure 6-37: Second floor 5%-damped acceleration response spectra

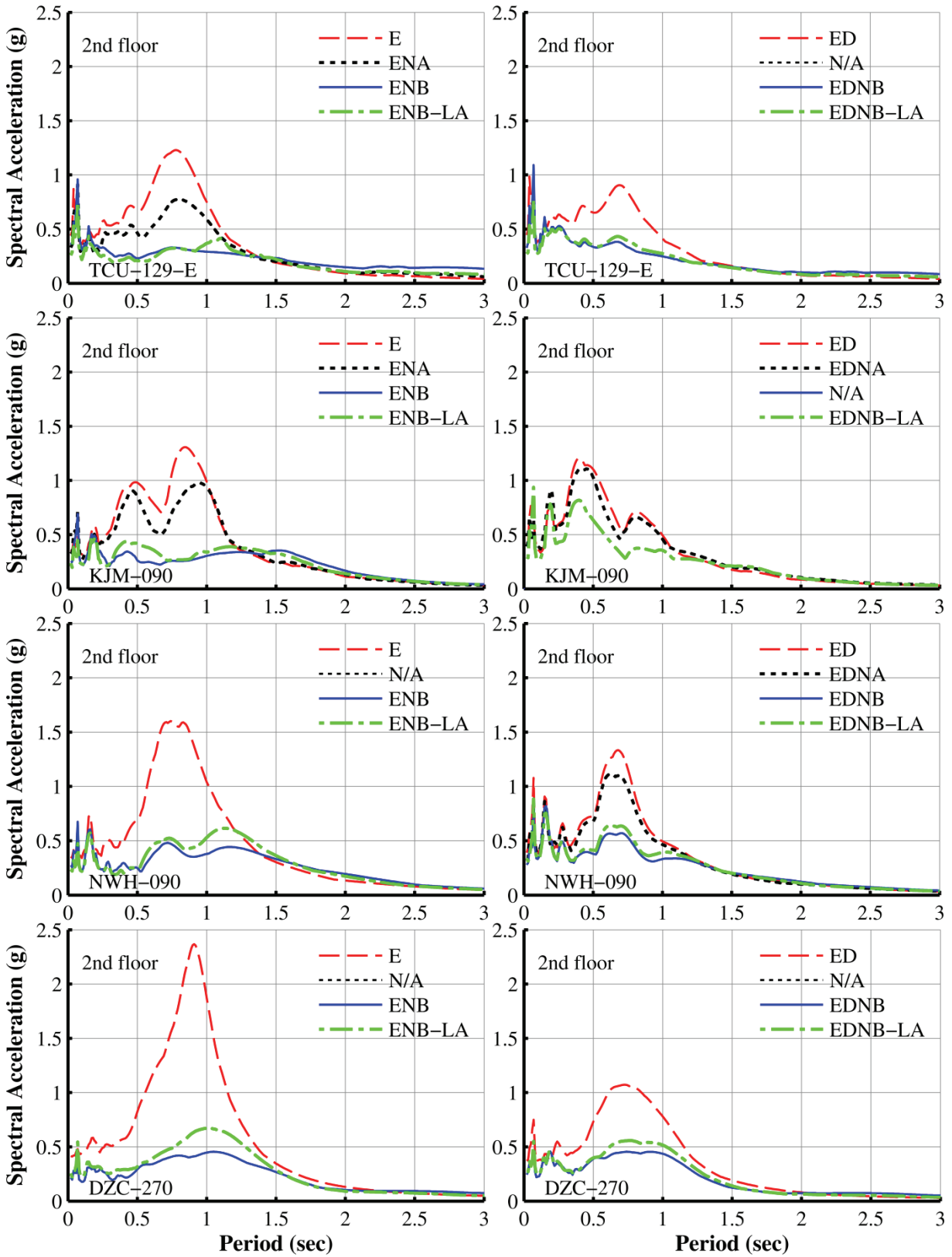


Figure 6-37 (cont'd): Second floor 5%-damped acceleration response spectra

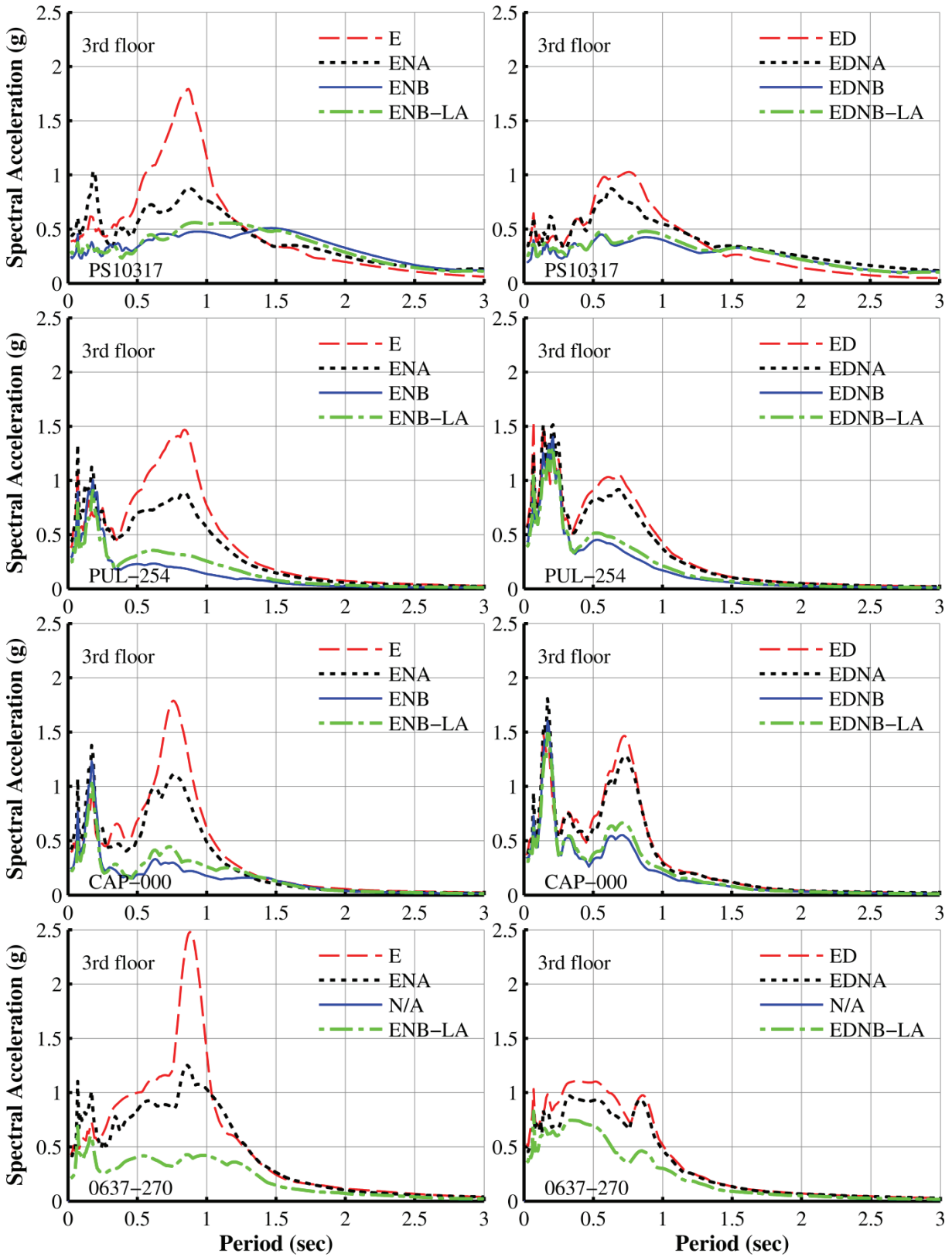


Figure 6-38: Third floor 5%-damped acceleration response spectra

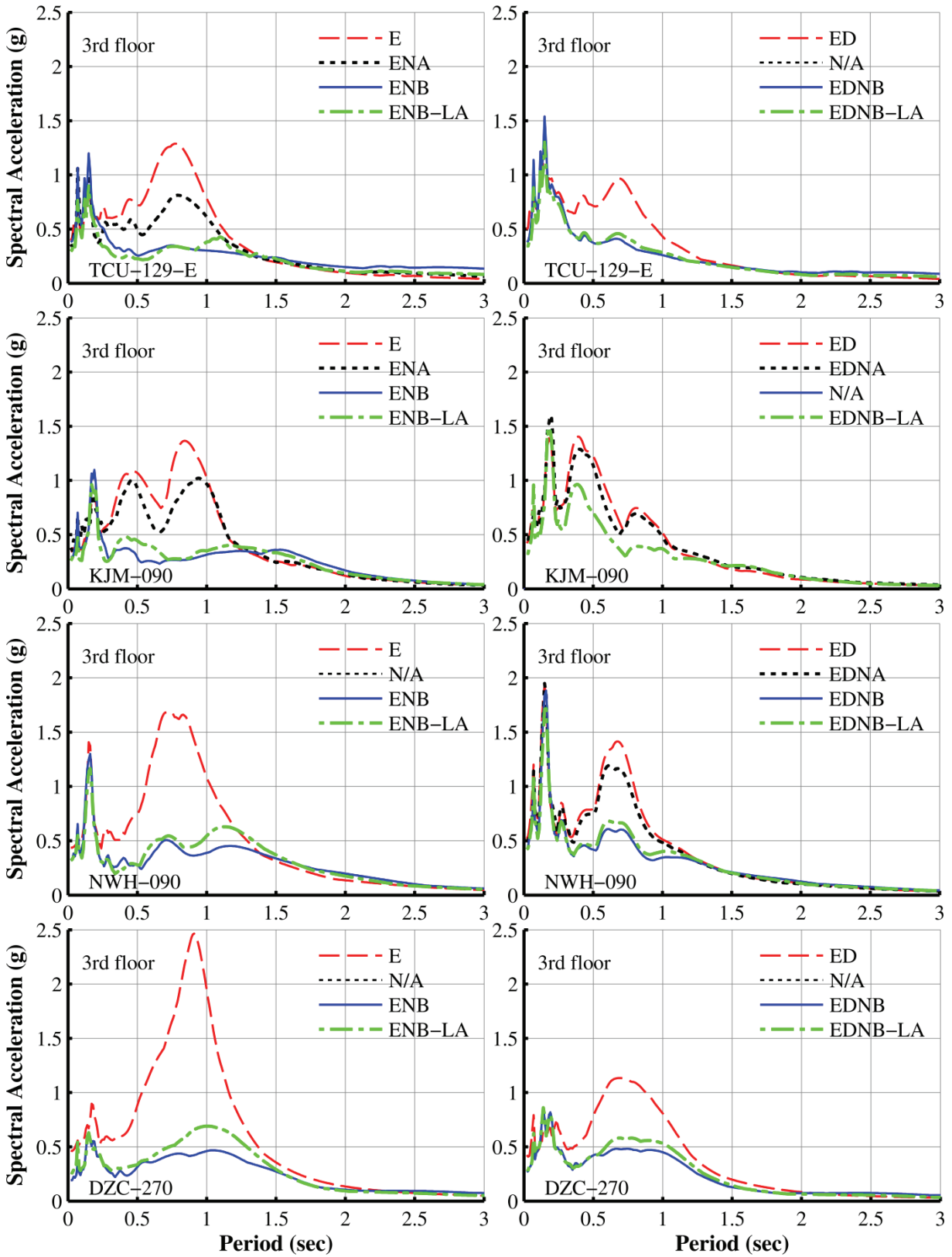


Figure 6-38 (cont'd): Third floor 5%-damped acceleration response spectra

Table 6-7: Peak recorded inter-story drift ratio

Motion	1st story drift ratio (% of story height)							
	Without Dampers				With Dampers			
	E	ENA	ENB	ENB-LA	ED	EDNA	EDNB	EDNB-LA
PS-10317	0.35	0.29	0.21	0.18	0.27	0.27	0.17	0.18
PUL-254	0.30	0.29	0.12	0.15	0.30	0.32	0.23	0.23
CAP-000	0.35	0.29	0.13	0.13	0.31	0.27	0.17	0.20
0637-270	0.38	0.30	-	0.16	0.36	0.33	-	0.26
TCU-129-E	0.36	0.27	0.27	0.13	0.27	-	0.22	0.18
KJM-090	0.28	0.24	0.23	0.16	0.35	0.29	-	0.22
NWH-090	0.30	-	0.22	0.15	0.35	0.33	0.28	0.28
DZC-270	0.46	-	0.19	0.17	0.36	-	0.18	0.24
Motion	2nd story drift ratio (% of story height)							
	Without Dampers				With Dampers			
	E	ENA	ENB	ENB-LA	ED	EDNA	EDNB	EDNB-LA
PS-10317	0.45	0.40	0.28	0.31	0.35	0.28	0.27	0.23
PUL-254	0.45	0.39	0.20	0.17	0.47	0.42	0.28	0.28
CAP-000	0.42	0.31	0.19	0.19	0.32	0.34	0.25	0.24
0637-270	0.53	0.46	-	0.23	0.55	0.52	-	0.32
TCU-129-E	0.42	0.30	0.38	0.31	0.36	-	0.33	0.33
KJM-090	0.46	0.32	0.31	0.28	0.37	0.36	-	0.27
NWH-090	0.43	-	0.31	0.30	0.45	0.38	0.32	0.30
DZC-270	0.58	-	0.25	0.30	0.45	-	0.29	0.30
Motion	3rd story drift ratio (% of story height)							
	Without Dampers				With Dampers			
	E	ENA	ENB	ENB-LA	ED	EDNA	EDNB	EDNB-LA
PS-10317	0.36	0.33	0.25	0.20	0.28	0.32	0.15	0.19
PUL-254	0.26	0.21	0.12	0.11	0.24	0.27	0.21	0.18
CAP-000	0.25	0.25	0.13	0.12	0.23	0.24	0.17	0.15
0637-270	0.32	0.21	-	0.08	0.29	0.24	-	0.21
TCU-129-E	0.23	0.21	0.20	0.13	0.20	-	0.22	0.17
KJM-090	0.27	0.20	0.18	0.16	0.29	0.26	-	0.21
NWH-090	0.30	-	0.14	0.16	0.24	0.24	0.22	0.23
DZC-270	0.44	-	0.13	0.14	0.27	-	0.17	0.15

Table 6-8: Peak recorded floor acceleration

Motion	Base Acceleration (g)							
	Without Dampers				With Dampers			
	E	ENA	ENB	ENB-LA	ED	EDNA	EDNB	EDNB-LA
PS-10317	0.31	0.39	0.19	0.25	0.27	0.29	0.19	0.22
PUL-254	0.33	0.34	0.24	0.19	0.41	0.33	0.26	0.25
CAP-000	0.32	0.28	0.21	0.22	0.30	0.32	0.25	0.25
0637-270	0.37	0.33	-	0.17	0.35	0.28	-	0.21
TCU-129-E	0.33	0.32	0.28	0.21	0.38	-	0.31	0.26
KJM-090	0.25	0.25	0.23	0.20	0.28	0.28	-	0.23
NWH-090	0.28	-	0.22	0.20	0.40	0.36	0.34	0.32
DZC-270	0.42	-	0.20	0.24	0.34	-	0.22	0.24
Motion	1st floor Acceleration (g)							
	Without Dampers				With Dampers			
	E	ENA	ENB	ENB-LA	ED	EDNA	EDNB	EDNB-LA
PS-10317	0.34	0.33	0.22	0.24	0.32	0.35	0.18	0.20
PUL-254	0.38	0.40	0.20	0.22	0.39	0.40	0.24	0.26
CAP-000	0.34	0.29	0.14	0.15	0.31	0.26	0.18	0.24
0637-270	0.39	0.37	-	0.16	0.44	0.34	-	0.28
TCU-129-E	0.38	0.31	0.29	0.21	0.40	-	0.29	0.24
KJM-090	0.29	0.25	0.19	0.17	0.36	0.31	-	0.22
NWH-090	0.31	-	0.21	0.20	0.32	0.30	0.24	0.23
DZC-270	0.38	-	0.21	0.23	0.37	-	0.21	0.23
Motion	2nd floor Acceleration (g)							
	Without Dampers				With Dampers			
	E	ENA	ENB	ENB-LA	ED	EDNA	EDNB	EDNB-LA
PS-10317	0.36	0.37	0.22	0.27	0.32	0.35	0.20	0.23
PUL-254	0.40	0.38	0.22	0.22	0.42	0.38	0.29	0.30
CAP-000	0.36	0.35	0.13	0.17	0.34	0.31	0.18	0.22
0637-270	0.43	0.36	-	0.18	0.48	0.38	-	0.28
TCU-129-E	0.40	0.30	0.35	0.25	0.39	-	0.26	0.23
KJM-090	0.34	0.30	0.23	0.20	0.36	0.36	-	0.25
NWH-090	0.33	-	0.24	0.20	0.39	0.31	0.25	0.29
DZC-270	0.41	-	0.18	0.22	0.35	-	0.23	0.25
Motion	3rd floor Acceleration (g)							
	Without Dampers				With Dampers			
	E	ENA	ENB	ENB-LA	ED	EDNA	EDNB	EDNB-LA
PS-10317	0.38	0.43	0.23	0.28	0.34	0.33	0.19	0.26
PUL-254	0.37	0.43	0.28	0.23	0.56	0.53	0.42	0.37
CAP-000	0.38	0.41	0.22	0.21	0.37	0.38	0.33	0.29
0637-270	0.42	0.39	-	0.21	0.50	0.45	-	0.34
TCU-129-E	0.38	0.33	0.36	0.29	0.45	-	0.37	0.33
KJM-090	0.34	0.34	0.27	0.26	0.41	0.44	-	0.30
NWH-090	0.43	-	0.31	0.31	0.50	0.48	0.43	0.41
DZC-270	0.46	-	0.18	0.25	0.41	-	0.26	0.27

Table 6-9: Peak recorded base displacement and base shear force

Motion	Base Displacement (cm) ¹							
	Without Dampers				With Dampers			
	E	ENA	ENB	ENB-LA	ED	EDNA	EDNB	EDNB-LA
PS-10317	5.80	5.92	7.57	6.89	3.98	4.49	4.15	4.31
PUL-254	4.97	4.74	3.73	3.84	3.43	3.35	2.88	2.97
CAP-000	4.93	3.50	3.54	2.75	2.94	2.98	2.43	2.33
0637-270	6.11	6.52	-	4.46	4.31	4.48	-	3.80
TCU-129-E	4.77	3.76	4.41	4.38	2.79	-	2.97	2.75
KJM-090	4.82	4.56	4.87	4.03	3.04	3.16	-	3.04
NWH-090	5.03	-	6.98	5.34	2.98	2.78	3.05	3.11
DZC-270	6.68	-	7.17	6.28	4.30	-	4.47	4.22
Motion	Base Shear (kN)							
	Without Dampers				With Dampers			
	E	ENA	ENB	ENB-LA	ED	EDNA	EDNB	EDNB-LA
PS-10317	65.6	58.7	38.8	43.3	54.5	49.9	30.4	34.6
PUL-254	57.0	39.7	16.8	24.0	48.3	44.4	25.7	27.9
CAP-000	56.6	36.1	14.5	19.3	43.8	40.5	19.7	23.8
0637-270	67.1	57.9	-	25.8	68.3	63.8	-	44.7
TCU-129-E	54.8	37.3	39.4	29.3	45.3	-	33.4	30.4
KJM-090	55.3	38.8	28.4	26.8	49.3	46.5	N/A	33.9
NWH-090	56.7	-	35.3	30.8	45.9	43.2	29.2	30.2
DZC-270	73.9	-	29.2	36.3	56.4	-	27.9	33.8
1. This is the maximum value of base displacement minus initial displacement which was nonzero for tests with configurations ENB,EDNB,ENB-LA,EDNB-LA								

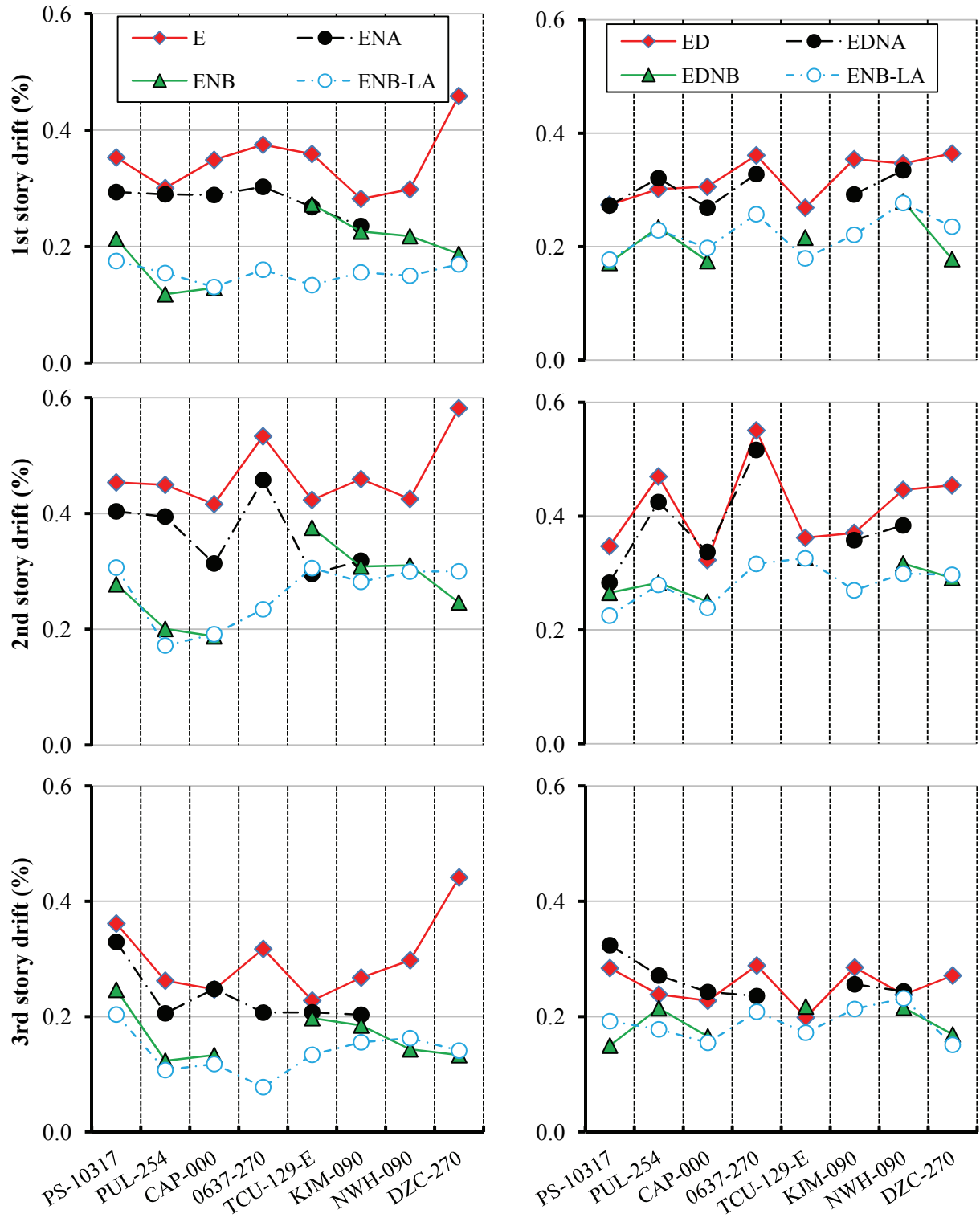


Figure 6-39: Comparison of recorded peak inter-story drift ratio for all configurations and tests (left column is for systems without dampers; right column is for systems with dampers)

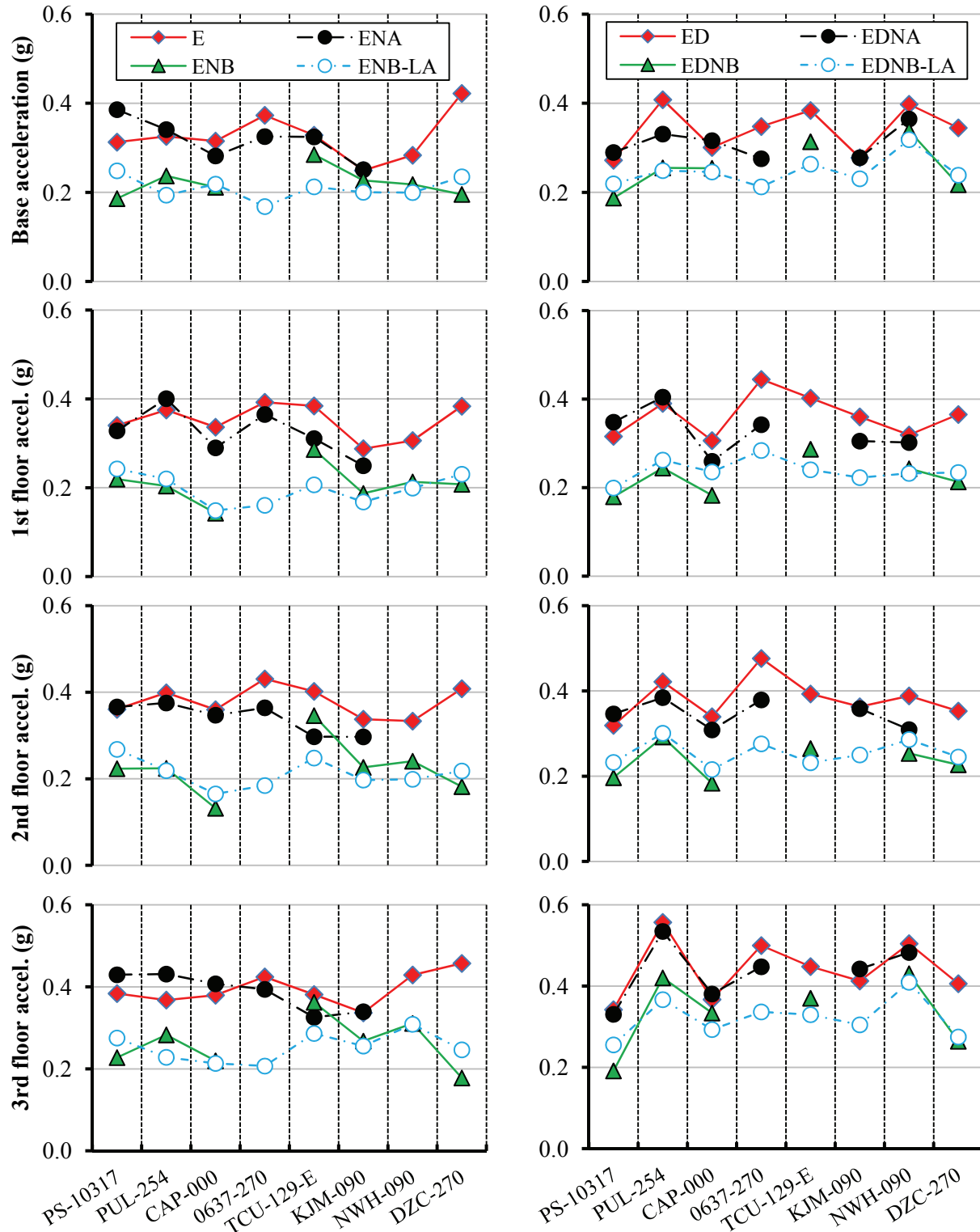


Figure 6-40: Comparison of recorded peak floor acceleration for all configurations and tests (left column is for systems without dampers; right column is for systems with dampers)

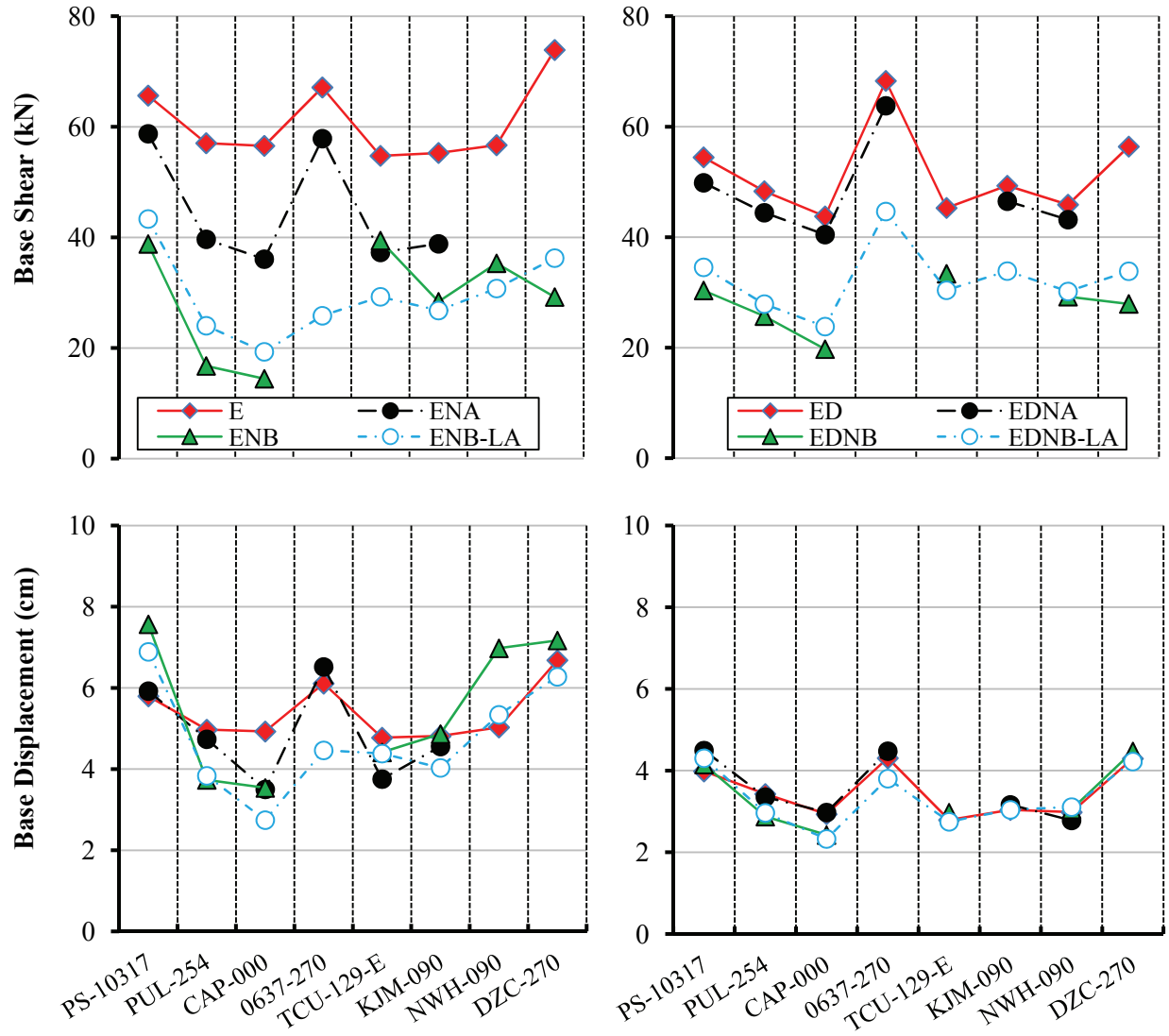


Figure 6-41: Comparison of recorded peak base displacement and base shear force for all configurations and tests (left column is for systems without dampers; right column is for systems with dampers)

SECTION 7

ANALYTICAL PREDICTION OF RESPONSE

7.1 Introduction

This section presents details of modeling of the tested model in program SAP2000 and compares experimental results to the predictions of the analytical model. The section presents only sample results in graphical form. Appendix C presents comparisons of experimental and analytical histories of all response quantities and of the floor acceleration spectra for all tests.

7.2 Modeling of Superstructure in Program SAP2000

The superstructure, fixed at its base, was modeled in program SAP2000 using linear elastic frame elements for all beams, columns and braces. The diaphragm bracing of the superstructure was explicitly modeled and therefore no diaphragm constraints have been assigned. The concrete blocks were modeled as lumped masses without mass moment of inertia. The self-weight of the frame was explicitly captured using the steel density value for the material in SAP2000. Additional small masses were added at the base-mat to capture the difference in the total weight calculated by the program and the one obtained from measurement by the load cells. This additional weight was contributed by elements not accounted for in the model, such as steel connecting plates, stiffeners, bolts and connection angles. Due to the large dimensions of the base-mat beams compared to the superstructure elements, rigid beam elements have been used to connect the bottom of the columns to the centerline of the W14x90 beams of the base-mat. Rigid offsets have not been used for any beam-to-column connection in the rest of the structure. Table 7-1 presents results for the modal properties of the model, fixed at the base, as obtained by program SAP2000 for the first three modes. The damping ratio is the value assigned for each mode in SAP2000 for the construction of the inherent damping matrix. Note that the assigned damping ratio values are between the values identified in the experiments and presented in Table 6-4 and 6-5. There is reasonably good agreement between the mode shapes and period values obtained in the experimental identification (Table 6-4 and 6-5) and the results of the modal analysis in SAP2000.

Analysis of the fixed-base superstructure with seismic motion at its base was conducted and results are compared to experimental results in Figure 7-1, which shows histories of inter-story drift, in Figure 7-2, which shows histories of floor accelerations and in Figure 7-3, which shows 5%-damped floor acceleration spectra. Results are in good agreement but the peak values of response may be over-estimated or under-estimated by the analytical model. There are two reasons for this: a) The experimental response has not been filtered (except for a filter at 50Hz) so that it contains some noise, and b) The analytical model assumes rigidity in the connections of masses to floors and of braces to beams and columns, whereas some sliding occurred at these

connections during strong shaking. The latter resulted in recordings of spikes in response that could not be analytically predicted.

Table 7-1: Modal characteristics of analytical model in SAP2000

Mode	Period (sec)	Assigned Damping Ratio	Mode Shape		
			1 st floor	2 nd floor	3 rd floor
1 st	0.292	0.0650	0.331	0.741	1.000
2 nd	0.092	0.0100	-1.176	-0.808	1.000
3 rd	0.053	0.0078	2.286	-2.397	1.000

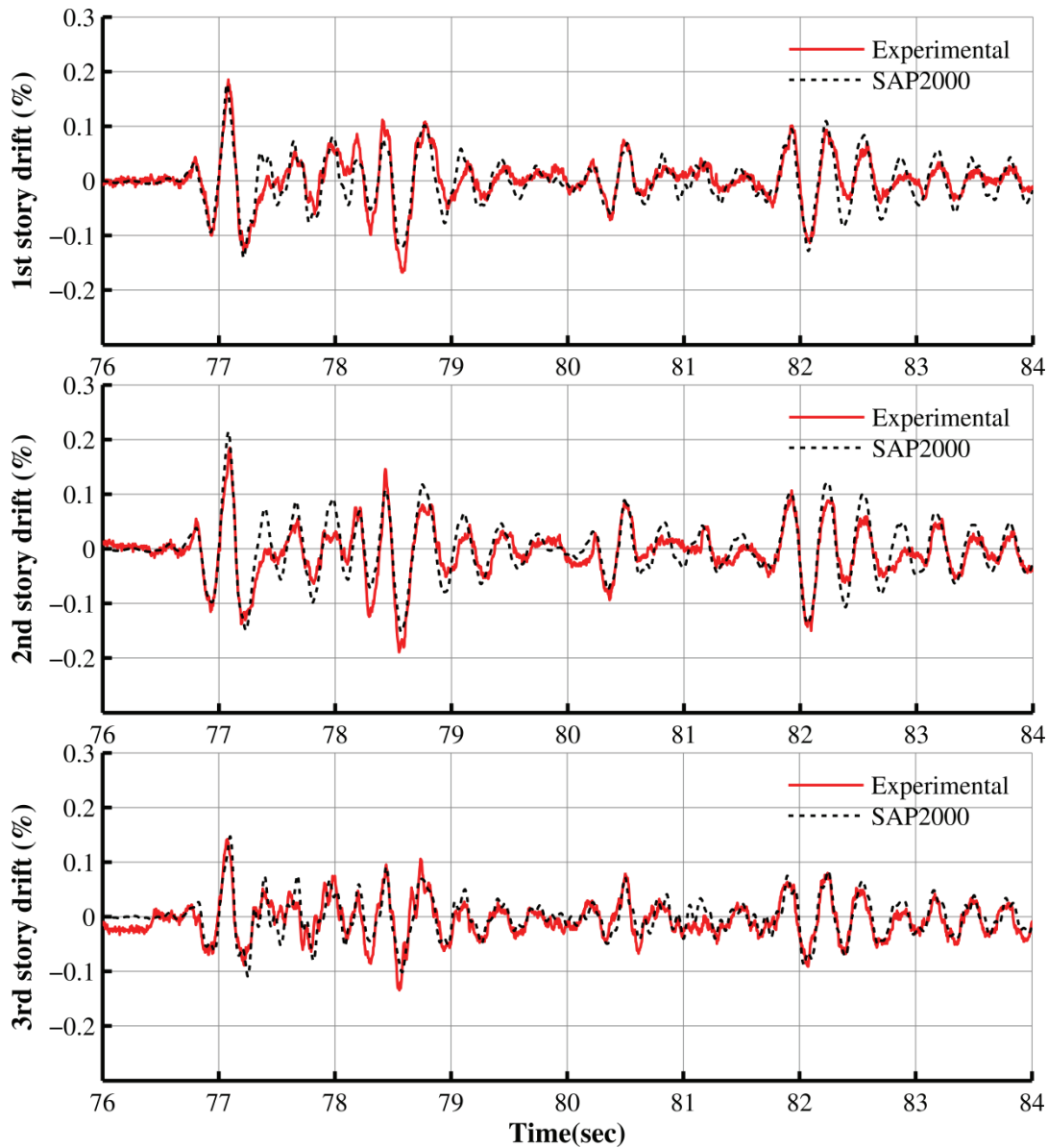


Figure 7-1: Comparison of analytical and experimental results for inner-story drift of fixed structure obtained for ground motion ATL-270

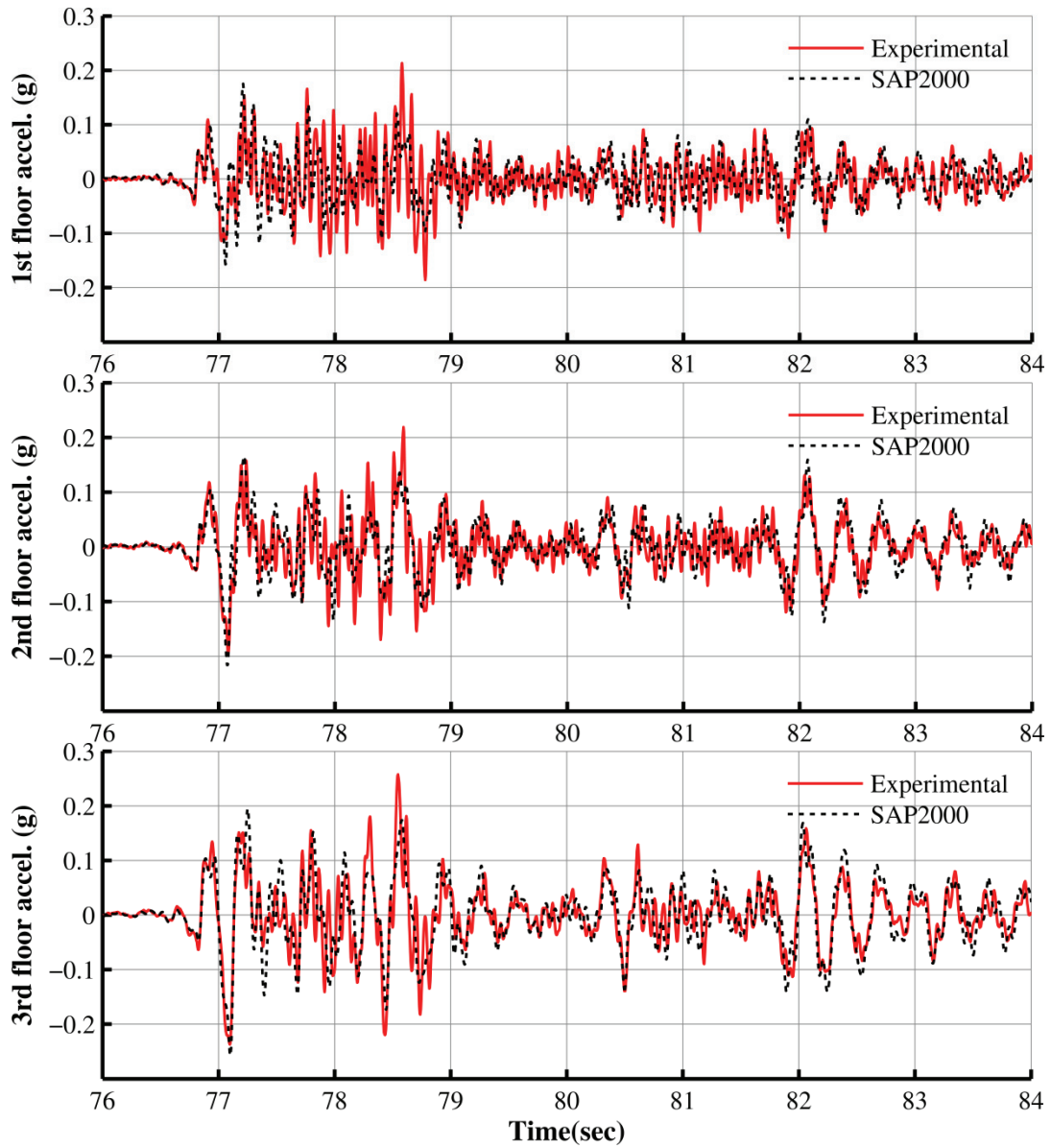


Figure 7-2: Comparison of analytical and experimental results for floor acceleration of fixed structure obtained for ground motion ATL-270

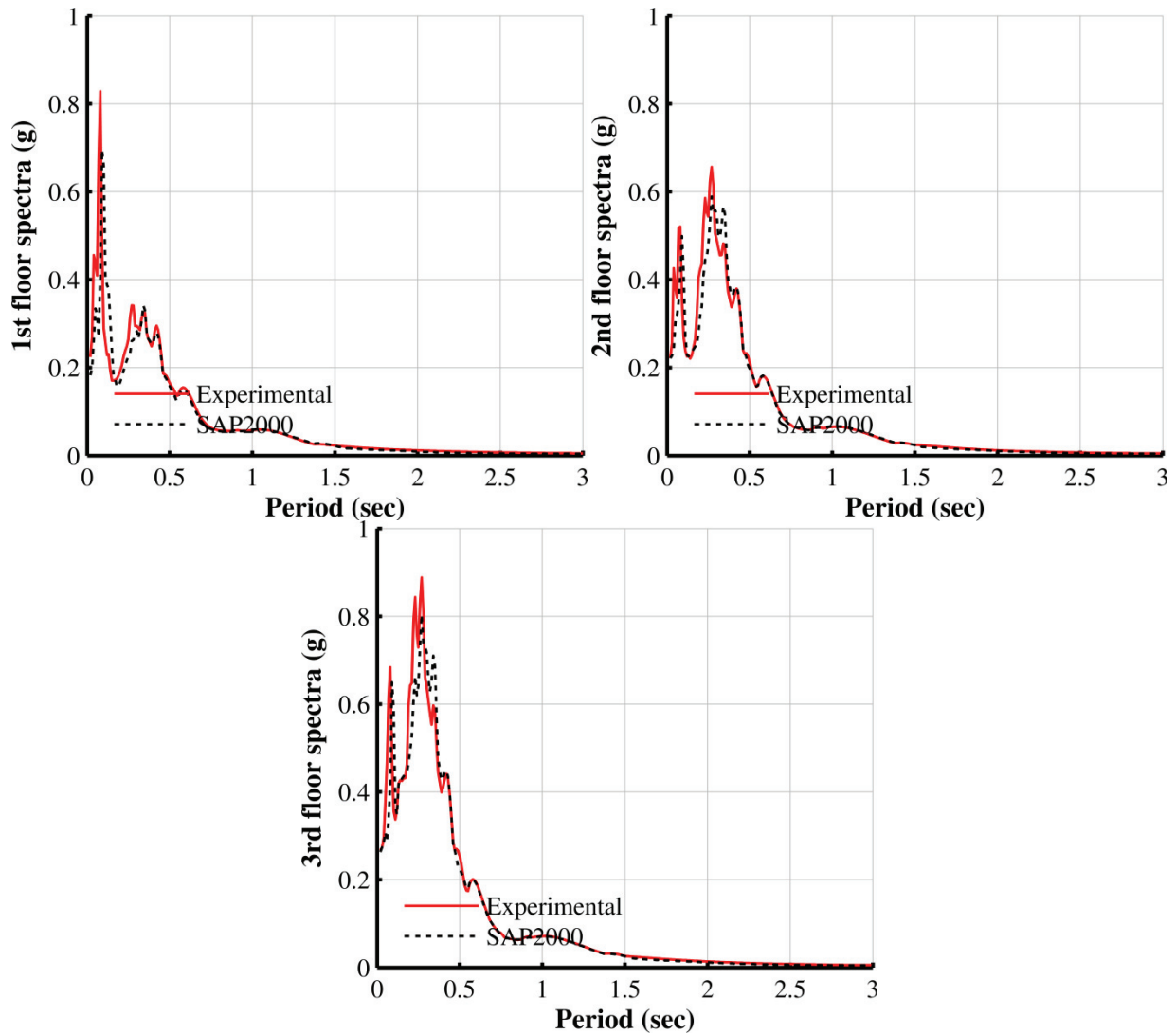


Figure 7-3: Comparison of analytical and experimental results for 5%-damped floor acceleration spectra of fixed structure obtained for ground motion ATL-270

7.3 Modeling of Elastomeric Bearings

Low damping elastomeric bearings are typically modeled as bilinear hysteretic elements. The particular bearing used in the testing exhibited a more complex behavior in which the stiffness reduced for displacement larger than about 1.5 to 2cm. Techniques for modeling these two types of behavior for elastomeric bearings in programs SAP2000 and 3D-BASIS-ME (Tsopeles et al., 1994) have been presented in Wolff and Constantinou (2004).

In this study a more complex model is employed for modeling in program SAP2000 the observed multi-linear hysteretic behavior of the bearings. As observed in Wolff and Constantinou (2004), this type of modeling improved the quality of prediction of the experimental response by comparison to the simpler bilinear hysteretic model. This was

particularly evident in the prediction of the floor acceleration response and of the floor acceleration response spectra.

Each elastomeric bearing was modeled using five different elements, combined in parallel as illustrated in Figure 7-4. An example of the combined force-displacement relation from the five elements is shown in Figure 7-5. The elements share the same joints at top and bottom.

Table 7-2 presents values of the model parameters for each of the four bearings that were identified from tests conducted on individual bearings as described in Section 6.3 and assigned in SAP2000. Figure 7-6 presents a comparison of experimental with analytical force-displacement loops of the isolation system (force from 4 bearings) in a displacement controlled test at 0.1Hz frequency and displacement amplitude that varied between 4 and 6.5cm. The analytical model predicts the observed behavior with very good accuracy.

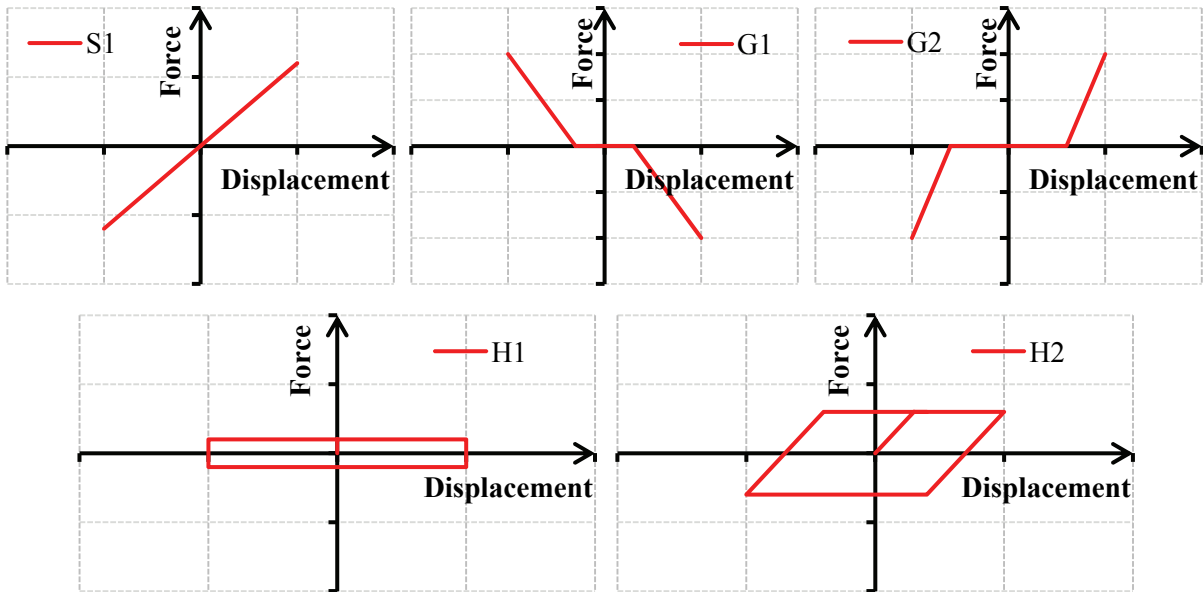


Figure 7-4: Force-displacement relations of five parallel elements representing an elastomeric bearing

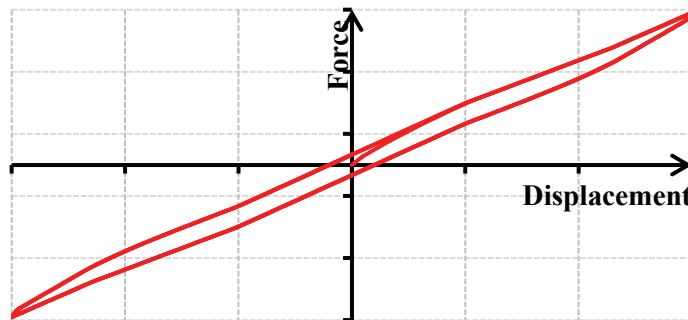


Figure 7-5: Analytical force-displacement loop of an elastomeric bearing obtained by the combination of the five parallel elements of Figure 7-4

Table 7-2: Properties of five elements representing each elastomeric bearing

Property	Bearing location on the shake table			
	NE	NW	SE	SW
G1 (Multi-Linear Elastic Element)				
Engagement displacement (<i>cm</i>)	2.36	1.60	1.37	1.83
Stiffness after engagement (<i>kN/cm</i>)	-0.51	-0.53	-0.65	-0.56
G2(Gap element)				
Engagement displacement (<i>cm</i>)	5.56	5.84	6.10	5.72
Stiffness after engagement (<i>kN/cm</i>)	0.58	0.39	1.24	0.77
H1 (Wen Element)				
Elastic stiffness (<i>kN/cm</i>)	175	175	175	175
Yield force (<i>kN</i>)	0.089	0.089	0.089	0.089
Yielding exponent	1	1	1	1
H2 (Wen Element)				
Elastic stiffness (<i>kN/cm</i>)	1.52	1.52	1.52	1.52
Yield force (<i>kN</i>)	1.34	1.34	2.23	1.20
Yielding exponent	0.27	0.27	0.27	0.27
S1 (Linear elastic spring)				
Horizontal Stiffness (<i>kN/cm</i>)	2.87	3.00	3.08	3.15
1. The effective stiffness of all elements is zero except for S1 which should have a very small value 2. The vertical stiffness of all elements except for H1 is zero. For H1, the vertical stiffness is the vertical stiffness of the bearing, equal to 964kN/cm (Wolff and Constantinou, 2004) 3. Element G1 has negative stiffness value and therefore negative force for positive displacement				

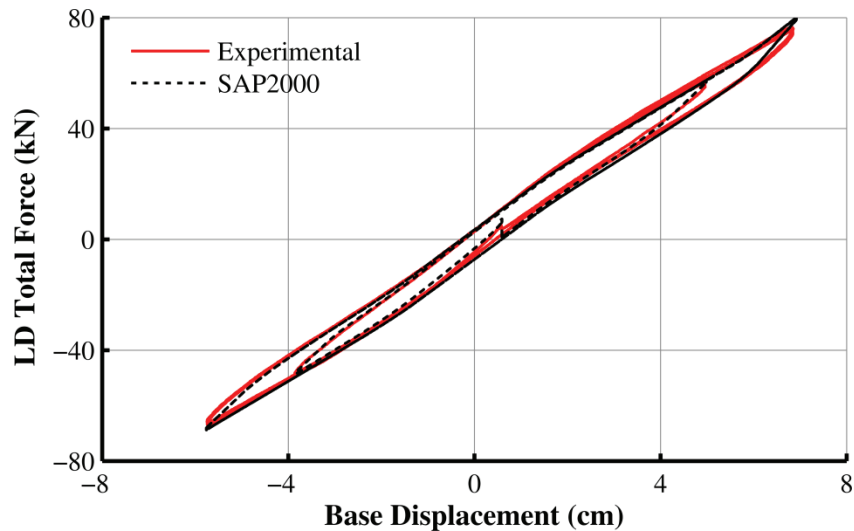


Figure 7-6: Comparison of analytical and experimental force-displacement loops of elastomeric isolation system

7.4 Modeling of Viscous Dampers

The dampers had linear viscous behavior with a damping constant measured in the displacement controlled tests to be 0.63kN-sec/cm for each damper. Figure 7-7 demonstrates that the dampers have this behavior by comparing experimental and analytical damper force-displacement loops (force of two dampers; displacement is the average of the displacement measured for the two dampers) in a displacement-controlled test at frequency of 0.5Hz. The analytical force was determined as twice the value of 0.63kN-sec/cm times the velocity of the damper obtained in the experiments. For the analytical prediction, the average velocity of the two dampers was used which was numerically calculated as the derivative of the damper displacement as measured by the damper potentiometers. Note that the deviation of the loop shape from the perfect elliptical shape is due to waviness in the velocity history during testing.

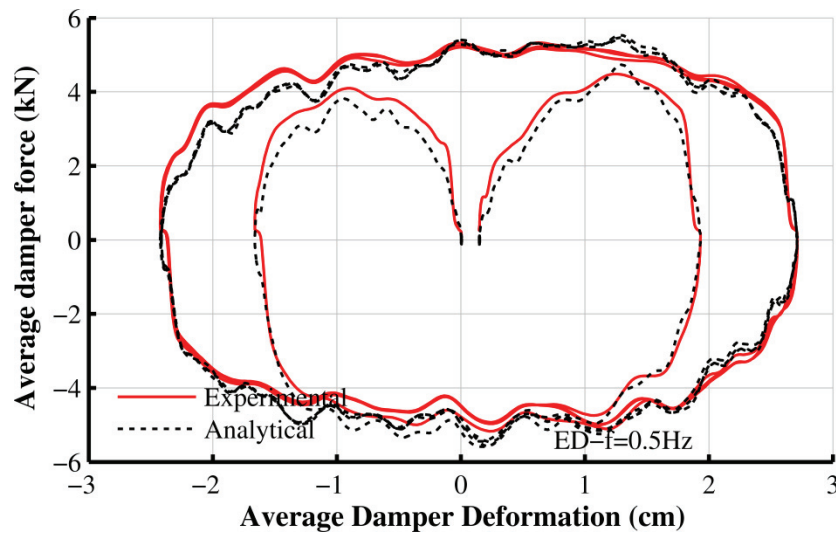


Figure 7-7: Comparison of analytical and experimental damper force-displacement loops

In program SAP2000, the linear viscous dampers were modeled as link damper elements together with their extenders as inclined elements in space exactly as installed in the model. The elastic stiffness of the damper extender was set to the arbitrarily large value of 1752kN/cm (1000kip/in) as it was determined that the stiffness did not affect the behavior of the assembly when varied within a range of estimated values (the exact stiffness was not known as the extender consisted of many complex parts including the load cell, etc.).

A sample comparison of experimental and analytical (predicted by response history analysis in SAP2000) results is presented in Figure 7-8 which shows the total horizontal (longitudinal) component of the damper force versus the base displacement in a shake table test of configuration ED (elastomeric bearings and dampers) with ground motion PS-10317 (see Table 6-2).

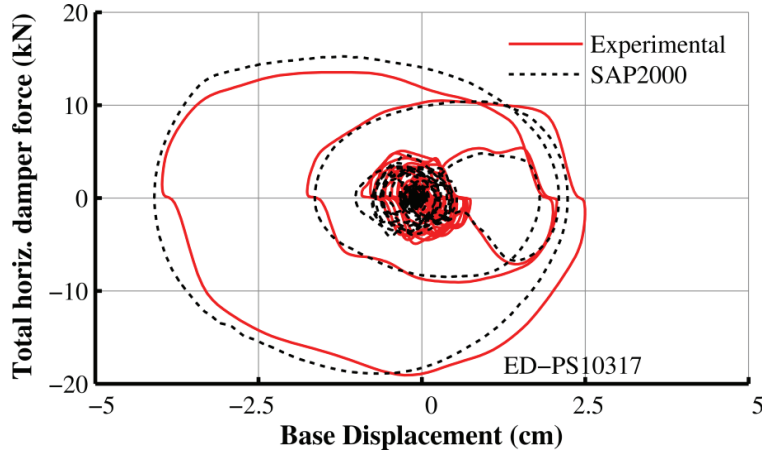


Figure 7-8: Comparison of experimental and analytically predicted (program SAP2000) damper longitudinal component of damper force versus base displacement in test of configuration ED and ground motion PS10317

7.5 Modeling of GSA

The force-displacement relation of the GSA was derived in Section 3.3 and is described by Equation (3-13). The properties of the four GSA units used in the two NSD devices are presented in Table 7-3 as obtained from individual GSA testing described in Section 6.4. The stiffness of spring S1 (see Figure 3-11), k_{s1} , was identified as the initial stiffness, the pre-load of spring S2, P_{is2} , was identified as the load where softening initiates and the engagement displacement u_y was identified as the displacement where softening initiates. The stiffness of spring S2, k_{s2} , was calculated as the pre-load P_{is2} divided by the specified (or nominal) pre-load displacement of spring S2 (equal to 27.2cm). Note that on the basis of Equation (3-13), the post-softening stiffness is given by $k_{psGSA} = k_{s2}k_{s1}/(k_{s2} + k_{s1})$. Therefore, stiffness k_{s2} could be calculated as $k_{s2} = k_{psGSA}k_{s1}/(k_{s1} - k_{psGSA})$. Stiffness k_{s2} was calculated both ways and is shown in Table 7-3. The two values of stiffness k_{s2} in Table 7-3 differ substantially. The source of this discrepancy was identified and explained in Section 6.4: stiffness k_{s2} was larger than the theoretical value due blockage of coils of spring S2.

Table 7-3: Properties of individual GSA

Location of GSA	NW	SW	NE	SE
k_{s1} (kN/cm)	3.24	3.33	3.49	4.64
P_{is2} (kN)	7.08	7.08	6.45	10.68
u_y (cm)	2.18	2.13	1.85	2.30
k_{psGSA} (kN/cm)	0.44	0.30	0.37	0.58
k_{s2} (kN/cm) ¹	0.26	0.26	0.24	0.39
k_{s2} (kN/cm) ²	0.51	0.33	0.41	0.66
1. Calculated as $k_{s2} = P_{is2}/(27.2\text{cm})$. Value used in analysis of Figure 7-9.				
2. Calculated as $k_{s2} = k_{psGSA}k_{s1}/(k_{s1} - k_{psGSA})$				

A comparison of experimental and analytical force-displacement loops of the four GSA is presented in Figure 7-9. Note that the analytical prediction is based on the value of stiffness k_{s2} determined as the spring preload divided by the preload displacement, which does not account for the fact that some coils of spring S2 were blocked so that the stiffness was actually larger. This is evident in Figure 7-9 where the post softening stiffness is under-predicted by the analytical model. Note that the problems with coil blockage and others discussed in Section 6.4 have been later resolved by redesigning the GSA (see Figure 6-7).

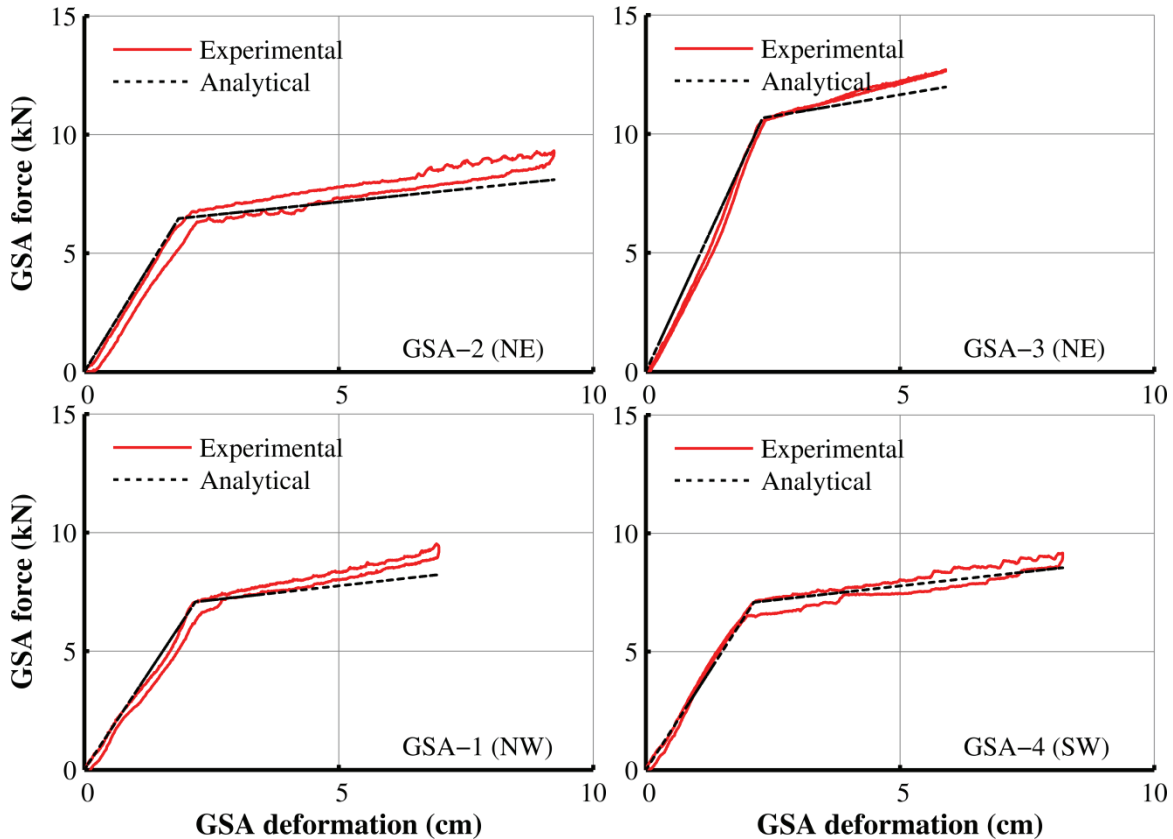


Figure 7-9: Comparison of analytical and experimental force-displacement relations of individual GSA

The force-displacement relations of the GSA in Figure 7-9 were obtained in testing of individual GSA removed from the NSD. When installed in the NSD, the GSA exhibited different behavior, as discussed in Section 6.4, due to (a) reduction in the physical gap opening and (b) due to the gap closing ($d_{gap} < u'_y$). Under such conditions Equations (4-63) to (4-69) should be used instead of Equation (3-13) to model the GSA behavior. Using the identified properties of the GSA in Table 7-3, the force-displacement relations of the GSA obtained by (a) Equations (4-63) to (4-69) and (b) by Equation (3-13) are compared in Figure 7-10. For the analysis, the following values for the physical gap were used: for the original gap $d_{gap} = 1.65\text{cm}$ and for the reduced gap $d'_{gap} = 1.27\text{cm}$ (the reduced gap value was the actual value during the shake table testing).

As a result of the reduction in the gap, spring S1 has a preload equal to $P_{s1} = k_{s1} (d_{gap} - d'_{gap})$, resulting in a non-zero force at zero displacement for the GSA. This is evident in the force-displacement relations of Figure 7-10. The deviation of the GSA behavior from ideal is relatively small but coupled with other problems (friction and blockage of springs), affected the performance of the GSA.

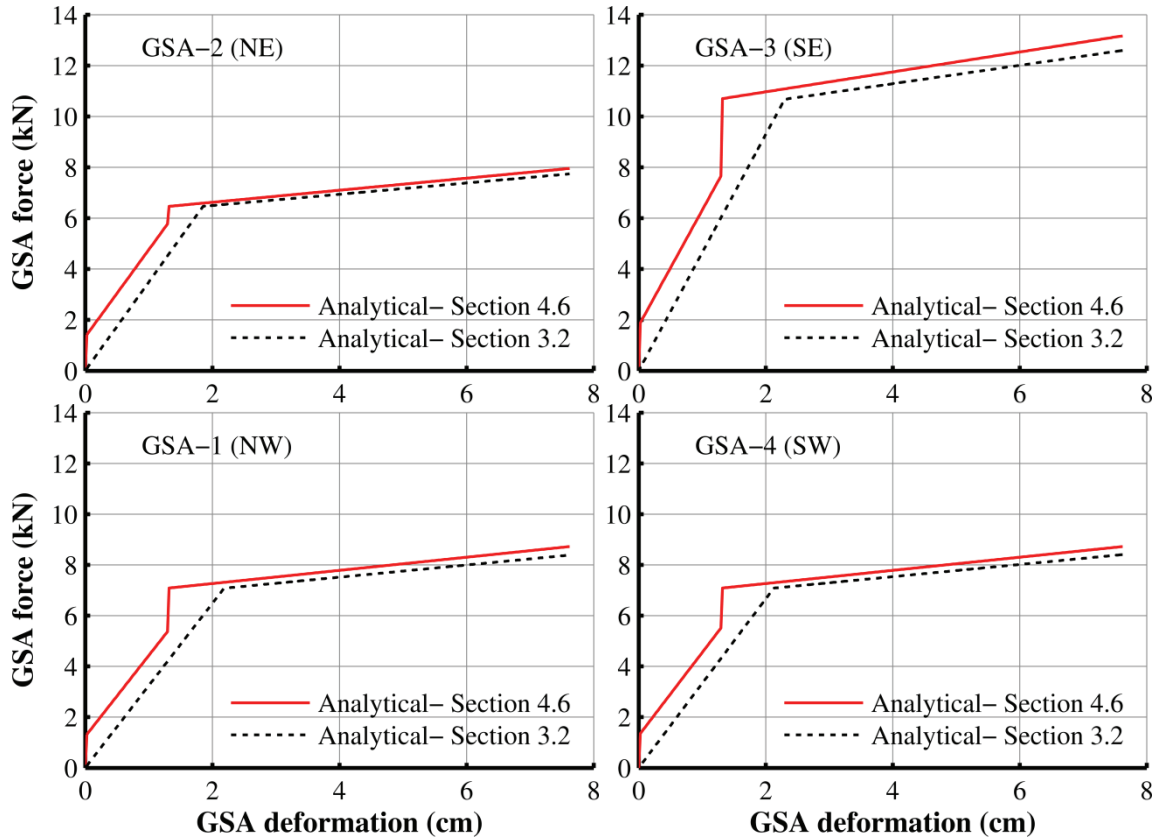


Figure 7-10: Comparison of GSA analytical results using the basic equation of Section 3.2 (Equation (3-13)) and the detailed equations of Section 4.6 for modeling GSA abnormal behavior

7.6 Modeling of NSD

Models for the NSD behavior have been presented in Sections 3 and 4. The results produced by these models are compared in this section to experimental results for configurations ENA, ENB and ENB-LA. In these configurations without dampers, the total NSD forces could be accurately calculated from acceleration records and from the elastomeric bearing load cell measurements (accelerometer base shear calculated from acceleration records times the effective mass F_{acc} subtracted from the sum of the bearing load cell measurements F_{ld}). The displacement input for all analytical predictions was the base displacement obtained in the experiments.

Figure 7-11 presents a comparison of experimental and analytical force-displacement relations for the total NSD force (sum of forces from two NSD) in a shake table test of configuration ENB (without GSA) and earthquake motion DZC-270. The NSD exhibits some hysteresis due to friction in its joints. The elastic baseline (obtained by subtracting friction) agrees very well with the analytical prediction based on Equation (3-11) with $F_g=0$ (multiplied by two for NSD East and West) and using the nominal properties of Table 3-1. For the analytical prediction, the recorded history of base displacement was used in Equation (3-11). Note that Equation (3-11) does not include any inertia, flexibility or friction effects.

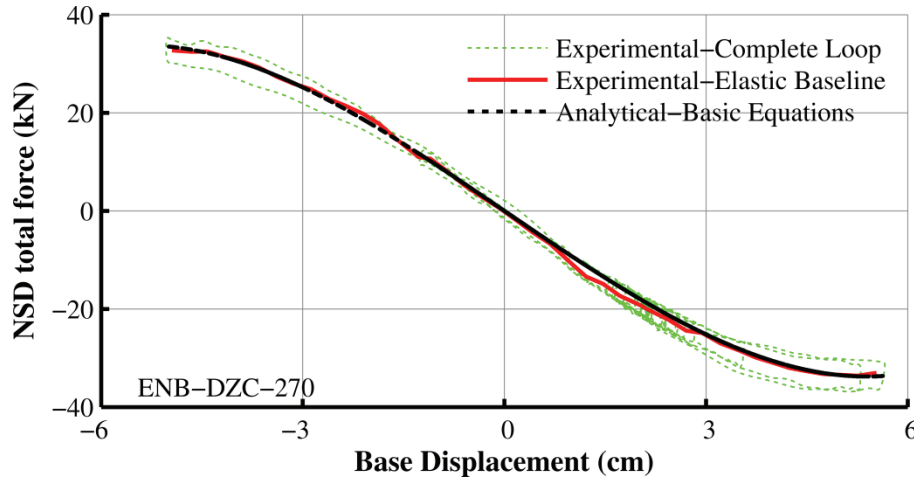


Figure 7-11: Comparison of experimental and basic analytical force-displacement relations of NSD in test with configuration ENB (without GSA)

The effects of inertia of the moving parts of the NSD are investigated in Figure 7-12 which compares the experimental force-displacement relations of the NSD in configuration ENB (without GSA) in test with motion DZC-270 to analytical predictions that include inertia effects as described in Section 4.3. For the analytical prediction the nominal properties of Table 3-1 and the mass and inertia properties of Table 4-1 have been used. It is evident that the NSD inertia has insignificant effects.

The effects of NSD flexibility are investigated in Figure 7-13 which compares the experimental force-displacement relations of the NSD in configuration ENB (without GSA) in test with motion DZC-270 to analytical predictions that include flexibility (but not inertia) effects as described in Section 4.5. For the analytical prediction, the nominal properties of Table 3-1 have been used together with a stiffness value of $k_b=131.4\text{kN/cm}$ for the bottom chevron and a stiffness value of $k_t=26.3\text{kN/cm}$ for the top chevron. The stiffness value for the bottom chevron k_b was identified using a) the measured (using the Krypton camera) peak displacement of point C in Figure 6-12, b) Equation (4-53) and c) the peak NSD force from Figure 7-11 (divided by two for each NSD). It is noted that the so calculated value of stiffness k_b is much smaller than the value calculated for the bottom chevron when assumed to be rigidly connected to the shake table. As tested, the connection details at the bottom of the NSD introduced significant flexibility. The

stiffness value for the top chevron k_t was conservatively estimated from the Krypton camera data in Figure 6-16 and use of Equation (4-54). The results of Figure 7-13 demonstrate that the NSD flexibility has no important effects.

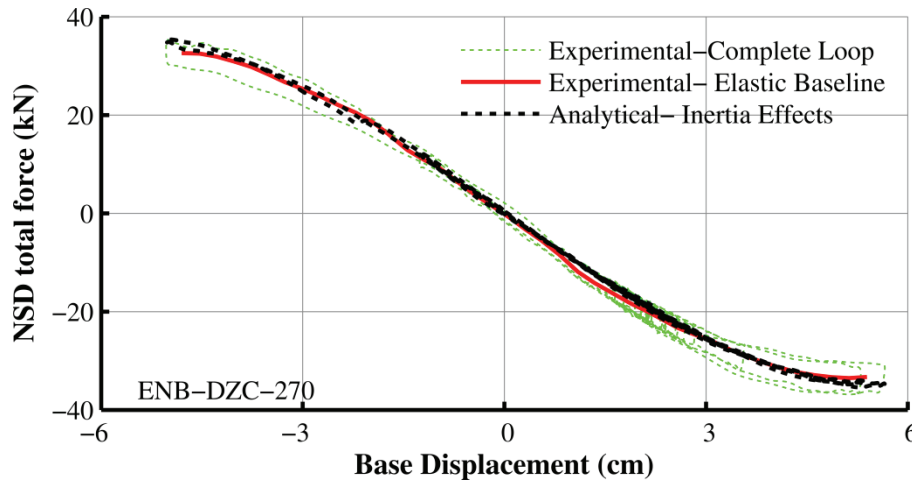


Figure 7-12: Comparison of experimental and analytical force-displacement relations with inertia effects of NSD in test with configuration ENB (without GSA)

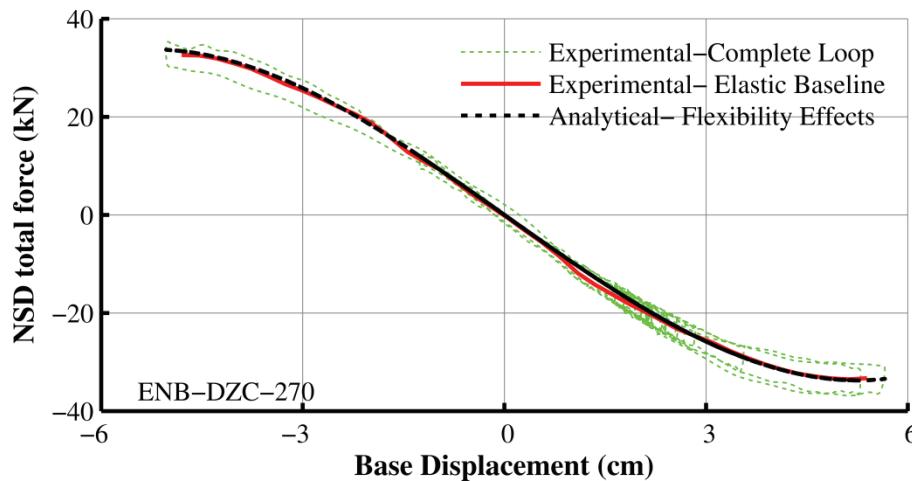


Figure 7-13: Comparison of experimental and analytical force-displacement relations with flexibility effects of NSD in test with configuration ENB (without GSA)

Figure 7-14 compares the experimental force-displacement loops of the NSD in configuration ENB (without GSA) in test with motion DZC-270 to analytical predictions that include hysteresis (but not inertia and flexibility) effects as described in Section 4.4. For the analytical prediction, the nominal properties of Table 3-1 with pin friction coefficient equal to 0.2 and a pin radius of 1.43cm were used. Evidently, the analytical prediction is excellent. Nearly identical analytical results were obtained when a constant hysteretic force was assumed instead of the more complex pin friction model.

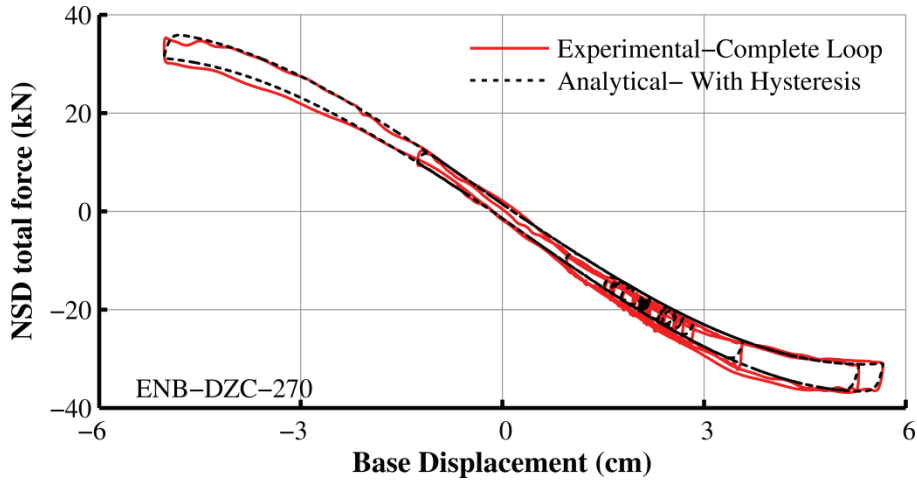


Figure 7-14: Comparison of experimental and analytical force-displacement loops with pin friction effects of NSD in test with configuration ENB (without GSA)

Further comparisons of experimental and analytical results are based on models of the NSD that include hysteresis but not inertia and flexibility effects. Figure 7-15 and Figure 7-16 present comparisons of experimental force-displacement loops of the NSD with GSA in configuration ENA in two shake table tests with motions PS10317 and 0637-270. The analytical model of the NSD included pin friction as described in Section 4.4 and the GSA model followed the procedures of Section 4.6 and made use of the parameters listed in Table 7-4. Furthermore, the small friction force observed in the GSA (see Figure 6-6) was ignored. The results of Figure 7-15 and Figure 7-16 demonstrate good agreement between experimental and analytical results. It should be noted, however, that the analysis is based on using the measured base displacement history as input to solve the equations describing the NSD with GSA force-displacement relation (dynamic response history analysis of the entire system is addressed later in Section 7.8).

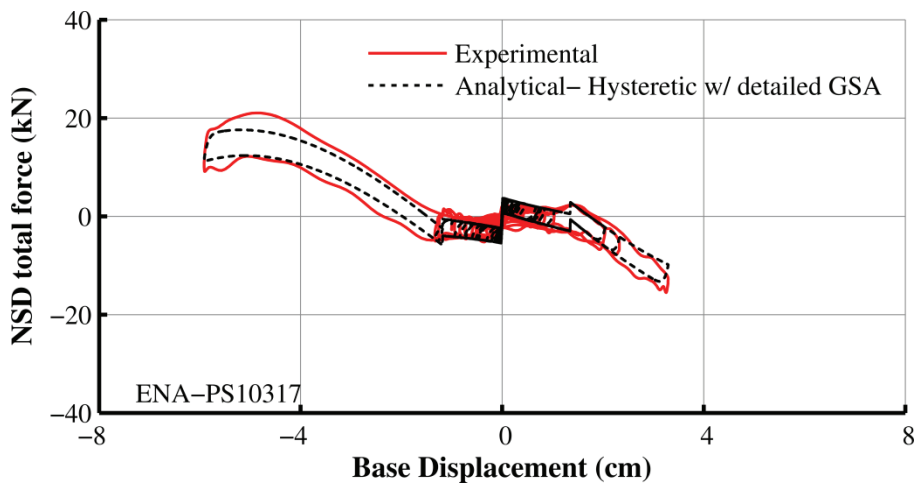


Figure 7-15: Comparison of experimental and analytical force-displacement loops of NSD with GSA in configuration ENA in test with motion PS10317

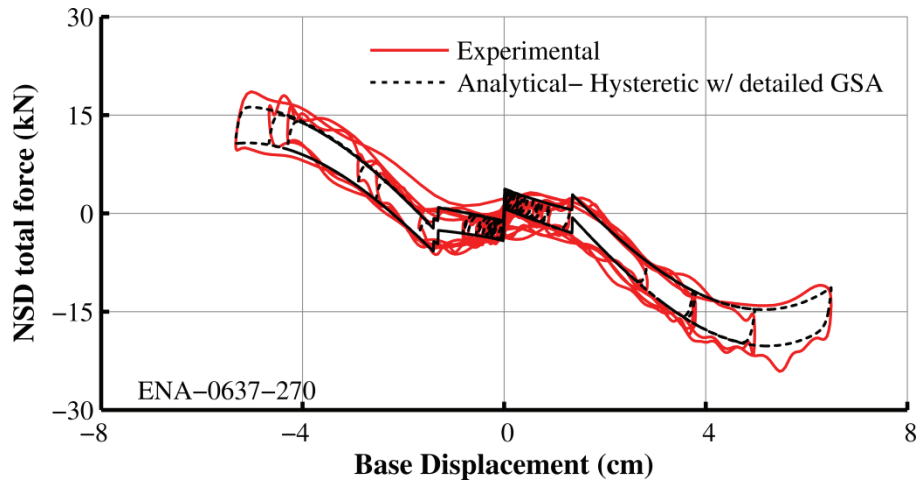


Figure 7-16: Comparison of experimental and analytical force-displacement loops of NSD with GSA in configuration ENA in test with motion 0637-270

The GSA properties used in the analytical model for prediction of the response due to seismic ground motion that were also used in generating Figure 7-15 and Figure 7-16 are presented in Table 7-4 and subject to the following details:

1. The values of gap opening d_{gap} varied during testing. The original value of the gap was 1.65cm for all GSA. Adjustments to the gap resulted in pre-loading of spring S1, which otherwise should be unloaded. These adjustments occurred because the GSA were removed and re-installed in the NSD several times. Also note that all GSA needed to be shimmed during re-installation as shown in Figure 7-17 which caused an initial external load to the GSA. For tests in configuration ENA and EDNA with motions 0637-270 and TCU-129-E, the modified gap opening was as listed in Table 7-4. Subsequently, the GSA were modified resulting in a new set of gap opening values as listed in Table 7-4. Also, shimming resulted in higher loads applied by the shims to the GSA and this is reflected by the different values of P_{is2} listed in Table 7-4. The differences between the two sets of modified gap openings are small and did not have any important effect on the behavior of the GSA.
2. The value of stiffness of spring S2 k_{s2} used in analysis of the model structure subjected to ground motion was calculated based on the measured value of the post-softening stiffness of each GSA, k_{psGSA} , as reported in Table 7-3, and using $k_{s2} = k_{psGSA}k_{s1} / (k_{s1} - k_{psGSA})$. This resulting value of k_{s2} is larger than the theoretical spring constant due to the fact that during testing, coils of spring S2 were blocked resulting in higher stiffness.
3. A reduced value for the rod stiffness $k_r = 210 \text{ kN/cm}$ was used in Equations (4-63) to (4-69) in order to approximately account for stiffness reduction due to the series arrangement of the rods with reaction plates, shims, etc.

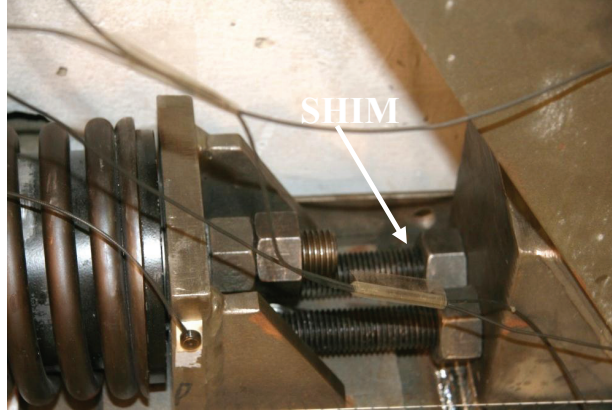


Figure 7-17: Shimming of GSA resulting in modified gap opening

Table 7-4: Properties used in modeling GSA per theory of Section 4.6

Property	Location of GSA			
	NW	SW	NE	SE
k_{s1} (kN/cm)	3.24	3.33	3.49	4.64
P_{is2} (kN)	7.08	7.08, 6.19 ¹	6.45	9.79, 8.9 ²
Modified gap d_{gap} '(cm)	1.32	1.37, 1.17 ³	1.32	1.27, 1.14 ⁴
k_{s2} (kN/cm) ⁵	0.51	0.33	0.41	0.66
$P_{is1} = k_{s1} (d_{gap} - d'_{gap})$ $d_{gap} = 1.65cm$				
<p>1. This value was 7.08kN for tests ENA_0637-270 and ENA_TCU-129-E; 6.19kN for other tests 2. This value was 9.79kN for tests ENA_0637-270 and ENA_TCU-129-E; 8.9kN for other tests 3. This value was 1.37cm for tests ENA_0637-270 and ENA_TCU-129-E, 1.17cm for other tests 4. This value was 1.27cm for tests ENA_0637-270 and ENA_TCU-129-E; 1.14cm for other tests 5. The stiffness of spring S2 was based on the value of stiffness k_{psGSA} identified from the individual GSA testing as $k_{s2} = k_{psGSA} k_{s1} / (k_{s1} - k_{psGSA})$. Values are as listed in Table 7-3.</p>				

7.7 Implementation of NSD Model in Program SAP2000

The NSD was modeled in program SAP2000 using the element described in Section 4.4.2. This element is the most complex at capturing the behavior of the NSD, including displacement-dependent hysteresis. It does not account for NSD inertia and flexibility effects, which have been demonstrated to be insignificant.

Based on the definition of parameters in Figure 4-20, the following force parameters have been identified for each NSD on the basis of analytical force-displacement loop shown in Figure 7-14 (which is in very good agreement with the experimental loop of the NSD without GSA):

$$F_y = 1.46kN; F_{max} = 36.6kN; F_{el,max} = 33.9kN \quad (8-1)$$

The coefficient of friction assigned for elements FPL and FPR was calculated using Equation (4-44) and the values of force in Equation (8-1) to be $\bar{\mu} = 0.037$. The elastic stiffness of these

elements was assigned the value of 175kN/cm and their radius the value zero (flat sliders). The yield force for element WEN (Wen Element) was 0.73kN, the exponent was 2, the elastic stiffness was 175kN/cm and the post elastic stiffness was zero. The vertical stiffness of elements FPL and FPR was 175kN/cm. Also, the tension-only vertical stiffness of elements LINL and LINR was assigned the value 175kN/cm. The height of the elements was 50.8cm.

For configuration ENA, the force-displacement relation of the NSD exclusive of the GSA was constructed using Equations (3-4) and (3-11) with $F_g=0$ and directly imported into program SAP2000 as the force-displacement relation for element ML1 (see Figure 4-17). The relation was calculated using the nominal properties of the device listed in Table 3-1. The force-displacement relation of the GSA was calculated using Equations (4-63) to (4-69) using the properties of Table 7-4 and imported into program SAP2000 as the force-displacement relation for element ML2.

Figure 7-18 compares experimental and analytical force-displacement loops for the NSD, inclusive of the GSA, in a test of configuration ENA with motion 0637-270. Note that the analytical results in Figure 7-18 were obtained in response history analysis of the tested structural system in program SAP2000. The analytical model predicts well the NSD force-displacement loop.

For configurations ENB, ENB-LA, EDNB and EDNB-LA (without the GSA), the elements of the NSD model in SAP2000 had the properties described above except that element ML2, representing the GSA, was removed and element ML1 was assigned properties based on a different procedure. Specifically for the configurations lacking the GSA, the NSD (and the isolation system) had a non-zero displacement at the start of some experiments and also had comparable permanent displacement at the end of the experiment (see Figures 6-27 and Figure 6-28). This behavior was found to be important in the analytical prediction of the response so that the analysis model required the introduction of a non-zero initial force in the NSD.

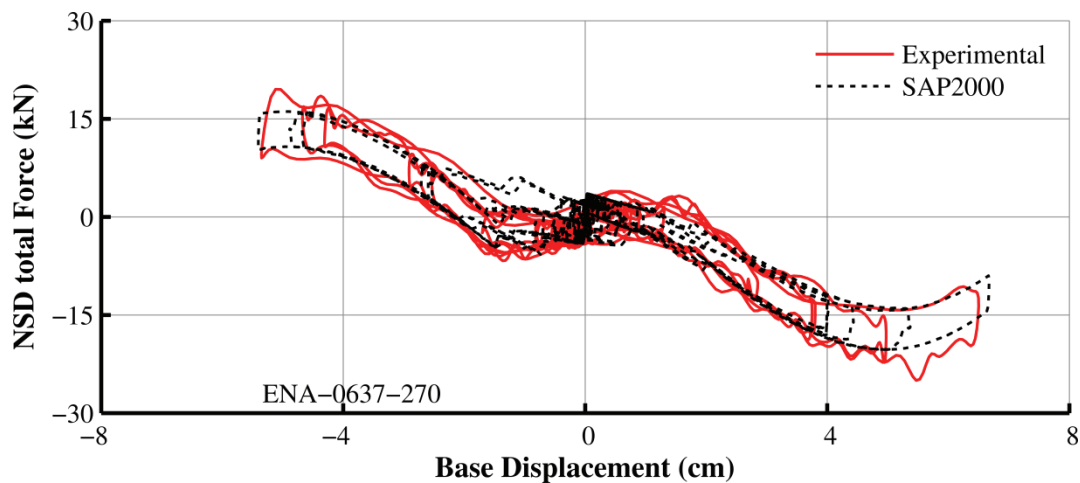


Figure 7-18: Comparison of experimental and response history analysis (program SAP2000) results for NSD force-displacement loops for configuration ENA in test with motion 0637-270

To account for initial force in the NSD, it was arbitrarily assumed that the pre-compressed spring of the NSD on the East side had permanent curvature due to damage caused by repeated testing as shown in Figure 7-19. The behavior of the NSD with initial curvature of the spring can be captured by Equations (3-4) to (3-11) except for Equation (3-7) which is replaced by the following equation:

$$\sin \theta_s = \arcsin \left[\frac{u}{l_s} \left(1 + \frac{l_1}{l_2} \right) \right] + \psi \quad (8-2)$$

In this equation, ψ is a parameter that represents the initial angle of the pre-loaded springs at pins D and E as shown in Figure 7-19. When parameter ψ is introduced, the force-displacement of the NSD exhibits a shift with a non-zero force at zero displacement as shown in Figure 7-20 for the case of $\psi=0.07rad$. The implementation of this behavior in program SAP2000 requires two steps:

1. Force F_o is subtracted from the calculated force-displacement relation of the NSD and the result is imported to the program as the force-displacement relation for element ML1.
2. A constant force F_o is applied as external load to node J1 (Figure 4-17) during the response history analysis.

Figure 7-21 compares force-displacement loops of the NSD in tests with motion PS10317 for configurations ENB and ENB-LA (without GSA) when the analytical model includes the initial curvature effects. The analytical results were obtained in response history analysis of the tested structure in program SAP2000. The force-offset at zero displacement is apparent in the experimental loops and is captured well in the analysis.

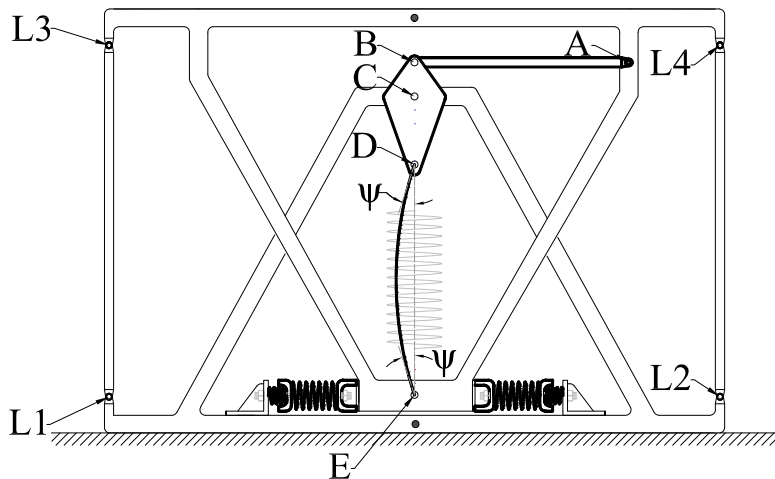


Figure 7-19: NSD with initial curvature of the pre-compressed spring

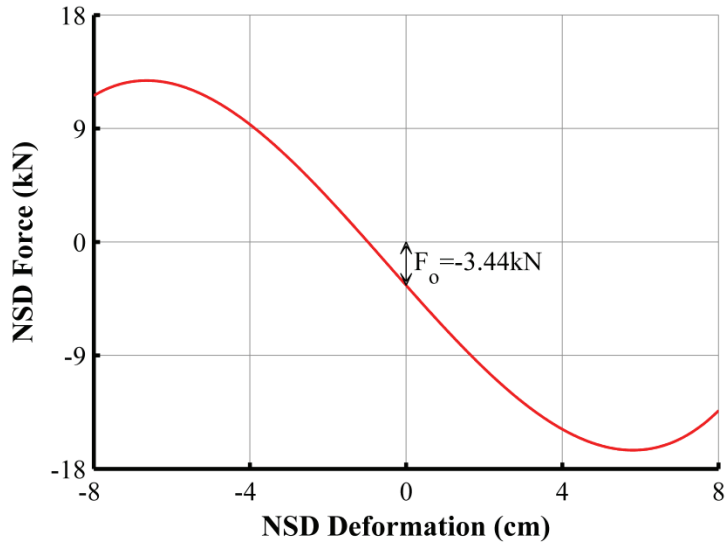


Figure 7-20: NSD force-displacement relation with initial spring curvature

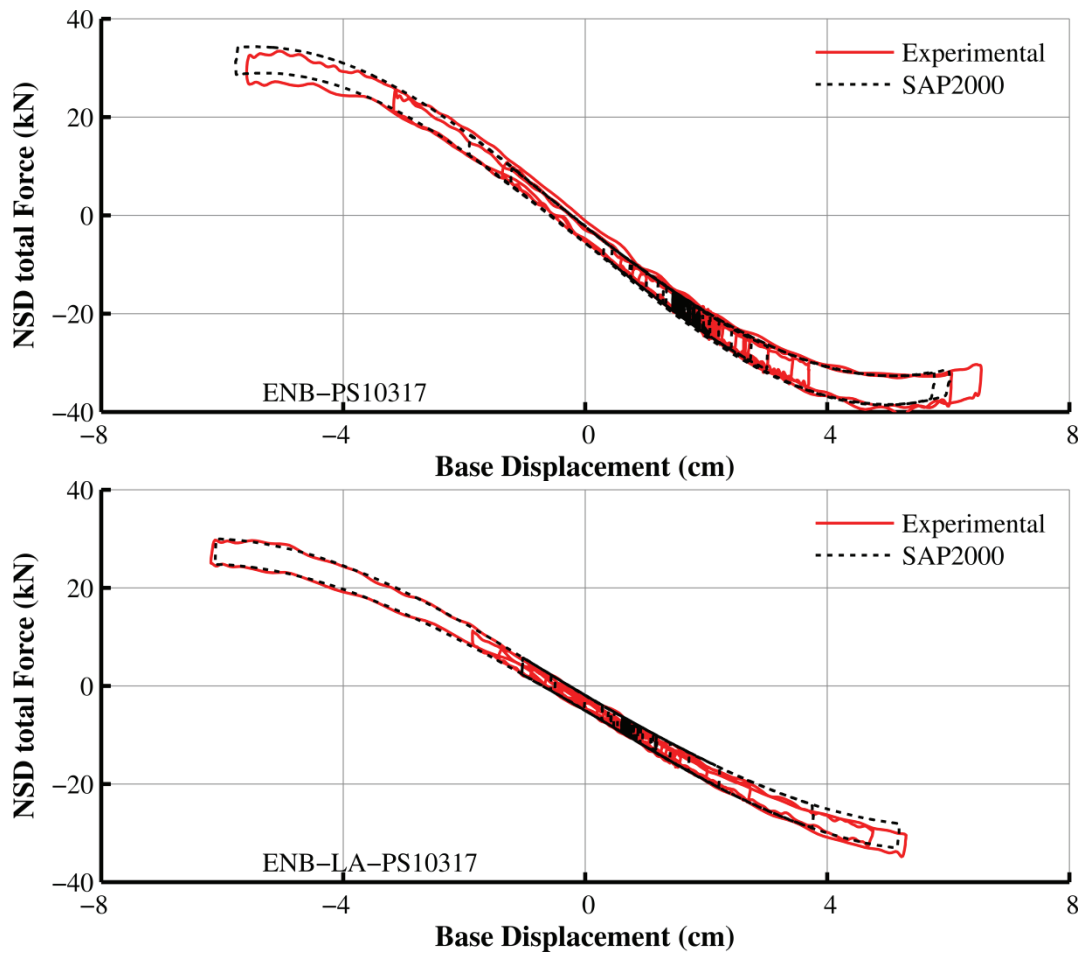


Figure 7-21: Comparison of experimental and analytical (program SAP2000 with initial curvature of spring) force-displacement loops of NSD without GSA for configurations ENB and ENB-LA and motion PS10317

7.8 Comparison of Experimental and Analytical Results

This section presents comparisons of the experimental results obtained in the shake table testing to response history analysis results obtained by program SAP2000 in which the structure, elastomeric bearing, viscous damper and NSD models described in Sections 7.2 to 7.7 have been implemented.

Figure 7-22 to Figure 7-29 present selected experimental and analytical results for all tested configurations and for earthquake motion PS10317. Appendix C presents comparisons of experimental and analytical results for all tested configurations and earthquake motions. The response quantities compared in these figures and Appendix C are: (a) loops of base shear force versus base displacement, (b) histories of base displacement and inter-story drift (for the figures of this section only the largest second story drift is presented), (c) histories of base acceleration and floor acceleration (for the figures of this section only the largest third floor acceleration is presented), (d) histories of elastomeric bearing axial force, and (e) base and floor acceleration 5%-damped response spectra. It is presumed here that the experimental response is exact. However, it should be noted that the experimental data contain noise as only a 50Hz low pass filter has been used in the processing of data. This affected to some extent the measurement of peak values.

The figures in this section and in Appendix C demonstrate that the analytical model predicts well the experimental response in terms of frequency content of the response and shape of loops but it occasionally over-predicts or under-predicts the experimental peak response. However, the predicted peak base displacement and peak base shear force are in very good agreement with the experimental peak values. The occasional over or under-prediction of the peak structural response was also observed in the analysis of the structure without the isolation system (see Figures 7-2 and 7-3). It is believed that this is due to inability of the model of the structural system in program SAP2000 to capture sliding and minor impact in the connections of the masses of the model to the floors and in the connections of the braces to beams and columns during strong shaking.

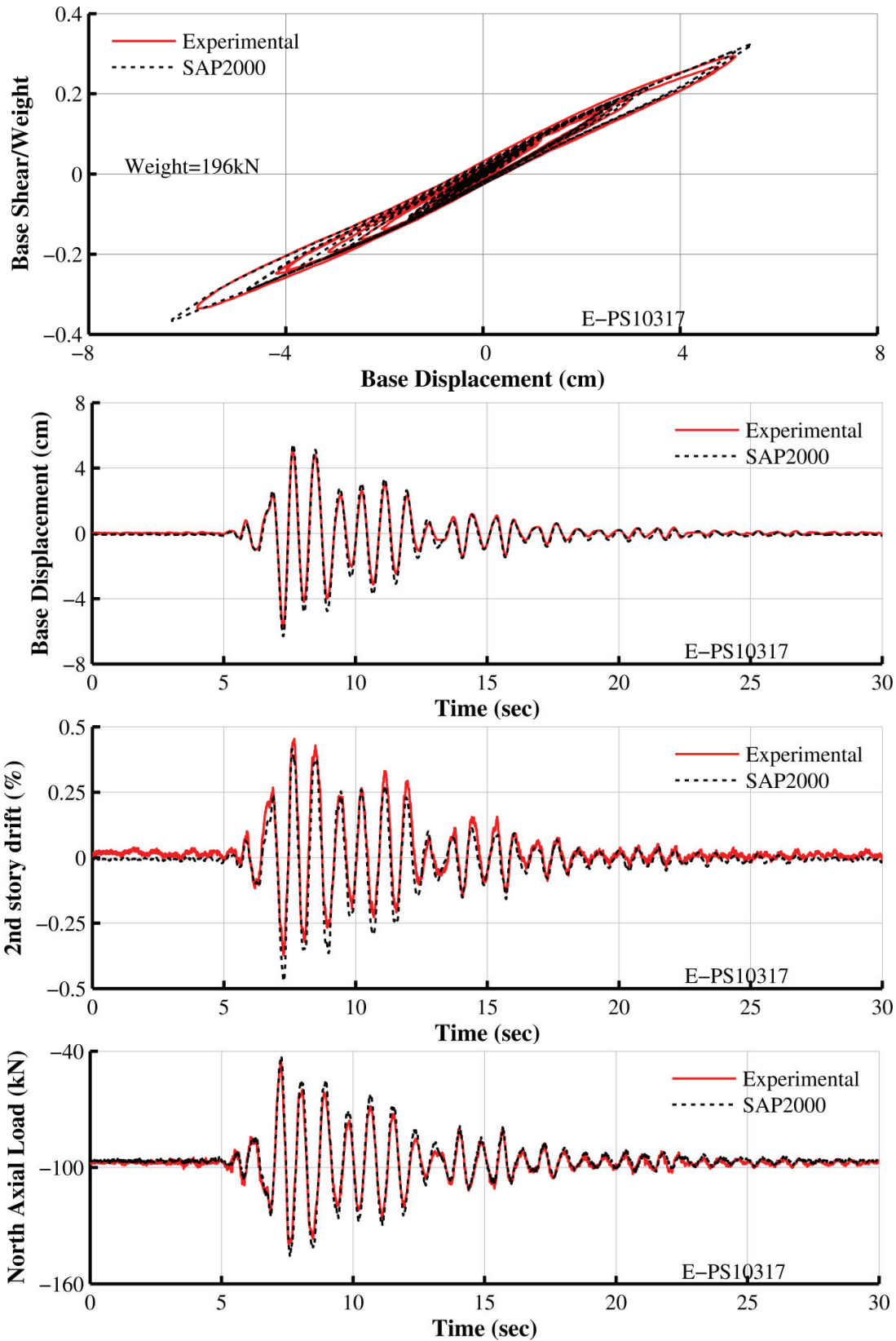


Figure 7-22: Comparison of experimental and analytical results for configuration E and ground motion PS-10317

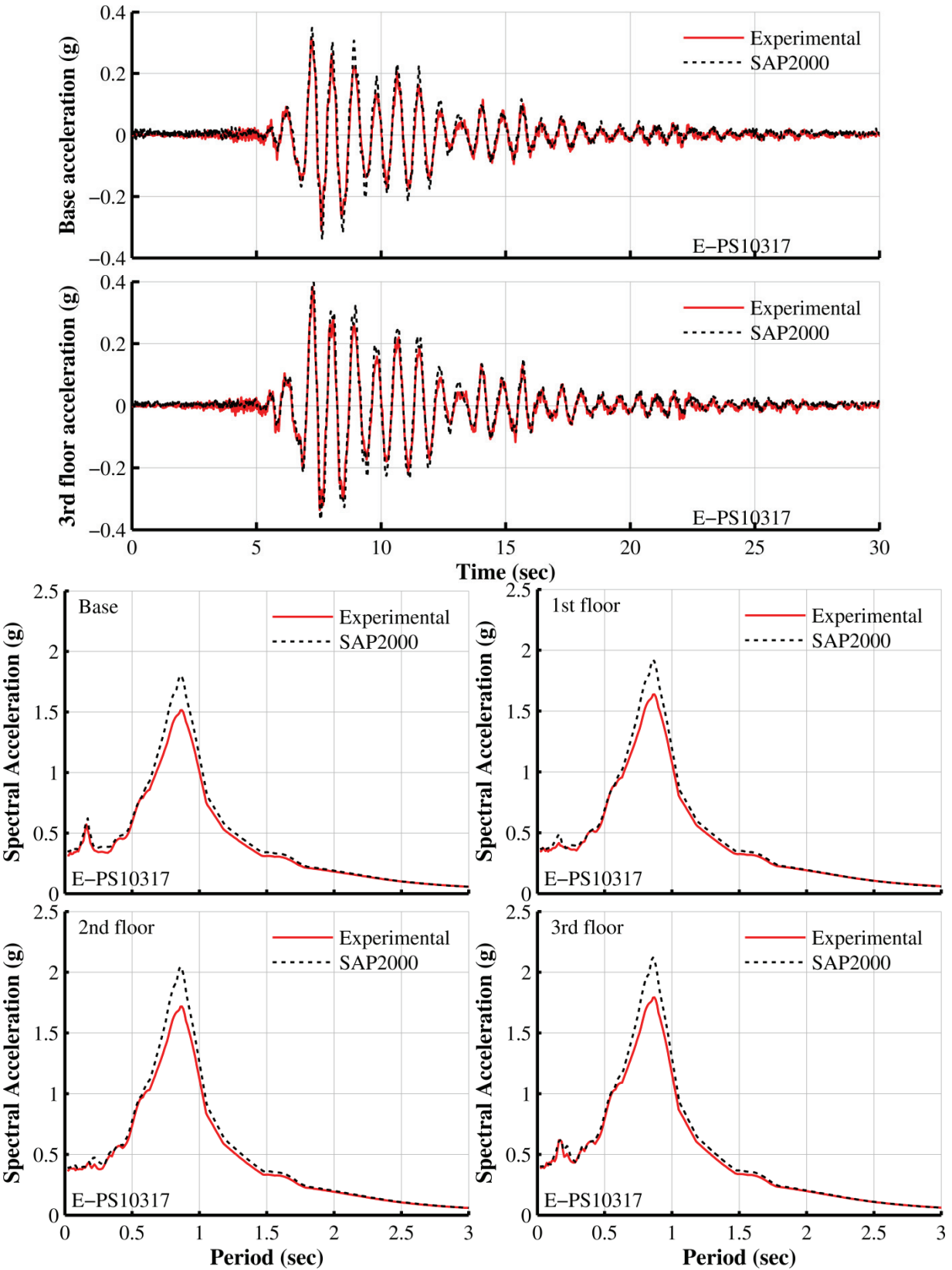


Figure 7-22 (cont'd): Comparison of experimental and analytical results for configuration E and ground motion PS-10317

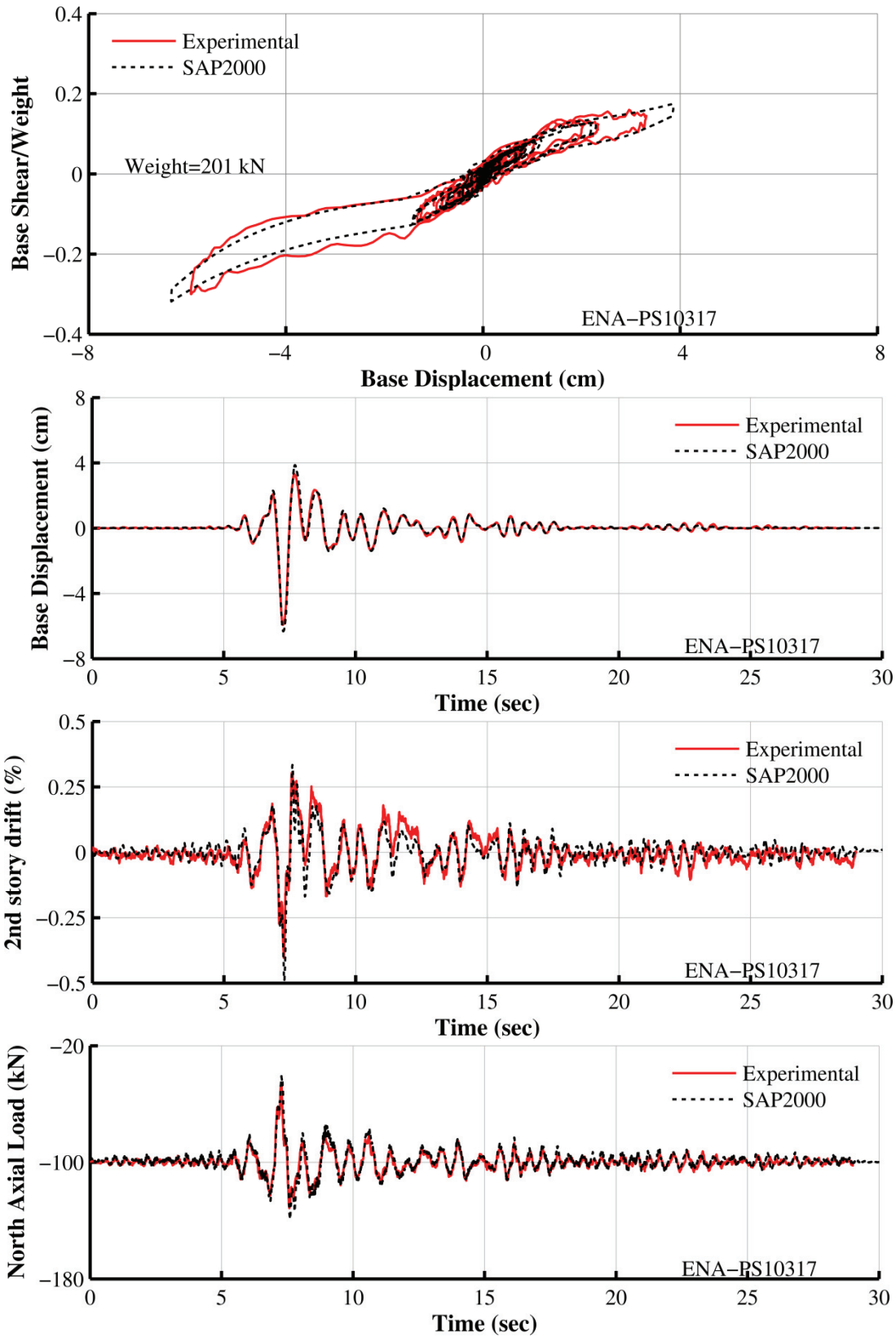


Figure 7-23: Comparison of experimental and analytical results for configuration ENA and ground motion PS-10317

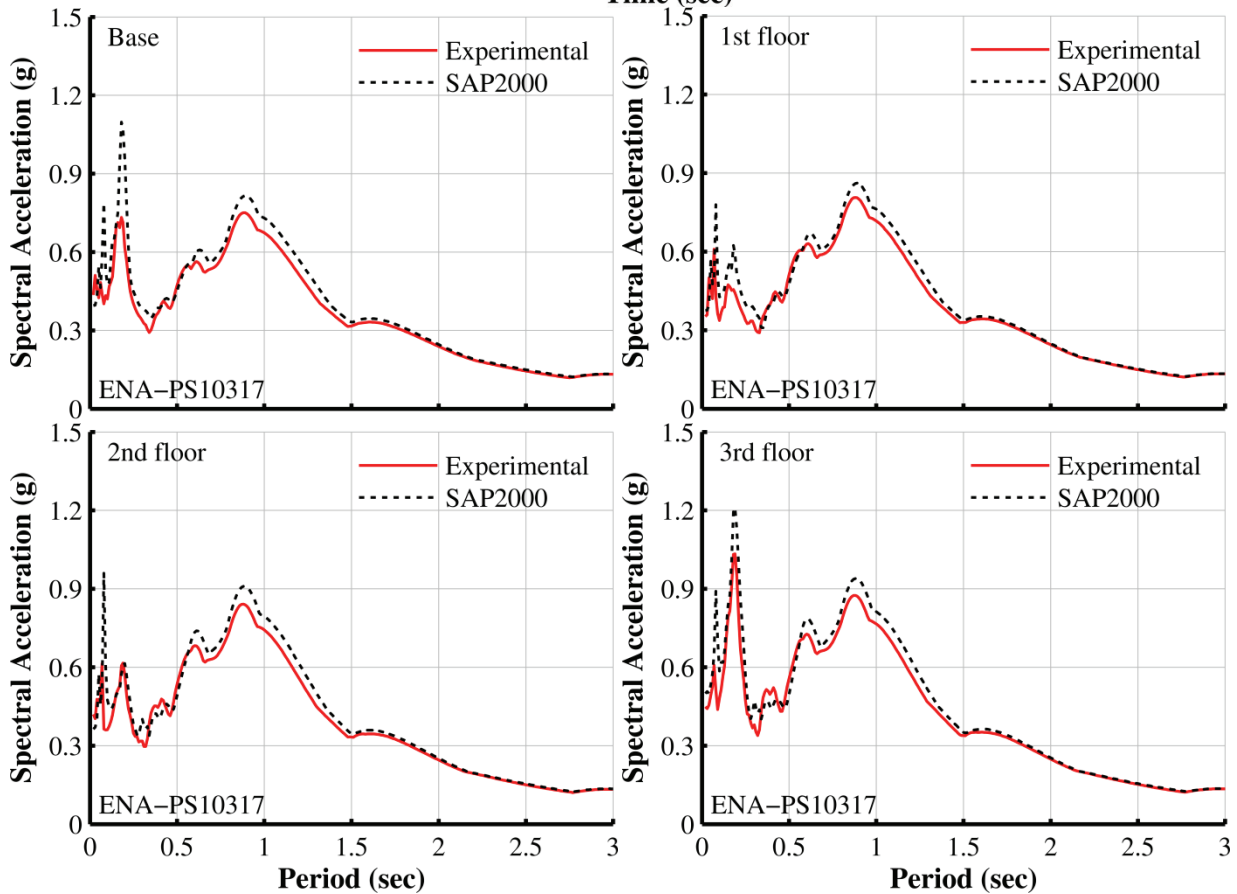
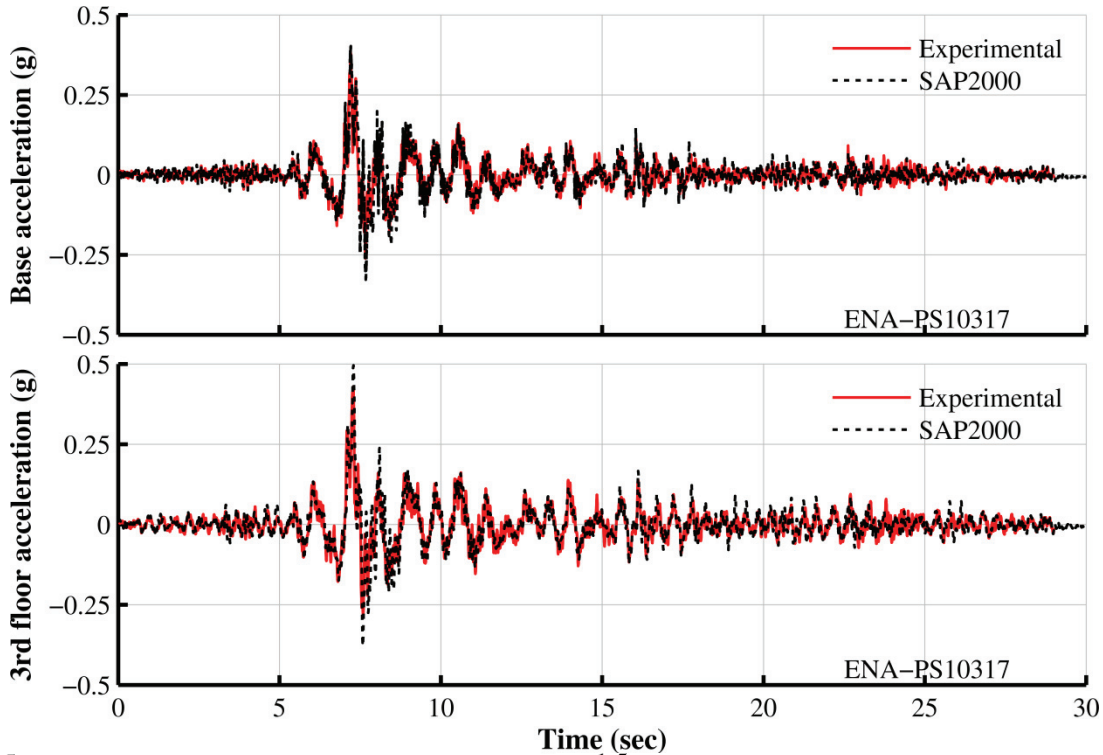


Figure 7-23 (cont'd): Comparison of experimental and analytical results for configuration ENA and ground motion PS-10317

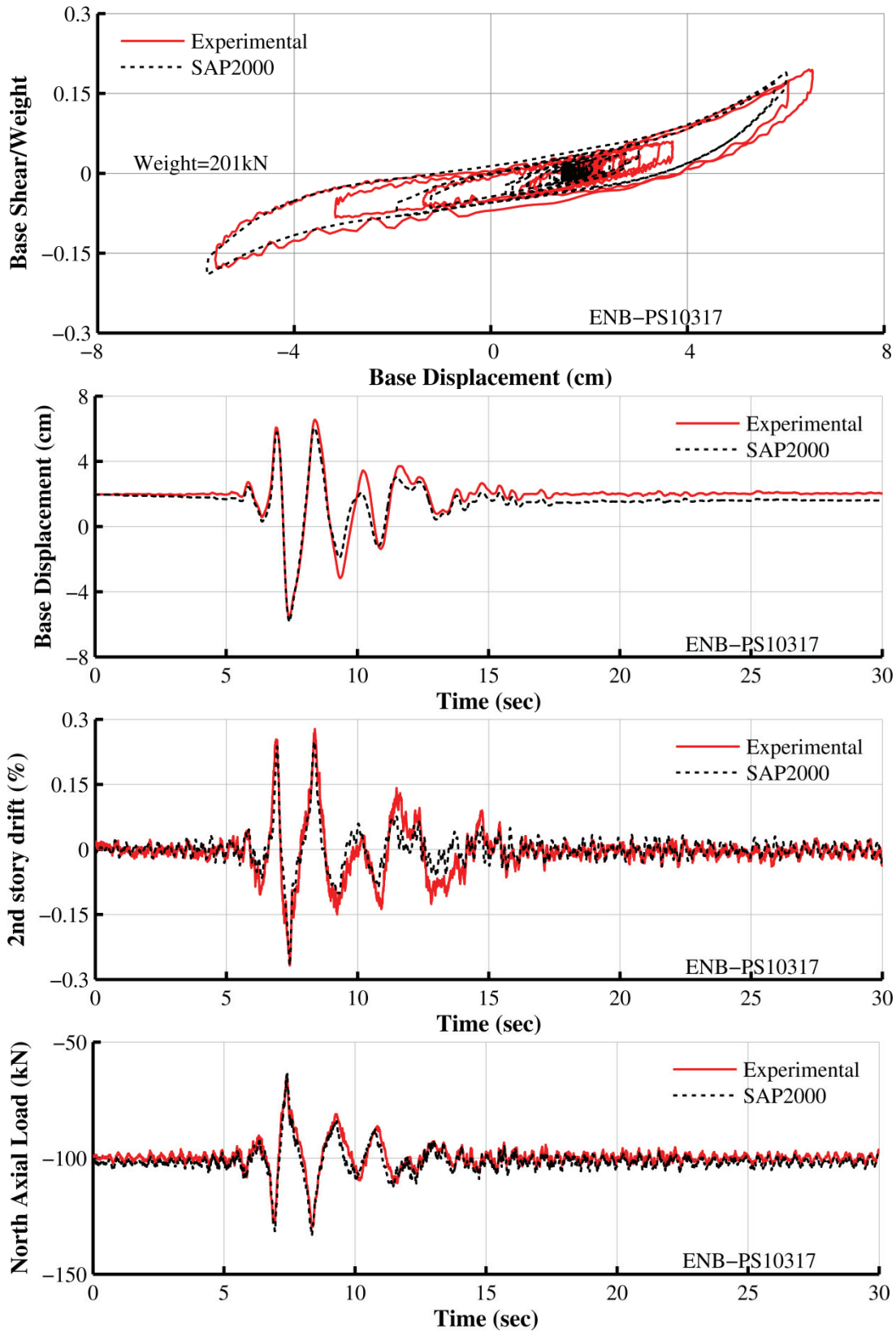


Figure 7-24: Comparison of experimental and analytical results for configuration ENB and ground motion PS-10317

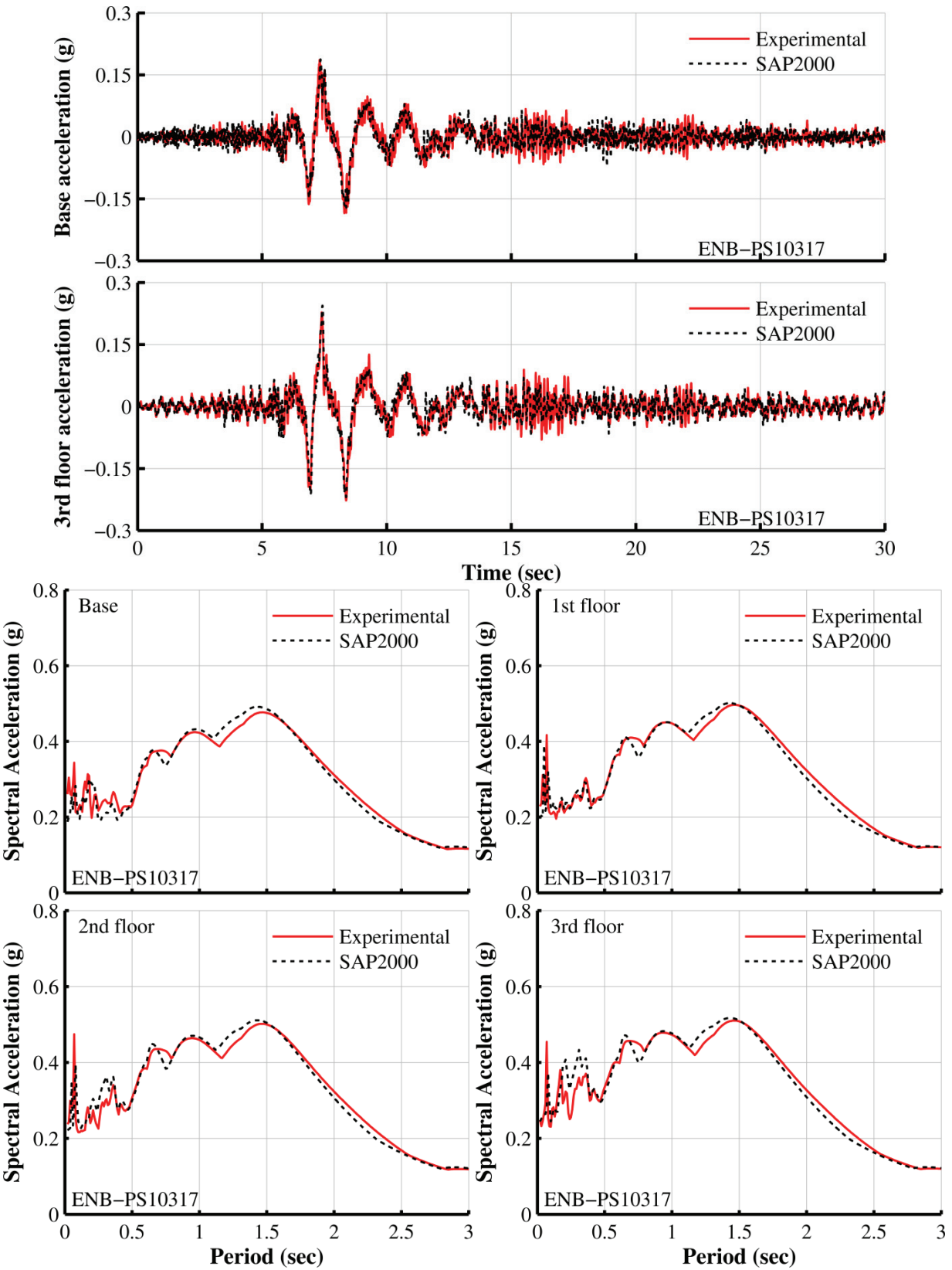


Figure 7-24 (cont'd): Comparison of experimental and analytical results for configuration ENB and ground motion PS-10317

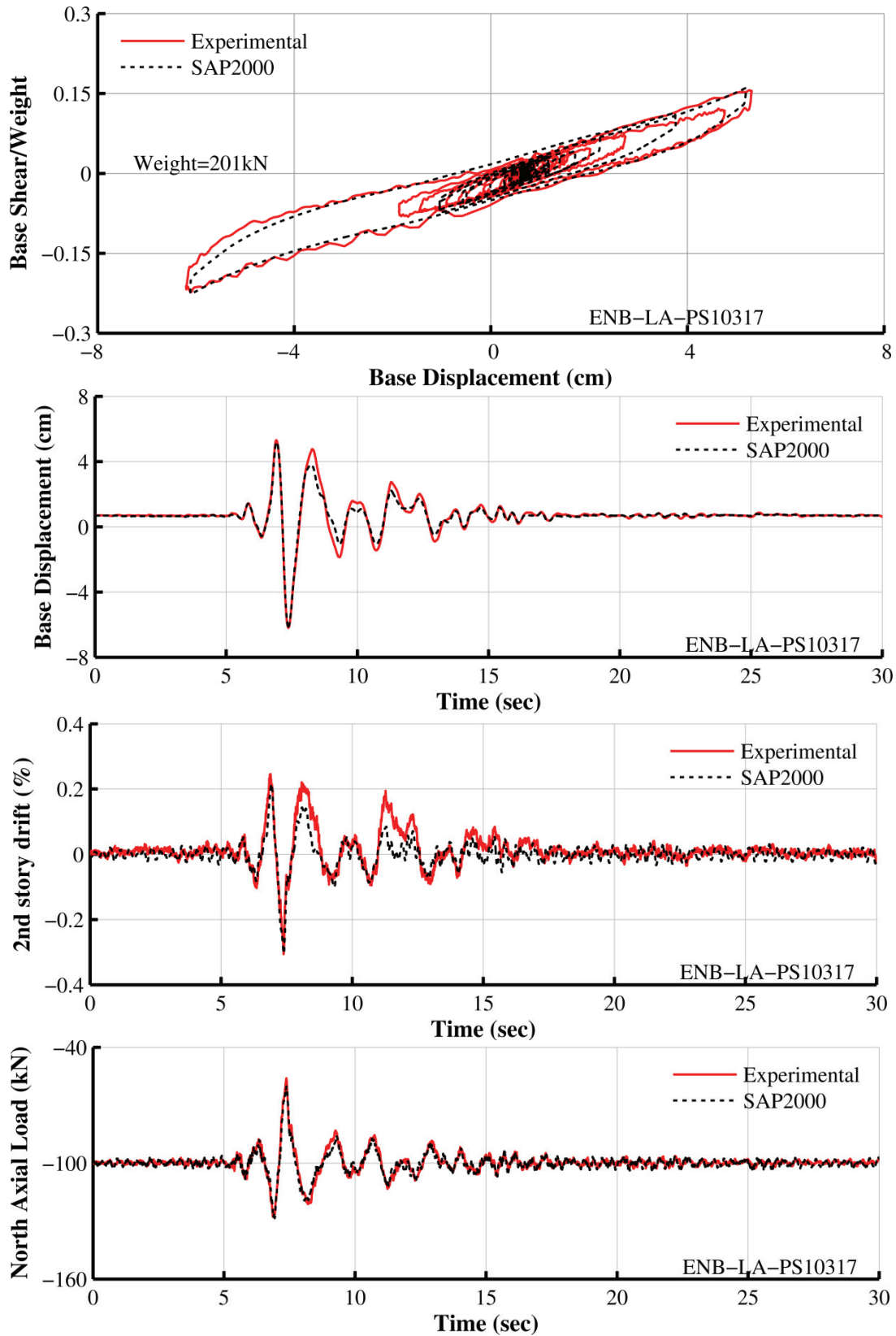


Figure 7-25: Comparison of experimental and analytical results for configuration ENB-LA and ground motion PS-10317

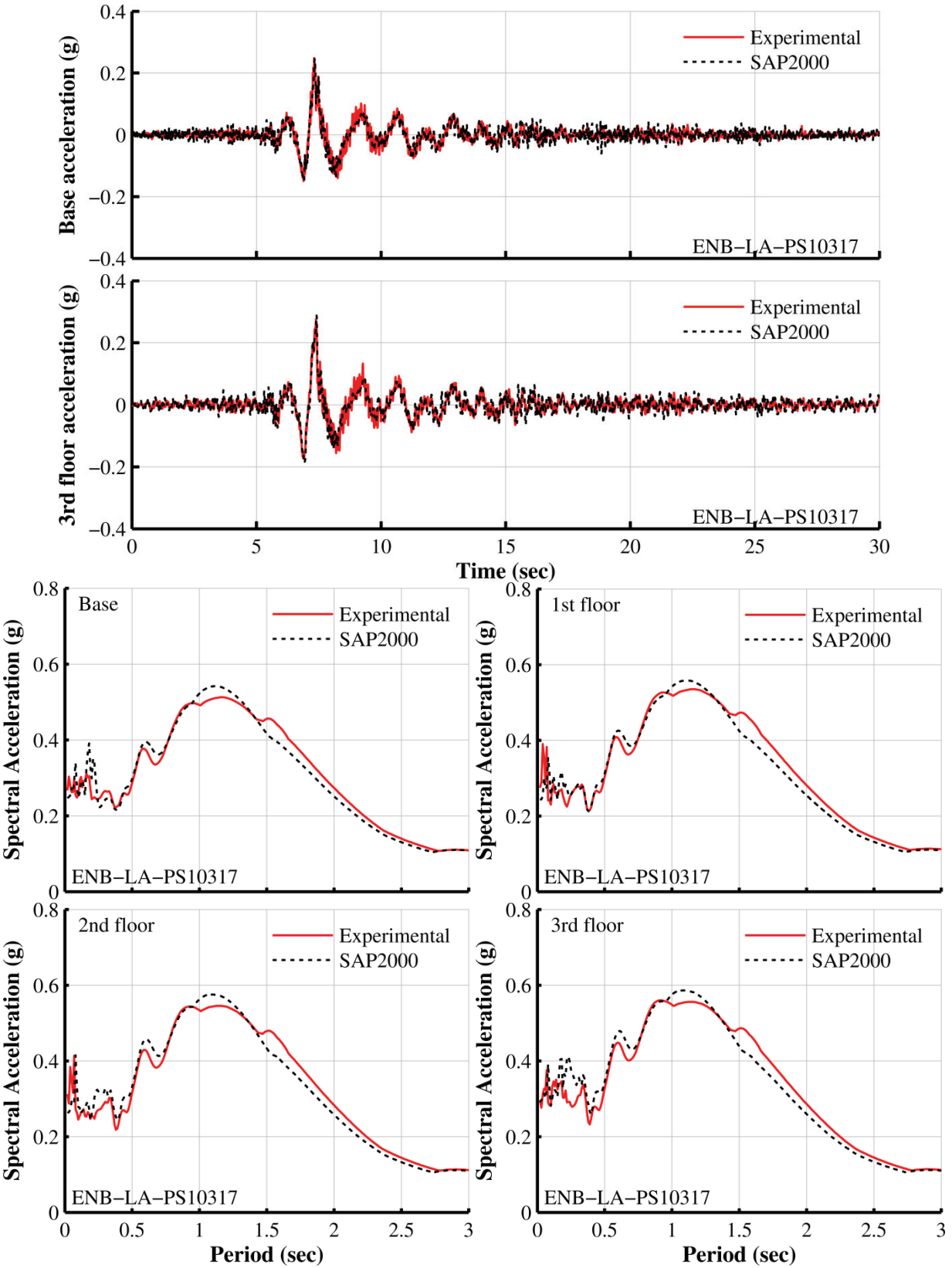


Figure 7-25 (cont'd): Comparison of experimental and analytical results for configuration ENB-LA and ground motion PS-10317

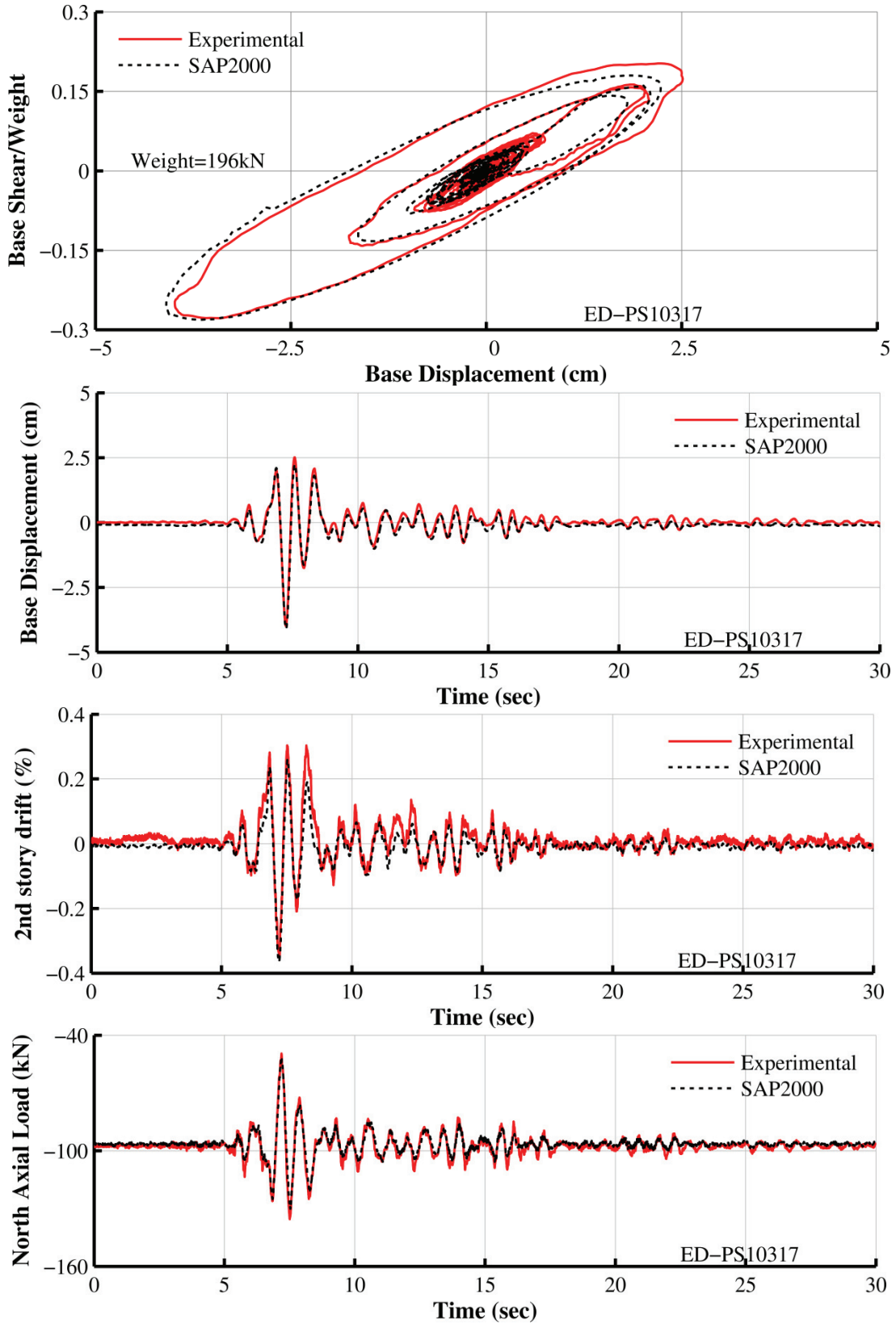


Figure 7-26: Comparison of experimental and analytical results for configuration ED and ground motion PS-10317

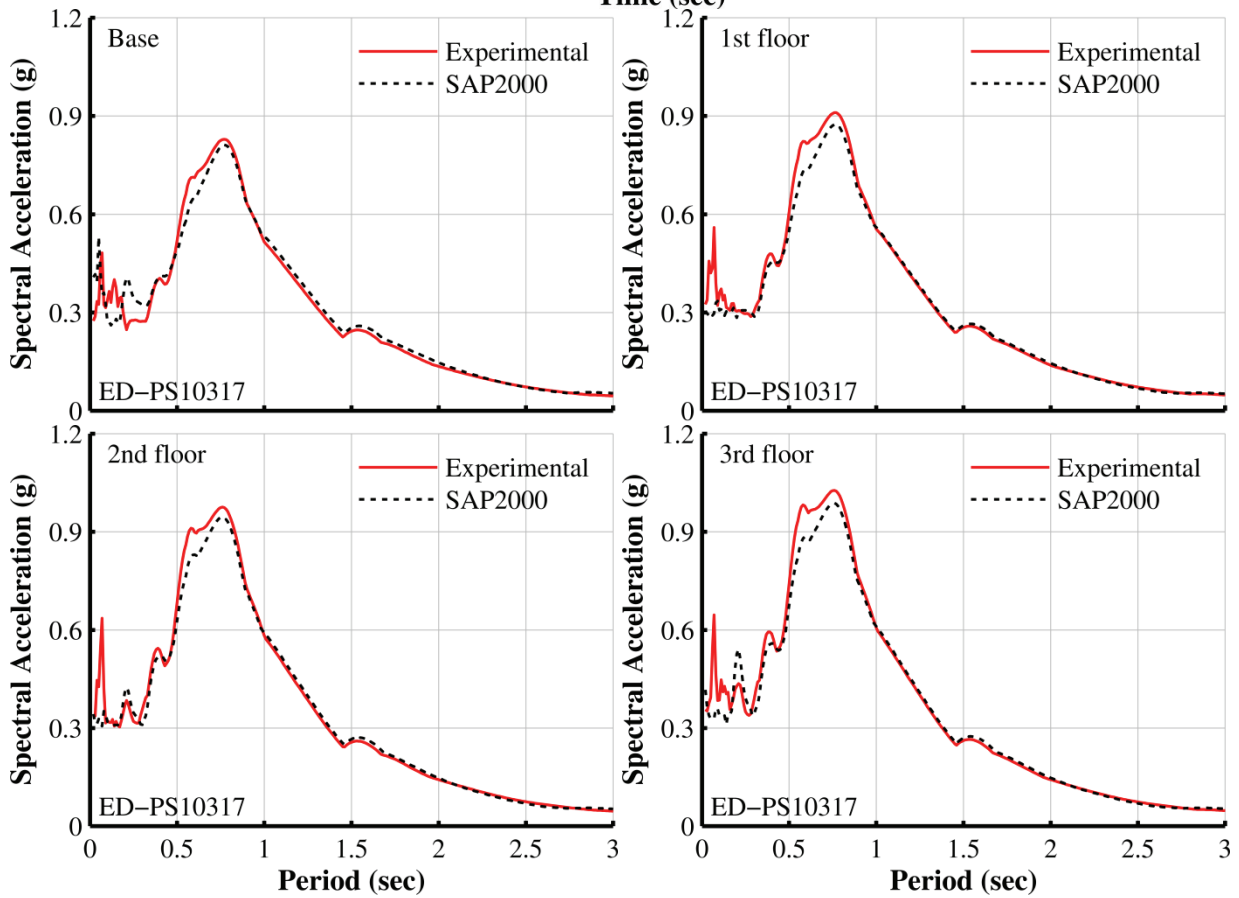
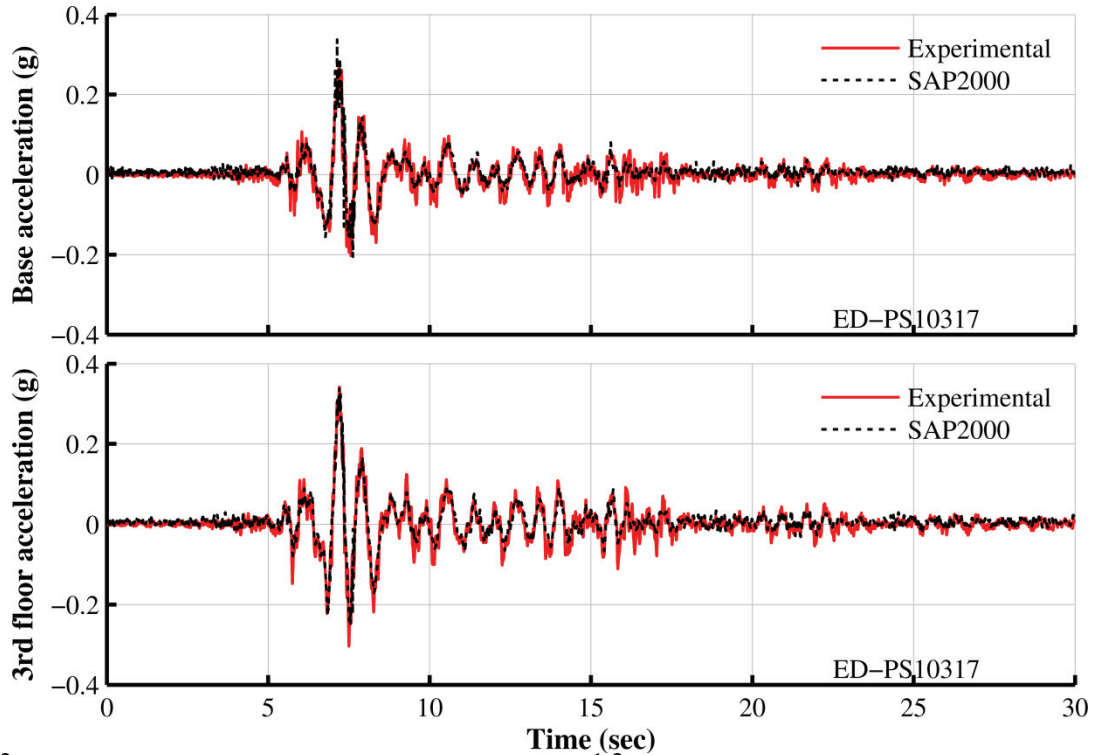


Figure 7-26 (cont'd): Comparison of experimental and analytical results for configuration ED and ground motion PS-10317

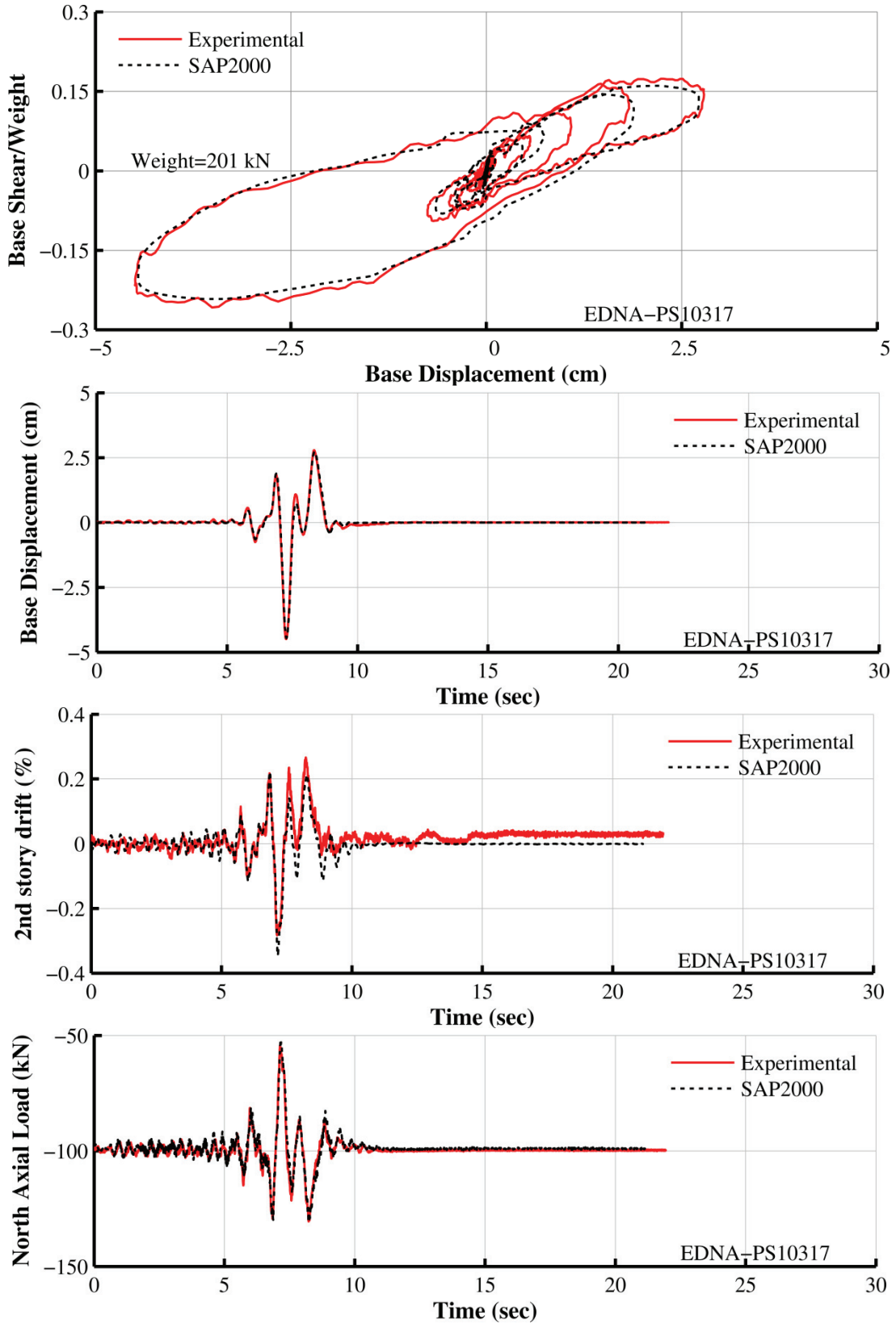


Figure 7-27: Comparison of experimental and analytical results for configuration EDNA and ground motion PS-10317

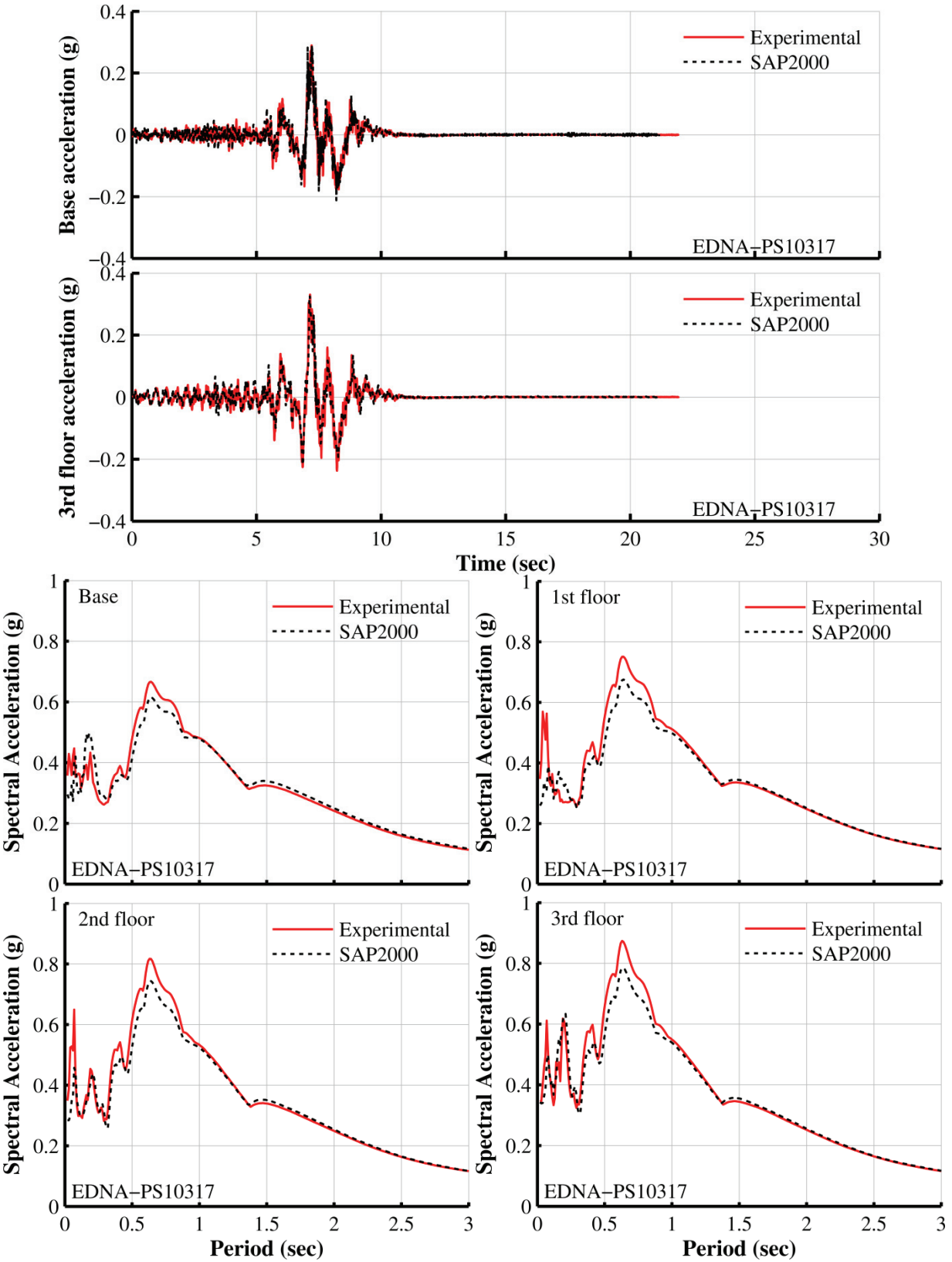


Figure 7-27 (cont'd): Comparison of experimental and analytical results for configuration EDNA and ground motion PS-10317

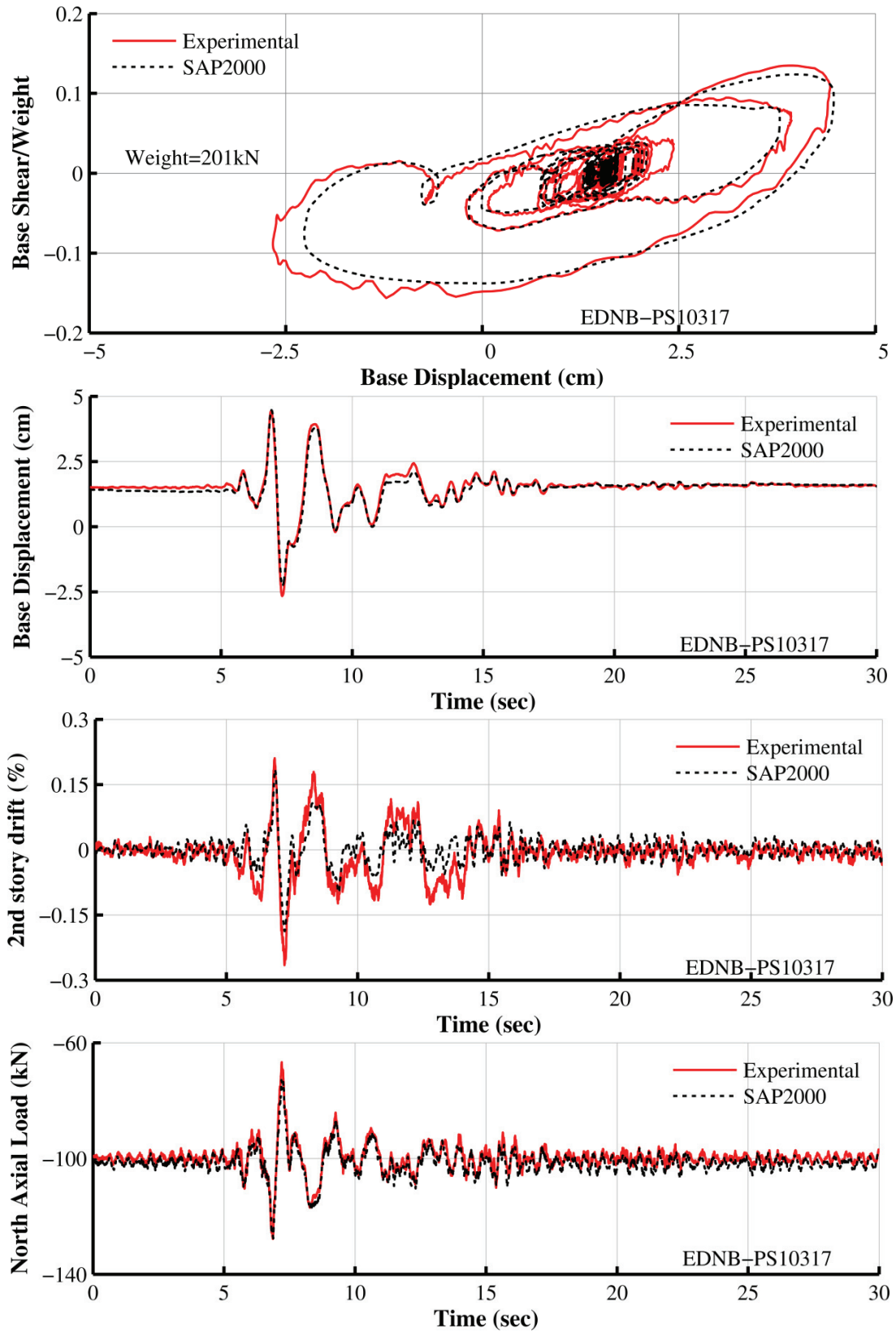


Figure 7-28: Comparison of experimental and analytical results for configuration EDNB and ground motion PS-10317

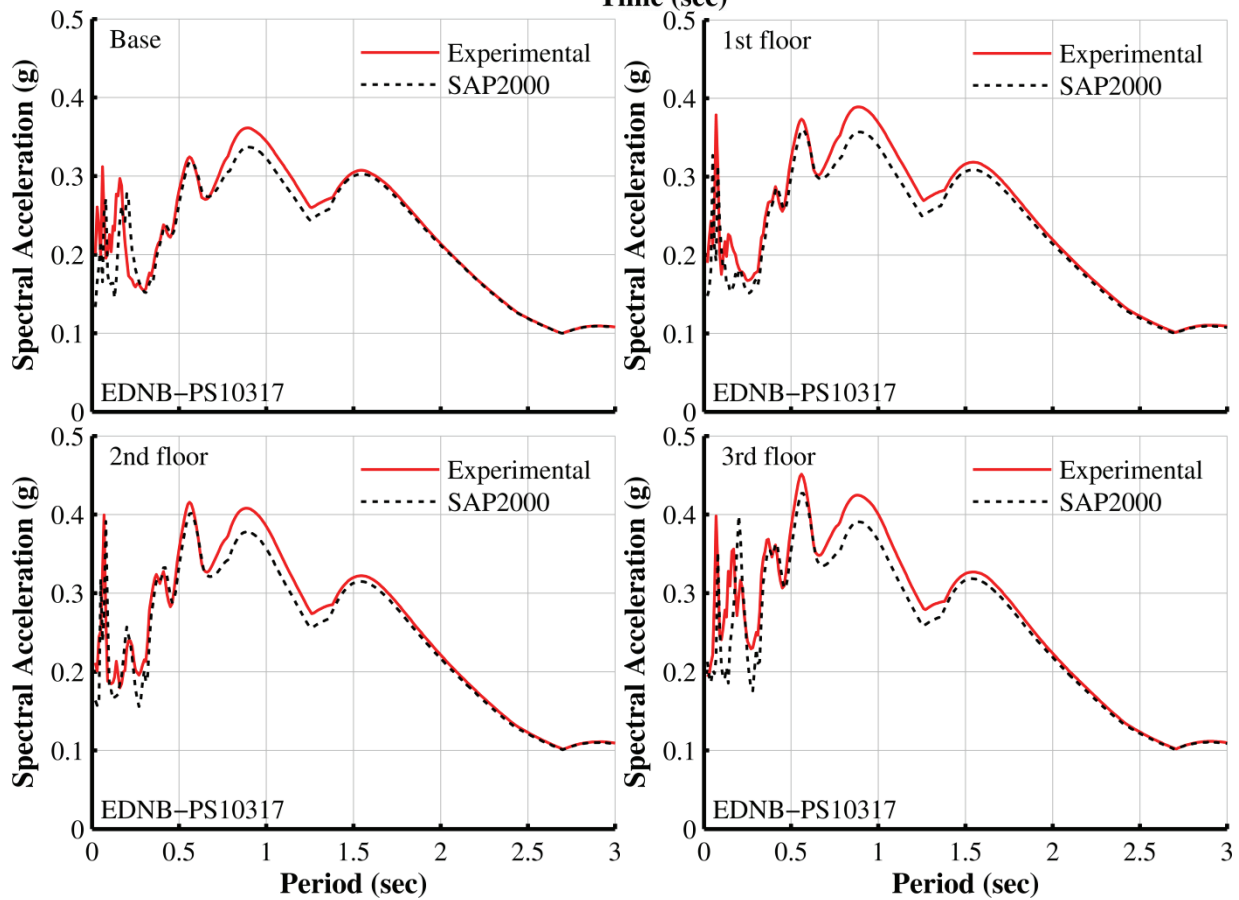
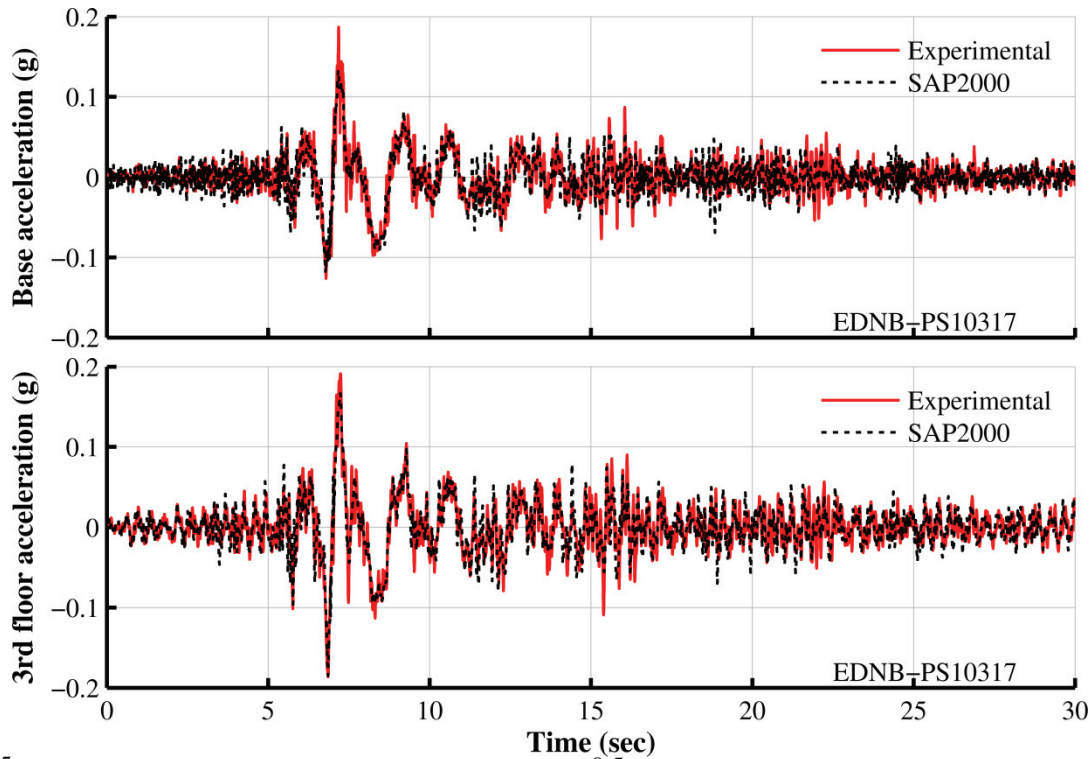


Figure 7-28 (cont'd): Comparison of experimental and analytical results for configuration EDNB and ground motion PS-10317

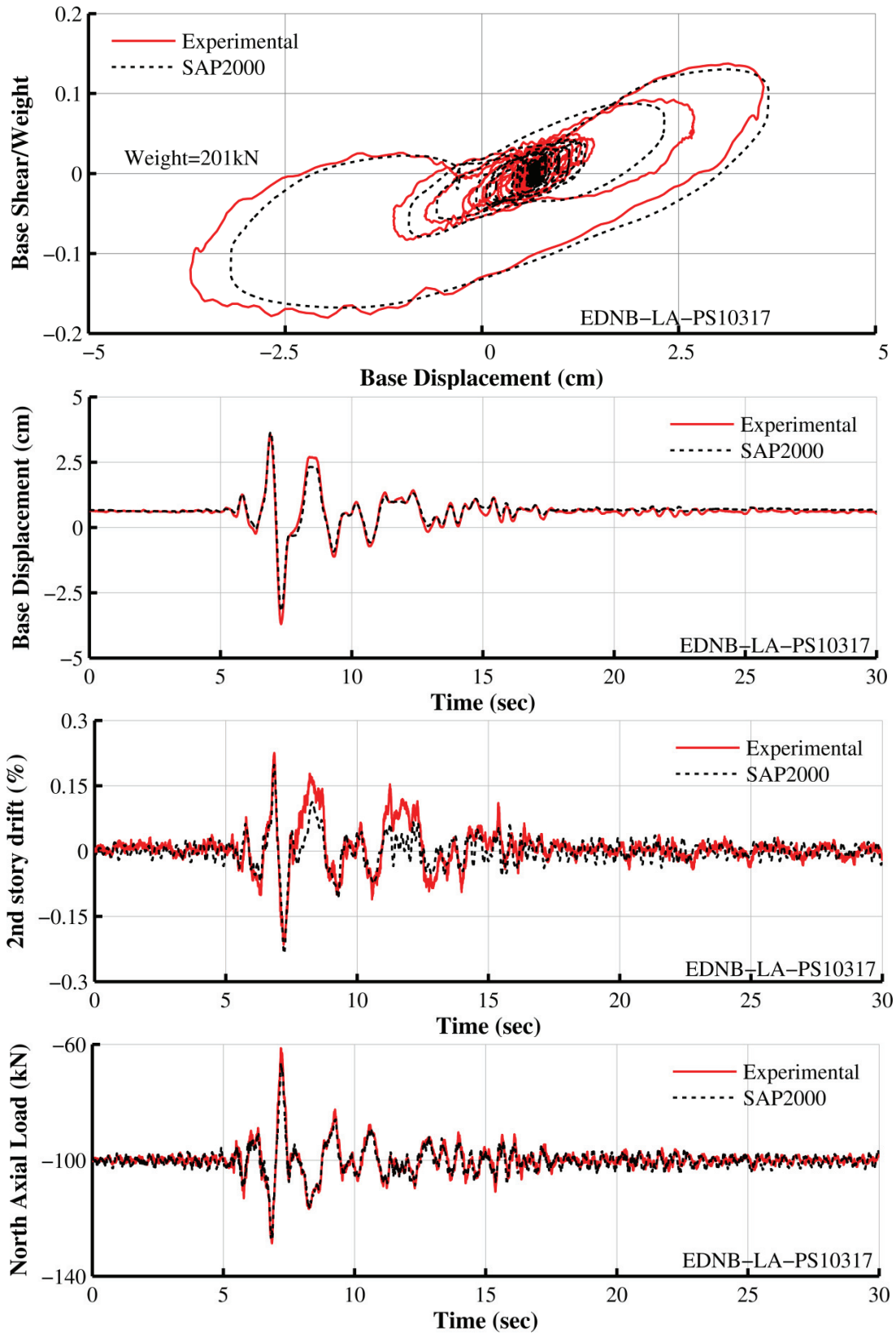


Figure 7-29: Comparison of experimental and analytical results for configuration EDNB-LA and ground motion PS-10317

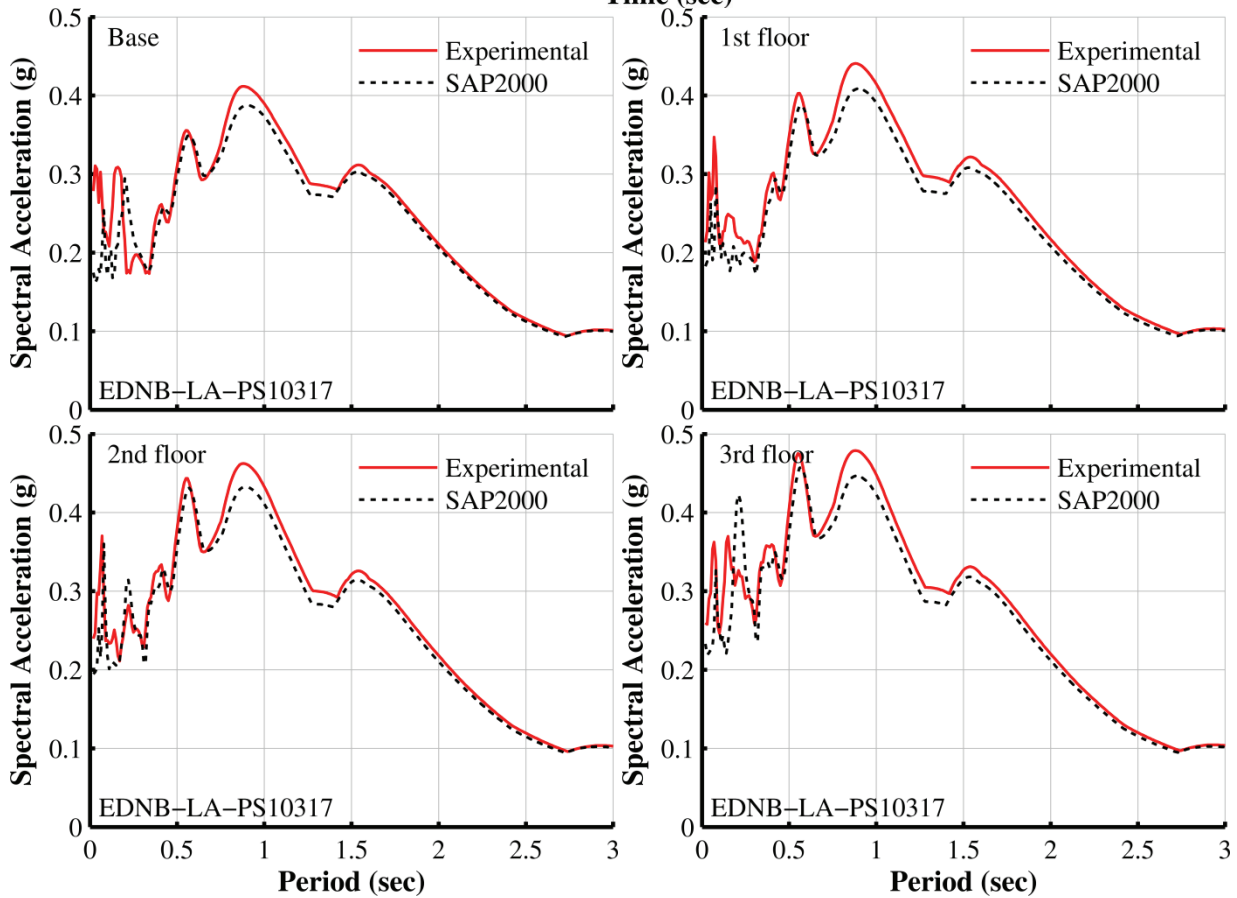
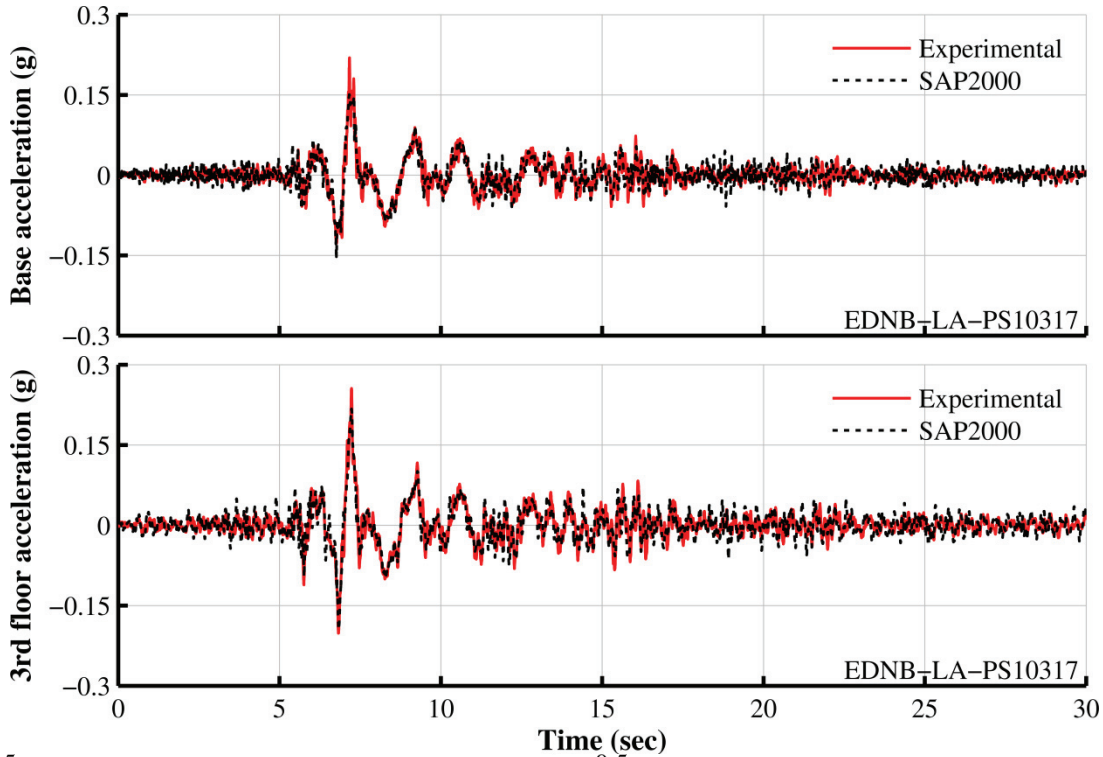


Figure 7-29 (cont'd): Comparison of experimental and analytical results for configuration EDNB-LA and ground motion PS-10317

SECTION 8

REPORT SUMMARY

This report described the construction, behavior and modeling of a novel Negative Stiffness Device (NSD), presented an experimental study of a model seismically isolated 3-story structure equipped with various configurations of NSD in an effort to reduce the response of the structure and presented comparisons of analytical and experimental results in an effort to validate the analytical models of the NSD. Section 1 summarized the Negative Stiffness Concept and the beneficial effects in a structure's response that can be obtained by adding negative stiffness. Section 2 presented the description of operation of the NSD and the identification of the most important points on the NSD behavior; the apparent yield displacement, stiffening displacement, peak force and stiffness at zero displacement. Section 3 presented analytical and computational models of the NSD for use in design. Also, an analytical study was also shown that demonstrated the advantages of the NSD over other simpler systems. Section 4 presented analytical equations that included flexibilities, inertia, large deformations and hysteresis into the NSD equations. With the exception of hysteresis, these were shown to be in most cases negligible and therefore established the validity of the simpler equations of Section 3. In the unlikely case that these sensitivities become important, modeling techniques were presented. Section 5, presented the description of an experimental program that included displacement-controlled tests of individual NSD and shake table tests of a model structure equipped with NSD. Connection details of the NSD to the structure were also presented there. Section 6, presented experimental results from the experimental program mentioned above and showed the significant reductions that can be achieved in a structure's response by the addition of the NSD. Section 7 presented result comparisons of shake table experiments and analytical predictions in order to establish the validity and accuracy of the analytical prediction.

The three story structure was tested in shake table tests in eight different configurations denoted (E, ENA, ENB, ENBLA, ED, EDNA, EDNB and EDNB-LA) with and without dampers and with and without NSD. Each configuration was tested in shake table tests at a minimum of 6 and maximum of 8 ground motions that were the same for all configurations tested. For each configuration with NSD (ENA, ENB, ENBLA, ED, EDNA, EDNB and EDNB-LA) the average of the peak values of several response quantities from these earthquake motions was obtained and then compared to the average response quantities obtained for the same motions and for the model structure without NSD (E, ED). These comparisons and the characteristics of each configuration tested are described herein.

Configuration E consisted of the isolated structure with elastomeric bearings (no NSD, no dampers) with effective stiffness of roughly 12kN/cm, period of roughly 0.8sec and effective damping of roughly 5% for displacements less than 4cm. This configuration was tested in a total

of 8 ground motions and was used as the benchmark un-damped system, on the basis of which, the effect of adding NSD and dampers or NSD without dampers could be studied.

Configuration ENA consisted of elastomeric bearings and NSD with Gap Spring Assembly (GSA) and had the same properties as configuration E for displacements less than 1.7cm, but substantially reduced stiffness than configuration E for displacements more than 1.7cm due to the engagement of the NSD. The effective damping was about 6% for displacements less than 1.7cm (1% effective damping was added by the NSD). Results from configuration ENA (tested in six ground motions) were compared to results from configuration E, and showed reductions in the measured quantities by an average of 25% for the base shear, 17% for the inter-story drifts (for all stories) and 4% for the peak floor accelerations (base, 1st, 2nd and 3rd floor). In some cases, the peak floor accelerations were increased however the floor spectra which are a better measurement of the response for these cases were still reduced. Base displacements were reduced by 9%.

Configuration ENB consisted of elastomeric bearings and NSD without GSA (the NSD engages at a small perturbation from zero displacement) and had an effective stiffness of 5kN/cm, period of roughly 1.3sec and effective damping of roughly 17% (15% from elastomeric bearings and 2% from friction in the NSD) for displacements less than 4cm. Note that the effective damping was increased when compared to configuration E, due to the reduction in the effective stiffness caused by the NSD. Configuration ENB was tested in seven ground motions and when compared to the results of configuration E, configuration ENB reduced the measured response quantities by an average of 52% for the base shear, 41% for inter story drifts and 35% for peak floor accelerations. Base displacements were increased by 2% however in the absence of viscous dampers this increase could have been substantially higher if other ground motions were selected for the shake table tests.

Configuration ENB-LA consisted of elastomeric bearings and NSD with modified lever and without GSA that lead to an effective stiffness of 7kN/cm effective period of roughly 1.1sec and effective damping of roughly 12% for displacements less than 4cm. Configuration ENB-LA was similar to configuration B but the modified level reduced the negative stiffness generated by the NSD and also increased the stiffening displacement (displacement at which the NSD switches from negative stiffness to positive stiffness). Configuration ENB-LA was tested in a total of eight ground motions same as those used in configuration E. When compared to configuration E, this configuration reduced base shear by an average of 52%, inter-story drifts by 51%, peak floor accelerations by 39% and base displacements by an average of 12%.

Configuration ED was identical to configuration E but for the addition of dampers which increased the effective damping of this configuration to 25% (5% was the effective damping of Configuration E). This configuration was used as the benchmark damped system. It was tested in a total of 8 ground motions and when compared to configuration E, this configuration reduced

response quantities by an average of 15% for the base shear, 10% for inter-story drifts, and 36% for base displacements. Peak floor accelerations were however increased by an average of 6%.

Configuration EDNA was identical to configuration ENA but for the addition of dampers. The effective damping of EDNA was the same as the effective damping of ED for displacements less than 1.7cm but was significantly higher for EDNA for displacements larger than 1.7cm due to the reduction of stiffness caused by the NSD engagement. This configuration was tested in 6 ground motions and when compared to configuration ED, reduced the base shear by an average of 7%, the inter-story drifts by an average of 4% and peak floor accelerations by an average of 6%. When this configuration is compared to the original configuration E, response was reduced by an average of 20% for the base shear, 11% for inter-story drifts and 33% for base displacements. Peak floor accelerations were increased by an average of 1%.

Configuration EDNB was identical to configuration ENB, but for the addition of dampers which increased the effective damping to 65%. The substantially higher effective damping for this configuration in comparison to configuration ED, is due to the significant stiffness reduction cause by the NSD (the effective damping is inversely proportional to the effective stiffness). This configuration was tested in a total of six ground motions and when compared to configuration ED, reduced the base shear by an average of 43%, the inter-story drifts by an average of 26%, peak floor accelerations by an average of 31% and base displacements by an average of 3%. The latter is significant as it shows that the substantial reduction in stiffness, did not affect the base displacement since it was accompanied by significant increase of effective damping (65% for ENDB and 25% for ED). When this configuration is compared to the original configuration E, base shear was reduced by an average of 54%, inter-story drifts by an average of 36%, peak floor accelerations by an average of 27% and base displacements by 39%.

Configuration EDNB-LA was identical to configuration ENB-LA, but for the addition of dampers which increased the effective damping to 46%. This configuration was tested in eight ground motions and when results from this configuration are compared to the results of configuration ED, it reduced the base shear by an average of 37%, inter-story drifts by an average of 29%, peak floor accelerations by an average of 30% and base displacements by an average of 5%. When compared to the results of configuration E, this configuration reduced base shear by an average of 47%, inter-story drifts by an average of 36%, peak floor accelerations by an average of 26% and base displacements by an average of 39%.

The comparisons above show that largest reductions in response for all quantities are achieved by configurations EDNB and EDNB-LA (structure with elastomeric bearings, NSD without the GSA and viscous dampers). The reason why these configurations were so effective is that the NSD was able to reduce the lateral stiffness of the structure, which reduced forces and thus drifts and accelerations (similar to the concept of base isolation). The NSD did so without the addition of significant friction. Dampers were able to reduce base displacements since the stiffness drop caused by the NSD (which usually causes increase in base displacements) was counteracted by

the significant increase of effective damping caused by this stiffness reduction. This can be seen by inspecting the base displacement obtained by configurations EDNB, EDNB-LA and configuration ED. All these configurations have almost the same base displacement despite the fact that configurations EDNB, EDNB-LA have significantly lower stiffness than configuration ED.

Significant reductions were also observed for configurations ENA (NSD with GSA without dampers) and EDNA (NSD with GSA and with dampers) however these reductions were not as large as those for configurations ENB and EDNB since the engagement displacement for the NSD that was selected for this study was much larger than needed and therefore the NSD was not engaged for a big portion of the excitation. Especially for configurations with dampers (where base displacements were reduced significantly) the NSD was engaged only for a small portion of the response. Particularly for quantities such as peak floor accelerations, peak values occurred prior to the engagement of the NSD. If a smaller engagement displacement was used (e.g 0.5cm instead of 1.27cm), then the observed reductions would have been closer to the reductions observed when the NSD without the GSA was used. Note that configurations ENB and EDNB are simply special cases of ENA and EDNA respectively when the engagement displacement is zero.

Finally, the NSD offers the additional advantage of accurate response prediction. The NSD without the GSA is constructed using machined springs and its behavior is based on the properties of the springs and geometric nonlinearity. Also due to the very low variability in the properties of machined springs and very high precision manufacturing (similar to the one utilized in the preloaded springs of the tested NSD), when a large number of NSD are installed in a structure they can all have almost identical behavior. The GSA however is comprised of coil springs that exhibit higher variability in their properties and therefore the final properties need to be determined from testing. This disadvantage can be eliminated by constructing the GSA with machined springs as well. Using the analytical equations and computational models developed in SAP2000, the response of the structure was simulated in program SAP2000. Peak values for all 50 ground motions were predicted by an average of 5% error for base displacements, 7% error for base shear, 16% error for inter-story drifts and 15% error for peak floor accelerations. The last two quantities have lower prediction accuracy due to additional uncertainties involved in the modeling of the superstructure.

SECTION 9 CONCLUSIONS

This report described the construction, behavior and modeling of a novel Negative Stiffness Device (NSD) with the following characteristics:

1. The NSD reduces the structure's lateral stiffness after a pre-determined displacement (engagement displacement). This is achieved through a system (called *Gap Spring Assembly* or GSA) that provides positive stiffness up to a predefined displacement such that the combined effective stiffness of NSD and GSA is almost zero until the engagement displacement. The NSD generates negative stiffness through the use of a highly compressed machined spring that develops a force in the direction of motion. The magnitude of the spring force is magnified through the use of a double negative stiffness magnification and therefore the NSD can be constructed using realistic spring stiffness and preload. The NSD is nonlinear elastic and the negative stiffness magnitude reduces with increasing displacement so that stability of the system is ensured at large displacements. The device is self contained and does not add forces in the vertical direction of the structure.
2. When Viscous damping devices are added in parallel to the negative stiffness device their effective damping is substantially larger than the equivalent system without the NSD due to the stiffness reduction caused by the NSD. This causes substantial reduction of the displacements at the level of installation of the NSD.

The efficiency of the NSD in reducing the response was investigated by conducting shake table tests on a model seismically isolated 3-story structure with elastomeric bearings equipped with various configurations of NSD in a total of eight different configurations. In four configurations, linear viscous dampers were added in parallel to the bearings. For each group of tests (with and without dampers) the NSD was used in three different configurations; one configuration with the GSA and two configurations without the GSA (one configuration exhibited larger negative stiffness and smaller stiffening displacement than the other). Each configuration was tested in six to eight ground motions. It was concluded that:

1. The largest reduction in response for all quantities except for base displacements was achieved by the configuration that included the NSD without the GSA and without dampers (configuration ENB). When dampers were added to this configuration (configuration EDNB), similar reductions were observed for all response quantities, with the additional advantage of significant base displacement reductions.
2. Reduction in the response was also observed for configurations of NSD with GSA which was much smaller than the reduction observed for configurations of NSD without GSA. Also these configurations, in some cases, the addition of the NSD slightly increased peak

floor accelerations however floor spectra were still reduced. However, the NSD without GSA is a special case of the NSD with GSA when the engagement displacement is zero. If a smaller engagement displacement for the NSD with GSA was used, then the observed reductions would have been closer to the reductions observed for the NSD without the GSA.

Key conclusions with respect to the analytical modeling and analytical prediction are:

1. The presented analytical models of the NSD could reliably capture the behavior of the NSD as observed in experiments, including hysteresis effects.
2. The analytical models of the NSD could be implemented in standard computer programs used for response history analysis. Details of implementation of the models in program SAP2000 have been presented.
3. The developed analytical model in program SAP2000 predicted well the observed experimental response of the tested model structure in a total of eight configurations of isolators and NSD, and eight earthquake motions (total of 50 tests-not all motions were run for all configurations). The models predicted well the frequency content of the response and shape of loops but it occasionally either over-predicted or under-predicted the measured peak response but for the peak base displacement and peak base shear force, which were in very good agreement with the experimental peak values. It is believed that the occasional over or under-prediction of the peak experimental response is due to inability of the model of the structural system in program SAP2000 to capture sliding and minor impact in the connections of the model. The analytical model assumes rigidity in the connections of masses to floors and of braces to beams and columns, whereas some sliding occurred at these connections during strong shaking. The latter resulted in recordings of spikes in response that could not be analytically predicted.
4. The developed analytical models of the NSD were based on fundamental principles. They were not phenomenological models calibrated by testing. Exception was the model of the GSA used in the prediction of the shake table test results. In this case experimental results were used to calibrate the analytical model because some GSA exhibited higher stiffness than the theory predicted due to blockage of spring coils and the gap displacement was accidentally reduced.

In practical applications the NSD can be used with or without the GSA in the design of new or existing isolated or fixed structures in order to achieve systems with low lateral stiffness and high vertical stiffness without friction. The GSA is essential to provide the combined system with sufficient stiffness for small displacements for service loading especially if the combined stiffness of the main structural system and NSD (without GSA) is not sufficient for service loading. With appropriate selection of parameters the GSA can also add stiffness to the main system around small displacements if the existing system does not have sufficient stiffness for service loading. When implemented to seismically isolated structure's the NSDs have the disadvantage of having large size and therefore requiring larger space for installation than the

space that is typically available below the base-mat of the building. Such was the case in the current experimental study. This can be accommodated by placing the devices horizontally. In fixed structures, the story height in combination with the displacement demands (that controls the NSD height) is sufficient for straightforward installation. These two cases will be demonstrated in subsequent phases of the project.

SECTION 10 REFERENCES

1. American Society of Civil Engineers (2010), “Minimum design Loads for Buildings and Other Structures”, *Standard ASCE 7-10*, Reston, VA.
2. Bracci, J.M., Reinhorn, A.M. and Mander, J.B. (1992). “ Seismic Resistance of Reinforced Concrete Frame Structures Designed Only for Gravity Loads: Part I- Design and Properties of a One- Third Scale Model Structure”, Technical Report NCEER-92-0027, National Center for Earthquake Engineering Research, State University of New York at Buffalo, Buffalo, NY.
3. Computers and Structures Inc. (2007), “SAP2000: Integrated Finite Element Analysis and Design of Structures”, Version 11.0.8, Berkeley, CA.
4. Fenz, D.M. and Constantinou, M.C. (2008a), "Mechanical Behavior of Multi-spherical Sliding Bearings", Report No. MCEER-08-0007, Multidisciplinary Center for Earthquake Engineering Research, Buffalo, NY.
5. Fenz, D.M. and Constantinou, M.C. (2008b), "Development, Implementation and Verification of Dynamic Analysis Models for Multi-spherical Sliding Bearings", Report No. MCEER-08-0018, Multidisciplinary Center for Earthquake Engineering Research, Buffalo, NY.
6. Iemura, H., Kouchiyama, O., Toyooka, A. and Shimoda, I. (2008). “Development of the Friction-Based Passive Negative Stiffness Damper and its Verification Tests using Shaking Table”. 14th World Conference on Earthquake Engineering, October 12-17, 2008, Beijing, China
7. Iemura, H. and Pradono, M.H. (2009), “Advances in the development of pseudo-negative-stiffness dampers for seismic response control,” *Structural Control and Health Monitoring*, 16(7-8), 1545-2255.
8. Kasalanati, A. and Constantinou, M.C. (1999). “Experimental Study of Bridge Elastomeric and Other Isolation and Energy Dissipation Systems with Emphasis on Uplift Prevention and High Velocity Near Source Seismic Excitation”, Technical Report MCEER-99-0004, Multidisciplinary Center for Earthquake Engineering Research, State University of New York at Buffalo, Buffalo, NY.
9. Lee, C.M., Goverdovskiy, V. and Temnikov, A. (2007), “Design of springs with ‘negative’ stiffness to improve vehicle driver vibration isolation”, *Journal of Sound and Vibration* 302 (4-5) (2007) 865–874 URL: <http://dx.doi.org/10.1016/j.jsv.2006.12.024>
10. Mokha, A.S., Constantinou, M.C. and Reinhorn, A.M. (1990). “ Experimental Study and Analytical Prediction of Earthquake Response of a Sliding Isolation System with Spherical Surface”, Technical Report NCEER-90-0020, National Center for Earthquake Engineering Research, State University of New York at Buffalo, Buffalo, NY.

11. Molyneaux, W. G. (1957), "Supports for vibration isolation", ARC/CP-322, Aeronautical Research Council, Great Britain.
12. Nagarajaiah, S., Reinhorn, A.M., Constantinou, M.C., Taylor D., Pasala, D.T.R. and Sarlis, A.A. (2010), "True Adaptive Negative Stiffness: A New Structural Modification Approach for Seismic Protection", *5th World Conference on Structural Control and Monitoring*, Tokyo, Japan, July 12-14.
13. Pasala, D.T.R, Sarlis, A.A., Nagarajaiah, S., Reinhorn, A.M, Constantinou, M.C, and Taylor, D., (2012), "Adaptive Negative Stiffness: A New Structural Modification Approach for Seismic Protection", *Journal of Structural Engineering*, ASCE, 10.1061/(ASCE)ST.1943-541X.0000615, Posted ahead of print, 3 April 2012.
14. Pavlou, E. and Constantinou, M.C., (2006), "Response of Nonstructural Components in Structures with Damping Systems", *Journal of Structural Engineering*, ASCE, Vol. 132, No. 7, 1108-1117.
15. Platus, D.L. (2004), "Vibration Isolation System", US Patent No. 6676101B2, Washington DC: US Patent and Trademark Office.
16. Ramirez, O.M., Constantinou, M.C., Kircher, C.A., Whittaker, A.S., Johnson, M.W., Gomez, J.D., and Chrysostomou, C.Z., (2001), "Development and Evaluation of Simplified Procedures for Analysis and Design of Buildings with Passive Energy Dissipation Systems", *Report No. MCEER-00-0010, Revision 1, Multidisciplinary Center for Earthquake Engineering Research*, Buffalo, NY.
17. Reinhorn, A.M., Soong, T.T., Lin, R.C., Yang, Y.P., Fukao, Y., Abe, H. and Nakai, M. (1989), "1:4 Scale Model Studies of Active Tendon Systems and Active Mass Dampers for Aseismic Protection", Technical Report NCEER-89-0026, National Center for Earthquake Engineering Research, State University of New York at Buffalo, Buffalo, NY.
18. Reinhorn, A.M., Viti, S., and Cimellaro, G.P. (2005), "Retrofit of Structures: Strength Reduction with Damping Enhancement", *Proceeding of the 37th UJNR Panel Meeting on Wind and Seismic Effects*, Tsukuba, Japan.
19. Roussis, P. C. and Constantinou, M. C. (2006), "Uplift-Restraining Friction Pendulum Seismic Isolation System," *Earthquake Engineering and Structural Dynamics*, Vol. 35, No.5, 577-593.
20. Sarlis, A.A., Pasala, D.T.R, Constantinou, M.C, Reinhorn, A.M, Nagarajaiah, S., and Taylor, D., (2012), "Negative Stiffness Device for Seismic Protection of Structures ", *Journal of Structural Engineering*, ASCE, 10.1061/(ASCE)ST.1943-541X.0000616, Posted ahead of print, 11 April 2012.
21. Sivaselvan, M.V. and Reinhorn, A.M. (2001). "Hysteretic Models for Deteriorating Inelastic Structures", *ASCE Journal of Structural Engineering*, 126(6) 633-640.
22. Structural Engineering and Earthquake Simulation Laboratory (2004). "Laboratory Manual" SEESL, Buffalo, NY USA. Available online: <http://nees.buffalo.edu/docs/labmanual/html/>.
23. Tsopelas, P.C., Constantinou, M.C., and Reinhorn, A.M. (1994), "3D-BASIS-ME: Computer Program for Nonlinear Dynamic Analysis of Seismically Isolated Single and Multiple

Structures and Liquid Storage Tanks”, Report NCEER-94-0010, National Center for Earthquake Engineering Research, State University of New York, Buffalo, NY.

24. Viti, S., Cimellaro, G. P., and Reinhorn, A. M. (2006), Retrofit of a Hospital through Strength Reduction and Enhanced Damping. *Smart Structures and Systems*, 2(4), 339-355.
25. Wolff, E.D. and Constantinou, M.C. (2004). “Experimental Study of Seismic Isolation Systems with Emphasis on Secondary System Response and Verification of Accuracy of Dynamic Response History Analysis Methods”, Technical Report MCEER-04-0001, Multidisciplinary Center for Earthquake Engineering Research, State University of New York at Buffalo, Buffalo, NY.

MCEER Technical Reports

MCEER publishes technical reports on a variety of subjects written by authors funded through MCEER. These reports are available from both MCEER Publications and the National Technical Information Service (NTIS). Requests for reports should be directed to MCEER Publications, MCEER, University at Buffalo, State University of New York, 133A Ketter Hall, Buffalo, New York 14260. Reports can also be requested through NTIS, P.O. Box 1425, Springfield, Virginia 22151. NTIS accession numbers are shown in parenthesis, if available.

- NCEER-87-0001 "First-Year Program in Research, Education and Technology Transfer," 3/5/87, (PB88-134275, A04, MF-A01).
- NCEER-87-0002 "Experimental Evaluation of Instantaneous Optimal Algorithms for Structural Control," by R.C. Lin, T.T. Soong and A.M. Reinhorn, 4/20/87, (PB88-134341, A04, MF-A01).
- NCEER-87-0003 "Experimentation Using the Earthquake Simulation Facilities at University at Buffalo," by A.M. Reinhorn and R.L. Ketter, not available.
- NCEER-87-0004 "The System Characteristics and Performance of a Shaking Table," by J.S. Hwang, K.C. Chang and G.C. Lee, 6/1/87, (PB88-134259, A03, MF-A01). This report is available only through NTIS (see address given above).
- NCEER-87-0005 "A Finite Element Formulation for Nonlinear Viscoplastic Material Using a Q Model," by O. Gyebe and G. Dasgupta, 11/2/87, (PB88-213764, A08, MF-A01).
- NCEER-87-0006 "Symbolic Manipulation Program (SMP) - Algebraic Codes for Two and Three Dimensional Finite Element Formulations," by X. Lee and G. Dasgupta, 11/9/87, (PB88-218522, A05, MF-A01).
- NCEER-87-0007 "Instantaneous Optimal Control Laws for Tall Buildings Under Seismic Excitations," by J.N. Yang, A. Akbarpour and P. Ghaemmaghami, 6/10/87, (PB88-134333, A06, MF-A01). This report is only available through NTIS (see address given above).
- NCEER-87-0008 "IDARC: Inelastic Damage Analysis of Reinforced Concrete Frame - Shear-Wall Structures," by Y.J. Park, A.M. Reinhorn and S.K. Kunnath, 7/20/87, (PB88-134325, A09, MF-A01). This report is only available through NTIS (see address given above).
- NCEER-87-0009 "Liquefaction Potential for New York State: A Preliminary Report on Sites in Manhattan and Buffalo," by M. Budhu, V. Vijayakumar, R.F. Giese and L. Baumgras, 8/31/87, (PB88-163704, A03, MF-A01). This report is available only through NTIS (see address given above).
- NCEER-87-0010 "Vertical and Torsional Vibration of Foundations in Inhomogeneous Media," by A.S. Veletsos and K.W. Dotson, 6/1/87, (PB88-134291, A03, MF-A01). This report is only available through NTIS (see address given above).
- NCEER-87-0011 "Seismic Probabilistic Risk Assessment and Seismic Margins Studies for Nuclear Power Plants," by Howard H.M. Hwang, 6/15/87, (PB88-134267, A03, MF-A01). This report is only available through NTIS (see address given above).
- NCEER-87-0012 "Parametric Studies of Frequency Response of Secondary Systems Under Ground-Acceleration Excitations," by Y. Yong and Y.K. Lin, 6/10/87, (PB88-134309, A03, MF-A01). This report is only available through NTIS (see address given above).
- NCEER-87-0013 "Frequency Response of Secondary Systems Under Seismic Excitation," by J.A. HoLung, J. Cai and Y.K. Lin, 7/31/87, (PB88-134317, A05, MF-A01). This report is only available through NTIS (see address given above).
- NCEER-87-0014 "Modelling Earthquake Ground Motions in Seismically Active Regions Using Parametric Time Series Methods," by G.W. Ellis and A.S. Cakmak, 8/25/87, (PB88-134283, A08, MF-A01). This report is only available through NTIS (see address given above).
- NCEER-87-0015 "Detection and Assessment of Seismic Structural Damage," by E. DiPasquale and A.S. Cakmak, 8/25/87, (PB88-163712, A05, MF-A01). This report is only available through NTIS (see address given above).

- NCEER-87-0016 "Pipeline Experiment at Parkfield, California," by J. Isenberg and E. Richardson, 9/15/87, (PB88-163720, A03, MF-A01). This report is available only through NTIS (see address given above).
- NCEER-87-0017 "Digital Simulation of Seismic Ground Motion," by M. Shinozuka, G. Deodatis and T. Harada, 8/31/87, (PB88-155197, A04, MF-A01). This report is available only through NTIS (see address given above).
- NCEER-87-0018 "Practical Considerations for Structural Control: System Uncertainty, System Time Delay and Truncation of Small Control Forces," J.N. Yang and A. Akbarpour, 8/10/87, (PB88-163738, A08, MF-A01). This report is only available through NTIS (see address given above).
- NCEER-87-0019 "Modal Analysis of Nonclassically Damped Structural Systems Using Canonical Transformation," by J.N. Yang, S. Sarkani and F.X. Long, 9/27/87, (PB88-187851, A04, MF-A01).
- NCEER-87-0020 "A Nonstationary Solution in Random Vibration Theory," by J.R. Red-Horse and P.D. Spanos, 11/3/87, (PB88-163746, A03, MF-A01).
- NCEER-87-0021 "Horizontal Impedances for Radially Inhomogeneous Viscoelastic Soil Layers," by A.S. Veletsos and K.W. Dotson, 10/15/87, (PB88-150859, A04, MF-A01).
- NCEER-87-0022 "Seismic Damage Assessment of Reinforced Concrete Members," by Y.S. Chung, C. Meyer and M. Shinozuka, 10/9/87, (PB88-150867, A05, MF-A01). This report is available only through NTIS (see address given above).
- NCEER-87-0023 "Active Structural Control in Civil Engineering," by T.T. Soong, 11/11/87, (PB88-187778, A03, MF-A01).
- NCEER-87-0024 "Vertical and Torsional Impedances for Radially Inhomogeneous Viscoelastic Soil Layers," by K.W. Dotson and A.S. Veletsos, 12/87, (PB88-187786, A03, MF-A01).
- NCEER-87-0025 "Proceedings from the Symposium on Seismic Hazards, Ground Motions, Soil-Liquefaction and Engineering Practice in Eastern North America," October 20-22, 1987, edited by K.H. Jacob, 12/87, (PB88-188115, A23, MF-A01). This report is available only through NTIS (see address given above).
- NCEER-87-0026 "Report on the Whittier-Narrows, California, Earthquake of October 1, 1987," by J. Pantelic and A. Reinhorn, 11/87, (PB88-187752, A03, MF-A01). This report is available only through NTIS (see address given above).
- NCEER-87-0027 "Design of a Modular Program for Transient Nonlinear Analysis of Large 3-D Building Structures," by S. Srivastav and J.F. Abel, 12/30/87, (PB88-187950, A05, MF-A01). This report is only available through NTIS (see address given above).
- NCEER-87-0028 "Second-Year Program in Research, Education and Technology Transfer," 3/8/88, (PB88-219480, A04, MF-A01).
- NCEER-88-0001 "Workshop on Seismic Computer Analysis and Design of Buildings With Interactive Graphics," by W. McGuire, J.F. Abel and C.H. Conley, 1/18/88, (PB88-187760, A03, MF-A01). This report is only available through NTIS (see address given above).
- NCEER-88-0002 "Optimal Control of Nonlinear Flexible Structures," by J.N. Yang, F.X. Long and D. Wong, 1/22/88, (PB88-213772, A06, MF-A01).
- NCEER-88-0003 "Substructuring Techniques in the Time Domain for Primary-Secondary Structural Systems," by G.D. Manolis and G. Juhn, 2/10/88, (PB88-213780, A04, MF-A01).
- NCEER-88-0004 "Iterative Seismic Analysis of Primary-Secondary Systems," by A. Singhal, L.D. Lutes and P.D. Spanos, 2/23/88, (PB88-213798, A04, MF-A01).
- NCEER-88-0005 "Stochastic Finite Element Expansion for Random Media," by P.D. Spanos and R. Ghanem, 3/14/88, (PB88-213806, A03, MF-A01).

- NCEER-88-0006 "Combining Structural Optimization and Structural Control," by F.Y. Cheng and C.P. Pantelides, 1/10/88, (PB88-213814, A05, MF-A01).
- NCEER-88-0007 "Seismic Performance Assessment of Code-Designed Structures," by H.H-M. Hwang, J-W. Jaw and H-J. Shau, 3/20/88, (PB88-219423, A04, MF-A01). This report is only available through NTIS (see address given above).
- NCEER-88-0008 "Reliability Analysis of Code-Designed Structures Under Natural Hazards," by H.H-M. Hwang, H. Ushiba and M. Shinozuka, 2/29/88, (PB88-229471, A07, MF-A01). This report is only available through NTIS (see address given above).
- NCEER-88-0009 "Seismic Fragility Analysis of Shear Wall Structures," by J-W Jaw and H.H-M. Hwang, 4/30/88, (PB89-102867, A04, MF-A01).
- NCEER-88-0010 "Base Isolation of a Multi-Story Building Under a Harmonic Ground Motion - A Comparison of Performances of Various Systems," by F-G Fan, G. Ahmadi and I.G. Tadjbakhsh, 5/18/88, (PB89-122238, A06, MF-A01). This report is only available through NTIS (see address given above).
- NCEER-88-0011 "Seismic Floor Response Spectra for a Combined System by Green's Functions," by F.M. Lavelle, L.A. Bergman and P.D. Spanos, 5/1/88, (PB89-102875, A03, MF-A01).
- NCEER-88-0012 "A New Solution Technique for Randomly Excited Hysteretic Structures," by G.Q. Cai and Y.K. Lin, 5/16/88, (PB89-102883, A03, MF-A01).
- NCEER-88-0013 "A Study of Radiation Damping and Soil-Structure Interaction Effects in the Centrifuge," by K. Weissman, supervised by J.H. Prevost, 5/24/88, (PB89-144703, A06, MF-A01).
- NCEER-88-0014 "Parameter Identification and Implementation of a Kinematic Plasticity Model for Frictional Soils," by J.H. Prevost and D.V. Griffiths, not available.
- NCEER-88-0015 "Two- and Three- Dimensional Dynamic Finite Element Analyses of the Long Valley Dam," by D.V. Griffiths and J.H. Prevost, 6/17/88, (PB89-144711, A04, MF-A01).
- NCEER-88-0016 "Damage Assessment of Reinforced Concrete Structures in Eastern United States," by A.M. Reinhorn, M.J. Seidel, S.K. Kunnath and Y.J. Park, 6/15/88, (PB89-122220, A04, MF-A01). This report is only available through NTIS (see address given above).
- NCEER-88-0017 "Dynamic Compliance of Vertically Loaded Strip Foundations in Multilayered Viscoelastic Soils," by S. Ahmad and A.S.M. Israil, 6/17/88, (PB89-102891, A04, MF-A01).
- NCEER-88-0018 "An Experimental Study of Seismic Structural Response With Added Viscoelastic Dampers," by R.C. Lin, Z. Liang, T.T. Soong and R.H. Zhang, 6/30/88, (PB89-122212, A05, MF-A01). This report is available only through NTIS (see address given above).
- NCEER-88-0019 "Experimental Investigation of Primary - Secondary System Interaction," by G.D. Manolis, G. Juhn and A.M. Reinhorn, 5/27/88, (PB89-122204, A04, MF-A01).
- NCEER-88-0020 "A Response Spectrum Approach For Analysis of Nonclassically Damped Structures," by J.N. Yang, S. Sarkani and F.X. Long, 4/22/88, (PB89-102909, A04, MF-A01).
- NCEER-88-0021 "Seismic Interaction of Structures and Soils: Stochastic Approach," by A.S. Veletsos and A.M. Prasad, 7/21/88, (PB89-122196, A04, MF-A01). This report is only available through NTIS (see address given above).
- NCEER-88-0022 "Identification of the Serviceability Limit State and Detection of Seismic Structural Damage," by E. DiPasquale and A.S. Cakmak, 6/15/88, (PB89-122188, A05, MF-A01). This report is available only through NTIS (see address given above).
- NCEER-88-0023 "Multi-Hazard Risk Analysis: Case of a Simple Offshore Structure," by B.K. Bhartia and E.H. Vanmarcke, 7/21/88, (PB89-145213, A05, MF-A01).

- NCEER-88-0024 "Automated Seismic Design of Reinforced Concrete Buildings," by Y.S. Chung, C. Meyer and M. Shinozuka, 7/5/88, (PB89-122170, A06, MF-A01). This report is available only through NTIS (see address given above).
- NCEER-88-0025 "Experimental Study of Active Control of MDOF Structures Under Seismic Excitations," by L.L. Chung, R.C. Lin, T.T. Soong and A.M. Reinhorn, 7/10/88, (PB89-122600, A04, MF-A01).
- NCEER-88-0026 "Earthquake Simulation Tests of a Low-Rise Metal Structure," by J.S. Hwang, K.C. Chang, G.C. Lee and R.L. Ketter, 8/1/88, (PB89-102917, A04, MF-A01).
- NCEER-88-0027 "Systems Study of Urban Response and Reconstruction Due to Catastrophic Earthquakes," by F. Kozin and H.K. Zhou, 9/22/88, (PB90-162348, A04, MF-A01).
- NCEER-88-0028 "Seismic Fragility Analysis of Plane Frame Structures," by H.H-M. Hwang and Y.K. Low, 7/31/88, (PB89-131445, A06, MF-A01).
- NCEER-88-0029 "Response Analysis of Stochastic Structures," by A. Kardara, C. Bucher and M. Shinozuka, 9/22/88, (PB89-174429, A04, MF-A01).
- NCEER-88-0030 "Nonnormal Accelerations Due to Yielding in a Primary Structure," by D.C.K. Chen and L.D. Lutes, 9/19/88, (PB89-131437, A04, MF-A01).
- NCEER-88-0031 "Design Approaches for Soil-Structure Interaction," by A.S. Veletsos, A.M. Prasad and Y. Tang, 12/30/88, (PB89-174437, A03, MF-A01). This report is available only through NTIS (see address given above).
- NCEER-88-0032 "A Re-evaluation of Design Spectra for Seismic Damage Control," by C.J. Turkstra and A.G. Tallin, 11/7/88, (PB89-145221, A05, MF-A01).
- NCEER-88-0033 "The Behavior and Design of Noncontact Lap Splices Subjected to Repeated Inelastic Tensile Loading," by V.E. Sagan, P. Gergely and R.N. White, 12/8/88, (PB89-163737, A08, MF-A01).
- NCEER-88-0034 "Seismic Response of Pile Foundations," by S.M. Mamoon, P.K. Banerjee and S. Ahmad, 11/1/88, (PB89-145239, A04, MF-A01).
- NCEER-88-0035 "Modeling of R/C Building Structures With Flexible Floor Diaphragms (IDARC2)," by A.M. Reinhorn, S.K. Kunnath and N. Panahshahi, 9/7/88, (PB89-207153, A07, MF-A01).
- NCEER-88-0036 "Solution of the Dam-Reservoir Interaction Problem Using a Combination of FEM, BEM with Particular Integrals, Modal Analysis, and Substructuring," by C-S. Tsai, G.C. Lee and R.L. Ketter, 12/31/88, (PB89-207146, A04, MF-A01).
- NCEER-88-0037 "Optimal Placement of Actuators for Structural Control," by F.Y. Cheng and C.P. Pantelides, 8/15/88, (PB89-162846, A05, MF-A01).
- NCEER-88-0038 "Teflon Bearings in Aseismic Base Isolation: Experimental Studies and Mathematical Modeling," by A. Mokha, M.C. Constantinou and A.M. Reinhorn, 12/5/88, (PB89-218457, A10, MF-A01). This report is available only through NTIS (see address given above).
- NCEER-88-0039 "Seismic Behavior of Flat Slab High-Rise Buildings in the New York City Area," by P. Weidlinger and M. Ettouney, 10/15/88, (PB90-145681, A04, MF-A01).
- NCEER-88-0040 "Evaluation of the Earthquake Resistance of Existing Buildings in New York City," by P. Weidlinger and M. Ettouney, 10/15/88, not available.
- NCEER-88-0041 "Small-Scale Modeling Techniques for Reinforced Concrete Structures Subjected to Seismic Loads," by W. Kim, A. El-Attar and R.N. White, 11/22/88, (PB89-189625, A05, MF-A01).
- NCEER-88-0042 "Modeling Strong Ground Motion from Multiple Event Earthquakes," by G.W. Ellis and A.S. Cakmak, 10/15/88, (PB89-174445, A03, MF-A01).

- NCEER-88-0043 "Nonstationary Models of Seismic Ground Acceleration," by M. Grigoriu, S.E. Ruiz and E. Rosenblueth, 7/15/88, (PB89-189617, A04, MF-A01).
- NCEER-88-0044 "SARCF User's Guide: Seismic Analysis of Reinforced Concrete Frames," by Y.S. Chung, C. Meyer and M. Shinozuka, 11/9/88, (PB89-174452, A08, MF-A01).
- NCEER-88-0045 "First Expert Panel Meeting on Disaster Research and Planning," edited by J. Pantelic and J. Stoyke, 9/15/88, (PB89-174460, A05, MF-A01).
- NCEER-88-0046 "Preliminary Studies of the Effect of Degrading Infill Walls on the Nonlinear Seismic Response of Steel Frames," by C.Z. Chrysostomou, P. Gergely and J.F. Abel, 12/19/88, (PB89-208383, A05, MF-A01).
- NCEER-88-0047 "Reinforced Concrete Frame Component Testing Facility - Design, Construction, Instrumentation and Operation," by S.P. Pessiki, C. Conley, T. Bond, P. Gergely and R.N. White, 12/16/88, (PB89-174478, A04, MF-A01).
- NCEER-89-0001 "Effects of Protective Cushion and Soil Compliancy on the Response of Equipment Within a Seismically Excited Building," by J.A. HoLung, 2/16/89, (PB89-207179, A04, MF-A01).
- NCEER-89-0002 "Statistical Evaluation of Response Modification Factors for Reinforced Concrete Structures," by H.H-M. Hwang and J-W. Jaw, 2/17/89, (PB89-207187, A05, MF-A01).
- NCEER-89-0003 "Hysteretic Columns Under Random Excitation," by G-Q. Cai and Y.K. Lin, 1/9/89, (PB89-196513, A03, MF-A01).
- NCEER-89-0004 "Experimental Study of 'Elephant Foot Bulge' Instability of Thin-Walled Metal Tanks," by Z-H. Jia and R.L. Ketter, 2/22/89, (PB89-207195, A03, MF-A01).
- NCEER-89-0005 "Experiment on Performance of Buried Pipelines Across San Andreas Fault," by J. Isenberg, E. Richardson and T.D. O'Rourke, 3/10/89, (PB89-218440, A04, MF-A01). This report is available only through NTIS (see address given above).
- NCEER-89-0006 "A Knowledge-Based Approach to Structural Design of Earthquake-Resistant Buildings," by M. Subramani, P. Gergely, C.H. Conley, J.F. Abel and A.H. Zaghaw, 1/15/89, (PB89-218465, A06, MF-A01).
- NCEER-89-0007 "Liquefaction Hazards and Their Effects on Buried Pipelines," by T.D. O'Rourke and P.A. Lane, 2/1/89, (PB89-218481, A09, MF-A01).
- NCEER-89-0008 "Fundamentals of System Identification in Structural Dynamics," by H. Imai, C-B. Yun, O. Maruyama and M. Shinozuka, 1/26/89, (PB89-207211, A04, MF-A01).
- NCEER-89-0009 "Effects of the 1985 Michoacan Earthquake on Water Systems and Other Buried Lifelines in Mexico," by A.G. Ayala and M.J. O'Rourke, 3/8/89, (PB89-207229, A06, MF-A01).
- NCEER-89-R010 "NCEER Bibliography of Earthquake Education Materials," by K.E.K. Ross, Second Revision, 9/1/89, (PB90-125352, A05, MF-A01). This report is replaced by NCEER-92-0018.
- NCEER-89-0011 "Inelastic Three-Dimensional Response Analysis of Reinforced Concrete Building Structures (IDARC-3D), Part I - Modeling," by S.K. Kunnath and A.M. Reinhorn, 4/17/89, (PB90-114612, A07, MF-A01). This report is available only through NTIS (see address given above).
- NCEER-89-0012 "Recommended Modifications to ATC-14," by C.D. Poland and J.O. Malley, 4/12/89, (PB90-108648, A15, MF-A01).
- NCEER-89-0013 "Repair and Strengthening of Beam-to-Column Connections Subjected to Earthquake Loading," by M. Corazao and A.J. Durrani, 2/28/89, (PB90-109885, A06, MF-A01).
- NCEER-89-0014 "Program EXKAL2 for Identification of Structural Dynamic Systems," by O. Maruyama, C-B. Yun, M. Hoshiya and M. Shinozuka, 5/19/89, (PB90-109877, A09, MF-A01).

- NCEER-89-0015 "Response of Frames With Bolted Semi-Rigid Connections, Part I - Experimental Study and Analytical Predictions," by P.J. DiCorso, A.M. Reinhorn, J.R. Dickerson, J.B. Radzimirski and W.L. Harper, 6/1/89, not available.
- NCEER-89-0016 "ARMA Monte Carlo Simulation in Probabilistic Structural Analysis," by P.D. Spanos and M.P. Mignolet, 7/10/89, (PB90-109893, A03, MF-A01).
- NCEER-89-P017 "Preliminary Proceedings from the Conference on Disaster Preparedness - The Place of Earthquake Education in Our Schools," Edited by K.E.K. Ross, 6/23/89, (PB90-108606, A03, MF-A01).
- NCEER-89-0017 "Proceedings from the Conference on Disaster Preparedness - The Place of Earthquake Education in Our Schools," Edited by K.E.K. Ross, 12/31/89, (PB90-207895, A012, MF-A02). This report is available only through NTIS (see address given above).
- NCEER-89-0018 "Multidimensional Models of Hysteretic Material Behavior for Vibration Analysis of Shape Memory Energy Absorbing Devices, by E.J. Graesser and F.A. Cozzarelli, 6/7/89, (PB90-164146, A04, MF-A01).
- NCEER-89-0019 "Nonlinear Dynamic Analysis of Three-Dimensional Base Isolated Structures (3D-BASIS)," by S. Nagarajaiah, A.M. Reinhorn and M.C. Constantinou, 8/3/89, (PB90-161936, A06, MF-A01). This report has been replaced by NCEER-93-0011.
- NCEER-89-0020 "Structural Control Considering Time-Rate of Control Forces and Control Rate Constraints," by F.Y. Cheng and C.P. Pantelides, 8/3/89, (PB90-120445, A04, MF-A01).
- NCEER-89-0021 "Subsurface Conditions of Memphis and Shelby County," by K.W. Ng, T-S. Chang and H-H.M. Hwang, 7/26/89, (PB90-120437, A03, MF-A01).
- NCEER-89-0022 "Seismic Wave Propagation Effects on Straight Jointed Buried Pipelines," by K. Elhmadi and M.J. O'Rourke, 8/24/89, (PB90-162322, A10, MF-A02).
- NCEER-89-0023 "Workshop on Serviceability Analysis of Water Delivery Systems," edited by M. Grigoriu, 3/6/89, (PB90-127424, A03, MF-A01).
- NCEER-89-0024 "Shaking Table Study of a 1/5 Scale Steel Frame Composed of Tapered Members," by K.C. Chang, J.S. Hwang and G.C. Lee, 9/18/89, (PB90-160169, A04, MF-A01).
- NCEER-89-0025 "DYNA1D: A Computer Program for Nonlinear Seismic Site Response Analysis - Technical Documentation," by Jean H. Prevost, 9/14/89, (PB90-161944, A07, MF-A01). This report is available only through NTIS (see address given above).
- NCEER-89-0026 "1:4 Scale Model Studies of Active Tendon Systems and Active Mass Dampers for Aseismic Protection," by A.M. Reinhorn, T.T. Soong, R.C. Lin, Y.P. Yang, Y. Fukao, H. Abe and M. Nakai, 9/15/89, (PB90-173246, A10, MF-A02). This report is available only through NTIS (see address given above).
- NCEER-89-0027 "Scattering of Waves by Inclusions in a Nonhomogeneous Elastic Half Space Solved by Boundary Element Methods," by P.K. Hadley, A. Askar and A.S. Cakmak, 6/15/89, (PB90-145699, A07, MF-A01).
- NCEER-89-0028 "Statistical Evaluation of Deflection Amplification Factors for Reinforced Concrete Structures," by H.H.M. Hwang, J-W. Jaw and A.L. Ch'ng, 8/31/89, (PB90-164633, A05, MF-A01).
- NCEER-89-0029 "Bedrock Accelerations in Memphis Area Due to Large New Madrid Earthquakes," by H.H.M. Hwang, C.H.S. Chen and G. Yu, 11/7/89, (PB90-162330, A04, MF-A01).
- NCEER-89-0030 "Seismic Behavior and Response Sensitivity of Secondary Structural Systems," by Y.Q. Chen and T.T. Soong, 10/23/89, (PB90-164658, A08, MF-A01).
- NCEER-89-0031 "Random Vibration and Reliability Analysis of Primary-Secondary Structural Systems," by Y. Ibrahim, M. Grigoriu and T.T. Soong, 11/10/89, (PB90-161951, A04, MF-A01).

- NCEER-89-0032 "Proceedings from the Second U.S. - Japan Workshop on Liquefaction, Large Ground Deformation and Their Effects on Lifelines, September 26-29, 1989," Edited by T.D. O'Rourke and M. Hamada, 12/1/89, (PB90-209388, A22, MF-A03).
- NCEER-89-0033 "Deterministic Model for Seismic Damage Evaluation of Reinforced Concrete Structures," by J.M. Bracci, A.M. Reinhorn, J.B. Mander and S.K. Kunnath, 9/27/89, (PB91-108803, A06, MF-A01).
- NCEER-89-0034 "On the Relation Between Local and Global Damage Indices," by E. DiPasquale and A.S. Cakmak, 8/15/89, (PB90-173865, A05, MF-A01).
- NCEER-89-0035 "Cyclic Undrained Behavior of Nonplastic and Low Plasticity Silts," by A.J. Walker and H.E. Stewart, 7/26/89, (PB90-183518, A10, MF-A01).
- NCEER-89-0036 "Liquefaction Potential of Surficial Deposits in the City of Buffalo, New York," by M. Budhu, R. Giese and L. Baumgrass, 1/17/89, (PB90-208455, A04, MF-A01).
- NCEER-89-0037 "A Deterministic Assessment of Effects of Ground Motion Incoherence," by A.S. Veletsos and Y. Tang, 7/15/89, (PB90-164294, A03, MF-A01).
- NCEER-89-0038 "Workshop on Ground Motion Parameters for Seismic Hazard Mapping," July 17-18, 1989, edited by R.V. Whitman, 12/1/89, (PB90-173923, A04, MF-A01).
- NCEER-89-0039 "Seismic Effects on Elevated Transit Lines of the New York City Transit Authority," by C.J. Costantino, C.A. Miller and E. Heymsfield, 12/26/89, (PB90-207887, A06, MF-A01).
- NCEER-89-0040 "Centrifugal Modeling of Dynamic Soil-Structure Interaction," by K. Weissman, Supervised by J.H. Prevost, 5/10/89, (PB90-207879, A07, MF-A01).
- NCEER-89-0041 "Linearized Identification of Buildings With Cores for Seismic Vulnerability Assessment," by I-K. Ho and A.E. Aktan, 11/1/89, (PB90-251943, A07, MF-A01).
- NCEER-90-0001 "Geotechnical and Lifeline Aspects of the October 17, 1989 Loma Prieta Earthquake in San Francisco," by T.D. O'Rourke, H.E. Stewart, F.T. Blackburn and T.S. Dickerman, 1/90, (PB90-208596, A05, MF-A01).
- NCEER-90-0002 "Nonnormal Secondary Response Due to Yielding in a Primary Structure," by D.C.K. Chen and L.D. Lutes, 2/28/90, (PB90-251976, A07, MF-A01).
- NCEER-90-0003 "Earthquake Education Materials for Grades K-12," by K.E.K. Ross, 4/16/90, (PB91-251984, A05, MF-A05). This report has been replaced by NCEER-92-0018.
- NCEER-90-0004 "Catalog of Strong Motion Stations in Eastern North America," by R.W. Busby, 4/3/90, (PB90-251984, A05, MF-A01).
- NCEER-90-0005 "NCEER Strong-Motion Data Base: A User Manual for the GeoBase Release (Version 1.0 for the Sun3)," by P. Friberg and K. Jacob, 3/31/90 (PB90-258062, A04, MF-A01).
- NCEER-90-0006 "Seismic Hazard Along a Crude Oil Pipeline in the Event of an 1811-1812 Type New Madrid Earthquake," by H.H.M. Hwang and C-H.S. Chen, 4/16/90, (PB90-258054, A04, MF-A01).
- NCEER-90-0007 "Site-Specific Response Spectra for Memphis Sheahan Pumping Station," by H.H.M. Hwang and C.S. Lee, 5/15/90, (PB91-108811, A05, MF-A01).
- NCEER-90-0008 "Pilot Study on Seismic Vulnerability of Crude Oil Transmission Systems," by T. Ariman, R. Dobry, M. Grigoriu, F. Kozin, M. O'Rourke, T. O'Rourke and M. Shinozuka, 5/25/90, (PB91-108837, A06, MF-A01).
- NCEER-90-0009 "A Program to Generate Site Dependent Time Histories: EQGEN," by G.W. Ellis, M. Srinivasan and A.S. Cakmak, 1/30/90, (PB91-108829, A04, MF-A01).
- NCEER-90-0010 "Active Isolation for Seismic Protection of Operating Rooms," by M.E. Talbott, Supervised by M. Shinozuka, 6/8/9, (PB91-110205, A05, MF-A01).

- NCEER-90-0011 "Program LINEARID for Identification of Linear Structural Dynamic Systems," by C-B. Yun and M. Shinozuka, 6/25/90, (PB91-110312, A08, MF-A01).
- NCEER-90-0012 "Two-Dimensional Two-Phase Elasto-Plastic Seismic Response of Earth Dams," by A.N. Yiagos, Supervised by J.H. Prevost, 6/20/90, (PB91-110197, A13, MF-A02).
- NCEER-90-0013 "Secondary Systems in Base-Isolated Structures: Experimental Investigation, Stochastic Response and Stochastic Sensitivity," by G.D. Manolis, G. Juhn, M.C. Constantinou and A.M. Reinhorn, 7/1/90, (PB91-110320, A08, MF-A01).
- NCEER-90-0014 "Seismic Behavior of Lightly-Reinforced Concrete Column and Beam-Column Joint Details," by S.P. Pessiki, C.H. Conley, P. Gergely and R.N. White, 8/22/90, (PB91-108795, A11, MF-A02).
- NCEER-90-0015 "Two Hybrid Control Systems for Building Structures Under Strong Earthquakes," by J.N. Yang and A. Daniellians, 6/29/90, (PB91-125393, A04, MF-A01).
- NCEER-90-0016 "Instantaneous Optimal Control with Acceleration and Velocity Feedback," by J.N. Yang and Z. Li, 6/29/90, (PB91-125401, A03, MF-A01).
- NCEER-90-0017 "Reconnaissance Report on the Northern Iran Earthquake of June 21, 1990," by M. Mehrain, 10/4/90, (PB91-125377, A03, MF-A01).
- NCEER-90-0018 "Evaluation of Liquefaction Potential in Memphis and Shelby County," by T.S. Chang, P.S. Tang, C.S. Lee and H. Hwang, 8/10/90, (PB91-125427, A09, MF-A01).
- NCEER-90-0019 "Experimental and Analytical Study of a Combined Sliding Disc Bearing and Helical Steel Spring Isolation System," by M.C. Constantinou, A.S. Mokha and A.M. Reinhorn, 10/4/90, (PB91-125385, A06, MF-A01). This report is available only through NTIS (see address given above).
- NCEER-90-0020 "Experimental Study and Analytical Prediction of Earthquake Response of a Sliding Isolation System with a Spherical Surface," by A.S. Mokha, M.C. Constantinou and A.M. Reinhorn, 10/11/90, (PB91-125419, A05, MF-A01).
- NCEER-90-0021 "Dynamic Interaction Factors for Floating Pile Groups," by G. Gazetas, K. Fan, A. Kaynia and E. Kausel, 9/10/90, (PB91-170381, A05, MF-A01).
- NCEER-90-0022 "Evaluation of Seismic Damage Indices for Reinforced Concrete Structures," by S. Rodriguez-Gomez and A.S. Cakmak, 9/30/90, PB91-171322, A06, MF-A01).
- NCEER-90-0023 "Study of Site Response at a Selected Memphis Site," by H. Desai, S. Ahmad, E.S. Gazetas and M.R. Oh, 10/11/90, (PB91-196857, A03, MF-A01).
- NCEER-90-0024 "A User's Guide to Strongmo: Version 1.0 of NCEER's Strong-Motion Data Access Tool for PCs and Terminals," by P.A. Friberg and C.A.T. Susch, 11/15/90, (PB91-171272, A03, MF-A01).
- NCEER-90-0025 "A Three-Dimensional Analytical Study of Spatial Variability of Seismic Ground Motions," by L-L. Hong and A.H.-S. Ang, 10/30/90, (PB91-170399, A09, MF-A01).
- NCEER-90-0026 "MUMOID User's Guide - A Program for the Identification of Modal Parameters," by S. Rodriguez-Gomez and E. DiPasquale, 9/30/90, (PB91-171298, A04, MF-A01).
- NCEER-90-0027 "SARCF-II User's Guide - Seismic Analysis of Reinforced Concrete Frames," by S. Rodriguez-Gomez, Y.S. Chung and C. Meyer, 9/30/90, (PB91-171280, A05, MF-A01).
- NCEER-90-0028 "Viscous Dampers: Testing, Modeling and Application in Vibration and Seismic Isolation," by N. Makris and M.C. Constantinou, 12/20/90 (PB91-190561, A06, MF-A01).
- NCEER-90-0029 "Soil Effects on Earthquake Ground Motions in the Memphis Area," by H. Hwang, C.S. Lee, K.W. Ng and T.S. Chang, 8/2/90, (PB91-190751, A05, MF-A01).

- NCEER-91-0001 "Proceedings from the Third Japan-U.S. Workshop on Earthquake Resistant Design of Lifeline Facilities and Countermeasures for Soil Liquefaction, December 17-19, 1990," edited by T.D. O'Rourke and M. Hamada, 2/1/91, (PB91-179259, A99, MF-A04).
- NCEER-91-0002 "Physical Space Solutions of Non-Proportionally Damped Systems," by M. Tong, Z. Liang and G.C. Lee, 1/15/91, (PB91-179242, A04, MF-A01).
- NCEER-91-0003 "Seismic Response of Single Piles and Pile Groups," by K. Fan and G. Gazetas, 1/10/91, (PB92-174994, A04, MF-A01).
- NCEER-91-0004 "Damping of Structures: Part 1 - Theory of Complex Damping," by Z. Liang and G. Lee, 10/10/91, (PB92-197235, A12, MF-A03).
- NCEER-91-0005 "3D-BASIS - Nonlinear Dynamic Analysis of Three Dimensional Base Isolated Structures: Part II," by S. Nagarajaiah, A.M. Reinhorn and M.C. Constantinou, 2/28/91, (PB91-190553, A07, MF-A01). This report has been replaced by NCEER-93-0011.
- NCEER-91-0006 "A Multidimensional Hysteretic Model for Plasticity Deforming Metals in Energy Absorbing Devices," by E.J. Graesser and F.A. Cozzarelli, 4/9/91, (PB92-108364, A04, MF-A01).
- NCEER-91-0007 "A Framework for Customizable Knowledge-Based Expert Systems with an Application to a KBES for Evaluating the Seismic Resistance of Existing Buildings," by E.G. Ibarra-Anaya and S.J. Fenves, 4/9/91, (PB91-210930, A08, MF-A01).
- NCEER-91-0008 "Nonlinear Analysis of Steel Frames with Semi-Rigid Connections Using the Capacity Spectrum Method," by G.G. Deierlein, S-H. Hsieh, Y-J. Shen and J.F. Abel, 7/2/91, (PB92-113828, A05, MF-A01).
- NCEER-91-0009 "Earthquake Education Materials for Grades K-12," by K.E.K. Ross, 4/30/91, (PB91-212142, A06, MF-A01). This report has been replaced by NCEER-92-0018.
- NCEER-91-0010 "Phase Wave Velocities and Displacement Phase Differences in a Harmonically Oscillating Pile," by N. Makris and G. Gazetas, 7/8/91, (PB92-108356, A04, MF-A01).
- NCEER-91-0011 "Dynamic Characteristics of a Full-Size Five-Story Steel Structure and a 2/5 Scale Model," by K.C. Chang, G.C. Yao, G.C. Lee, D.S. Hao and Y.C. Yeh, 7/2/91, (PB93-116648, A06, MF-A02).
- NCEER-91-0012 "Seismic Response of a 2/5 Scale Steel Structure with Added Viscoelastic Dampers," by K.C. Chang, T.T. Soong, S-T. Oh and M.L. Lai, 5/17/91, (PB92-110816, A05, MF-A01).
- NCEER-91-0013 "Earthquake Response of Retaining Walls; Full-Scale Testing and Computational Modeling," by S. Alampalli and A-W.M. Elgamal, 6/20/91, not available.
- NCEER-91-0014 "3D-BASIS-M: Nonlinear Dynamic Analysis of Multiple Building Base Isolated Structures," by P.C. Tsopelas, S. Nagarajaiah, M.C. Constantinou and A.M. Reinhorn, 5/28/91, (PB92-113885, A09, MF-A02).
- NCEER-91-0015 "Evaluation of SEAOC Design Requirements for Sliding Isolated Structures," by D. Theodossiou and M.C. Constantinou, 6/10/91, (PB92-114602, A11, MF-A03).
- NCEER-91-0016 "Closed-Loop Modal Testing of a 27-Story Reinforced Concrete Flat Plate-Core Building," by H.R. Somaprasad, T. Toksoy, H. Yoshiyuki and A.E. Aktan, 7/15/91, (PB92-129980, A07, MF-A02).
- NCEER-91-0017 "Shake Table Test of a 1/6 Scale Two-Story Lightly Reinforced Concrete Building," by A.G. El-Attar, R.N. White and P. Gergely, 2/28/91, (PB92-222447, A06, MF-A02).
- NCEER-91-0018 "Shake Table Test of a 1/8 Scale Three-Story Lightly Reinforced Concrete Building," by A.G. El-Attar, R.N. White and P. Gergely, 2/28/91, (PB93-116630, A08, MF-A02).
- NCEER-91-0019 "Transfer Functions for Rigid Rectangular Foundations," by A.S. Veletsos, A.M. Prasad and W.H. Wu, 7/31/91, not available.

- NCEER-91-0020 "Hybrid Control of Seismic-Excited Nonlinear and Inelastic Structural Systems," by J.N. Yang, Z. Li and A. Daniellians, 8/1/91, (PB92-143171, A06, MF-A02).
- NCEER-91-0021 "The NCEER-91 Earthquake Catalog: Improved Intensity-Based Magnitudes and Recurrence Relations for U.S. Earthquakes East of New Madrid," by L. Seeber and J.G. Armbruster, 8/28/91, (PB92-176742, A06, MF-A02).
- NCEER-91-0022 "Proceedings from the Implementation of Earthquake Planning and Education in Schools: The Need for Change - The Roles of the Changemakers," by K.E.K. Ross and F. Winslow, 7/23/91, (PB92-129998, A12, MF-A03).
- NCEER-91-0023 "A Study of Reliability-Based Criteria for Seismic Design of Reinforced Concrete Frame Buildings," by H.H.M. Hwang and H-M. Hsu, 8/10/91, (PB92-140235, A09, MF-A02).
- NCEER-91-0024 "Experimental Verification of a Number of Structural System Identification Algorithms," by R.G. Ghanem, H. Gavin and M. Shinozuka, 9/18/91, (PB92-176577, A18, MF-A04).
- NCEER-91-0025 "Probabilistic Evaluation of Liquefaction Potential," by H.H.M. Hwang and C.S. Lee," 11/25/91, (PB92-143429, A05, MF-A01).
- NCEER-91-0026 "Instantaneous Optimal Control for Linear, Nonlinear and Hysteretic Structures - Stable Controllers," by J.N. Yang and Z. Li, 11/15/91, (PB92-163807, A04, MF-A01).
- NCEER-91-0027 "Experimental and Theoretical Study of a Sliding Isolation System for Bridges," by M.C. Constantinou, A. Kartoum, A.M. Reinhorn and P. Bradford, 11/15/91, (PB92-176973, A10, MF-A03).
- NCEER-92-0001 "Case Studies of Liquefaction and Lifeline Performance During Past Earthquakes, Volume 1: Japanese Case Studies," Edited by M. Hamada and T. O'Rourke, 2/17/92, (PB92-197243, A18, MF-A04).
- NCEER-92-0002 "Case Studies of Liquefaction and Lifeline Performance During Past Earthquakes, Volume 2: United States Case Studies," Edited by T. O'Rourke and M. Hamada, 2/17/92, (PB92-197250, A20, MF-A04).
- NCEER-92-0003 "Issues in Earthquake Education," Edited by K. Ross, 2/3/92, (PB92-222389, A07, MF-A02).
- NCEER-92-0004 "Proceedings from the First U.S. - Japan Workshop on Earthquake Protective Systems for Bridges," Edited by I.G. Buckle, 2/4/92, (PB94-142239, A99, MF-A06).
- NCEER-92-0005 "Seismic Ground Motion from a Haskell-Type Source in a Multiple-Layered Half-Space," A.P. Theoharis, G. Deodatis and M. Shinozuka, 1/2/92, not available.
- NCEER-92-0006 "Proceedings from the Site Effects Workshop," Edited by R. Whitman, 2/29/92, (PB92-197201, A04, MF-A01).
- NCEER-92-0007 "Engineering Evaluation of Permanent Ground Deformations Due to Seismically-Induced Liquefaction," by M.H. Baziar, R. Dobry and A-W.M. Elgamal, 3/24/92, (PB92-222421, A13, MF-A03).
- NCEER-92-0008 "A Procedure for the Seismic Evaluation of Buildings in the Central and Eastern United States," by C.D. Poland and J.O. Malley, 4/2/92, (PB92-222439, A20, MF-A04).
- NCEER-92-0009 "Experimental and Analytical Study of a Hybrid Isolation System Using Friction Controllable Sliding Bearings," by M.Q. Feng, S. Fujii and M. Shinozuka, 5/15/92, (PB93-150282, A06, MF-A02).
- NCEER-92-0010 "Seismic Resistance of Slab-Column Connections in Existing Non-Ductile Flat-Plate Buildings," by A.J. Durrani and Y. Du, 5/18/92, (PB93-116812, A06, MF-A02).
- NCEER-92-0011 "The Hysteretic and Dynamic Behavior of Brick Masonry Walls Upgraded by Ferrocement Coatings Under Cyclic Loading and Strong Simulated Ground Motion," by H. Lee and S.P. Prawel, 5/11/92, not available.
- NCEER-92-0012 "Study of Wire Rope Systems for Seismic Protection of Equipment in Buildings," by G.F. Demetriades, M.C. Constantinou and A.M. Reinhorn, 5/20/92, (PB93-116655, A08, MF-A02).

- NCEER-92-0013 "Shape Memory Structural Dampers: Material Properties, Design and Seismic Testing," by P.R. Witting and F.A. Cozzarelli, 5/26/92, (PB93-116663, A05, MF-A01).
- NCEER-92-0014 "Longitudinal Permanent Ground Deformation Effects on Buried Continuous Pipelines," by M.J. O'Rourke, and C. Nordberg, 6/15/92, (PB93-116671, A08, MF-A02).
- NCEER-92-0015 "A Simulation Method for Stationary Gaussian Random Functions Based on the Sampling Theorem," by M. Grigoriu and S. Balopoulou, 6/11/92, (PB93-127496, A05, MF-A01).
- NCEER-92-0016 "Gravity-Load-Designed Reinforced Concrete Buildings: Seismic Evaluation of Existing Construction and Detailing Strategies for Improved Seismic Resistance," by G.W. Hoffmann, S.K. Kunnath, A.M. Reinhorn and J.B. Mander, 7/15/92, (PB94-142007, A08, MF-A02).
- NCEER-92-0017 "Observations on Water System and Pipeline Performance in the Limón Area of Costa Rica Due to the April 22, 1991 Earthquake," by M. O'Rourke and D. Ballantyne, 6/30/92, (PB93-126811, A06, MF-A02).
- NCEER-92-0018 "Fourth Edition of Earthquake Education Materials for Grades K-12," Edited by K.E.K. Ross, 8/10/92, (PB93-114023, A07, MF-A02).
- NCEER-92-0019 "Proceedings from the Fourth Japan-U.S. Workshop on Earthquake Resistant Design of Lifeline Facilities and Countermeasures for Soil Liquefaction," Edited by M. Hamada and T.D. O'Rourke, 8/12/92, (PB93-163939, A99, MF-E11).
- NCEER-92-0020 "Active Bracing System: A Full Scale Implementation of Active Control," by A.M. Reinhorn, T.T. Soong, R.C. Lin, M.A. Riley, Y.P. Wang, S. Aizawa and M. Higashino, 8/14/92, (PB93-127512, A06, MF-A02).
- NCEER-92-0021 "Empirical Analysis of Horizontal Ground Displacement Generated by Liquefaction-Induced Lateral Spreads," by S.F. Bartlett and T.L. Youd, 8/17/92, (PB93-188241, A06, MF-A02).
- NCEER-92-0022 "IDARC Version 3.0: Inelastic Damage Analysis of Reinforced Concrete Structures," by S.K. Kunnath, A.M. Reinhorn and R.F. Lobo, 8/31/92, (PB93-227502, A07, MF-A02).
- NCEER-92-0023 "A Semi-Empirical Analysis of Strong-Motion Peaks in Terms of Seismic Source, Propagation Path and Local Site Conditions, by M. Kamiyama, M.J. O'Rourke and R. Flores-Berrones, 9/9/92, (PB93-150266, A08, MF-A02).
- NCEER-92-0024 "Seismic Behavior of Reinforced Concrete Frame Structures with Nonductile Details, Part I: Summary of Experimental Findings of Full Scale Beam-Column Joint Tests," by A. Beres, R.N. White and P. Gergely, 9/30/92, (PB93-227783, A05, MF-A01).
- NCEER-92-0025 "Experimental Results of Repaired and Retrofitted Beam-Column Joint Tests in Lightly Reinforced Concrete Frame Buildings," by A. Beres, S. El-Borgi, R.N. White and P. Gergely, 10/29/92, (PB93-227791, A05, MF-A01).
- NCEER-92-0026 "A Generalization of Optimal Control Theory: Linear and Nonlinear Structures," by J.N. Yang, Z. Li and S. Vongchavalitkul, 11/2/92, (PB93-188621, A05, MF-A01).
- NCEER-92-0027 "Seismic Resistance of Reinforced Concrete Frame Structures Designed Only for Gravity Loads: Part I - Design and Properties of a One-Third Scale Model Structure," by J.M. Bracci, A.M. Reinhorn and J.B. Mander, 12/1/92, (PB94-104502, A08, MF-A02).
- NCEER-92-0028 "Seismic Resistance of Reinforced Concrete Frame Structures Designed Only for Gravity Loads: Part II - Experimental Performance of Subassemblages," by L.E. Aycaardi, J.B. Mander and A.M. Reinhorn, 12/1/92, (PB94-104510, A08, MF-A02).
- NCEER-92-0029 "Seismic Resistance of Reinforced Concrete Frame Structures Designed Only for Gravity Loads: Part III - Experimental Performance and Analytical Study of a Structural Model," by J.M. Bracci, A.M. Reinhorn and J.B. Mander, 12/1/92, (PB93-227528, A09, MF-A01).

- NCEER-92-0030 "Evaluation of Seismic Retrofit of Reinforced Concrete Frame Structures: Part I - Experimental Performance of Retrofitted Subassemblages," by D. Choudhuri, J.B. Mander and A.M. Reinhorn, 12/8/92, (PB93-198307, A07, MF-A02).
- NCEER-92-0031 "Evaluation of Seismic Retrofit of Reinforced Concrete Frame Structures: Part II - Experimental Performance and Analytical Study of a Retrofitted Structural Model," by J.M. Bracci, A.M. Reinhorn and J.B. Mander, 12/8/92, (PB93-198315, A09, MF-A03).
- NCEER-92-0032 "Experimental and Analytical Investigation of Seismic Response of Structures with Supplemental Fluid Viscous Dampers," by M.C. Constantinou and M.D. Symans, 12/21/92, (PB93-191435, A10, MF-A03). This report is available only through NTIS (see address given above).
- NCEER-92-0033 "Reconnaissance Report on the Cairo, Egypt Earthquake of October 12, 1992," by M. Khater, 12/23/92, (PB93-188621, A03, MF-A01).
- NCEER-92-0034 "Low-Level Dynamic Characteristics of Four Tall Flat-Plate Buildings in New York City," by H. Gavin, S. Yuan, J. Grossman, E. Pekelis and K. Jacob, 12/28/92, (PB93-188217, A07, MF-A02).
- NCEER-93-0001 "An Experimental Study on the Seismic Performance of Brick-Infilled Steel Frames With and Without Retrofit," by J.B. Mander, B. Nair, K. Wojtkowski and J. Ma, 1/29/93, (PB93-227510, A07, MF-A02).
- NCEER-93-0002 "Social Accounting for Disaster Preparedness and Recovery Planning," by S. Cole, E. Pantoja and V. Razak, 2/22/93, (PB94-142114, A12, MF-A03).
- NCEER-93-0003 "Assessment of 1991 NEHRP Provisions for Nonstructural Components and Recommended Revisions," by T.T. Soong, G. Chen, Z. Wu, R-H. Zhang and M. Grigoriu, 3/1/93, (PB93-188639, A06, MF-A02).
- NCEER-93-0004 "Evaluation of Static and Response Spectrum Analysis Procedures of SEAOC/UBC for Seismic Isolated Structures," by C.W. Winters and M.C. Constantinou, 3/23/93, (PB93-198299, A10, MF-A03).
- NCEER-93-0005 "Earthquakes in the Northeast - Are We Ignoring the Hazard? A Workshop on Earthquake Science and Safety for Educators," edited by K.E.K. Ross, 4/2/93, (PB94-103066, A09, MF-A02).
- NCEER-93-0006 "Inelastic Response of Reinforced Concrete Structures with Viscoelastic Braces," by R.F. Lobo, J.M. Bracci, K.L. Shen, A.M. Reinhorn and T.T. Soong, 4/5/93, (PB93-227486, A05, MF-A02).
- NCEER-93-0007 "Seismic Testing of Installation Methods for Computers and Data Processing Equipment," by K. Kosar, T.T. Soong, K.L. Shen, J.A. HoLung and Y.K. Lin, 4/12/93, (PB93-198299, A07, MF-A02).
- NCEER-93-0008 "Retrofit of Reinforced Concrete Frames Using Added Dampers," by A. Reinhorn, M. Constantinou and C. Li, not available.
- NCEER-93-0009 "Seismic Behavior and Design Guidelines for Steel Frame Structures with Added Viscoelastic Dampers," by K.C. Chang, M.L. Lai, T.T. Soong, D.S. Hao and Y.C. Yeh, 5/1/93, (PB94-141959, A07, MF-A02).
- NCEER-93-0010 "Seismic Performance of Shear-Critical Reinforced Concrete Bridge Piers," by J.B. Mander, S.M. Waheed, M.T.A. Chaudhary and S.S. Chen, 5/12/93, (PB93-227494, A08, MF-A02).
- NCEER-93-0011 "3D-BASIS-TABS: Computer Program for Nonlinear Dynamic Analysis of Three Dimensional Base Isolated Structures," by S. Nagarajaiah, C. Li, A.M. Reinhorn and M.C. Constantinou, 8/2/93, (PB94-141819, A09, MF-A02).
- NCEER-93-0012 "Effects of Hydrocarbon Spills from an Oil Pipeline Break on Ground Water," by O.J. Helweg and H.H.M. Hwang, 8/3/93, (PB94-141942, A06, MF-A02).
- NCEER-93-0013 "Simplified Procedures for Seismic Design of Nonstructural Components and Assessment of Current Code Provisions," by M.P. Singh, L.E. Suarez, E.E. Matheu and G.O. Maldonado, 8/4/93, (PB94-141827, A09, MF-A02).
- NCEER-93-0014 "An Energy Approach to Seismic Analysis and Design of Secondary Systems," by G. Chen and T.T. Soong, 8/6/93, (PB94-142767, A11, MF-A03).

- NCEER-93-0015 "Proceedings from School Sites: Becoming Prepared for Earthquakes - Commemorating the Third Anniversary of the Loma Prieta Earthquake," Edited by F.E. Winslow and K.E.K. Ross, 8/16/93, (PB94-154275, A16, MF-A02).
- NCEER-93-0016 "Reconnaissance Report of Damage to Historic Monuments in Cairo, Egypt Following the October 12, 1992 Dahshur Earthquake," by D. Sykora, D. Look, G. Croci, E. Karaesmen and E. Karaesmen, 8/19/93, (PB94-142221, A08, MF-A02).
- NCEER-93-0017 "The Island of Guam Earthquake of August 8, 1993," by S.W. Swan and S.K. Harris, 9/30/93, (PB94-141843, A04, MF-A01).
- NCEER-93-0018 "Engineering Aspects of the October 12, 1992 Egyptian Earthquake," by A.W. Elgamal, M. Amer, K. Adalier and A. Abul-Fadl, 10/7/93, (PB94-141983, A05, MF-A01).
- NCEER-93-0019 "Development of an Earthquake Motion Simulator and its Application in Dynamic Centrifuge Testing," by I. Krstelj, Supervised by J.H. Prevost, 10/23/93, (PB94-181773, A-10, MF-A03).
- NCEER-93-0020 "NCEER-Taisei Corporation Research Program on Sliding Seismic Isolation Systems for Bridges: Experimental and Analytical Study of a Friction Pendulum System (FPS)," by M.C. Constantinou, P. Tsopelas, Y-S. Kim and S. Okamoto, 11/1/93, (PB94-142775, A08, MF-A02).
- NCEER-93-0021 "Finite Element Modeling of Elastomeric Seismic Isolation Bearings," by L.J. Billings, Supervised by R. Shepherd, 11/8/93, not available.
- NCEER-93-0022 "Seismic Vulnerability of Equipment in Critical Facilities: Life-Safety and Operational Consequences," by K. Porter, G.S. Johnson, M.M. Zadeh, C. Scawthorn and S. Eder, 11/24/93, (PB94-181765, A16, MF-A03).
- NCEER-93-0023 "Hokkaido Nansei-oki, Japan Earthquake of July 12, 1993, by P.I. Yanev and C.R. Scawthorn, 12/23/93, (PB94-181500, A07, MF-A01).
- NCEER-94-0001 "An Evaluation of Seismic Serviceability of Water Supply Networks with Application to the San Francisco Auxiliary Water Supply System," by I. Markov, Supervised by M. Grigoriu and T. O'Rourke, 1/21/94, (PB94-204013, A07, MF-A02).
- NCEER-94-0002 "NCEER-Taisei Corporation Research Program on Sliding Seismic Isolation Systems for Bridges: Experimental and Analytical Study of Systems Consisting of Sliding Bearings, Rubber Restoring Force Devices and Fluid Dampers," Volumes I and II, by P. Tsopelas, S. Okamoto, M.C. Constantinou, D. Ozaki and S. Fujii, 2/4/94, (PB94-181740, A09, MF-A02 and PB94-181757, A12, MF-A03).
- NCEER-94-0003 "A Markov Model for Local and Global Damage Indices in Seismic Analysis," by S. Rahman and M. Grigoriu, 2/18/94, (PB94-206000, A12, MF-A03).
- NCEER-94-0004 "Proceedings from the NCEER Workshop on Seismic Response of Masonry Infills," edited by D.P. Abrams, 3/1/94, (PB94-180783, A07, MF-A02).
- NCEER-94-0005 "The Northridge, California Earthquake of January 17, 1994: General Reconnaissance Report," edited by J.D. Goltz, 3/11/94, (PB94-193943, A10, MF-A03).
- NCEER-94-0006 "Seismic Energy Based Fatigue Damage Analysis of Bridge Columns: Part I - Evaluation of Seismic Capacity," by G.A. Chang and J.B. Mander, 3/14/94, (PB94-219185, A11, MF-A03).
- NCEER-94-0007 "Seismic Isolation of Multi-Story Frame Structures Using Spherical Sliding Isolation Systems," by T.M. Al-Hussaini, V.A. Zayas and M.C. Constantinou, 3/17/94, (PB94-193745, A09, MF-A02).
- NCEER-94-0008 "The Northridge, California Earthquake of January 17, 1994: Performance of Highway Bridges," edited by I.G. Buckle, 3/24/94, (PB94-193851, A06, MF-A02).
- NCEER-94-0009 "Proceedings of the Third U.S.-Japan Workshop on Earthquake Protective Systems for Bridges," edited by I.G. Buckle and I. Friedland, 3/31/94, (PB94-195815, A99, MF-A06).

- NCEER-94-0010 "3D-BASIS-ME: Computer Program for Nonlinear Dynamic Analysis of Seismically Isolated Single and Multiple Structures and Liquid Storage Tanks," by P.C. Tsopelas, M.C. Constantinou and A.M. Reinhorn, 4/12/94, (PB94-204922, A09, MF-A02).
- NCEER-94-0011 "The Northridge, California Earthquake of January 17, 1994: Performance of Gas Transmission Pipelines," by T.D. O'Rourke and M.C. Palmer, 5/16/94, (PB94-204989, A05, MF-A01).
- NCEER-94-0012 "Feasibility Study of Replacement Procedures and Earthquake Performance Related to Gas Transmission Pipelines," by T.D. O'Rourke and M.C. Palmer, 5/25/94, (PB94-206638, A09, MF-A02).
- NCEER-94-0013 "Seismic Energy Based Fatigue Damage Analysis of Bridge Columns: Part II - Evaluation of Seismic Demand," by G.A. Chang and J.B. Mander, 6/1/94, (PB95-18106, A08, MF-A02).
- NCEER-94-0014 "NCEER-Taisei Corporation Research Program on Sliding Seismic Isolation Systems for Bridges: Experimental and Analytical Study of a System Consisting of Sliding Bearings and Fluid Restoring Force/Damping Devices," by P. Tsopelas and M.C. Constantinou, 6/13/94, (PB94-219144, A10, MF-A03).
- NCEER-94-0015 "Generation of Hazard-Consistent Fragility Curves for Seismic Loss Estimation Studies," by H. Hwang and J-R. Huo, 6/14/94, (PB95-181996, A09, MF-A02).
- NCEER-94-0016 "Seismic Study of Building Frames with Added Energy-Absorbing Devices," by W.S. Pong, C.S. Tsai and G.C. Lee, 6/20/94, (PB94-219136, A10, A03).
- NCEER-94-0017 "Sliding Mode Control for Seismic-Excited Linear and Nonlinear Civil Engineering Structures," by J. Yang, J. Wu, A. Agrawal and Z. Li, 6/21/94, (PB95-138483, A06, MF-A02).
- NCEER-94-0018 "3D-BASIS-TABS Version 2.0: Computer Program for Nonlinear Dynamic Analysis of Three Dimensional Base Isolated Structures," by A.M. Reinhorn, S. Nagarajaiah, M.C. Constantinou, P. Tsopelas and R. Li, 6/22/94, (PB95-182176, A08, MF-A02).
- NCEER-94-0019 "Proceedings of the International Workshop on Civil Infrastructure Systems: Application of Intelligent Systems and Advanced Materials on Bridge Systems," Edited by G.C. Lee and K.C. Chang, 7/18/94, (PB95-252474, A20, MF-A04).
- NCEER-94-0020 "Study of Seismic Isolation Systems for Computer Floors," by V. Lambrou and M.C. Constantinou, 7/19/94, (PB95-138533, A10, MF-A03).
- NCEER-94-0021 "Proceedings of the U.S.-Italian Workshop on Guidelines for Seismic Evaluation and Rehabilitation of Unreinforced Masonry Buildings," Edited by D.P. Abrams and G.M. Calvi, 7/20/94, (PB95-138749, A13, MF-A03).
- NCEER-94-0022 "NCEER-Taisei Corporation Research Program on Sliding Seismic Isolation Systems for Bridges: Experimental and Analytical Study of a System Consisting of Lubricated PTFE Sliding Bearings and Mild Steel Dampers," by P. Tsopelas and M.C. Constantinou, 7/22/94, (PB95-182184, A08, MF-A02).
- NCEER-94-0023 "Development of Reliability-Based Design Criteria for Buildings Under Seismic Load," by Y.K. Wen, H. Hwang and M. Shinozuka, 8/1/94, (PB95-211934, A08, MF-A02).
- NCEER-94-0024 "Experimental Verification of Acceleration Feedback Control Strategies for an Active Tendon System," by S.J. Dyke, B.F. Spencer, Jr., P. Quast, M.K. Sain, D.C. Kaspari, Jr. and T.T. Soong, 8/29/94, (PB95-212320, A05, MF-A01).
- NCEER-94-0025 "Seismic Retrofitting Manual for Highway Bridges," Edited by I.G. Buckle and I.F. Friedland, published by the Federal Highway Administration (PB95-212676, A15, MF-A03).
- NCEER-94-0026 "Proceedings from the Fifth U.S.-Japan Workshop on Earthquake Resistant Design of Lifeline Facilities and Countermeasures Against Soil Liquefaction," Edited by T.D. O'Rourke and M. Hamada, 11/7/94, (PB95-220802, A99, MF-E08).

- NCEER-95-0001 “Experimental and Analytical Investigation of Seismic Retrofit of Structures with Supplemental Damping: Part 1 - Fluid Viscous Damping Devices,” by A.M. Reinhorn, C. Li and M.C. Constantinou, 1/3/95, (PB95-266599, A09, MF-A02).
- NCEER-95-0002 “Experimental and Analytical Study of Low-Cycle Fatigue Behavior of Semi-Rigid Top-And-Seat Angle Connections,” by G. Pekcan, J.B. Mander and S.S. Chen, 1/5/95, (PB95-220042, A07, MF-A02).
- NCEER-95-0003 “NCEER-ATC Joint Study on Fragility of Buildings,” by T. Anagnos, C. Rojahn and A.S. Kiremidjian, 1/20/95, (PB95-220026, A06, MF-A02).
- NCEER-95-0004 “Nonlinear Control Algorithms for Peak Response Reduction,” by Z. Wu, T.T. Soong, V. Gattulli and R.C. Lin, 2/16/95, (PB95-220349, A05, MF-A01).
- NCEER-95-0005 “Pipeline Replacement Feasibility Study: A Methodology for Minimizing Seismic and Corrosion Risks to Underground Natural Gas Pipelines,” by R.T. Eguchi, H.A. Seligson and D.G. Honegger, 3/2/95, (PB95-252326, A06, MF-A02).
- NCEER-95-0006 “Evaluation of Seismic Performance of an 11-Story Frame Building During the 1994 Northridge Earthquake,” by F. Naeim, R. DiSulio, K. Benuska, A. Reinhorn and C. Li, not available.
- NCEER-95-0007 “Prioritization of Bridges for Seismic Retrofitting,” by N. Basöz and A.S. Kiremidjian, 4/24/95, (PB95-252300, A08, MF-A02).
- NCEER-95-0008 “Method for Developing Motion Damage Relationships for Reinforced Concrete Frames,” by A. Singhal and A.S. Kiremidjian, 5/11/95, (PB95-266607, A06, MF-A02).
- NCEER-95-0009 “Experimental and Analytical Investigation of Seismic Retrofit of Structures with Supplemental Damping: Part II - Friction Devices,” by C. Li and A.M. Reinhorn, 7/6/95, (PB96-128087, A11, MF-A03).
- NCEER-95-0010 “Experimental Performance and Analytical Study of a Non-Ductile Reinforced Concrete Frame Structure Retrofitted with Elastomeric Spring Dampers,” by G. Pekcan, J.B. Mander and S.S. Chen, 7/14/95, (PB96-137161, A08, MF-A02).
- NCEER-95-0011 “Development and Experimental Study of Semi-Active Fluid Damping Devices for Seismic Protection of Structures,” by M.D. Symans and M.C. Constantinou, 8/3/95, (PB96-136940, A23, MF-A04).
- NCEER-95-0012 “Real-Time Structural Parameter Modification (RSPM): Development of Innervated Structures,” by Z. Liang, M. Tong and G.C. Lee, 4/11/95, (PB96-137153, A06, MF-A01).
- NCEER-95-0013 “Experimental and Analytical Investigation of Seismic Retrofit of Structures with Supplemental Damping: Part III - Viscous Damping Walls,” by A.M. Reinhorn and C. Li, 10/1/95, (PB96-176409, A11, MF-A03).
- NCEER-95-0014 “Seismic Fragility Analysis of Equipment and Structures in a Memphis Electric Substation,” by J-R. Huo and H.H.M. Hwang, 8/10/95, (PB96-128087, A09, MF-A02).
- NCEER-95-0015 “The Hanshin-Awaji Earthquake of January 17, 1995: Performance of Lifelines,” Edited by M. Shinozuka, 11/3/95, (PB96-176383, A15, MF-A03).
- NCEER-95-0016 “Highway Culvert Performance During Earthquakes,” by T.L. Youd and C.J. Beckman, available as NCEER-96-0015.
- NCEER-95-0017 “The Hanshin-Awaji Earthquake of January 17, 1995: Performance of Highway Bridges,” Edited by I.G. Buckle, 12/1/95, not available.
- NCEER-95-0018 “Modeling of Masonry Infill Panels for Structural Analysis,” by A.M. Reinhorn, A. Madan, R.E. Valles, Y. Reichmann and J.B. Mander, 12/8/95, (PB97-110886, MF-A01, A06).
- NCEER-95-0019 “Optimal Polynomial Control for Linear and Nonlinear Structures,” by A.K. Agrawal and J.N. Yang, 12/11/95, (PB96-168737, A07, MF-A02).

- NCEER-95-0020 “Retrofit of Non-Ductile Reinforced Concrete Frames Using Friction Dampers,” by R.S. Rao, P. Gergely and R.N. White, 12/22/95, (PB97-133508, A10, MF-A02).
- NCEER-95-0021 “Parametric Results for Seismic Response of Pile-Supported Bridge Bents,” by G. Mylonakis, A. Nikolaou and G. Gazetas, 12/22/95, (PB97-100242, A12, MF-A03).
- NCEER-95-0022 “Kinematic Bending Moments in Seismically Stressed Piles,” by A. Nikolaou, G. Mylonakis and G. Gazetas, 12/23/95, (PB97-113914, MF-A03, A13).
- NCEER-96-0001 “Dynamic Response of Unreinforced Masonry Buildings with Flexible Diaphragms,” by A.C. Costley and D.P. Abrams, 10/10/96, (PB97-133573, MF-A03, A15).
- NCEER-96-0002 “State of the Art Review: Foundations and Retaining Structures,” by I. Po Lam, not available.
- NCEER-96-0003 “Ductility of Rectangular Reinforced Concrete Bridge Columns with Moderate Confinement,” by N. Wehbe, M. Saiidi, D. Sanders and B. Douglas, 11/7/96, (PB97-133557, A06, MF-A02).
- NCEER-96-0004 “Proceedings of the Long-Span Bridge Seismic Research Workshop,” edited by I.G. Buckle and I.M. Friedland, not available.
- NCEER-96-0005 “Establish Representative Pier Types for Comprehensive Study: Eastern United States,” by J. Kulicki and Z. Prucz, 5/28/96, (PB98-119217, A07, MF-A02).
- NCEER-96-0006 “Establish Representative Pier Types for Comprehensive Study: Western United States,” by R. Imbsen, R.A. Schamber and T.A. Osterkamp, 5/28/96, (PB98-118607, A07, MF-A02).
- NCEER-96-0007 “Nonlinear Control Techniques for Dynamical Systems with Uncertain Parameters,” by R.G. Ghanem and M.I. Bujakov, 5/27/96, (PB97-100259, A17, MF-A03).
- NCEER-96-0008 “Seismic Evaluation of a 30-Year Old Non-Ductile Highway Bridge Pier and Its Retrofit,” by J.B. Mander, B. Mahmoodzadegan, S. Bhadra and S.S. Chen, 5/31/96, (PB97-110902, MF-A03, A10).
- NCEER-96-0009 “Seismic Performance of a Model Reinforced Concrete Bridge Pier Before and After Retrofit,” by J.B. Mander, J.H. Kim and C.A. Ligozio, 5/31/96, (PB97-110910, MF-A02, A10).
- NCEER-96-0010 “IDARC2D Version 4.0: A Computer Program for the Inelastic Damage Analysis of Buildings,” by R.E. Valles, A.M. Reinhorn, S.K. Kunnath, C. Li and A. Madan, 6/3/96, (PB97-100234, A17, MF-A03).
- NCEER-96-0011 “Estimation of the Economic Impact of Multiple Lifeline Disruption: Memphis Light, Gas and Water Division Case Study,” by S.E. Chang, H.A. Seligson and R.T. Eguchi, 8/16/96, (PB97-133490, A11, MF-A03).
- NCEER-96-0012 “Proceedings from the Sixth Japan-U.S. Workshop on Earthquake Resistant Design of Lifeline Facilities and Countermeasures Against Soil Liquefaction, Edited by M. Hamada and T. O’Rourke, 9/11/96, (PB97-133581, A99, MF-A06).
- NCEER-96-0013 “Chemical Hazards, Mitigation and Preparedness in Areas of High Seismic Risk: A Methodology for Estimating the Risk of Post-Earthquake Hazardous Materials Release,” by H.A. Seligson, R.T. Eguchi, K.J. Tierney and K. Richmond, 11/7/96, (PB97-133565, MF-A02, A08).
- NCEER-96-0014 “Response of Steel Bridge Bearings to Reversed Cyclic Loading,” by J.B. Mander, D-K. Kim, S.S. Chen and G.J. Premus, 11/13/96, (PB97-140735, A12, MF-A03).
- NCEER-96-0015 “Highway Culvert Performance During Past Earthquakes,” by T.L. Youd and C.J. Beckman, 11/25/96, (PB97-133532, A06, MF-A01).
- NCEER-97-0001 “Evaluation, Prevention and Mitigation of Pounding Effects in Building Structures,” by R.E. Valles and A.M. Reinhorn, 2/20/97, (PB97-159552, A14, MF-A03).
- NCEER-97-0002 “Seismic Design Criteria for Bridges and Other Highway Structures,” by C. Rojahn, R. Mayes, D.G. Anderson, J. Clark, J.H. Hom, R.V. Nutt and M.J. O’Rourke, 4/30/97, (PB97-194658, A06, MF-A03).

- NCEER-97-0003 "Proceedings of the U.S.-Italian Workshop on Seismic Evaluation and Retrofit," Edited by D.P. Abrams and G.M. Calvi, 3/19/97, (PB97-194666, A13, MF-A03).
- NCEER-97-0004 "Investigation of Seismic Response of Buildings with Linear and Nonlinear Fluid Viscous Dampers," by A.A. Seleemah and M.C. Constantinou, 5/21/97, (PB98-109002, A15, MF-A03).
- NCEER-97-0005 "Proceedings of the Workshop on Earthquake Engineering Frontiers in Transportation Facilities," edited by G.C. Lee and I.M. Friedland, 8/29/97, (PB98-128911, A25, MR-A04).
- NCEER-97-0006 "Cumulative Seismic Damage of Reinforced Concrete Bridge Piers," by S.K. Kunnath, A. El-Bahy, A. Taylor and W. Stone, 9/2/97, (PB98-108814, A11, MF-A03).
- NCEER-97-0007 "Structural Details to Accommodate Seismic Movements of Highway Bridges and Retaining Walls," by R.A. Imbsen, R.A. Schamber, E. Thorkildsen, A. Kartoum, B.T. Martin, T.N. Rosser and J.M. Kulicki, 9/3/97, (PB98-108996, A09, MF-A02).
- NCEER-97-0008 "A Method for Earthquake Motion-Damage Relationships with Application to Reinforced Concrete Frames," by A. Singhal and A.S. Kiremidjian, 9/10/97, (PB98-108988, A13, MF-A03).
- NCEER-97-0009 "Seismic Analysis and Design of Bridge Abutments Considering Sliding and Rotation," by K. Fishman and R. Richards, Jr., 9/15/97, (PB98-108897, A06, MF-A02).
- NCEER-97-0010 "Proceedings of the FHWA/NCEER Workshop on the National Representation of Seismic Ground Motion for New and Existing Highway Facilities," edited by I.M. Friedland, M.S. Power and R.L. Mayes, 9/22/97, (PB98-128903, A21, MF-A04).
- NCEER-97-0011 "Seismic Analysis for Design or Retrofit of Gravity Bridge Abutments," by K.L. Fishman, R. Richards, Jr. and R.C. Divito, 10/2/97, (PB98-128937, A08, MF-A02).
- NCEER-97-0012 "Evaluation of Simplified Methods of Analysis for Yielding Structures," by P. Tsopelas, M.C. Constantinou, C.A. Kircher and A.S. Whittaker, 10/31/97, (PB98-128929, A10, MF-A03).
- NCEER-97-0013 "Seismic Design of Bridge Columns Based on Control and Repairability of Damage," by C-T. Cheng and J.B. Mander, 12/8/97, (PB98-144249, A11, MF-A03).
- NCEER-97-0014 "Seismic Resistance of Bridge Piers Based on Damage Avoidance Design," by J.B. Mander and C-T. Cheng, 12/10/97, (PB98-144223, A09, MF-A02).
- NCEER-97-0015 "Seismic Response of Nominally Symmetric Systems with Strength Uncertainty," by S. Balopoulou and M. Grigoriu, 12/23/97, (PB98-153422, A11, MF-A03).
- NCEER-97-0016 "Evaluation of Seismic Retrofit Methods for Reinforced Concrete Bridge Columns," by T.J. Wipf, F.W. Klaiber and F.M. Russo, 12/28/97, (PB98-144215, A12, MF-A03).
- NCEER-97-0017 "Seismic Fragility of Existing Conventional Reinforced Concrete Highway Bridges," by C.L. Mullen and A.S. Cakmak, 12/30/97, (PB98-153406, A08, MF-A02).
- NCEER-97-0018 "Loss Assessment of Memphis Buildings," edited by D.P. Abrams and M. Shinozuka, 12/31/97, (PB98-144231, A13, MF-A03).
- NCEER-97-0019 "Seismic Evaluation of Frames with Infill Walls Using Quasi-static Experiments," by K.M. Mosalam, R.N. White and P. Gergely, 12/31/97, (PB98-153455, A07, MF-A02).
- NCEER-97-0020 "Seismic Evaluation of Frames with Infill Walls Using Pseudo-dynamic Experiments," by K.M. Mosalam, R.N. White and P. Gergely, 12/31/97, (PB98-153430, A07, MF-A02).
- NCEER-97-0021 "Computational Strategies for Frames with Infill Walls: Discrete and Smeared Crack Analyses and Seismic Fragility," by K.M. Mosalam, R.N. White and P. Gergely, 12/31/97, (PB98-153414, A10, MF-A02).

- NCEER-97-0022 "Proceedings of the NCEER Workshop on Evaluation of Liquefaction Resistance of Soils," edited by T.L. Youd and I.M. Idriss, 12/31/97, (PB98-155617, A15, MF-A03).
- MCEER-98-0001 "Extraction of Nonlinear Hysteretic Properties of Seismically Isolated Bridges from Quick-Release Field Tests," by Q. Chen, B.M. Douglas, E.M. Maragakis and I.G. Buckle, 5/26/98, (PB99-118838, A06, MF-A01).
- MCEER-98-0002 "Methodologies for Evaluating the Importance of Highway Bridges," by A. Thomas, S. Eshenaur and J. Kulicki, 5/29/98, (PB99-118846, A10, MF-A02).
- MCEER-98-0003 "Capacity Design of Bridge Piers and the Analysis of Overstrength," by J.B. Mander, A. Dutta and P. Goel, 6/1/98, (PB99-118853, A09, MF-A02).
- MCEER-98-0004 "Evaluation of Bridge Damage Data from the Loma Prieta and Northridge, California Earthquakes," by N. Basoz and A. Kiremidjian, 6/2/98, (PB99-118861, A15, MF-A03).
- MCEER-98-0005 "Screening Guide for Rapid Assessment of Liquefaction Hazard at Highway Bridge Sites," by T. L. Youd, 6/16/98, (PB99-118879, A06, not available on microfiche).
- MCEER-98-0006 "Structural Steel and Steel/Concrete Interface Details for Bridges," by P. Ritchie, N. Kaulh and J. Kulicki, 7/13/98, (PB99-118945, A06, MF-A01).
- MCEER-98-0007 "Capacity Design and Fatigue Analysis of Confined Concrete Columns," by A. Dutta and J.B. Mander, 7/14/98, (PB99-118960, A14, MF-A03).
- MCEER-98-0008 "Proceedings of the Workshop on Performance Criteria for Telecommunication Services Under Earthquake Conditions," edited by A.J. Schiff, 7/15/98, (PB99-118952, A08, MF-A02).
- MCEER-98-0009 "Fatigue Analysis of Unconfined Concrete Columns," by J.B. Mander, A. Dutta and J.H. Kim, 9/12/98, (PB99-123655, A10, MF-A02).
- MCEER-98-0010 "Centrifuge Modeling of Cyclic Lateral Response of Pile-Cap Systems and Seat-Type Abutments in Dry Sands," by A.D. Gadre and R. Dobry, 10/2/98, (PB99-123606, A13, MF-A03).
- MCEER-98-0011 "IDARC-BRIDGE: A Computational Platform for Seismic Damage Assessment of Bridge Structures," by A.M. Reinhorn, V. Simeonov, G. Mylonakis and Y. Reichman, 10/2/98, (PB99-162919, A15, MF-A03).
- MCEER-98-0012 "Experimental Investigation of the Dynamic Response of Two Bridges Before and After Retrofitting with Elastomeric Bearings," by D.A. Wendichansky, S.S. Chen and J.B. Mander, 10/2/98, (PB99-162927, A15, MF-A03).
- MCEER-98-0013 "Design Procedures for Hinge Restrainers and Hinge Sear Width for Multiple-Frame Bridges," by R. Des Roches and G.L. Fenves, 11/3/98, (PB99-140477, A13, MF-A03).
- MCEER-98-0014 "Response Modification Factors for Seismically Isolated Bridges," by M.C. Constantinou and J.K. Quarshie, 11/3/98, (PB99-140485, A14, MF-A03).
- MCEER-98-0015 "Proceedings of the U.S.-Italy Workshop on Seismic Protective Systems for Bridges," edited by I.M. Friedland and M.C. Constantinou, 11/3/98, (PB2000-101711, A22, MF-A04).
- MCEER-98-0016 "Appropriate Seismic Reliability for Critical Equipment Systems: Recommendations Based on Regional Analysis of Financial and Life Loss," by K. Porter, C. Scawthorn, C. Taylor and N. Blais, 11/10/98, (PB99-157265, A08, MF-A02).
- MCEER-98-0017 "Proceedings of the U.S. Japan Joint Seminar on Civil Infrastructure Systems Research," edited by M. Shinozuka and A. Rose, 11/12/98, (PB99-156713, A16, MF-A03).
- MCEER-98-0018 "Modeling of Pile Footings and Drilled Shafts for Seismic Design," by I. PoLam, M. Kapuskar and D. Chaudhuri, 12/21/98, (PB99-157257, A09, MF-A02).

- MCEER-99-0001 "Seismic Evaluation of a Masonry Infilled Reinforced Concrete Frame by Pseudodynamic Testing," by S.G. Buonopane and R.N. White, 2/16/99, (PB99-162851, A09, MF-A02).
- MCEER-99-0002 "Response History Analysis of Structures with Seismic Isolation and Energy Dissipation Systems: Verification Examples for Program SAP2000," by J. Scheller and M.C. Constantinou, 2/22/99, (PB99-162869, A08, MF-A02).
- MCEER-99-0003 "Experimental Study on the Seismic Design and Retrofit of Bridge Columns Including Axial Load Effects," by A. Dutta, T. Kokorina and J.B. Mander, 2/22/99, (PB99-162877, A09, MF-A02).
- MCEER-99-0004 "Experimental Study of Bridge Elastomeric and Other Isolation and Energy Dissipation Systems with Emphasis on Uplift Prevention and High Velocity Near-source Seismic Excitation," by A. Kasalanati and M. C. Constantinou, 2/26/99, (PB99-162885, A12, MF-A03).
- MCEER-99-0005 "Truss Modeling of Reinforced Concrete Shear-flexure Behavior," by J.H. Kim and J.B. Mander, 3/8/99, (PB99-163693, A12, MF-A03).
- MCEER-99-0006 "Experimental Investigation and Computational Modeling of Seismic Response of a 1:4 Scale Model Steel Structure with a Load Balancing Supplemental Damping System," by G. Pekcan, J.B. Mander and S.S. Chen, 4/2/99, (PB99-162893, A11, MF-A03).
- MCEER-99-0007 "Effect of Vertical Ground Motions on the Structural Response of Highway Bridges," by M.R. Button, C.J. Cronin and R.L. Mayes, 4/10/99, (PB2000-101411, A10, MF-A03).
- MCEER-99-0008 "Seismic Reliability Assessment of Critical Facilities: A Handbook, Supporting Documentation, and Model Code Provisions," by G.S. Johnson, R.E. Sheppard, M.D. Quilici, S.J. Eder and C.R. Scawthorn, 4/12/99, (PB2000-101701, A18, MF-A04).
- MCEER-99-0009 "Impact Assessment of Selected MCEER Highway Project Research on the Seismic Design of Highway Structures," by C. Rojahn, R. Mayes, D.G. Anderson, J.H. Clark, D'Appolonia Engineering, S. Gloyd and R.V. Nutt, 4/14/99, (PB99-162901, A10, MF-A02).
- MCEER-99-0010 "Site Factors and Site Categories in Seismic Codes," by R. Dobry, R. Ramos and M.S. Power, 7/19/99, (PB2000-101705, A08, MF-A02).
- MCEER-99-0011 "Restrainer Design Procedures for Multi-Span Simply-Supported Bridges," by M.J. Randall, M. Saiidi, E. Maragakis and T. Isakovic, 7/20/99, (PB2000-101702, A10, MF-A02).
- MCEER-99-0012 "Property Modification Factors for Seismic Isolation Bearings," by M.C. Constantinou, P. Tsopelas, A. Kasalanati and E. Wolff, 7/20/99, (PB2000-103387, A11, MF-A03).
- MCEER-99-0013 "Critical Seismic Issues for Existing Steel Bridges," by P. Ritchie, N. Kauh and J. Kulicki, 7/20/99, (PB2000-101697, A09, MF-A02).
- MCEER-99-0014 "Nonstructural Damage Database," by A. Kao, T.T. Soong and A. Vender, 7/24/99, (PB2000-101407, A06, MF-A01).
- MCEER-99-0015 "Guide to Remedial Measures for Liquefaction Mitigation at Existing Highway Bridge Sites," by H.G. Cooke and J. K. Mitchell, 7/26/99, (PB2000-101703, A11, MF-A03).
- MCEER-99-0016 "Proceedings of the MCEER Workshop on Ground Motion Methodologies for the Eastern United States," edited by N. Abrahamson and A. Becker, 8/11/99, (PB2000-103385, A07, MF-A02).
- MCEER-99-0017 "Quindío, Colombia Earthquake of January 25, 1999: Reconnaissance Report," by A.P. Asfura and P.J. Flores, 10/4/99, (PB2000-106893, A06, MF-A01).
- MCEER-99-0018 "Hysteretic Models for Cyclic Behavior of Deteriorating Inelastic Structures," by M.V. Sivaselvan and A.M. Reinhorn, 11/5/99, (PB2000-103386, A08, MF-A02).

- MCEER-99-0019 "Proceedings of the 7th U.S.- Japan Workshop on Earthquake Resistant Design of Lifeline Facilities and Countermeasures Against Soil Liquefaction," edited by T.D. O'Rourke, J.P. Bardet and M. Hamada, 11/19/99, (PB2000-103354, A99, MF-A06).
- MCEER-99-0020 "Development of Measurement Capability for Micro-Vibration Evaluations with Application to Chip Fabrication Facilities," by G.C. Lee, Z. Liang, J.W. Song, J.D. Shen and W.C. Liu, 12/1/99, (PB2000-105993, A08, MF-A02).
- MCEER-99-0021 "Design and Retrofit Methodology for Building Structures with Supplemental Energy Dissipating Systems," by G. Pekcan, J.B. Mander and S.S. Chen, 12/31/99, (PB2000-105994, A11, MF-A03).
- MCEER-00-0001 "The Marmara, Turkey Earthquake of August 17, 1999: Reconnaissance Report," edited by C. Scawthorn; with major contributions by M. Bruneau, R. Eguchi, T. Holzer, G. Johnson, J. Mander, J. Mitchell, W. Mitchell, A. Papageorgiou, C. Scaethorn, and G. Webb, 3/23/00, (PB2000-106200, A11, MF-A03).
- MCEER-00-0002 "Proceedings of the MCEER Workshop for Seismic Hazard Mitigation of Health Care Facilities," edited by G.C. Lee, M. Ettouney, M. Grigoriu, J. Hauer and J. Nigg, 3/29/00, (PB2000-106892, A08, MF-A02).
- MCEER-00-0003 "The Chi-Chi, Taiwan Earthquake of September 21, 1999: Reconnaissance Report," edited by G.C. Lee and C.H. Loh, with major contributions by G.C. Lee, M. Bruneau, I.G. Buckle, S.E. Chang, P.J. Flores, T.D. O'Rourke, M. Shinozuka, T.T. Soong, C-H. Loh, K-C. Chang, Z-J. Chen, J-S. Hwang, M-L. Lin, G-Y. Liu, K-C. Tsai, G.C. Yao and C-L. Yen, 4/30/00, (PB2001-100980, A10, MF-A02).
- MCEER-00-0004 "Seismic Retrofit of End-Sway Frames of Steel Deck-Truss Bridges with a Supplemental Tendon System: Experimental and Analytical Investigation," by G. Pekcan, J.B. Mander and S.S. Chen, 7/1/00, (PB2001-100982, A10, MF-A02).
- MCEER-00-0005 "Sliding Fragility of Unrestrained Equipment in Critical Facilities," by W.H. Chong and T.T. Soong, 7/5/00, (PB2001-100983, A08, MF-A02).
- MCEER-00-0006 "Seismic Response of Reinforced Concrete Bridge Pier Walls in the Weak Direction," by N. Abo-Shadi, M. Saiidi and D. Sanders, 7/17/00, (PB2001-100981, A17, MF-A03).
- MCEER-00-0007 "Low-Cycle Fatigue Behavior of Longitudinal Reinforcement in Reinforced Concrete Bridge Columns," by J. Brown and S.K. Kunnath, 7/23/00, (PB2001-104392, A08, MF-A02).
- MCEER-00-0008 "Soil Structure Interaction of Bridges for Seismic Analysis," I. PoLam and H. Law, 9/25/00, (PB2001-105397, A08, MF-A02).
- MCEER-00-0009 "Proceedings of the First MCEER Workshop on Mitigation of Earthquake Disaster by Advanced Technologies (MEDAT-1), edited by M. Shinozuka, D.J. Inman and T.D. O'Rourke, 11/10/00, (PB2001-105399, A14, MF-A03).
- MCEER-00-0010 "Development and Evaluation of Simplified Procedures for Analysis and Design of Buildings with Passive Energy Dissipation Systems, Revision 01," by O.M. Ramirez, M.C. Constantinou, C.A. Kircher, A.S. Whittaker, M.W. Johnson, J.D. Gomez and C. Chrysostomou, 11/16/01, (PB2001-105523, A23, MF-A04).
- MCEER-00-0011 "Dynamic Soil-Foundation-Structure Interaction Analyses of Large Caissons," by C-Y. Chang, C-M. Mok, Z-L. Wang, R. Settgast, F. Waggoner, M.A. Ketchum, H.M. Gonnermann and C-C. Chin, 12/30/00, (PB2001-104373, A07, MF-A02).
- MCEER-00-0012 "Experimental Evaluation of Seismic Performance of Bridge Restrainers," by A.G. Vlassis, E.M. Maragakis and M. Saiid Saiidi, 12/30/00, (PB2001-104354, A09, MF-A02).
- MCEER-00-0013 "Effect of Spatial Variation of Ground Motion on Highway Structures," by M. Shinozuka, V. Saxena and G. Deodatis, 12/31/00, (PB2001-108755, A13, MF-A03).
- MCEER-00-0014 "A Risk-Based Methodology for Assessing the Seismic Performance of Highway Systems," by S.D. Werner, C.E. Taylor, J.E. Moore, II, J.S. Walton and S. Cho, 12/31/00, (PB2001-108756, A14, MF-A03).

- MCEER-01-0001 “Experimental Investigation of P-Delta Effects to Collapse During Earthquakes,” by D. Vian and M. Bruneau, 6/25/01, (PB2002-100534, A17, MF-A03).
- MCEER-01-0002 “Proceedings of the Second MCEER Workshop on Mitigation of Earthquake Disaster by Advanced Technologies (MEDAT-2),” edited by M. Bruneau and D.J. Inman, 7/23/01, (PB2002-100434, A16, MF-A03).
- MCEER-01-0003 “Sensitivity Analysis of Dynamic Systems Subjected to Seismic Loads,” by C. Roth and M. Grigoriu, 9/18/01, (PB2003-100884, A12, MF-A03).
- MCEER-01-0004 “Overcoming Obstacles to Implementing Earthquake Hazard Mitigation Policies: Stage 1 Report,” by D.J. Alesch and W.J. Petak, 12/17/01, (PB2002-107949, A07, MF-A02).
- MCEER-01-0005 “Updating Real-Time Earthquake Loss Estimates: Methods, Problems and Insights,” by C.E. Taylor, S.E. Chang and R.T. Eguchi, 12/17/01, (PB2002-107948, A05, MF-A01).
- MCEER-01-0006 “Experimental Investigation and Retrofit of Steel Pile Foundations and Pile Bents Under Cyclic Lateral Loadings,” by A. Shama, J. Mander, B. Blabac and S. Chen, 12/31/01, (PB2002-107950, A13, MF-A03).
- MCEER-02-0001 “Assessment of Performance of Bolu Viaduct in the 1999 Duzce Earthquake in Turkey” by P.C. Roussis, M.C. Constantinou, M. Erdik, E. Durukal and M. Dicleli, 5/8/02, (PB2003-100883, A08, MF-A02).
- MCEER-02-0002 “Seismic Behavior of Rail Counterweight Systems of Elevators in Buildings,” by M.P. Singh, Rildova and L.E. Suarez, 5/27/02. (PB2003-100882, A11, MF-A03).
- MCEER-02-0003 “Development of Analysis and Design Procedures for Spread Footings,” by G. Mylonakis, G. Gazetas, S. Nikolaou and A. Chauncey, 10/02/02, (PB2004-101636, A13, MF-A03, CD-A13).
- MCEER-02-0004 “Bare-Earth Algorithms for Use with SAR and LIDAR Digital Elevation Models,” by C.K. Huyck, R.T. Eguchi and B. Houshmand, 10/16/02, (PB2004-101637, A07, CD-A07).
- MCEER-02-0005 “Review of Energy Dissipation of Compression Members in Concentrically Braced Frames,” by K.Lee and M. Bruneau, 10/18/02, (PB2004-101638, A10, CD-A10).
- MCEER-03-0001 “Experimental Investigation of Light-Gauge Steel Plate Shear Walls for the Seismic Retrofit of Buildings” by J. Berman and M. Bruneau, 5/2/03, (PB2004-101622, A10, MF-A03, CD-A10).
- MCEER-03-0002 “Statistical Analysis of Fragility Curves,” by M. Shinozuka, M.Q. Feng, H. Kim, T. Uzawa and T. Ueda, 6/16/03, (PB2004-101849, A09, CD-A09).
- MCEER-03-0003 “Proceedings of the Eighth U.S.-Japan Workshop on Earthquake Resistant Design of Lifeline Facilities and Countermeasures Against Liquefaction,” edited by M. Hamada, J.P. Bardet and T.D. O’Rourke, 6/30/03, (PB2004-104386, A99, CD-A99).
- MCEER-03-0004 “Proceedings of the PRC-US Workshop on Seismic Analysis and Design of Special Bridges,” edited by L.C. Fan and G.C. Lee, 7/15/03, (PB2004-104387, A14, CD-A14).
- MCEER-03-0005 “Urban Disaster Recovery: A Framework and Simulation Model,” by S.B. Miles and S.E. Chang, 7/25/03, (PB2004-104388, A07, CD-A07).
- MCEER-03-0006 “Behavior of Underground Piping Joints Due to Static and Dynamic Loading,” by R.D. Meis, M. Maragakis and R. Siddharthan, 11/17/03, (PB2005-102194, A13, MF-A03, CD-A00).
- MCEER-04-0001 “Experimental Study of Seismic Isolation Systems with Emphasis on Secondary System Response and Verification of Accuracy of Dynamic Response History Analysis Methods,” by E. Wolff and M. Constantinou, 1/16/04 (PB2005-102195, A99, MF-E08, CD-A00).
- MCEER-04-0002 “Tension, Compression and Cyclic Testing of Engineered Cementitious Composite Materials,” by K. Kesner and S.L. Billington, 3/1/04, (PB2005-102196, A08, CD-A08).

- MCEER-04-0003 "Cyclic Testing of Braces Laterally Restrained by Steel Studs to Enhance Performance During Earthquakes," by O.C. Celik, J.W. Berman and M. Bruneau, 3/16/04, (PB2005-102197, A13, MF-A03, CD-A00).
- MCEER-04-0004 "Methodologies for Post Earthquake Building Damage Detection Using SAR and Optical Remote Sensing: Application to the August 17, 1999 Marmara, Turkey Earthquake," by C.K. Huyck, B.J. Adams, S. Cho, R.T. Eguchi, B. Mansouri and B. Houshmand, 6/15/04, (PB2005-104888, A10, CD-A00).
- MCEER-04-0005 "Nonlinear Structural Analysis Towards Collapse Simulation: A Dynamical Systems Approach," by M.V. Sivaselvan and A.M. Reinhorn, 6/16/04, (PB2005-104889, A11, MF-A03, CD-A00).
- MCEER-04-0006 "Proceedings of the Second PRC-US Workshop on Seismic Analysis and Design of Special Bridges," edited by G.C. Lee and L.C. Fan, 6/25/04, (PB2005-104890, A16, CD-A00).
- MCEER-04-0007 "Seismic Vulnerability Evaluation of Axially Loaded Steel Built-up Laced Members," by K. Lee and M. Bruneau, 6/30/04, (PB2005-104891, A16, CD-A00).
- MCEER-04-0008 "Evaluation of Accuracy of Simplified Methods of Analysis and Design of Buildings with Damping Systems for Near-Fault and for Soft-Soil Seismic Motions," by E.A. Pavlou and M.C. Constantinou, 8/16/04, (PB2005-104892, A08, MF-A02, CD-A00).
- MCEER-04-0009 "Assessment of Geotechnical Issues in Acute Care Facilities in California," by M. Lew, T.D. O'Rourke, R. Dobry and M. Koch, 9/15/04, (PB2005-104893, A08, CD-A00).
- MCEER-04-0010 "Scissor-Jack-Damper Energy Dissipation System," by A.N. Sigaher-Boyle and M.C. Constantinou, 12/1/04 (PB2005-108221).
- MCEER-04-0011 "Seismic Retrofit of Bridge Steel Truss Piers Using a Controlled Rocking Approach," by M. Pollino and M. Bruneau, 12/20/04 (PB2006-105795).
- MCEER-05-0001 "Experimental and Analytical Studies of Structures Seismically Isolated with an Uplift-Restraint Isolation System," by P.C. Roussis and M.C. Constantinou, 1/10/05 (PB2005-108222).
- MCEER-05-0002 "A Versatile Experimentation Model for Study of Structures Near Collapse Applied to Seismic Evaluation of Irregular Structures," by D. Kusumastuti, A.M. Reinhorn and A. Rutenberg, 3/31/05 (PB2006-101523).
- MCEER-05-0003 "Proceedings of the Third PRC-US Workshop on Seismic Analysis and Design of Special Bridges," edited by L.C. Fan and G.C. Lee, 4/20/05, (PB2006-105796).
- MCEER-05-0004 "Approaches for the Seismic Retrofit of Braced Steel Bridge Piers and Proof-of-Concept Testing of an Eccentrically Braced Frame with Tubular Link," by J.W. Berman and M. Bruneau, 4/21/05 (PB2006-101524).
- MCEER-05-0005 "Simulation of Strong Ground Motions for Seismic Fragility Evaluation of Nonstructural Components in Hospitals," by A. Wanitkorkul and A. Filiatrault, 5/26/05 (PB2006-500027).
- MCEER-05-0006 "Seismic Safety in California Hospitals: Assessing an Attempt to Accelerate the Replacement or Seismic Retrofit of Older Hospital Facilities," by D.J. Alesch, L.A. Arendt and W.J. Petak, 6/6/05 (PB2006-105794).
- MCEER-05-0007 "Development of Seismic Strengthening and Retrofit Strategies for Critical Facilities Using Engineered Cementitious Composite Materials," by K. Kesner and S.L. Billington, 8/29/05 (PB2006-111701).
- MCEER-05-0008 "Experimental and Analytical Studies of Base Isolation Systems for Seismic Protection of Power Transformers," by N. Murota, M.Q. Feng and G-Y. Liu, 9/30/05 (PB2006-111702).
- MCEER-05-0009 "3D-BASIS-ME-MB: Computer Program for Nonlinear Dynamic Analysis of Seismically Isolated Structures," by P.C. Tsopelas, P.C. Roussis, M.C. Constantinou, R. Buchanan and A.M. Reinhorn, 10/3/05 (PB2006-111703).
- MCEER-05-0010 "Steel Plate Shear Walls for Seismic Design and Retrofit of Building Structures," by D. Vian and M. Bruneau, 12/15/05 (PB2006-111704).

- MCEER-05-0011 "The Performance-Based Design Paradigm," by M.J. Astrella and A. Whittaker, 12/15/05 (PB2006-111705).
- MCEER-06-0001 "Seismic Fragility of Suspended Ceiling Systems," H. Badillo-Almaraz, A.S. Whittaker, A.M. Reinhorn and G.P. Cimellaro, 2/4/06 (PB2006-111706).
- MCEER-06-0002 "Multi-Dimensional Fragility of Structures," by G.P. Cimellaro, A.M. Reinhorn and M. Bruneau, 3/1/06 (PB2007-106974, A09, MF-A02, CD A00).
- MCEER-06-0003 "Built-Up Shear Links as Energy Dissipators for Seismic Protection of Bridges," by P. Dusicka, A.M. Itani and I.G. Buckle, 3/15/06 (PB2006-111708).
- MCEER-06-0004 "Analytical Investigation of the Structural Fuse Concept," by R.E. Vargas and M. Bruneau, 3/16/06 (PB2006-111709).
- MCEER-06-0005 "Experimental Investigation of the Structural Fuse Concept," by R.E. Vargas and M. Bruneau, 3/17/06 (PB2006-111710).
- MCEER-06-0006 "Further Development of Tubular Eccentrically Braced Frame Links for the Seismic Retrofit of Braced Steel Truss Bridge Piers," by J.W. Berman and M. Bruneau, 3/27/06 (PB2007-105147).
- MCEER-06-0007 "REDARS Validation Report," by S. Cho, C.K. Huyck, S. Ghosh and R.T. Eguchi, 8/8/06 (PB2007-106983).
- MCEER-06-0008 "Review of Current NDE Technologies for Post-Earthquake Assessment of Retrofitted Bridge Columns," by J.W. Song, Z. Liang and G.C. Lee, 8/21/06 (PB2007-106984).
- MCEER-06-0009 "Liquefaction Remediation in Silty Soils Using Dynamic Compaction and Stone Columns," by S. Thevanayagam, G.R. Martin, R. Nashed, T. Shenthan, T. Kanagalingam and N. Ecemis, 8/28/06 (PB2007-106985).
- MCEER-06-0010 "Conceptual Design and Experimental Investigation of Polymer Matrix Composite Infill Panels for Seismic Retrofitting," by W. Jung, M. Chiewanichakorn and A.J. Aref, 9/21/06 (PB2007-106986).
- MCEER-06-0011 "A Study of the Coupled Horizontal-Vertical Behavior of Elastomeric and Lead-Rubber Seismic Isolation Bearings," by G.P. Warn and A.S. Whittaker, 9/22/06 (PB2007-108679).
- MCEER-06-0012 "Proceedings of the Fourth PRC-US Workshop on Seismic Analysis and Design of Special Bridges: Advancing Bridge Technologies in Research, Design, Construction and Preservation," Edited by L.C. Fan, G.C. Lee and L. Ziang, 10/12/06 (PB2007-109042).
- MCEER-06-0013 "Cyclic Response and Low Cycle Fatigue Characteristics of Plate Steels," by P. Dusicka, A.M. Itani and I.G. Buckle, 11/1/06 (PB2007-106987).
- MCEER-06-0014 "Proceedings of the Second US-Taiwan Bridge Engineering Workshop," edited by W.P. Yen, J. Shen, J-Y. Chen and M. Wang, 11/15/06 (PB2008-500041).
- MCEER-06-0015 "User Manual and Technical Documentation for the REDARSTM Import Wizard," by S. Cho, S. Ghosh, C.K. Huyck and S.D. Werner, 11/30/06 (PB2007-114766).
- MCEER-06-0016 "Hazard Mitigation Strategy and Monitoring Technologies for Urban and Infrastructure Public Buildings: Proceedings of the China-US Workshops," edited by X.Y. Zhou, A.L. Zhang, G.C. Lee and M. Tong, 12/12/06 (PB2008-500018).
- MCEER-07-0001 "Static and Kinetic Coefficients of Friction for Rigid Blocks," by C. Kafali, S. Fathali, M. Grigoriu and A.S. Whittaker, 3/20/07 (PB2007-114767).
- MCEER-07-0002 "Hazard Mitigation Investment Decision Making: Organizational Response to Legislative Mandate," by L.A. Arendt, D.J. Alesch and W.J. Petak, 4/9/07 (PB2007-114768).
- MCEER-07-0003 "Seismic Behavior of Bidirectional-Resistant Ductile End Diaphragms with Unbonded Braces in Straight or Skewed Steel Bridges," by O. Celik and M. Bruneau, 4/11/07 (PB2008-105141).

- MCEER-07-0004 “Modeling Pile Behavior in Large Pile Groups Under Lateral Loading,” by A.M. Dodds and G.R. Martin, 4/16/07(PB2008-105142).
- MCEER-07-0005 “Experimental Investigation of Blast Performance of Seismically Resistant Concrete-Filled Steel Tube Bridge Piers,” by S. Fujikura, M. Bruneau and D. Lopez-Garcia, 4/20/07 (PB2008-105143).
- MCEER-07-0006 “Seismic Analysis of Conventional and Isolated Liquefied Natural Gas Tanks Using Mechanical Analogs,” by I.P. Christovasilis and A.S. Whittaker, 5/1/07, not available.
- MCEER-07-0007 “Experimental Seismic Performance Evaluation of Isolation/Restraint Systems for Mechanical Equipment – Part 1: Heavy Equipment Study,” by S. Fathali and A. Filiatrault, 6/6/07 (PB2008-105144).
- MCEER-07-0008 “Seismic Vulnerability of Timber Bridges and Timber Substructures,” by A.A. Sharma, J.B. Mander, I.M. Friedland and D.R. Allicock, 6/7/07 (PB2008-105145).
- MCEER-07-0009 “Experimental and Analytical Study of the XY-Friction Pendulum (XY-FP) Bearing for Bridge Applications,” by C.C. Marin-Artieda, A.S. Whittaker and M.C. Constantinou, 6/7/07 (PB2008-105191).
- MCEER-07-0010 “Proceedings of the PRC-US Earthquake Engineering Forum for Young Researchers,” Edited by G.C. Lee and X.Z. Qi, 6/8/07 (PB2008-500058).
- MCEER-07-0011 “Design Recommendations for Perforated Steel Plate Shear Walls,” by R. Purba and M. Bruneau, 6/18/07, (PB2008-105192).
- MCEER-07-0012 “Performance of Seismic Isolation Hardware Under Service and Seismic Loading,” by M.C. Constantinou, A.S. Whittaker, Y. Kalpakidis, D.M. Fenz and G.P. Warn, 8/27/07, (PB2008-105193).
- MCEER-07-0013 “Experimental Evaluation of the Seismic Performance of Hospital Piping Subassemblies,” by E.R. Goodwin, E. Maragakis and A.M. Itani, 9/4/07, (PB2008-105194).
- MCEER-07-0014 “A Simulation Model of Urban Disaster Recovery and Resilience: Implementation for the 1994 Northridge Earthquake,” by S. Miles and S.E. Chang, 9/7/07, (PB2008-106426).
- MCEER-07-0015 “Statistical and Mechanistic Fragility Analysis of Concrete Bridges,” by M. Shinozuka, S. Banerjee and S-H. Kim, 9/10/07, (PB2008-106427).
- MCEER-07-0016 “Three-Dimensional Modeling of Inelastic Buckling in Frame Structures,” by M. Schachter and AM. Reinhorn, 9/13/07, (PB2008-108125).
- MCEER-07-0017 “Modeling of Seismic Wave Scattering on Pile Groups and Caissons,” by I. Po Lam, H. Law and C.T. Yang, 9/17/07 (PB2008-108150).
- MCEER-07-0018 “Bridge Foundations: Modeling Large Pile Groups and Caissons for Seismic Design,” by I. Po Lam, H. Law and G.R. Martin (Coordinating Author), 12/1/07 (PB2008-111190).
- MCEER-07-0019 “Principles and Performance of Roller Seismic Isolation Bearings for Highway Bridges,” by G.C. Lee, Y.C. Ou, Z. Liang, T.C. Niu and J. Song, 12/10/07 (PB2009-110466).
- MCEER-07-0020 “Centrifuge Modeling of Permeability and Pinning Reinforcement Effects on Pile Response to Lateral Spreading,” by L.L Gonzalez-Lagos, T. Abdoun and R. Dobry, 12/10/07 (PB2008-111191).
- MCEER-07-0021 “Damage to the Highway System from the Pisco, Perú Earthquake of August 15, 2007,” by J.S. O’Connor, L. Mesa and M. Nykamp, 12/10/07, (PB2008-108126).
- MCEER-07-0022 “Experimental Seismic Performance Evaluation of Isolation/Restraint Systems for Mechanical Equipment – Part 2: Light Equipment Study,” by S. Fathali and A. Filiatrault, 12/13/07 (PB2008-111192).
- MCEER-07-0023 “Fragility Considerations in Highway Bridge Design,” by M. Shinozuka, S. Banerjee and S.H. Kim, 12/14/07 (PB2008-111193).

- MCEER-07-0024 "Performance Estimates for Seismically Isolated Bridges," by G.P. Warn and A.S. Whittaker, 12/30/07 (PB2008-112230).
- MCEER-08-0001 "Seismic Performance of Steel Girder Bridge Superstructures with Conventional Cross Frames," by L.P. Carden, A.M. Itani and I.G. Buckle, 1/7/08, (PB2008-112231).
- MCEER-08-0002 "Seismic Performance of Steel Girder Bridge Superstructures with Ductile End Cross Frames with Seismic Isolators," by L.P. Carden, A.M. Itani and I.G. Buckle, 1/7/08 (PB2008-112232).
- MCEER-08-0003 "Analytical and Experimental Investigation of a Controlled Rocking Approach for Seismic Protection of Bridge Steel Truss Piers," by M. Pollino and M. Bruneau, 1/21/08 (PB2008-112233).
- MCEER-08-0004 "Linking Lifeline Infrastructure Performance and Community Disaster Resilience: Models and Multi-Stakeholder Processes," by S.E. Chang, C. Pasion, K. Tatebe and R. Ahmad, 3/3/08 (PB2008-112234).
- MCEER-08-0005 "Modal Analysis of Generally Damped Linear Structures Subjected to Seismic Excitations," by J. Song, Y-L. Chu, Z. Liang and G.C. Lee, 3/4/08 (PB2009-102311).
- MCEER-08-0006 "System Performance Under Multi-Hazard Environments," by C. Kafali and M. Grigoriu, 3/4/08 (PB2008-112235).
- MCEER-08-0007 "Mechanical Behavior of Multi-Spherical Sliding Bearings," by D.M. Fenz and M.C. Constantinou, 3/6/08 (PB2008-112236).
- MCEER-08-0008 "Post-Earthquake Restoration of the Los Angeles Water Supply System," by T.H.P. Tabucchi and R.A. Davidson, 3/7/08 (PB2008-112237).
- MCEER-08-0009 "Fragility Analysis of Water Supply Systems," by A. Jacobson and M. Grigoriu, 3/10/08 (PB2009-105545).
- MCEER-08-0010 "Experimental Investigation of Full-Scale Two-Story Steel Plate Shear Walls with Reduced Beam Section Connections," by B. Qu, M. Bruneau, C-H. Lin and K-C. Tsai, 3/17/08 (PB2009-106368).
- MCEER-08-0011 "Seismic Evaluation and Rehabilitation of Critical Components of Electrical Power Systems," S. Ersoy, B. Feizi, A. Ashrafi and M. Ala Saadeghvaziri, 3/17/08 (PB2009-105546).
- MCEER-08-0012 "Seismic Behavior and Design of Boundary Frame Members of Steel Plate Shear Walls," by B. Qu and M. Bruneau, 4/26/08 . (PB2009-106744).
- MCEER-08-0013 "Development and Appraisal of a Numerical Cyclic Loading Protocol for Quantifying Building System Performance," by A. Filiatrault, A. Wanitkorkul and M. Constantinou, 4/27/08 (PB2009-107906).
- MCEER-08-0014 "Structural and Nonstructural Earthquake Design: The Challenge of Integrating Specialty Areas in Designing Complex, Critical Facilities," by W.J. Petak and D.J. Alesch, 4/30/08 (PB2009-107907).
- MCEER-08-0015 "Seismic Performance Evaluation of Water Systems," by Y. Wang and T.D. O'Rourke, 5/5/08 (PB2009-107908).
- MCEER-08-0016 "Seismic Response Modeling of Water Supply Systems," by P. Shi and T.D. O'Rourke, 5/5/08 (PB2009-107910).
- MCEER-08-0017 "Numerical and Experimental Studies of Self-Centering Post-Tensioned Steel Frames," by D. Wang and A. Filiatrault, 5/12/08 (PB2009-110479).
- MCEER-08-0018 "Development, Implementation and Verification of Dynamic Analysis Models for Multi-Spherical Sliding Bearings," by D.M. Fenz and M.C. Constantinou, 8/15/08 (PB2009-107911).
- MCEER-08-0019 "Performance Assessment of Conventional and Base Isolated Nuclear Power Plants for Earthquake Blast Loadings," by Y.N. Huang, A.S. Whittaker and N. Luco, 10/28/08 (PB2009-107912).

- MCEER-08-0020 “Remote Sensing for Resilient Multi-Hazard Disaster Response – Volume I: Introduction to Damage Assessment Methodologies,” by B.J. Adams and R.T. Eguchi, 11/17/08 (PB2010-102695).
- MCEER-08-0021 “Remote Sensing for Resilient Multi-Hazard Disaster Response – Volume II: Counting the Number of Collapsed Buildings Using an Object-Oriented Analysis: Case Study of the 2003 Bam Earthquake,” by L. Gusella, C.K. Huyck and B.J. Adams, 11/17/08 (PB2010-100925).
- MCEER-08-0022 “Remote Sensing for Resilient Multi-Hazard Disaster Response – Volume III: Multi-Sensor Image Fusion Techniques for Robust Neighborhood-Scale Urban Damage Assessment,” by B.J. Adams and A. McMillan, 11/17/08 (PB2010-100926).
- MCEER-08-0023 “Remote Sensing for Resilient Multi-Hazard Disaster Response – Volume IV: A Study of Multi-Temporal and Multi-Resolution SAR Imagery for Post-Katrina Flood Monitoring in New Orleans,” by A. McMillan, J.G. Morley, B.J. Adams and S. Chesworth, 11/17/08 (PB2010-100927).
- MCEER-08-0024 “Remote Sensing for Resilient Multi-Hazard Disaster Response – Volume V: Integration of Remote Sensing Imagery and VIEWS™ Field Data for Post-Hurricane Charley Building Damage Assessment,” by J.A. Womble, K. Mehta and B.J. Adams, 11/17/08 (PB2009-115532).
- MCEER-08-0025 “Building Inventory Compilation for Disaster Management: Application of Remote Sensing and Statistical Modeling,” by P. Sarabandi, A.S. Kiremidjian, R.T. Eguchi and B. J. Adams, 11/20/08 (PB2009-110484).
- MCEER-08-0026 “New Experimental Capabilities and Loading Protocols for Seismic Qualification and Fragility Assessment of Nonstructural Systems,” by R. Retamales, G. Mosqueda, A. Filiatrault and A. Reinhorn, 11/24/08 (PB2009-110485).
- MCEER-08-0027 “Effects of Heating and Load History on the Behavior of Lead-Rubber Bearings,” by I.V. Kalpakidis and M.C. Constantinou, 12/1/08 (PB2009-115533).
- MCEER-08-0028 “Experimental and Analytical Investigation of Blast Performance of Seismically Resistant Bridge Piers,” by S.Fujikura and M. Bruneau, 12/8/08 (PB2009-115534).
- MCEER-08-0029 “Evolutionary Methodology for Aseismic Decision Support,” by Y. Hu and G. Dargush, 12/15/08.
- MCEER-08-0030 “Development of a Steel Plate Shear Wall Bridge Pier System Conceived from a Multi-Hazard Perspective,” by D. Keller and M. Bruneau, 12/19/08 (PB2010-102696).
- MCEER-09-0001 “Modal Analysis of Arbitrarily Damped Three-Dimensional Linear Structures Subjected to Seismic Excitations,” by Y.L. Chu, J. Song and G.C. Lee, 1/31/09 (PB2010-100922).
- MCEER-09-0002 “Air-Blast Effects on Structural Shapes,” by G. Ballantyne, A.S. Whittaker, A.J. Aref and G.F. Dargush, 2/2/09 (PB2010-102697).
- MCEER-09-0003 “Water Supply Performance During Earthquakes and Extreme Events,” by A.L. Bonneau and T.D. O’Rourke, 2/16/09 (PB2010-100923).
- MCEER-09-0004 “Generalized Linear (Mixed) Models of Post-Earthquake Ignitions,” by R.A. Davidson, 7/20/09 (PB2010-102698).
- MCEER-09-0005 “Seismic Testing of a Full-Scale Two-Story Light-Frame Wood Building: NEESWood Benchmark Test,” by I.P. Christovasilis, A. Filiatrault and A. Wanitkorkul, 7/22/09 (PB2012-102401).
- MCEER-09-0006 “IDARC2D Version 7.0: A Program for the Inelastic Damage Analysis of Structures,” by A.M. Reinhorn, H. Roh, M. Sivaselvan, S.K. Kunnath, R.E. Valles, A. Madan, C. Li, R. Lobo and Y.J. Park, 7/28/09 (PB2010-103199).
- MCEER-09-0007 “Enhancements to Hospital Resiliency: Improving Emergency Planning for and Response to Hurricanes,” by D.B. Hess and L.A. Arendt, 7/30/09 (PB2010-100924).

- MCEER-09-0008 "Assessment of Base-Isolated Nuclear Structures for Design and Beyond-Design Basis Earthquake Shaking," by Y.N. Huang, A.S. Whittaker, R.P. Kennedy and R.L. Mayes, 8/20/09 (PB2010-102699).
- MCEER-09-0009 "Quantification of Disaster Resilience of Health Care Facilities," by G.P. Cimellaro, C. Fumo, A.M. Reinhorn and M. Bruneau, 9/14/09 (PB2010-105384).
- MCEER-09-0010 "Performance-Based Assessment and Design of Squat Reinforced Concrete Shear Walls," by C.K. Gulec and A.S. Whittaker, 9/15/09 (PB2010-102700).
- MCEER-09-0011 "Proceedings of the Fourth US-Taiwan Bridge Engineering Workshop," edited by W.P. Yen, J.J. Shen, T.M. Lee and R.B. Zheng, 10/27/09 (PB2010-500009).
- MCEER-09-0012 "Proceedings of the Special International Workshop on Seismic Connection Details for Segmental Bridge Construction," edited by W. Phillip Yen and George C. Lee, 12/21/09 (PB2012-102402).
- MCEER-10-0001 "Direct Displacement Procedure for Performance-Based Seismic Design of Multistory Woodframe Structures," by W. Pang and D. Rosowsky, 4/26/10 (PB2012-102403).
- MCEER-10-0002 "Simplified Direct Displacement Design of Six-Story NEESWood Capstone Building and Pre-Test Seismic Performance Assessment," by W. Pang, D. Rosowsky, J. van de Lindt and S. Pei, 5/28/10 (PB2012-102404).
- MCEER-10-0003 "Integration of Seismic Protection Systems in Performance-Based Seismic Design of Woodframed Structures," by J.K. Shinde and M.D. Symans, 6/18/10 (PB2012-102405).
- MCEER-10-0004 "Modeling and Seismic Evaluation of Nonstructural Components: Testing Frame for Experimental Evaluation of Suspended Ceiling Systems," by A.M. Reinhorn, K.P. Ryu and G. Maddaloni, 6/30/10 (PB2012-102406).
- MCEER-10-0005 "Analytical Development and Experimental Validation of a Structural-Fuse Bridge Pier Concept," by S. El-Bahey and M. Bruneau, 10/1/10 (PB2012-102407).
- MCEER-10-0006 "A Framework for Defining and Measuring Resilience at the Community Scale: The PEOPLES Resilience Framework," by C.S. Renschler, A.E. Frazier, L.A. Arendt, G.P. Cimellaro, A.M. Reinhorn and M. Bruneau, 10/8/10 (PB2012-102408).
- MCEER-10-0007 "Impact of Horizontal Boundary Elements Design on Seismic Behavior of Steel Plate Shear Walls," by R. Purba and M. Bruneau, 11/14/10 (PB2012-102409).
- MCEER-10-0008 "Seismic Testing of a Full-Scale Mid-Rise Building: The NEESWood Capstone Test," by S. Pei, J.W. van de Lindt, S.E. Pryor, H. Shimizu, H. Isoda and D.R. Rammer, 12/1/10 (PB2012-102410).
- MCEER-10-0009 "Modeling the Effects of Detonations of High Explosives to Inform Blast-Resistant Design," by P. Sherkar, A.S. Whittaker and A.J. Aref, 12/1/10 (PB2012-102411).
- MCEER-10-0010 "L'Aquila Earthquake of April 6, 2009 in Italy: Rebuilding a Resilient City to Withstand Multiple Hazards," by G.P. Cimellaro, I.P. Christovasilis, A.M. Reinhorn, A. De Stefano and T. Kirova, 12/29/10.
- MCEER-11-0001 "Numerical and Experimental Investigation of the Seismic Response of Light-Frame Wood Structures," by I.P. Christovasilis and A. Filiatrault, 8/8/11 (PB2012-102412).
- MCEER-11-0002 "Seismic Design and Analysis of a Precast Segmental Concrete Bridge Model," by M. Anagnostopoulou, A. Filiatrault and A. Aref, 9/15/11.
- MCEER-11-0003 "Proceedings of the Workshop on Improving Earthquake Response of Substation Equipment," Edited by A.M. Reinhorn, 9/19/11 (PB2012-102413).
- MCEER-11-0004 "LRFD-Based Analysis and Design Procedures for Bridge Bearings and Seismic Isolators," by M.C. Constantinou, I. Kalpakidis, A. Filiatrault and R.A. Ecker Lay, 9/26/11.

- MCEER-11-0005 “Experimental Seismic Evaluation, Model Parameterization, and Effects of Cold-Formed Steel-Framed Gypsum Partition Walls on the Seismic Performance of an Essential Facility,” by R. Davies, R. Retamales, G. Mosqueda and A. Filiatrault, 10/12/11.
- MCEER-11-0006 “Modeling and Seismic Performance Evaluation of High Voltage Transformers and Bushings,” by A.M. Reinhorn, K. Oikonomou, H. Roh, A. Schiff and L. Kempner, Jr., 10/3/11.
- MCEER-11-0007 “Extreme Load Combinations: A Survey of State Bridge Engineers,” by G.C. Lee, Z. Liang, J.J. Shen and J.S. O’Connor, 10/14/11.
- MCEER-12-0001 “Simplified Analysis Procedures in Support of Performance Based Seismic Design,” by Y.N. Huang and A.S. Whittaker.
- MCEER-12-0002 “Seismic Protection of Electrical Transformer Bushing Systems by Stiffening Techniques,” by M. Koliou, A. Filiatrault, A.M. Reinhorn and N. Oliveto, 6/1/12.
- MCEER-12-0003 “Post-Earthquake Bridge Inspection Guidelines,” by J.S. O’Connor and S. Alampalli, 6/8/12.
- MCEER-12-0004 “Integrated Design Methodology for Isolated Floor Systems in Single-Degree-of-Freedom Structural Fuse Systems,” by S. Cui, M. Bruneau and M.C. Constantinou, 6/13/12.
- MCEER-12-0005 “Characterizing the Rotational Components of Earthquake Ground Motion,” by D. Basu, A.S. Whittaker and M.C. Constantinou, 6/15/12.
- MCEER-12-0006 “Bayesian Fragility for Nonstructural Systems,” by C.H. Lee and M.D. Grigoriu, 9/12/12.
- MCEER-12-0007 “A Numerical Model for Capturing the In-Plane Seismic Response of Interior Metal Stud Partition Walls,” by R.L. Wood and T.C. Hutchinson, 9/12/12.
- MCEER-12-0008 “Assessment of Floor Accelerations in Yielding Buildings,” by J.D. Wieser, G. Pekcan, A.E. Zaghi, A.M. Itani and E. Maragakis, 10/5/12.
- MCEER-13-0001 “Experimental Seismic Study of Pressurized Fire Sprinkler Piping Systems,” by Y. Tian, A. Filiatrault and G. Mosqueda, 4/8/13.
- MCEER-13-0002 “Enhancing Resource Coordination for Multi-Modal Evacuation Planning,” by D.B. Hess, B.W. Conley and C.M. Farrell, 2/8/13.
- MCEER-13-0003 “Seismic Response of Base Isolated Buildings Considering Pounding to Moat Walls,” by A. Masroor and G. Mosqueda, 2/26/13.
- MCEER-13-0004 “Seismic Response Control of Structures Using Novel Adaptive Passive Negative Stiffness Device,” by D.T.R. Pasala, A.A. Sarlis, S. Nagarajaiah, A.M. Reinhorn, M.C. Constantinou and D.P. Taylor, 6/10/13.
- MCEER-13-0005 “Negative Stiffness Device for Seismic Protection of Structures,” by A.A. Sarlis, D.-T.R. Pasala, M.C. Constantinou, A.M. Reinhorn, S. Nagarajaiah and D.P. Taylor, 6/12/13.



EARTHQUAKE ENGINEERING TO EXTREME EVENTS

University at Buffalo, The State University of New York

133A Ketter Hall ■ Buffalo, New York 14260-4300

Phone: (716) 645-3391 ■ Fax: (716) 645-3399

Email: mceer@buffalo.edu ■ Web: <http://mceer.buffalo.edu>



University at Buffalo *The State University of New York*

ISSN 1520-295X